NANOPARTICLE BRIDGE DNA BIOSENSOR

by

HONG-WEN HUANG

Presented to the Faculty of the Graduate School of

The University of Texas at Arlington in Partial Fulfillment

of the Requirements

for the Degree of

DOCTOR OF PHILOSOPHY

THE UNIVERSITY OF TEXAS AT ARLINGTON

May 2010

Copyright © by Hong-Wen Huang 2009

All Rights Reserved

ACKNOWLEDGEMENTS

I am heartily thankful to my supervisor, Dr. Seong Jin Koh, whose encouragement, guidance and support from the initial to the final level enabled me to develop an understanding of the subject. It was his insistence and encouragement that helped me faced those difficulties during the whole research and found the way to overcome them. Without his help and support, this thesis could never been written.

I am indebted to my many of my colleagues-Ram, Jason, Ray, Pradeep and Ruqi to support me all the way through. It was their support and accompanying cheered me up when I was suffering from experiment failure. This group has been a source of friendships as well as good advice and collaboration. It is my pleasure to have them as my colleagues.

I owe my deepest gratitude to my family-my parents, my wife and my daughter. My parents show their greatest support in many ways. My wife taking care of everything and let me focus on study without worries. My daughter, Charlene, who was born two and half year before I finishing my degree is always the sweetest angel who makes me smile with her smile.

I would also like to show my gratitude to Dr. Samir Iqbal and his research group member Wan Yuan. They help me a lot in my research and always provide helpful suggestions when I needed.

Lastly, I offer my regards and blessings to all of those who supported me in any respect during the completion of this research.

This study was supported by the Office of Naval Research under Grant No. N00014-05-1-0030, by the National Science Foundation under Grant No. ECS-0449958 and ECCS-0925997, and by the Texas Higher Education Coordinating Board under Grant No. 003656-0014-2006

April 15, 2010

ABSTRACT

NANOPARTICLE BRIDGE DNA BIOSENSOR

Hong-Wen Huang, PhD.

The University of Texas at Arlington, 2009

Supervising Professor: Seong Jin Koh

A new DNA sensing method is demonstrated in which DNA hybridization events lead to the formation of nanoparticle satellites that bridge two electrodes and are detected electrically. The hybridization events are exclusively carried out only on specific locations, the surfaces of C-ssDNA modified 50 nm GNPs. The uniqueness of this work is that only a small number of T-ccDNA molecules (<10) is required to form the nanoparticle satellites, allowing ultra-sensitive DNA sensing. The principle of this new DNA sensing technique has been demonstrated using target DNA and three-base-pair-mismatched DNA in 20nM concentrations.

Three single-stranded DNA (ssDNA) system is used in our experiment which includes Capture-ssDNA (C-ssDNA), Target-ssDNA (T-ssDNA) and Probe-ssDNA (P-ssDNA). Both C-ssDNA and P-ssDNA are modified by a thiol group and can hybridize with different portions of T-ssDNA. T-ssDNA requires no modification in three ssDNA system, which is beneficial in many applications. C-ssDNA modified 50nm gold nanoparticle (C-50au) and P-ssDNA modified 30nm gold nanoparticle (P-30au) are prepared through the reaction of thiol-gold chemical bonding between thiolated ssDNA and gold nanoparticle (GNP) (C-ssDNA with 50nm GNP, P-ssDNA with 30nm GNP). We controllably place the C-50au only on the SiO_2 band surface (~ 90nm width) between two gold electrodes (source and drain electrodes) by forming positively- and

negatively-charged self-assembled monolayers (SAMs) on SiO_2 and gold surface, respectively. DNA modified GNP is negatively charged due to ionization of phosphate group on DNA back bone. C-50au therefore is negatively charged and can only be attracted toward SiO_2 area (repelled by negatively charged gold electrode surface). The amine group of positively-charged SAMs on SiO_2 surface is then passivated by converting to non-polar methyl functional group after C-50au placement. P-30au is first hybridized with T-ssDNA in the solution phase (T-P-30au formed) and is introduced into DNA detection device in which C-50au are immobilized on ~90nm width SiO_2 band (between two gold electrodes). The passivation step ensures every T-P-30au are attached only to C-50au through hybridization (T-P-30au will not be attracted toward SiO_2 surface or gold electrodes). GNP bridges are formed across the electrodes and provide an electrical path between two gold electrodes.

We ensure that every T-P-30au only hybridizes on the surface of C-50au by (1) accurately controlling C-50au placement between two gold electrodes, (2) passivating positively-charged SAMs on SiO2 surface after C-50au immobilization. When T-P-30au hybridize with C-50au on ~90nm wide SiO2 surface, GNP bridges form and provide an electrical path between two gold electrodes even with only a few hybridization events. Experimental results show that even a few GNP bridges formed on SiO2 band can provide a significant conductance change from an open circuit to a conductive circuit (current = 0.5 uA at voltage = 0.1 V with four GNP bridge). We also used 3-base-pair-mismatched ssDNA (3mm-ssDNA) as a control experiment, which always resulted in an open circuit (no GNP bridge formed). Our detection device is compatible with current CMOS fabrication technology and can be manufactured on a wafer scale. The direct electrical output of this DNA detection technique provides a promising basis for high-throughput screening (can be fabricated on a wafer scale) with no expensive equipment required.

TABLE OF CONTENTS

LIST OF ILLUSTRATIONS

LIST OF TABLES

CHAPTER 1

INTRODUCTION

1.1 Overview

Detection of specific DNA sequence is of significance in many biological research areas including clinical (how cells' work function are changed while infection), food analysis (genetic modification), DNA diagnostics and environmental analysis (harmful bacteria and virus detection). The basic principle of biosensor utilizes the characteristic of one-to-one recognization between those biomolecules (such as DNA hybridization, antibody-antigen and RNA-protein combination) and detects the signals generated during the recognizing process.

In our study, we chose DNA detection as an example for our detection method. We utilize GNP as signal amplifier which can be easily modified by thiolated ssDNA (C-50au: Capture-ssDNA modified 50nm GNP; P-30au: probe-ssDNA modified 30nm GNP). Also, we apply three-ssDNA system (Capture-Target-Probe ssDNA) in which thiolated capture and probe ssDNA can hybridize with different portion of target ssDNA and target ssDNA require no modification or amplification (PCR).

The major signal we detect is the conductance change before and after DNA hybridization by I-V measurement. When target ssDNA exist in the system, C-50au and P-30au can be linked together and form GNP bridges across two gold electrodes which provide electrical paths between electrodes. Our experiment results indicate that even with one GNP bridge can provide measureable signal and only one P-30au attached to C-50au by hybridization with T-ssDNA can sometimes form a useful GNP bridge. This is to say, our

detection limit could research an extremely low concentration (~10 target ssDNA molecules, sub zepto-M) theoretically.

1.2 DNA Biosensor Utilizing DNA Modified GNP

Utilizing DNA modified gold nanoparticle in DNA detection has many benefits. Gold nanoparticle can play a role of reliable signal amplifier in either optical or electrochemical detection method (will not decay with time). Also, utilizing DNA modified GNP in our detection method directly provides us measureable conductance change with even only one GNP bridge formed between two electrodes. This is to say, first, the signal generated from DNA hybridization events in our detection method can be directly exported to a read-friendly signal without any signal translation. Second, the detection limit from detection equipment does not exist in our method because the signal is strong enough to be recognized even with only one GNP bridge formed. Also, the melting transition of DNA linked GNP is sharper compared to free DNA melting transition which might give us much higher selectivity while mismatched ssDNA exist [1.3].

Thiol group modification for 3' end and 5' end ssDNA is commonly used and available commercially. Thiol group reaction with gold surface is also well known. Therefore, modification of GNP surface with thiolated ssDNA is robust and commonly used by many other researchers. DNA modified GNPs are stable even in high salt concentration environment which is important for DNA hybridization environment.

The pioneer of DNA modified GNPs, C.A. Mirkin et al [1.3], have done many great works in the study of characteristics of DNA modified GNPs and the applications of DNA modified GNP. Such as ssDNA modification density on GNP surface, the relationship of ssDNA surface modification density on GNP surface with the hybridization efficiency, melting temperature variation with the size of nanoparticle, and sequence-dependent interaction between ssDNA modified GNP.

Thanks to their work, we have more understanding about DNA modified GNP and can utilize their effort to improve our DNA detection mechanism.

1.3 Organization of This Thesis

The major focus of this work is to establish a new DNA detection mechanism utilizing DNA modified gold nanoparticles. There are many different kinds of fundamental knowledge applied in this detection mechanism including: (1) self-assembled monolayers formation on different substrate surface, (2) charged molecules or nanoparticles interaction in the electrolyte environment (electrical double layer and DLVO theory), (3) DNA hybridization and melting (kinetics and thermodynamics), (4) characteristic of DNA modified gold nanoparticle and how it affect DNA hybridization efficiency.

In chapter 2, we will discuss about the basic DNA structure, ssDNA hybridization, DNA melting transition and how those phenomena are affected while one of ssDNA is confined on the solid or nanoparticle surface. Also, the hybridization kinetics of how DNA hybridize in free solution differ from heterogeneous hybridization.

In chapter 3, we will have a brief review of different kinds of DNA detection methods including optical method, mechanical method and electrochemical method. We will specially focus on electrochemical method due to its fast, simple and low-cost benefits. Also, the electrochemical detection protocols are suitable for mass fabrication of miniaturized devices (microarray). Also, we will have a brief review of different kinds of transducer that we use to detect the biomolecular recognition event and translate into readable signal. At the end of the chapter, we will discuss briefly about the common methods used to immobilize the DNA on the solid surface.

In chapter 4, we will have a brief introduction about SAMs formation on different solid surface and how they interact with charged molecules or nanoparticles in the electrolyte environment base on DLVO theory. Those fundamentals are important in our DNA detection

mechanism because we have to utilize different SAMs to create positively and negatively charged surface on the guiding structure and accurate control the positioning of negatively charged DNA modified nanoparticles into the gap between two electrodes only. This is the most important step in all of our detection mechanism and also the most unique advantage compares to other similar detection methods.

Chapter 5 is the detail information of the experiment settings including experiment processing steps, reaction time, reaction concentration and temperature.

In chapter 6, all the experiment results for each step in our DNA detection method are shown and illustrated with detail sketches and SEM images. Including SAMs layer formation, accurate nanoparticle positioning, and how we can have a clear I-V signal with only less than 10 hybridization events occur without future amplification. The real device and the I-V measurements for the DNA detection between complementary target ssDNA and three base pair mismatched ssDNA are also compared.

In chapter 7 is the conclusion and future work of whole our DNA detection mechanism and possible suggestions that can improve the performance of our detection sensitivity and efficiency.

CHAPTER 2

BACKGROUND KNOWLEDGE OF DNA STRUCTURE AND HYBRIDIZATION

Deoxyribonucleic acid (DNA) is a long-term storage of genetic information and a long polymer chain with of simple repeating units (Adenine, Thymine, Guanine, and Cytosine). DNA contains genetic information used in development and functioning of all known living organisms and some viruses. Different DNA segments provide different functions; some segments that carry genetic information are called genes, and others have structure purposes or involved in regulating the use of this genetic information.

The nucleolus in cell is a non-membrane bound structure composed of proteins and nucleic acids found within the nucleus. Ribosomal RNA (rRNA) is transcribed and assembled whining the nucleolus (Fig. 2.1, (1)).

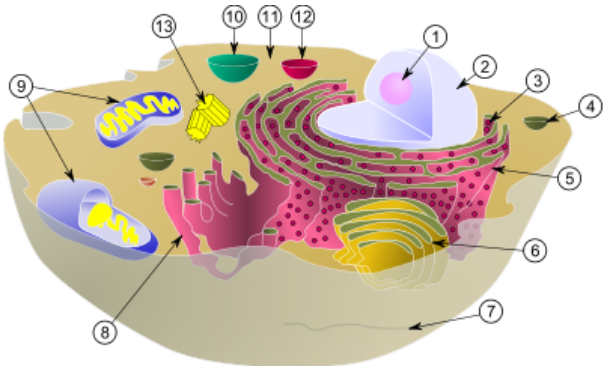

Fig. 2.1: Cell structure. (1)nucleolus (2)nucleus (3)ribosome (4)vesicle (5)rough endoplasmic reticulum (6)Golgi apparatus (7)Cytoskeleton (8)smooth endoplasmic reticulum (9) mitochondria (10) vacuole (11) cytoplasm (12) lysosome (13) centrioles [2.1]

DNA is organized into X-shaped structure called chromosomes and stored in the nucleolus. Chromosome is an organized structure of DNA and protein; it is a single piece of

coiled DNA containing genes, regulatory elements and other nucleotide sequences. DNA-bound proteins, which contained in chromosome, serve to package DNA and control its function. The DNA molecule may be circular or linear, and can be composed of 10,000 to 1,000,000,000 nucleotides in a long chain. Fig. 2.2 and Fig. 2.3 illustrate how DNA can be folded and form chromosome.

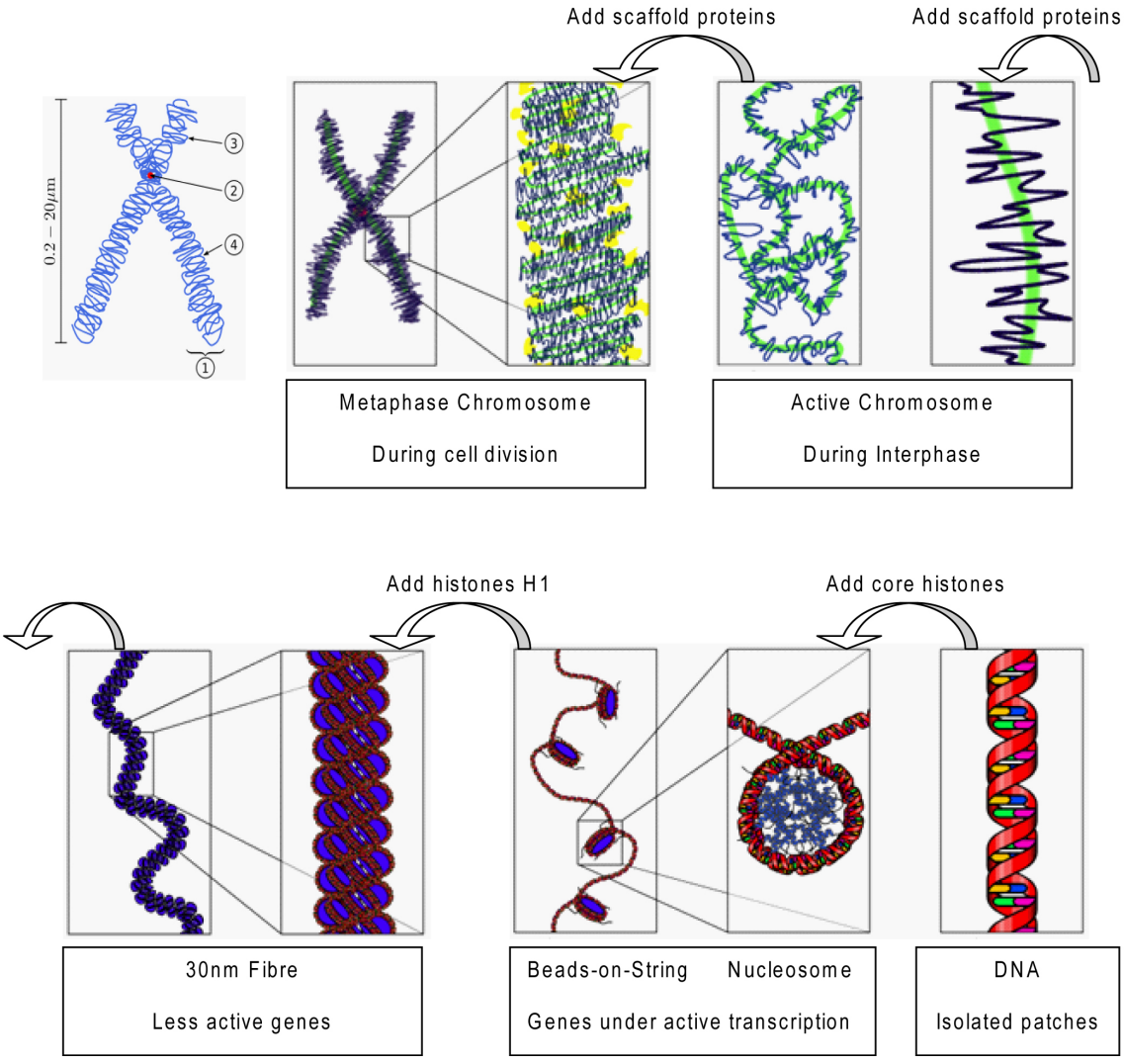

Fig. 2.2: How dsDNA can be folded and form Chromosome. (1) Chromatid, (2) Centromere–two chromatids touch, (3) Short arm, (4) Long arm. [2.1]

Histones are protein components which package and order the DNA into structure units called nucleosomes, act as spools around DNA winds and as play a role in gene regulation.

Histones are strongly alkaline proteins and can be grouped into five major classes: H1/H5, H2A, H2B, H3, and H4. H2A, H2B, H3, and H4 are classified as core histones which wrap up dsDNA chain into a ring shape as shown in Fig. 2.3. H1 and H5 are called linker histones which furture organize the wrapped-up DNA into less active genes as shown in Fig. 2.2.

Each human cell has about 1.8 meters of DNA, but wound on the histones it has about 90 millimeters of chromatin, which, when duplicated and condensed during mitosis, result in about 120 micrometers of chromosomes. The sketch how histones act as a package protein in dsDNA folding is shown in Fig. 2.3

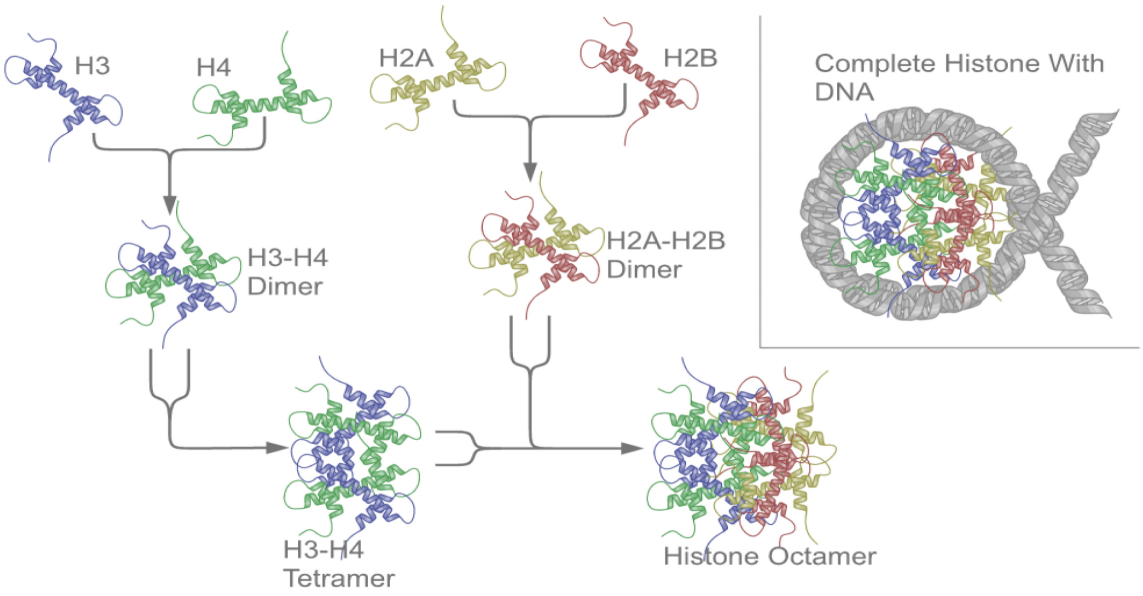

Fig. 2.3: The sketch of how Histones protein act as folding protein and help package dsDNA. [2.1]

2.1 DNA Structure

In 1953, J.D. Watson and F.H.C. Crick offered a model for the physical structure of DNA (Watson and Crick, 1953). They proposed that two antiparallel strands are coiled about one another to form a double-stranded helix. In this model, the bases of one strand are hydrogen-bonded to those of the other strand to form purine-pyrimidine base pairs. These are either adenine and thymine (A-T) or guanine and cytosine (G-C).

The three major portions of Deoxyribonucleic acid (DNA) are (a) five carbon sugar ring, (b) phosphate linker and (c) four types of bases molecular shown in Fig. 2.4. DNA is a long polymer made from repeating units called nucleotides [2.2-2.4].

DNA chain is 2.2~2.6nm wide, and one nucleotide unit is 0.33 nm long [2.5]. In living organisms, DNA exists as a double helix which is formed by to complementary single strand DNA hybridization. The length of one helical turn of dsDNA chain is around 3.4 nm with about 10 nucleotide pairs per helical turn. Although each individual repeating unit is very small, DNA polymers can be very large molecules containing millions of nucleotides.

The largest human chromosome, chromosome number 1, is approximately 220 million base pairs long (Chromosome 1 is gene-dense, with 3,141 genes and 991 pseudo-genes, and many coding sequences overlap) [2.6].

There are four different types of base in DNA strand which are Adenine (A), Thymine (T), Guanine (G) and Cytosine (C). Each type of base on one strand forms a bond with just one type of base on the other strand; this is called complementary base pairing.

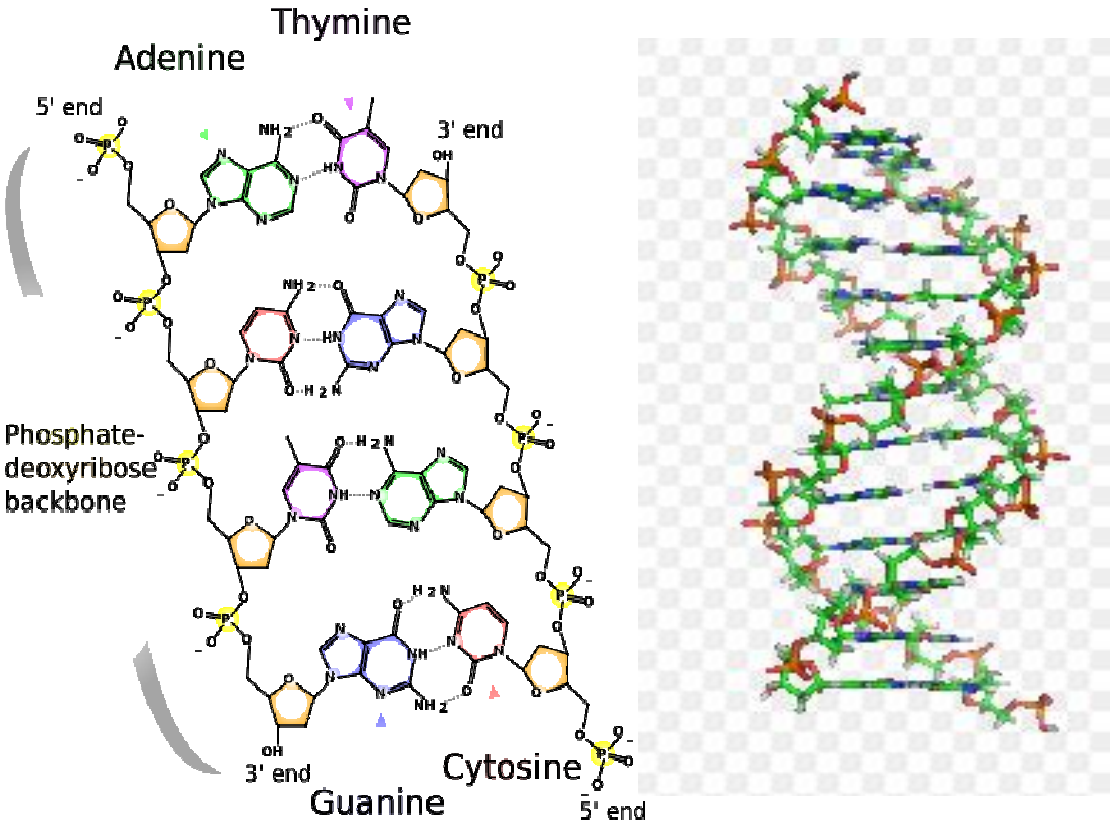

Fig. 2.4: The sketch of double strand DNA chemical structure and 3-D structure. [2.1]

Adenine ($C_5H_5N_5$, 9H-purin-6-amine) is a purine with a variety of roles in biochemistry and is one of the two purine nucleobases used in forming nucleotides. In DNA, adenine (A) binds to thymine (T) via two hydrogen bonds to assist in stabilizing the nucleic acid structure. Adenine forms adenosine, a nucleoside, when attached to ribose, and deoxyadneosine when attached to deoxyribose. The shape of adenine is complementary to either thymine (T) in DNA or uracil (U) in RNA.

Thymine ($C_5H_6N_2O_2$, 5-methylpyrimidine-2,4(1H,3H)-dione) is a pyrimidine nucleobase. In DNA, thymine (T) binds to adenine (A) via two hydrogen bonds to assist in stabilizing the nucleic acid structure. Thymine combined with deoxyribose creates the nucleoside deoxythymidine.

Guanine ($C_5H_5N_5O$, 2-amino-1H-purin-6(9H)-one) is a derivative of purine, consisting of a fused pyrimidine-imidazole ring system with conjugated double bonds. It is a unsaturated, bicyclic planar molecule.

Cytosine ($C_4H_5N_3O$, 4-amino-1H-pyrimidine-2-one) is a pyrimidine derivative with a heterocyclic aromatic ring and two substituents attached (an amine group at position 4 and a keto (R-CO-R') group at position 2)

The detail chemical structure and interaction between each base are shown as Fig. 2.5 and Fig. 2.6

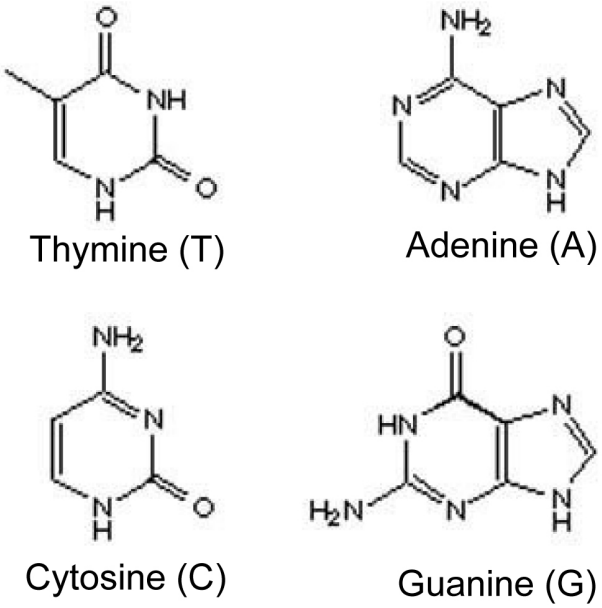

Fig. 2.5: Detail chemical structure of DNA bases. Thymine and Cytosine are pyrimidines, Adenine and Guanine are purines. [2.1]

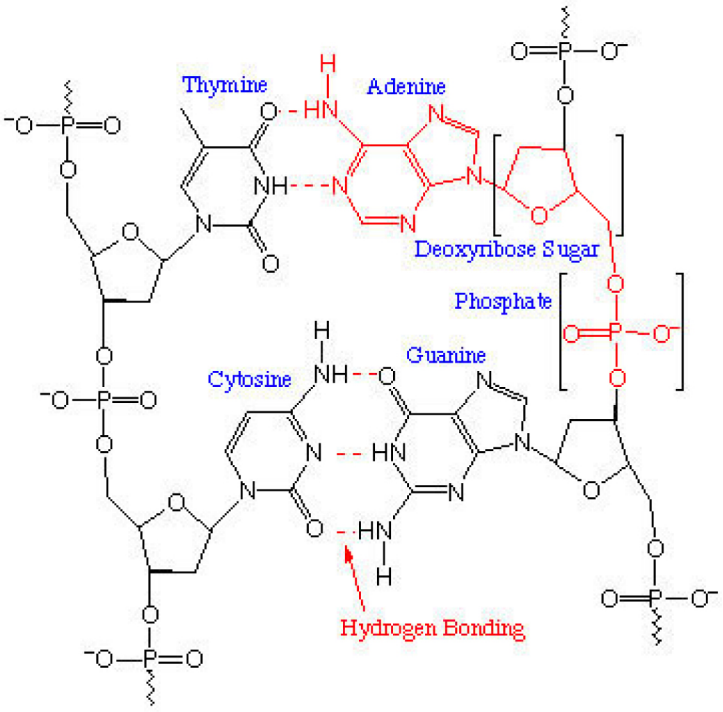

Fig. 2.6: DNA base pair interaction between two single strand DNA. [2.1]

2.1.1 Hydrogen Bonding and Stability of DNA Base Pair

Hydrogen bonding is forming between Hydrogen atom (hydrogen, which is connected to F, O or N atom) and F, O or N atoms. In the canonical Watson-Crick base pairing, Adenine (A) forms a base pair with Thymine (T) as does Guanine (G) with Cytosine (C) in DNA.

The larger nucleic acids, A and G, are members of class of doubly-ringed chemical structures called Purines; the smaller nucleic acids, C and T are singly-ringed chemical structure called Pyrimidines. Purines are only complementary with Pyrimidines (A-T; G-C). Pyrimidine - Pyrimidine pairings (C and T) are energetically unfavorable because the molecules are too far apart for hydrogen bonding formation. Purine - Purine pairings (A and G) are energetic unfavorable because the molecules are too close. The only other possible mismatch pairing are G-T and A-C, these pairings are mismatches because the pattern of hydrogen donors and acceptors do not correspond. The interaction between four bases including complementary and mis-match base pairing are shown at Fig. 2.7 [2.7].

Two of many possible mis-match base parings were shown in Fig. 2.7 (c) and (d). The purine-pyrimidine, guanine-thymine (G-T) and adenine, cytosine (A-C) mispairs adopt the so called wobble base-pair conformation. In these mis-matched base-pairs, in order to achieve some sort of hydrogen bonding complementarity, the two bases are moved (or "wobbled") with respect to one another. The results are base-pairs which are held together by two inter-base hydrogen bonds. For both possible hydrogen bonds to form in the A-C base-pair there is a requirement for the protonation of the adenine base and the result is more properly notated as an AH^+-C base-pair (Fig. 2.7(c)).

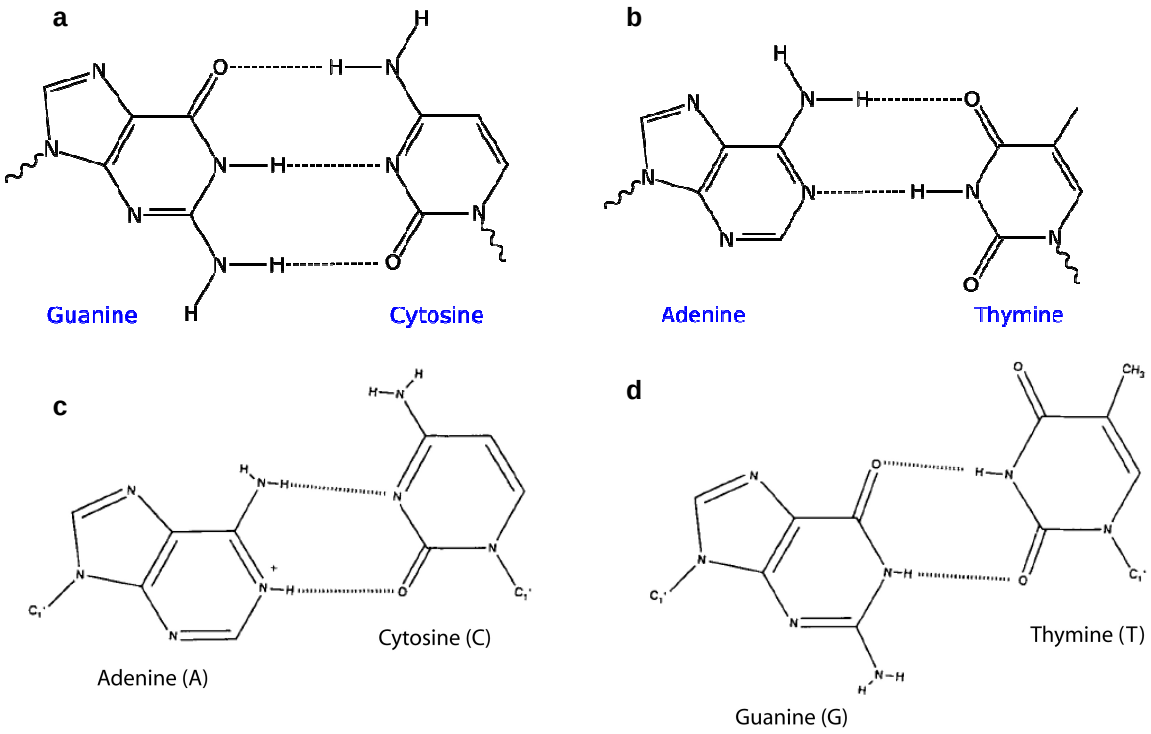

Fig. 2.7: Chemical structure and interaction between bases and mismatch. a) G-C interaction. b) A-T interaction. c) A-C mis match interaction. d) G-T mismatch interaction. For A-C mispair, Adenine is required to protonation to form two hydrogen bonding with Cytosine. For both A-C and G-T mispair, the molecules are both required to have some distortion. [2.7]

2.1.2 DNA Surface Charge

DNA is a polymer with alternating sugar-phosphate sequence. The monomer units of DNA are nucleotides. Each nucleotide consists of a deoxyribose sugar, a nitrogen-containing base attached to the sugar, and a phosphate group. DNA oligonucleotides have both ionic and hydrophobic characteristics which result in complex adsorption and surface diffusion behavior on glass silanized with a range of ionic and hydrophobic silanes. The orientation of the oligonucleotide lying on the surface and the quantity adsorbed appear to be influenced by whether the surface is cationic or hydrophobic [2.8].

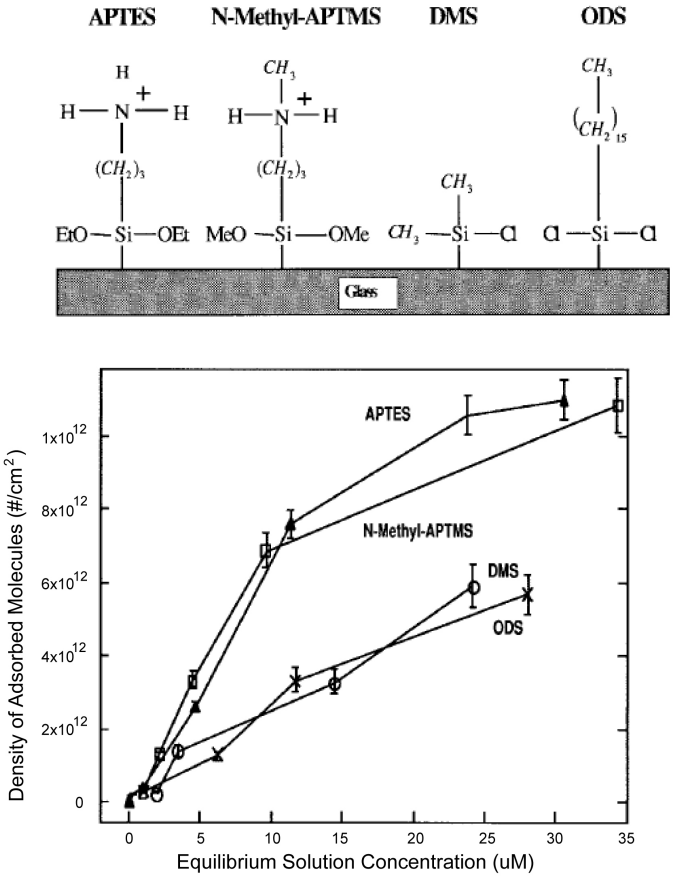

Fig. 2.8: Adsorption of oligonucleotide in PBS buffer on hydrophobic and ionic substrates. (A) Chemical structures of the four silanes which are coupled to the glass surfaces. (B) Adsorption isotherm measured by TIR/spot FRAP for various equilibrium concentrations on DMS-, ODS-, APTES- and N-methyl- APTMS-coated glass. [2.8]

On both hydrophobic surfaces, more than 80% of the oligonucleotides in all the samples studied adsorbed reversibly. But, the desorption rate constant of oligonucleotide on APTES coated glass is much slower than that of N-Methyl-APTMs, DMS and ODS [2.8].

The driving forces for oligonucleotide adsorption from buffer solution on the substrates can be divided into three categories: electrostatic interaction, hydrophobic interaction, and hydrogen bonding. However, in our study, we modify SiO_2 surface with APTES (positively charged), and gold electrode surfaces with MHA (negatively charged), therefore, electrostatic interactions were expected to predominate. Work done by Golub et al. indicates that the amino group in APTES is positively charged for all pH values less than approximately 10 [2.9, 2.10].

When single-stranded DNA molecules dissolve in aqueous solution, ionization of sites on the phosphate linkages and nitrogen-containing base result in a charge that is pH-dependent. [2.11]

A phosphodiester is a strong acid with pKa is around 1. Adenine (A) and cytosine (C) base can be found as neutral or positive forms, whereas thymine (T) is neutral or negative, and guanine (G) can exist in all three states [2.12].

The ionization of the bases and their corresponding dissociation constants may be described by the equilibria reported in Table 2.1.

Table 2.1: Ionization Equilibrium for the Four Different Bases Found in DNA [2.11].

Base	Equilibrium	Equilibrium constant
Adenine	$AH^+ \leftrightarrow A + H^+$	$K_A = 10^{-3.5}$
Cytosine	$CH^+ \leftrightarrow C + H^+$	$K_C = 10^{-4.2}$
Thymine	$TH \leftrightarrow T^- + H^+$	$K_T = 10^{-9.2}$
Guanine	$GH_2^+ \leftrightarrow GH + H^+$	$K_{G1} = 10^{-2.1}$
	$GH \leftrightarrow G^- + H^+$	$K_{G2} = 10^{-9.2}$

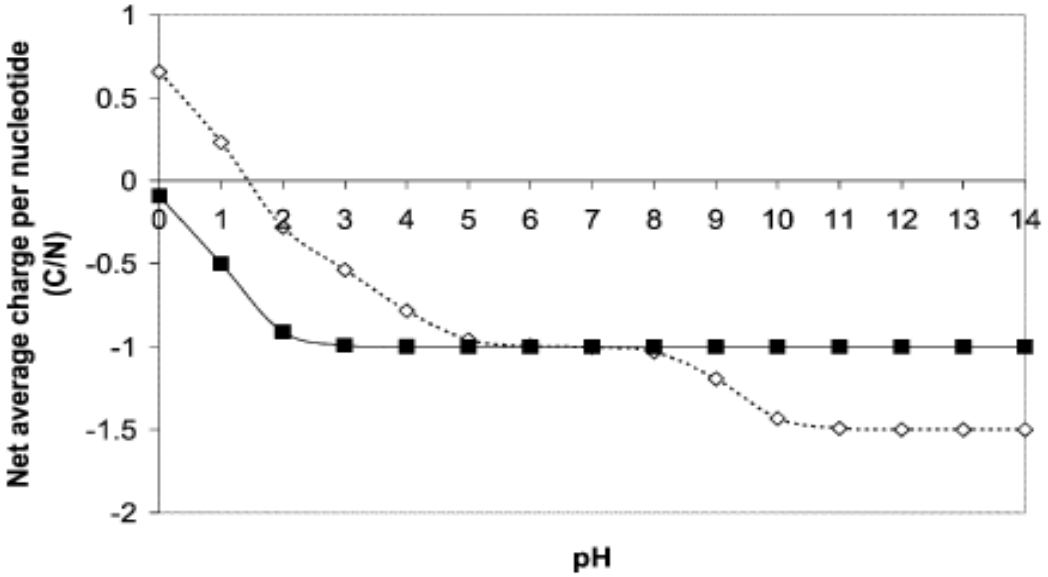

Fig. 2.9 Calculated net average charge per nucleotide of a double- or single-strand DNA molecule in solution. The solid line represents the charge of a double-stranded DNA (phosphate groups). The dotted line represents the charge of single-stranded DNA [2.11]

Science the amine group of APTES shows positive charge when pH is less than 10, and ssDNA molecule shows negative charge when pH is larger than 2, there is for sure that DNA molecules can be attracted by positively-charged APTES SAMs and therefore, DNA can be confined on the SiO_2 surface though APTES modification. APTES may interact with oligonucleotide by a combination of hydrogen bonding (through uncharged amino nitrogens) and charge interaction.

The study of DNA adsorption onto cationic aminated-latex particles and the ellipsometry of oligonucleotide adsorbed on APTES glass are done by Ganachaud et al (1997) and Chrisey et al (1994)[2.12, 2.13]. Proposed structures of adsorbed oligonucleotide on both positively charged and hydrophobic substrates based on data of Walker and Grant are shown in Fig. 2.10.

It should be noticed that, with cation silanized (APTES modified) surface, ssDNA attach to the surface by the negatively charged phosphate linker on DNA back bone, and the base are exposed. Which means the ssDNA still keep the hybridization ability with complementary ssDNA. On the other hand, when ssDNA attach to the hydrophobic surface, the negatively

charged phosphate linker is exposed, which means the hybridization with complementary ssDNA is prohibited. Also, for the ssDNA that attach to cationic silanized surface (Fig. 2.10(a)), although ssDNA is still keep the hybridization ability, but due to the distortion of is 3-D structure, the hybridization ability is lower than the free ssDNA in the free solution phase and the ssDNA which “stand straight ” (chemisorptions) on the surface.

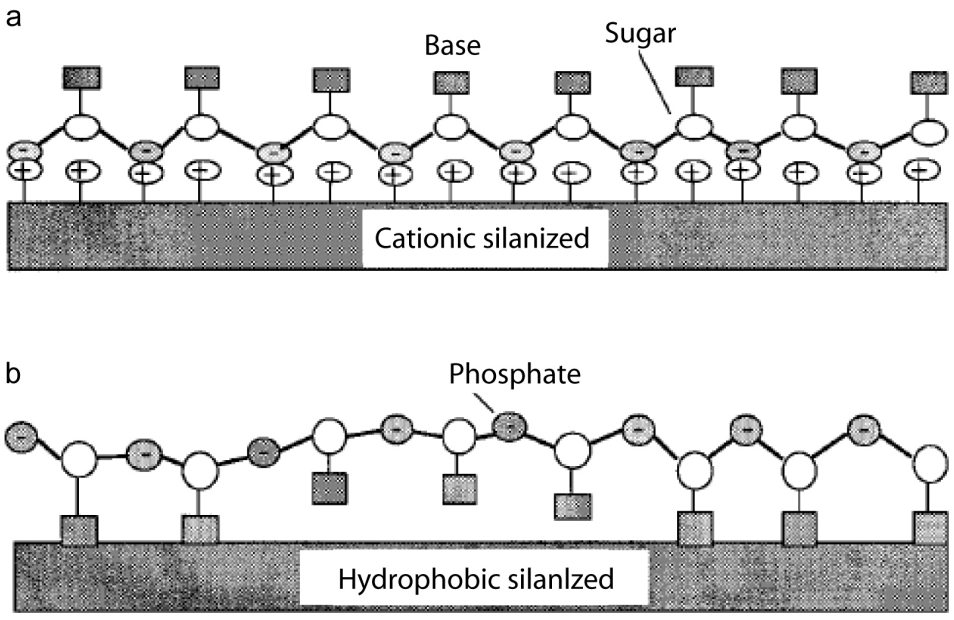

Fig. 2.10: Proposed structures for adsorbed oligonucleotide on positively charged and hydrophobic substrates [2.12, 2.13]. It should be noticed that for (a) cationic silanized surface, ssDNA attachs to the surface by the negatively charged phosphate linker, and the base is exposed which means the ssDNA is still able to hybridize with other complementary ssDNA. (b) For hydrophobic silanlzed surface, the ssDNA attach to surface with the base.

2.1.3 Melting Temperature of Double Strand DNA

Paired DNA and RNA molecules are comparatively stable at room temperature but two nucleotide strands will be separated when the temperature is above a melting point. When double-stranded DNA or native DNA is heated, the bonding forces between/within the strands are disrupted, and the two strands can separate. The chemical process, DNA melting or

denaturation involves breaking of three hydrogen bonds in every guanine-cytosine base pair and breaking of two hydrogen bonds in adenine-thymine base pair [2.14].

Pioneer melting experiments (Marmur and Doty, 1962 [2.15]) showed that DNA duplex melting and formation can be easily monitored through changes in the ultraviolet spectrum. Absorbance in the ultraviolet region increases as the double helix "melts" to two single strands. Reversibly, upon DNA duplex formation, the absorbance decreases. The optical UV-melting experiment is usually performed in the following way. Absorbance at 268 nm and temperature is monitored while the solution is slowly heated at a steady rate (6-60 ^{o}C / hour) from room temperature to 100 ^{o}C and cooled back to room temperature. The graph of absorbance vs temperature, the melting curve, is analyzed to obtain melting temperature (T_m), standard Gibbs free energy (ΔG^{o}), standard enthalpy (ΔH^{o}) and standard entropy (ΔS^{o}), of the helix-coil transition.

The melting temperature of DNA is often defined as the temperature when half of molecules are "melted", that is the temperature at the midpoint of the double helix to single strands transition.

The melting temperature of each double strand DNA (dsDNA) is determined by: (a) the length of the molecules (number of base pair); (b) the extent of mis-pairing (mismatch); (c) the GC content (the higher GC results in higher melting temperature due to three hydrogen bonding between G-C pairs); (d) the salt concentration ($[Na^{+}]$ or $[Mg^{+}]$).

In solution, DNA molecular is negative charged due to the ionization of phosphate linker (for both ssDNA and dsDNA at pH = 2~14). For hybridization, two ssDNA molecules need approach with each other first to allow hydrogen bond formation; however, they will be repelled from each other due to the electro-static force from their negatively charged phosphate linker. Reducing the hybridization temperature (increase thermal stability of hydrogen bonding between base pairs) can improve the hybridization rate between ssDNA but this will also increase the chance of non-complementary ssDNA mismatch. To reduce the repelling force between to negatively charged ssDNA molecules, we can add salt (NaCl) in to the solution. Due

to the screen effect from counter ions exist in the electrolyte solution, the affecting range of electro-static force can be reduced and the negatively charged ssDNA can get closer with each other to make hybridization occur easier.

2.1.3.1 Wallace Method

It was found that DNA stability depends on the chain length (number of hydrogen bonding) and the percentage of guanine-cytosine base pairs. The higher the G-C content, the greater the stability of DNA due to the number of hydrogen bonding formation is more than that of A-T base pair. The simplest interpretation is that when a guanine-cytosine base pair is formed, three hydrogen bonds are created in contrast to a adenine-thymine base pair that contains only two hydrogen bonds. Hence, higher G-C content increases the melting temperature and stability of duplex DNA.

Wallace method is base on this concept and provides the fastest and less accurate melting temperature estimation. Wallace method is suitable for oligos less than 18mers in length.

$$T_m = 2(A+T) + 3(G+C) \quad \text{(eq. 2.1)}$$

However, melting experiments showed that thermodynamic stability depends not only on G-C content but also on the sequence order or context. Two sequences with the same content of G-C base pairs can have different stabilities. The effect is less dramatic in comparison with two sequences having different G-C content, but is significant. To consider these effects, the nearest-neighbor (n-n) model has been employed (Wartell and Benight, 1985 [2.16]; Delcourt and Blake, 1991 [2.17]).

2.1.3.2 Nearest-Neighbor Method

The nearest-neighbor model of DNA predicts thermodynamics from n-n parameters for each doublet and assumes that there are no significant interactions beyond n-n doublets. In

DNA duplex, there are 10 n-n doublets (table 2.2). Consequently, the thermodynamics of double helix formation from single strands for any sequence can be calculated from 10 nearest-neighbor thermodynamic parameters. These ten nearest-neighbor parameters represent the thermodynamic values for formation of 10 possible n-n doublets in DNA duplexes.

The nearest-neighbor method (n-n method) is one method used to predict melting temperatures of nucleic acid duplexes which considering the effect of neighbor molecules. Instead of treating each base as an individual unit, n-n method considers adjacent base along the backbone two at a time due to the chemical bonding has certain angle and can not rotate freely[2.18]. Although GC content plays a large factor in the hybridization energy of double-stranded DNA, interactions between neighboring bases along the helix means that stacking energies are significant.

First, consider two single stranded DNA are complementary to each other (s1 and s2), the concentration of s1 and s2 are C_1 and C_2, respectively (assume $C_1 > C_2$). At initial state, no hybridization occurs and no double stranded DNA exists in the system. Assume all the s2 ssDNA is consuming by hybridizing with s1, the concentration of dsDNA now is C2. At certain temperature, a portion f of dsDNA is still remaining as double helix, the others (1-f) is melting as ssDNA. the equilibrium constant, K, can be written as following equation.

	s1	+	s2	=	ds
at initial state, $C_1 > C_2$	C_1		C_2		0
Assume all hybridized	$C_1 - C_2$		0		C_2
at equilibrium	$C_1 - C_2 + C_2 (1-f)$		$C_2 (1-f)$		$C_2\ f$

$$K = \frac{C_2\ f}{[C_1 - C_2 + C_2\ (1-f)]\ [C_2\ (1-f)]} = \frac{f}{(C_1 - C_2\ f)(1-f)}$$

at T = Tm, f = 1/2

$$K = \frac{1/2}{(C_1 - C_2/2)(1/2)} = \frac{1}{C_1 - C_2/2}$$

Where s1 is single strand DNA 1, s2 is complementary single strand DNA 2, ds is double helix formed by s1 and s2 hybridization. C_1 is concentration of s1 at initial stage, C_2 is

concentration of s2 at initial stage, f is the fraction of double helix compares to s2. Each of these has enthalpic and entropic parameters, the sums of which determine melting temperature according to the following equation:

$$\Delta G = \Delta H - T\Delta S = -RT\ln K$$
$$\Delta H = T\left(\Delta S - R\ln K\right)$$
$$T = Tm \Rightarrow K = \frac{1}{C_1 - C_2/2}$$
$$Tm(^oK) = \frac{\Delta H}{\Delta S - R\ln K} = \frac{\Delta H}{\Delta S + R\ln\left(C_1 - C_2/2\right)}$$
$$Tm(^oC) = \frac{\Delta H}{\Delta S + R\ln\left(C_1 - C_2/2\right)} - 273.15$$

(eq. 2.2)

where ΔH is the standard enthalpy and ΔS is the standard entropy for formation of the duplex from two single strands, C_1 is the initial concentration of the single strand that is in excess (usually probe, primer), C_2 is the initial concentration of the complementary strand that is limiting (usually target), R is the universal gas constant = 1.987 cal/(mol·K)

Standard enthalpies and entropies are negative for the annealing reaction and are assumed to be temperature independent. If C > > C_2 then C2 can be neglected.

Table 2.2: Unified Nearest-Neighbor Parameters for DNA/DNA Duplexes. Note that the ΔH values are given in kilocalories per mole and that the ΔS values are given in calories per mole per kelvin.

Nearest-neighbor sequence (5'-3'/5'-3')	ΔH kcal/mol	ΔS cal/(mol·K)
AA/TT	-7.9	-22.2
AG/CT	-7.8	-21.0
AT/AT	-7.2	-20.4
AC/GT	-8.4	-22.4
GA/TC	-8.2	-22.2
GG/CC	-8.0	-19.9
GC/GC	-9.8	-24.4
TA/TA	-7.2	-21.3
TG/CA	-8.5	-22.7
CG/CG	-10.6	-27.2
Terminal A-T base pair	2.3	4.1
Terminal G-C base pair	0.1	-2.8

(http://www.idtdna.com/analyzer/applications/Instructions/Default.aspx?AnalyzerDefinitions=true#MismatchMeltTemp)

2.1.3.3 Salt Concentration Affecting Tm of DNA

The influence of metal ions on nucleic acid melting is dramatic and was carefully investigated earlier in DNA polymers (Dove and Davidson, 1962; Gruenwedel and Chi-Hsia, 1969). They found that the melting temperature of DNA increases linearly with logarithm of alkali metal cation concentration (Owen et al., 1969; Frank-Kamenetskii, 1971) up to 1.0 M.

A nucleic acid duplex is a highly negatively charged polyelectrolyte due to ionized phosphate groups located in the backbone. Long-range electrostatic interactions between nucleic acids and counter-ions and co-ions in solution significantly affect the thermodynamics of nucleic acids. Strong repulsive electrostatic interactions exist between the negatively charged phosphate groups. Higher monovalent ion concentrations screen this interaction more effectively which results in higher stability of the DNA.

The effects of polyvalent ions is more complex, Mg^{2+} ions increase Tm but Cu^{2+} ions have the opposite effect and destabilize DNA duplexes (Eichhorn and Shin, 1968). Perhaps, Cu^{2+} exhibits a different mode of binding than $Mg^{2+,}$ and might prefer binding to the electron-donor groups on the bases instead of binding to phosphate moieties (Fig.2.11).

T_m depends on the mono-valent and divalent salt concentrations ($[Na^+]$ and $[Mg^{2+}]$, respectively) of the solvent. Linear T_m corrections were previously used to model the effects of cations on DNA hybridization. However, scientists at IDT determined that these linear functions are inaccurate. And they have developed new functions from several thousand ultraviolet and calorimetric melting experiments for over 100 short DNA duplexes in a variety of sodium, potassium, and magnesium buffers. OligoAnalyzer employs the improved Tm salt correction function for monovalent (Na^+) ions (Owczarzy,R. et al.[2.19]),

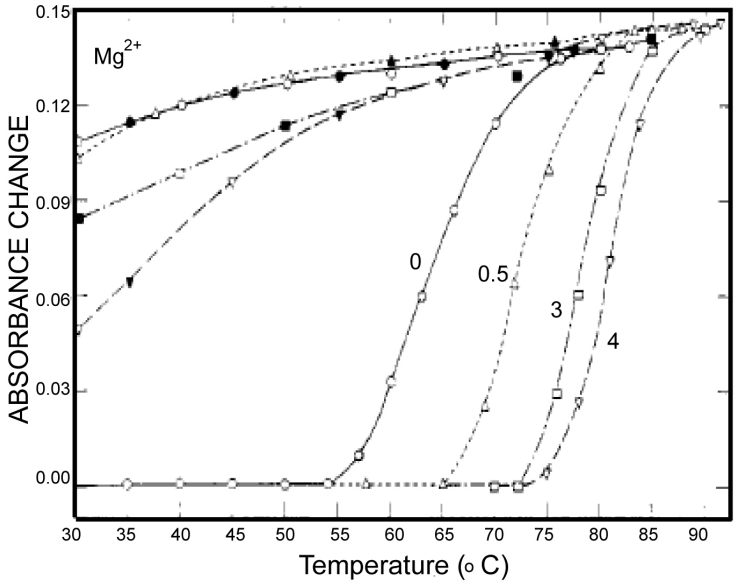

Fig. 2.11: Melting behavior of solutions containing $5x10^{-5}$ M DNA, $5x10^{-3}$ M sodium nitrate, and magnesium nitrate in the following mole ratios to DNA: 0; 0.5; 2; 4.

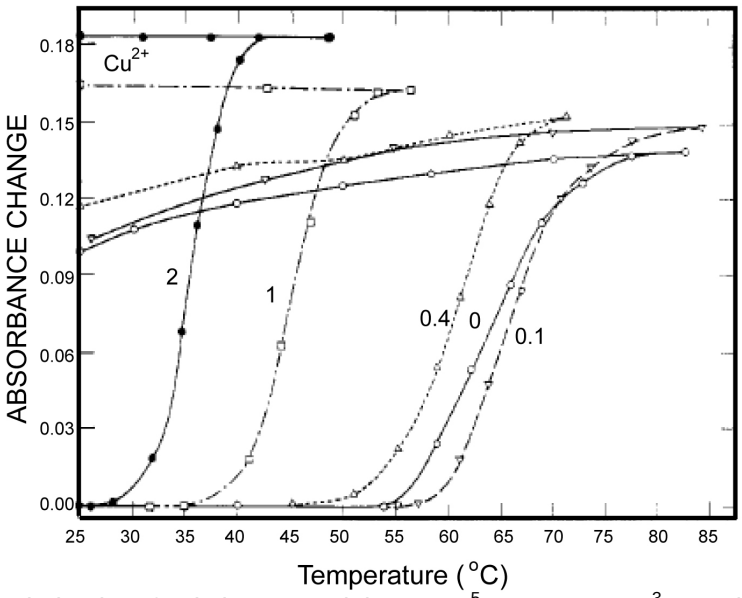

Fig. 2.12: Melting behavior of solutions containing $5x10^{-5}$ M DNA, $5x10^{-3}$ M sodium nitrate, and copper nitrate in the following mole ratios to DNA: 0; 0.1; 0.4; 1; 2. The maximum Tm occurs at only 0.1M Cu^{2+} /DNA. Ass salt containing Cu^{2+} will decrease the melting temperature of duplex DNA.

$$\frac{1}{T_M(Na^+)} = \frac{1}{T_M(1M\ Na^+)} + \left[(4.29 f_{GC} - 3.95)\ln[Na^+] + 0.940\ln^2[Na^+]\right]\times 10^{-5} \quad \text{(eq. 2.3)}$$

and for divalent (Mg^{2+}) ions (Owczarzy, R. et al., [2.20]),

$$\frac{1}{T_M(Mg^{++})} = \frac{1}{T_M(1M\ Na^+)} + \left[\begin{array}{l} a - 0.911\ln[Mg^{++}] + f_{GC}\times\left(6.26 + d\ln[Mg^{++}]\right) \\ + \dfrac{1}{2(N_{bp}-1)}\times\left[-48.2 + 52.5\ln[Mg^{++}] + g\ln^2[Mg^{++}]\right] \end{array}\right]\times 10^{-5}$$

(eq. 2.4)

where f_{GC} is the fraction of GC base pairs and N_{bp} is the number of base pairs. The monovalent ion or the divalent ion correction equations are used depending on the following ratio R of [Mg^{2+}] and [Na^+].

$$R = \frac{\sqrt{[Mg^{++}]}}{[Na^+]} \quad \text{(eq. 2.5)}$$

If R < 0.22, the mono-valent ion correction is employed otherwise the divalent correction is used, including the case when $[Na^+]$ is zero. If R value is in the range from 0.22 to 6.0, the divalent ion correction is applied using a, d, and g coefficients that varies with Na^+ concentration. These coefficients are constant for higher values of R (the second column of the following table).

Table 2.3: Variables Adjusted to Account for Monovalent Effects

Variables adjusted to account for monovalent effects	Constants
$a = 3.92 \times \left(0.843 - 0.352\sqrt{[Na^+]} \times \ln[Na^+]\right)$	$a = 3.92$
$d = 1.42 \times \left(1.279 - 4.03 \times 10^{-3} \ln[Na^+] - 8.03 \times 10^{-3} \ln^2[Na^+]\right)$	$d = 1.42$
$g = 8.31 \times \left(0.486 - 0.258 \ln[Na^+] + 5.25 \times 10^{-3} \ln^3[Na^+]\right)$	$g = 8.31$

Deoxynucleoside triphosphates (dNTPs) affects the concentration of free divalent ions that enters into the above correction functions and the calaculations of the ratio R. Free magnesium concentration is predicted from total Mg^{2+} concentration, $[tMg^{2+}]$, using relationships developed from the equilibrium binding constant of Mg++ and dNTPs.

$$[rMg^{++}] = \frac{-\left(K_a \times [dNTP] - K_a \times [tMg^{++}] + 1\right) + \sqrt{D}}{2 \times K_a}$$

$$\text{where } D = \left(K_a \times [dNTP] - K_a \times [tMg^{++}] + 1\right)^2 + 4 \times K_a \times [tMg^{++}] \qquad \text{(eq. 2.6)}$$

The association constant K_a is about 3x104 in biological buffers. These new parameters and methods are implemented within the OligoAnalyzer and improve the melting temperature accuracy, especially for standard PCR conditions. In the current version, however, these new parameters (Mg++ and dNTP concentrations) are defaulted to 0.0 mM, so that predicted melting temperature are identical to values predicted by the previous version of the OligoAnalyzer. To take advantage of these new, more accurate methods, the values for $[Mg^{2+}]$ and [dNTP] concentrations must be specified.

2.1.4 Melting Temperature of DNA Linked Nanoparticles

DNA-functionalized gold colloids hold promise for applications in nanotechnology and biotechnology and have been widely used to develop highly sensitive biosensors. The thermodynamics of individual DNA hybridization event on DNA-Au is central to these applications. Mirkin and Schatz et al. [2.22] have shown that DNA-Au aggregates are more stable than the isolated duplexes, and a detailed study has revealed the importance of cooperatively, probe density on the nanoparticle surface, gold nanoparticle size, salt concentration, and interparticle distance.

Compare to the DNA hybridized in free solution, the melting temperature of DNA linked nanoparticle, the melting temperature of the DNA duplex attached to gold particle surfaces is different from that of free DNA. Some research reports show that the Tm of DNA linked GNPs is lower than free DNA [2.23] and other reports show opposite way [2.22]. But there is one thing they agree with each other, the melting transition is much sharper for DNA linked GNP compares to free DAN in solution as shown at Fig. 2.13.

The factors that affect the melting temperature of DNA linked GNP (hybridize in solution) compare to DNA hybridize in free solution might include: (a) the size of the nanoparticles, (b) distance between nanoparticles, (c) the surface modification density of the oligonucleotides on the nanoparticles, (d) the dielectric constant of the surrounding medium.

However, compare all those experiments, we found out that all the experiment setting are different in (1) the length of oligonucleotides modified on GNP surface, (b) the ion concentration of the electrolyte. Which means the interaction forces between each case is different. The melting transition of DNA is the balance between repelling force from negatively-charged DNA phosphate back bone and attraction force provided by hydrogen bonding between base pairs. While GNP involved, the interaction force between GNPs should be taken into consideration. The favorite distance between two GNPs is decided by the interaction between electrical double layers which is strongly related to ion concentration. When DNA linked GNPs are forced to come closer than the favorite separation distance by hybridization, the extra

repelling force provided by GNPs will cause the Tm to be shifted lower. In the contrast, DNA linked GNP can have higher Tm compares to free DNA when the separation caused by DNA molecular is longer than favorite separation distance.

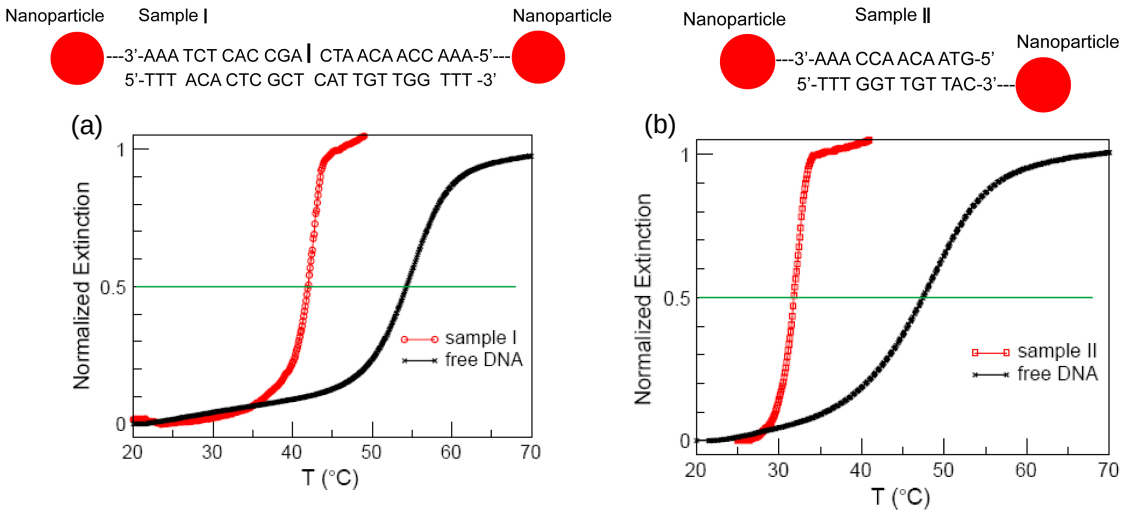

Fig. 2.13: Melting curves of DNA modified gold nanoparticles. (a) with a DNA linker (sample I), and (b) via direct hybridization of complementary surface-attached DNA (sample II). The corresponding free DNA melting curves are also shown. DNA linked GNPs shows lower melting temperature and sharper transition curve compares to free DNA. The shorter distance between nanoparticles, the greater difference of Tm compare to free DNA. [2.23]

Also, when one of the DNA modified nanoparticle A is fixed on a solid substrate, and then other DNA modified nanoparticle B from solution hybridize with A (fixed on the solid surface), the melting temperature is also different compares to the hybridizing in solution phase because the interaction between solid substrate and DNA modified GNP in the solution is needed to be taken into consideration, too.

2.1.4.1 Surface Probe Density Effect

When gold nanoparticle (GNP) surface is modified by ssDNA chemically (not by physical absorption), the stability of DNA modified GNP increasing with increasing density of surface modification. This is important for DNA modified GNP applications due to the high salt

concentration required during DNA hybridization process (>0.1M). Mirkin et al. [2.22] had explored the melting behavior of DNA modified GNP with different surface modification density. They observed that the Tm of DNA linked GNP will slightly increasing when surface modification density increasing. They contribute this Tm increasing to the increasing of the interaction between DNA modified GNPs due to the high surface DNA modification density (ssDNA can still have some interaction even when they are not complementary with each other).

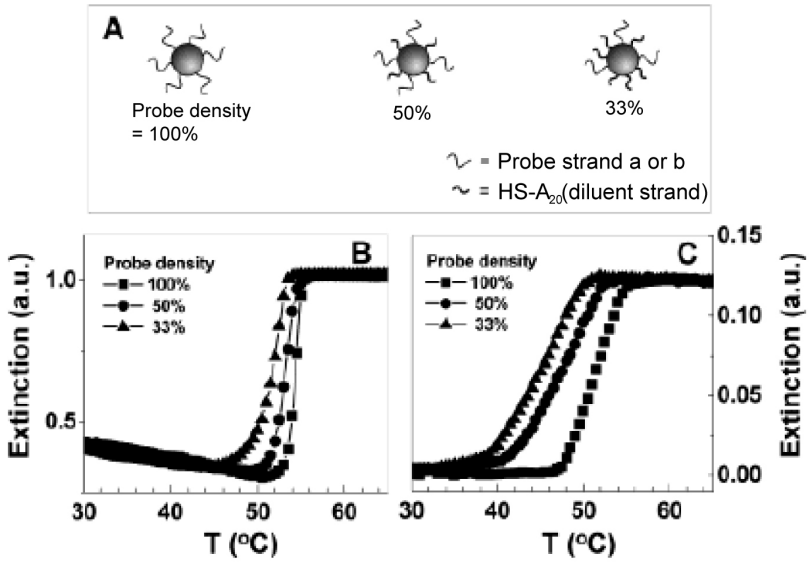

Fig. 2.14: The effect of probe oligonucleotide density on the Au nanoparticle surface on the melting properties (A) scheme, (B) in solution with aggregates, and (C) in the glass surface system (Au 13 nm particles were used; target concentration) 60 nM, 0.3 M NaCl, pH 7 PBS buffer, [2.22]

The melting analyses show that the Tm is directly proportional to the probe surface density when the nanoparticle and target concentrations are kept constant (Fig. 2.14 (B)). Also, a slight broadening of the melting transition was observed as the probe density decreased from 100% to 33% (Fig. 2.14 (C)). Also, similar behavior for nanoparticle probes with different surface probe densities that were hybridized to glass substrate surfaces were observed qualitatively.

2.1.4.2 Nanoparticle Size Effect

The relationship between melting temperature and different sizes of DNA modified GNPs is also investigated [2.22]. Fig. 2.15 (B) shows the melting curve of DNA linked GNP in the solution phase with different size GNPs. When the particle size increased, Tm reduced slightly and the melting curve became sharper compared with small GNP size. This means the interaction between GNPs (modified by DNA) become more significant with the larger size of GNP.

The sharper melting profiles observed for these DNA linked GNP might due to the creating multiple equivalent sites for cooperative dehybridization [2.22] or due to the interactions between GNPs increasing while GNPs are pulled close to each other. Science the GNP surface is heavily functionalized with oligo-nucleotides (~10^{13} strands/cm^2), which increasing the chance of forming multiple equivalent sites for cooperative dehybridization with larger particle size. Also, DNA linked GNPs again have sharper melting transition in the liquid phase compares to the heterogeneous phase (Fig. 2.15 (A)).

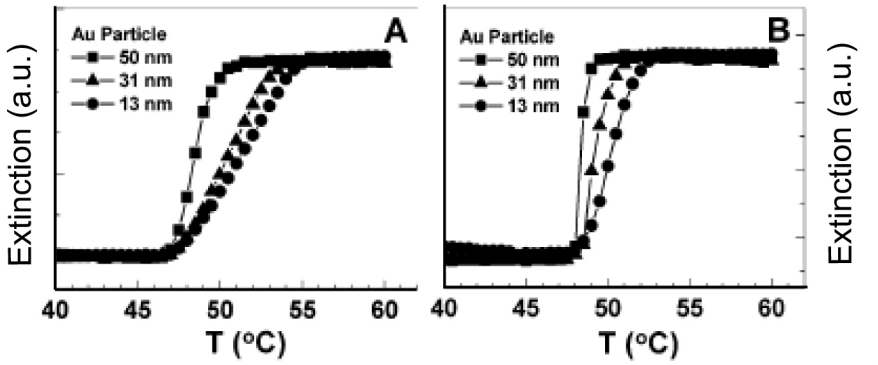

Fig. 2.15: The effect of nanoparticle size on the melting of (A) particle probes off of glass substrates (250-300 um beads) and (B) particle aggregates in the solution system. [2.22]

2.1.4.3 Salt Concentration Effect

The melting analyses show that salt concentration substantially affects the Tm of the DNA linked nanoparticles. As the salt concentration increased, the nanoparticle and target concentration constant, the Tm increased.

However, Mirkin et al. also observe that once the salt concentration is decreased to less than 0.05 M in their experiment, the Au nanoparticle probes do not hybridize at room temperature in the presence of target (60 nM), but complementary oligonucleotides (in the absence of nanoparticles) having the same sequence will hybridize at 0.05 M NaCl or less. This result might be due to the extra repelling force from nanoparticles reduce the stability of DNA linked GNP and therefore require higher salt concentration to stabilize the DNA duplex.

The salt concentration affect Tm of free DNA hybridize in free solution and DNA linked GNP is similar. The higher salt concentration in the environment, the more stable of DNA duplex and results in the higher thermal energy required to escape from the attraction force, which means, higher melting temperature.

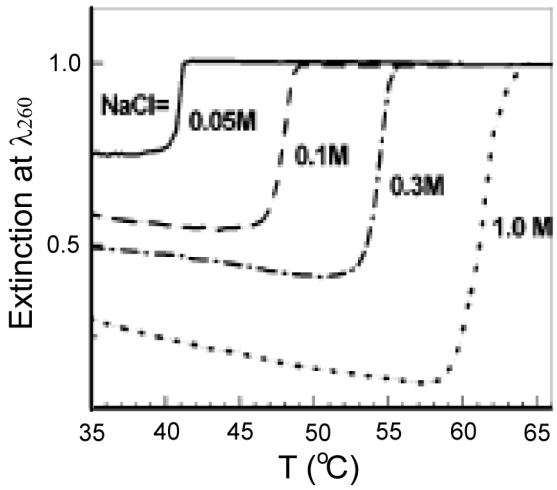

Fig. 2.16: The effect of salt concentration on the melting of nanoparticle aggregates in the solution system. [2.22]

2.1.4.4 Interparticle Distance Effect

As nanoparticles are linked together via DNA hybridization, electromagnetic coupling between the nanoparticles results in significant damping of their surface plasmon resonances and a distinct color change from red to purple. Interparticle distance also influences van der

Waals and electrostatic forces between the particles, affecting duplex DNA stability and hybridization/dehybridization properties.

The melting analyses show that the Tm increases with the length of spacer (or the interparticle distance) (Fig. 2.17 (a)). Which means, the longer interparticle distance, the more stable of DNA linked nanoparticles.

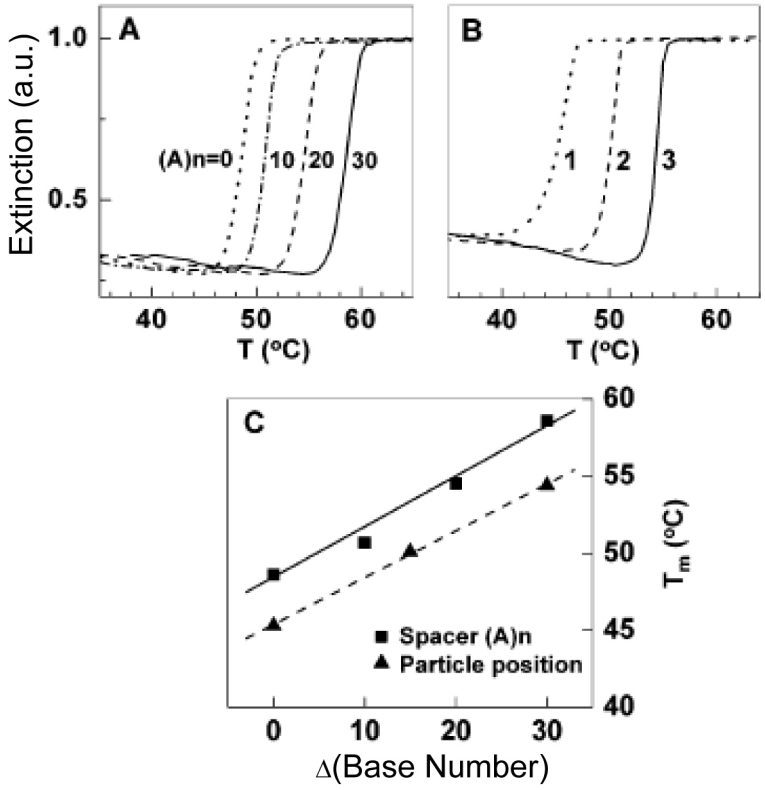

Fig. 2.17: The effect of interparticle distance on the melting properties of nanoparticle aggregates, (A) the length of the poly (A) n spacer (tail-to-tail hybridization mode), (B) hybridization modes of particles: 1, head-to-head; 2, head-to-tail; 3, tail-to-tail (see Scheme 2). (C) The plots of Tm as a function of changing spacer base number (solid line) and particle probe position (dash line) as a function of base separation (see Scheme 3). Au 13 nm particles were used; target concentration) 60 nM, 0.3 M NaCl PBS buffer. [2.22]

The melting behavior is the process of how molecules gain energy to escape from the attraction force. For free DNA hybridize in free solution, ssDNA is repelling with each other due to the negatively charged back bone but is attracted with each other by the hydrogen bonding between base pairs. However, compare with DNA linked GNP; the interaction force comes from

not only DNA molecules, but also from nanoparticles. The interaction force comes from nanoparticles including interactions between electrical double layers and van der Waals force.

In our DNA detecting device, the I-V signal is provided by whether DNA modified nanoparticle is linked through DNA hybridization or not, not DNA hybridization event itself. In other word, Instead of melting temperature of free ssDNA in free solution, the melting temperature of DNA linked GNP is the temperature we need.

The advantage of DNA modified nanoparticle is that the melting transition is a much sharper curve compares to free DNA in free solution. This means, if we choose the proper hybridization temperature, the difference between complementary and mis-matched DNA of DNA modified GNP should be more significant compares to free DNA.

Fig. 2.18 is the sketch to explain why we prefer a sharp melting transition behavior. When the melting transition is broad, the overlap between complementary and mismatched DNA increasing, therefore, in order to have high hybridization percentage for T-ssDNA, the hybridization temperature we chose also allows certain percentage of mismatched DNA hybridize(Fig. 2.18(a)). But with sharp melting transition behavior, both high sensitivity and good selectivity can be satisfied at the same time.

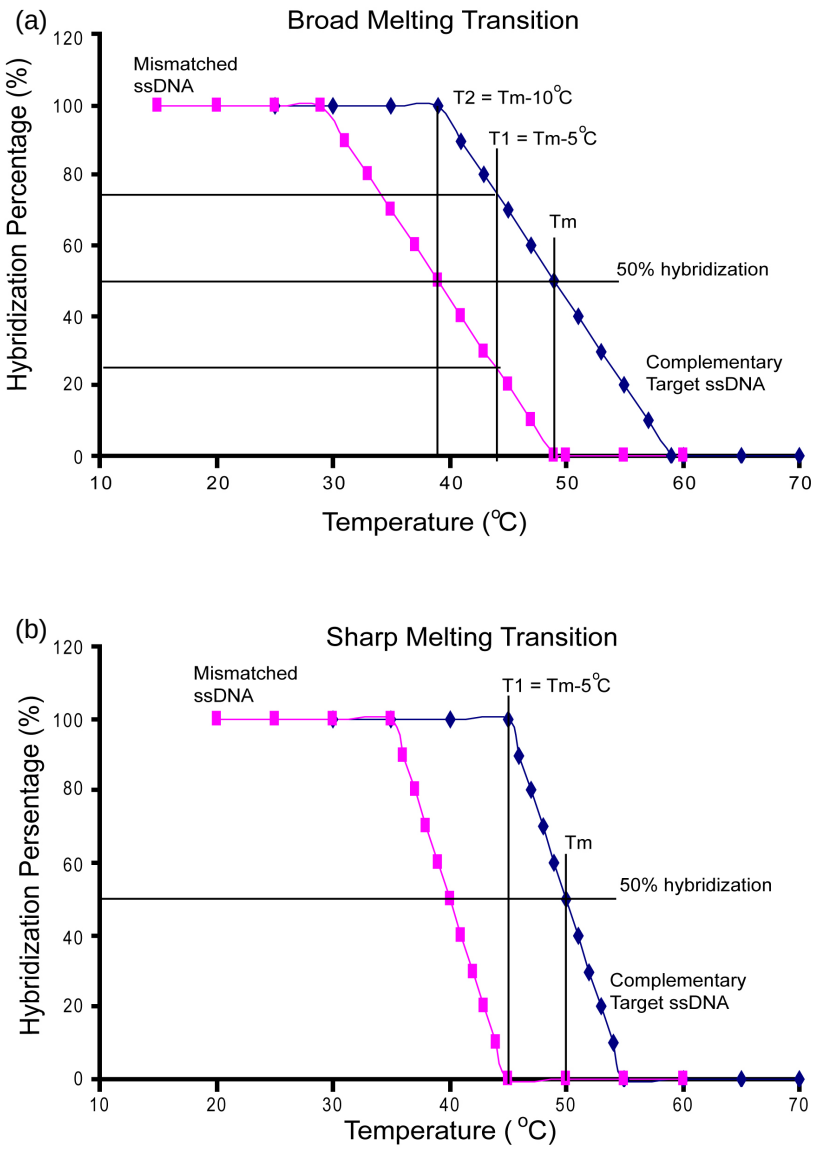

Fig. 2.18: Sketch of broad and sharp melting transition for complementary and mismatched DNA (a) Broad melting transition: difficult to have high hybridization % for T-ssDNA and low hybridization % for mismatched ssDNA at the same time. (b) Sharp melting transition: can have high hybridization % for T-ssDNA and low hybridization % for mismatched ssDNA at same time (T1).

2.2 DNA Hybridization

DNA hybridization is a process of two single-stranded DNA combining into a single molecule (double-stranded DNA) by hydrogen bonding between base pairs. This process also called annealing process. Two perfect complementary single-stranded DNA (ssDNA) will bind to each other readily in a bulk solution with higher thermal stability compares to mis-matched DNA. When mis-matched DNA hybridized, the mis-matched part will cause the distortion of the DNA chain and hence reduced the thermal stability.

DNA hybridization or melting process is a thermal equilibrium state between the repelling force generated from ionized phosphate group in DNA backbone and attracting force generated from hydrogen bonding formation between base pairs. DNA hybridization or melting temperature can be greatly affected by (1) DNA structure (length, sequence, G-C component), (2) ion concentration, (3) different kinds of ions.

The model of how two ssDNA hybridize with each other includes (1) a slow step of at least 3 complementary base pair from each ssDNA collides with each other. (2) a rapid zipping up process of double helix formation.

2.2.1 Hybridization efficiency and sensitivity in liquid phase

The process of single strand DNA hybridization in bulk solution is a specific interaction between two molecules and occurs homogeneously in solution. However, in the case of surface hybridization, the process may be treated as a specific adsorption process. Hybridization efficiency is a measure of the proportion of probe oligo-nucleotides that successfully hybridize to the complementary strand under optimum hybridization conditions at the surface. The hybridization rate describes the flux of target strand to the surface to facilitate hybridization.

The equilibrium constant for the hybridization process for two complementary single strand oligo-nucleotides is given by:

$$\text{Probe} + \text{Target} \rightarrow \text{Hybrid}$$

$$K = \frac{[Hybride]}{[\mathrm{Pr}obe] * [T\,\mathrm{arg}et]} \qquad \text{(eq. 2.7)}$$

Where K is the equilibrium constant. Experimental hybridization data may also be expressed as a ratio, v, of hybridized to single stranded probe oligo-nucleotide:

$$\nu = \frac{[Hybride]}{[\mathrm{Pr}obe] + [T\,\mathrm{arg}et]} \qquad \text{(eq. 2.8)}$$

2.2.2 Heterogeneous Hybridization (Liquid-Solid phase Hybridization)

Heterogeneous hybridization mechanism become more and more important due to the need of probe ssDNA immobilized on a solid substrate first and hybridizes with target ssDNA for DNA detection process. Heterogeneous hybridization mechanism is different from homogeneous DNA hybridization in the solution phase due to the target ssDNA need to reach the probe ssDNA through a diffusion process.

The modeling of the hybridization kinetics on the surface of DNA biochips is still in its infancy, and the literature on the measurement of the hybridization kinetics is diffuse and even contradictive. Some authors claim that the process is fully reaction-rate limited (Chan, Graves, & McKenzie, 1995; Jensen, Orum, Nielsen, & Norden, 1997), whereas others describe it as a diffusion-controlled process (Vontel, Ramakrishnan, & Sadana, 2000; Christensen, Jacobsen, Rajwanshi, Wengel, & Koch, 2001).

The existence of such strongly divergent observations and conclusions might be due to the fact that most of the experiments are undertaken on widely differing time scales and under totally different conditions (excess probe or not, different fluid layer heights, etc.).

2.2.2.1 Langmuir Model

The basic model of heterogeneous reaction is first order Langmuir model.

Whenever a gas is in contact with a solid, there will be an equilibrium established between the molecules in the gas/liquid phase and the corresponding adsorbed species

(molecules or atoms) which are bound to the surface of the solid. The Langmuir isotherm was developed by Irving Langmuir in 1916 to describe the dependence of the surface coverage of an adsorbed gas on the pressure of the gas above the surface at a fixed temperature.

The basic idea behind the Langmuir model is the coverage of the surface by a mono-molecularic layer. The model approach also assumes that only one gas is being adsorbed. Thus, at constant temperature a part of the surface will be covered with the adsorbed molecule another part not. Between the free gas and the adsorbed gas, a dynamic equilibrium will exist. Per time unit there will be as much molecules adsorbing as there will be desorbing. The rate of adsorption will be proportional with the equilibrium pressure of the gas and the free surface.

In mathematical terms we derive the following model.

q = molecule * = adsorption site q* = adsorbed molecule

Adsorption: $q + * \xrightarrow{k1} q^*$; rate of adsorption: $r_{ads} = k_1[q][*]$

Desorption: $q^* \xrightarrow{k2} q + *$; rate of desorption: $r_{des} = k_2[q^*]$

Therefore, adsorption rate equals to desorption rate when equilibrium is achieved.

$$r_{ads} = r_{des} = k_1[q][*] = k_2[q^*] \rightarrow \frac{[*]}{[q^*]} = \frac{k_2}{k_1[q]} = \frac{1}{K[q]} \quad ; \quad (K = \frac{k_1}{k_2})$$

(eq. 2.9)

2.2.2.2 Kinetics of DNA/DNA Hybridization with Langmuir Model

The Langmuir model was used to determine the association rate constant (K_{on}), the dissociation rate constant (K_{off}) and the affinity rate constant (K_A), for perfect matched DNA hybridization (Delan Li et al., 2007). [2.26] In their experiment setting, the thiolated DNA was assembled on the Au electrode surface first, and then followed by adsorption of a diluent of

16MHA. The diluent serves the purpose of displacing any weakly adsorbed DNA bases off the Au electrode surface. As a result, the probe DNA was projected out into the sample solution and target DNA nonspecifically adsorbed onto the interface could be resisted. [2.27]

The surface density of probe DNA in their study was estimated to be 3.79–6.78 pmol/cm^2 (2.28x10^{12}–4.08x10^{12} probe molecules/cm^2). Then the area occupied by each DNA strand is approximately from 44 nm^2 to 25 nm^2. With this experiment setting, the ssDNA strands have weak interaction with each other considering the 19-mer DNA probes are just less than 7 nm in length (DNA base distance ~ 0.34 nm).[2.28]

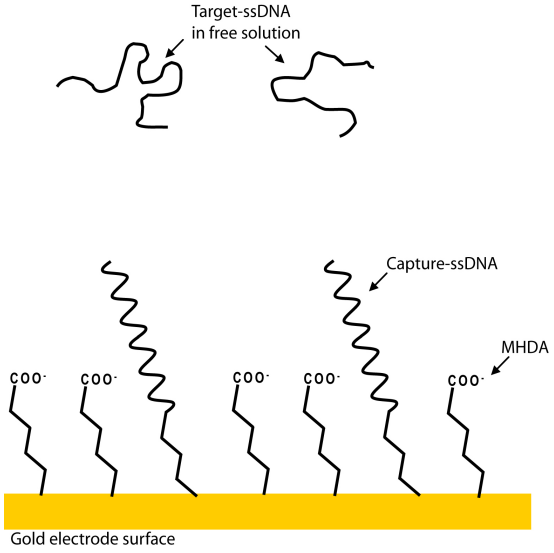

Fig. 2.19: Sketch of Langmuir model for DNA hybridization.

From their measurement by the electrochemical impedance spectroscopy, the adsorption rate constant and desorption rate constant was obtained:

K_{off} = 3.36x 10^{-3} min^{-1}

K_{on} = 4.93x10^5 M^{-1}min^{-1}

The affinity constant for complementary DNA/DNA complex was deduced.

$K_A = K_{on}/K_{off}$ = 1.47 · 10^8 M^{-1}, [2.28]

2.2.2.3 Kinetics of DNA/DNA Hybridization on microarray surfaces

There are all types of hybridizations which occur on a microarray surface: single-stranded DNA with single stranded DNA, DNA with RNA, RNA with RNA, proteins with enzymes, and antibodies with antigens.

Generally, the entity attached to the microarray surface is referred to as a probe and the other half of the hybridization process in solution on the microarray surface is the target. Hybridization between a probe and target forms a number of chemical bonds, thus hybridization is chemi-sorption. Generally, one target bonds with one probe, so first-order Langmuir kinetics is expected. [2.29]

$$P + T \rightarrow H \qquad \text{(eq. 2.10)}$$

P: the number of probes on the surface;
T: concentration of target in solution;
H: number of hybrids that form

If there are only limited number of probes on the surface and excess target in solution (T >> P), the maximum number of hybrids that can form will be equal to the original number of probes. So at any particular time, the number of hybrids is equal to the original number of probes minus the probes that are not hybridized.

$$H_t = P_0 - P_t \qquad \text{(eq. 2.11)}$$

H_t: number of hybrids at any time;
P_0: the original number of probes;
P_t: the number of probes that have not yet been hybridized.

If the above equation is divided by P0, then it becomes:

$$\varphi_H = 1 - \varphi_P \qquad \text{(eq. 2.12)}$$

Where $\varphi_H = H_t/P_o$; $\varphi_P = P_t/P_0$

Assuming no hybrids were present initially.

$$\frac{d\varphi_H}{dt} = k \cdot \varphi_P \cdot T = k \cdot (1 - \varphi_H) \cdot T \qquad \text{(eq. 2.13)}$$

k is the rate constant. If the amount of target, T is much greater than the number of probes, then T can be considered a constant and the solution of the above rate equation is:

$$\varphi_H = 1 - e^{-k \cdot T \cdot t} \quad \text{; t is time} \qquad \text{(eq. 2.14)}$$

Again, there are two assumptions for the equations above, a) the hybridization is a chemisorption process, which means no target ssDNA can goes back to the solution. b) the concentration of target ssDNA is much larger than the number of probe ssDNA. However, assumption b) might be true for certain hybridization environment, but reverse reaction need to be taken into account.

The bound hybrid may dissociate, especially those with mismatches, so a dissociative process should also be considered.

$$P + T \leftrightarrow H$$

$$r_f = k_f [P] [T] \; ; \; r_r = k_r [H] \qquad \text{(eq. 2.15)}$$

$$\frac{d\varphi_H}{dt} = k_f \cdot (1 - \varphi_H) \cdot T - k_r \cdot \varphi_H \qquad \text{(eq. 2.16)}$$

Where T is considered as a constant (T >> P), K_f is forward rate constant; K_r: reverse rate constant. And the first order Langmuir adsorptions model becomes: [2.29]

$$\varphi_H = \frac{k_f \cdot T - e^{-(k_f \cdot T + k_r) \cdot t}}{k_f \cdot T + k_r} \qquad \text{(eq. 2.17)}$$

2.2.2.4 Rate Constant “k” for Heterogeneous Hybridization

As it is well known in the field of chemical engineering that the thickness of the diffusion boundary layer in a heterogeneous reaction–diffusion problem continuously grows according to $t^{1/2}$ (Henry, Wilkins, Sun, & Kelso, 1999). Whereas other studies (Sadana & Vo-Dinh, 1998; Vontel etal., 2000) have clearly demonstrated that the use of a single kinetic rate constant k does not hold for the heterogeneous conditions on a biochip. They observed that k varies during the course of the hybridization process and should best be represented as

$$k = k' t^{-p} \qquad \text{(eq. 2.18)}$$

p: coefficient which is in turn also a function of time

For intermediate times, p appears to be given by (Sadana & Vo-Dinh, 1998; Vontel et al., 2000); p = ½.

It is normal to expect that on the short time scale the binding response will be dominated by the slow binding probability, whereas in the long time range, the slow diffusive DNA supply will become the rate limiting step.

CHAPTER 3

LITERATURE RESEARCH OF DNA BIOSENSOR

A chemical sensor is defined as a device which response to a particular analyte in a selective way through a chemical reaction and can be used for the qualitative or quantitative determination of this analyte [3.1]. Same as to the biosensor, a biosensor is a self-contained integrated receptor-transducer device, which is capable of providing quantitative or semi-quantitative analytical information using a biological recognition element [3.2].

Optical transducers include vibrational (IR, Raman), luminescence (Fluorescence, chemiluminescence) and Surface Plasmon Resonance (SPR).

Piezoelectric or mass change transducers include surface acoustic wave (SAW) and quartz crystal microbalance (QCM). This kind of transducer allows a binding event to be converted into a measurable signal such as resonance frequency shift for piezoelectric crystal oscillation or surface acoustic wave.

Electrochemical biosensors combine the analytical power of electrochemical techniques with the specificity biological recognition process. The bio-specific reagent is either immobilized or retained at a suitable electrode, which converts the biological recognition event into a quantitative amperometric or potentiometric response and the electrical signal is relates to the concentration of analytes. Electrochemical transducers include potentiometric, conductimetric and amperometric. Potentiometric biosensor monitors potentials at the working electrode with respect to the reference electrode while the analyte concentration changing. The charge accumulates on the electrode created by selective binding event in the electrode surface [3.3]. Conductimetric biosensor measure the effect of biological and chemical changes upon the conductance between a pair of metal electrodes. Amperometric biosensors measure changes in

the current on the working electrode due to the direct oxidation/reduction of products of a biochemical reaction in direct or indirect measuring systems.

The basic elements of bio-sensing are: (1) a powerful biomolecular recognition capability of bio-receptors such as antibody-antigen, DNA and enzymes. (2) The transducer that translates the interactions between biomolecular recognition processes into detectable signals.

This is to say, the limitation of a biosensor comes from (1) the limitation of transducers (how many recognition event required for equipment to get the readable signal), (2) the limitation of biomolecular recognition methods (the experiment environment or condition).

DNA detection is one of the most important analytical tools in molecular biology, disease diagnosis, forensic medicine, food science, and medicine development. We can classify DNA biosensor into two basic types: (1) Direct detection and (2) Indirect detection.

Direct detection means direct detect of physical, chemical, optical and electrochemical properties change caused by hybridization event. Direct detection includes surface Plasmon Resonance, UV absorption of 260nm, mass change, and dielectric or capacitance change,

Indirect detection means instead of directly detect DNA hybridization events; we detect the signal generated by a label or signal amplifier which modified directly on Target ssDNA or probes.

There are different kinds of labels which are commonly used in DNA detection including fluorescence label, Magnetic label, enzyme, Quantum dot, Dye and nanoparticles.

Also, there are other mechanism can be applied to assist the detection and becomes a very popular actuator for improving the detection limits such as microfluidic system (increase hybridization efficiency), PCR (increase the amount of target DNA), silver enhancement (increase the signal generated from DNA hybridization).

3.1 Direct Detection

3.1.1 Surface Plasmon Resonance (Optical)

The excitation of surface plasmon by light is denoted as a surface plasmon resonance (SPR). This phenomenon is the basis of many standard tools for measuring adsorption of material onto planar metal (typically gold and silver) surfaces or onto the surface of metal nanoparticles. It is behind many color based biosensor applications and different lab-on-a-chip sensors. SPR is surface electromagnetic wave that propagates in a direction parallel to the metal/dielectric (or metal/vacuum) interface. Since the surface plasma wave (SPW) is on the boundary of the metal and the external medium (air or water for example), these oscillations are very sensitive to any change of this boundary, such as the adsorption of molecules to the metal surface. The propagation constant of an SPW, β, can be expressed as [3.5]:

$$\beta = \frac{\omega}{c}\sqrt{\frac{\varepsilon_M \varepsilon_D}{\varepsilon_M + \varepsilon_D}} \qquad \text{(eq. 3.1)}$$

ω is the angular frequency, c is the speed of light in vacuum, and ε_D and ε_M are dielectric functions of the dielectric and metal, respectively.

Perturbation theory [3.5] suggests that if the binding occurs within the whole depth of the SPW field the binding-induced refractive index change, Δn, produces a change in the real part of the propagation constant, Δβ, which is directly proportional to the refractive index change:

$$\mathrm{Re}\{\Delta\beta\} \cong k\Delta n \qquad \text{(eq. 3.2)}$$

where k denotes the free-space wavenumber [3.6]. If the refractive index change is caused by a binding event occurring within a distance from the surface d, much smaller than the penetration depth of the SPW, the corresponding change in the real part of the propagation constant can be expressed as follows:

$$\mathrm{Re}\{\Delta\beta\} \cong \frac{2n_s n_f k^2 d}{\sqrt{|\mathrm{Re}\{\varepsilon_m\}|}} \Delta n = Fk\Delta n \qquad \text{(eq. 3.3)}$$

where n_f and n_s denote the refractive index of the biolayer and the refractive index of the background dielectric medium (sample), respectively. The binding-induced change in the propagation constant of the SPW is proportional to the refractive index change and the depth of the area within which the change occurs. The factor F (F<1) accounts for the fact that the interaction occurring within a thin layer is probed by only a fraction of the field of the SPW.

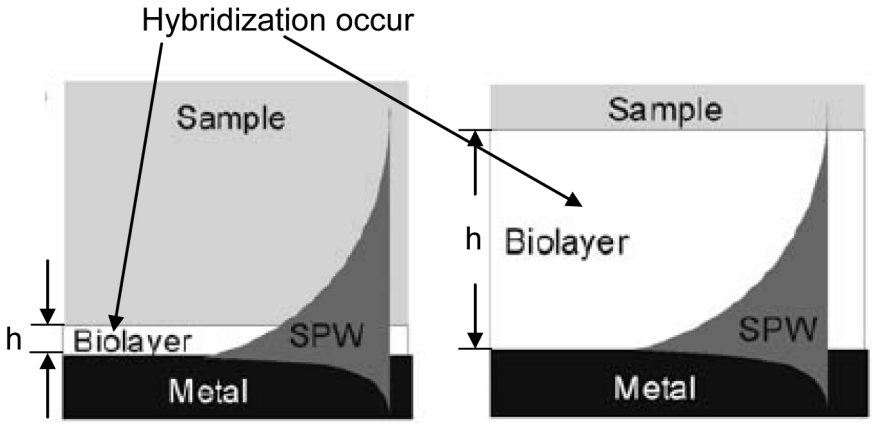

Fig. 3.1: Surface plasmon-polariton probing: (a) biomolecular interaction occurring within a short distance from metal surface, and (b) biomolecular interaction occurring within the whole extent of the field of a SPW. [3.4]

SPR can be applied in DNA detection base on detection of the electromagnetic wave change before/after target ssDNA hybridize with probes immobilized on the detection surface. Surface plasmon resonance (SPR) biosensors are optical sensors exploiting special electromagnetic waves– surface plasmon-polaritons – to probe interactions between an analyte in solution and a biomolecular recognition element immobilized on the SPR sensor surface.

The propagation constant, β, of the SPW is extremely sensitive to changes in the refractive index of the dielectric. This property of SPW is the underlying physical principle of affinity SPR biosensors – biomolecular recognition elements on the surface of metal recognize

and capture analyte present in a liquid sample producing a local increase in the refractive index at the metal surface.

The refractive index increase caused by target-probe hybridization gives rise to an increase in the propagation constant of SPW propagating along the metal surface which can be accurately measured by optical means. The magnitude of the change in the propagation constant of an SPW depends on the refractive index change.

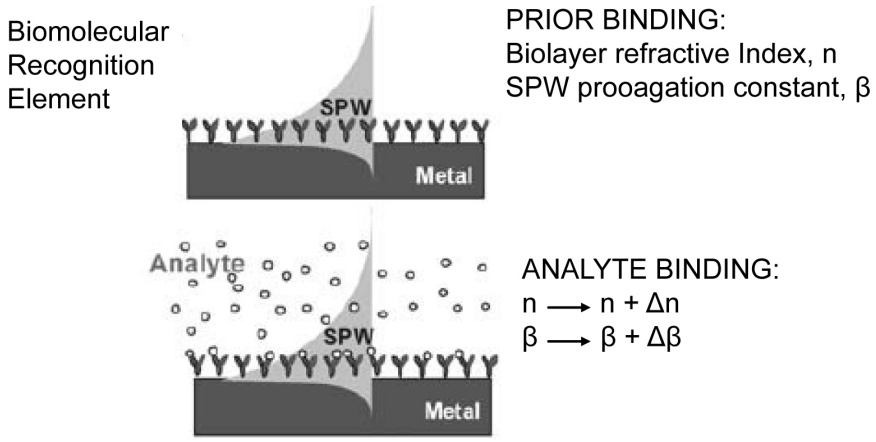

Fig. 3.2: Principle of SPR biosensing.[3.4]

The interaction of a light wave with an SPW can alter light's characteristics such as amplitude, phase, polarization and spectral distribution. Changes in these characteristics can be correlated with changes in the propagation constant of the SPW. Therefore, binding-induced changes in the refractive index at the sensor surface and, consequently, the propagation constant of the SPW can be determined by measuring changes in one of these characteristics. Based on which characteristic is measured, SPR biosensors can be classified as angle, wavelength, intensity, phase, or polarization modulation-based sensors.

The main performance characteristics relevant for SPR biosensors include sensitivity, accuracy, precision, repeatability, and the lowest detection limit. Sensor sensitivity, S, is the ratio of the change in sensor output, P (e.g. angle of incidence, wavelength, intensity, phase, and polarization of light wave interacting with an SPW) to the change in measurement (e.g.

analyte concentration, c). SPR biosensor sensitivity can be decomposed into two components – sensitivity to refractive index changes produced by the binding of analyte to biomolecular recognition elements on the sensor surface SRI, and the efficiency E, with which the presence of analyte at a concentration c is converted into the change in the refractive index n:

$$S = \frac{\partial P}{\partial n}\frac{\partial n}{\partial c} = S_{\mathrm{RI}}E \qquad \text{(eq. 3.4)}$$

3.1.2 UV absorption of 260nm (Optical)

Ultraviolet (UV) light is electromagnetic radiation with a wavelength shorter than that of visible light, but longer than x-rays, in the range 10 nm to 400 nm, and energies from 3 eV to 124 eV. UVB (315 nm–280 nm) light can cause direct DNA damage. The radiation excites DNA molecules in skin cells, causing aberrant covalent bonds to form between adjacent cytosine bases, producing a dimer. When DNA polymerase comes along to replicate this strand of DNA, it reads the dimer as "AA" and not the original "CC". This causes the DNA replication mechanism to add a "TT" on the growing strand. This is a mutation, which can result in cancerous growths and is known as a "classical C-T mutation". The mutations that are caused by the direct DNA damage carry a UV signature mutation that is commonly seen in skin cancers.

However, UV light at wavelength 260nm is the characteristic absorption peak for DNA (for the base pair); therefore, this technique can be applied as a DNA detection method.

This method works quite well if you have a pure sample of nucleic acid not badly contaminated by proteins (absorbency maximum at 280nm). DNA purity can be performed by the ratio of absorbance measurements at A260/ A280.

An absorbency of one A260 unit per ml = 50 micrograms/ml DNA (50 x 10^{-6}/ml). However, the disadvantage of this method are that RNA and DNA both absorb, as does protein to some extent; you can not tell how large your DNA fragments are (bacterial chromosome and plasmid both being detected); you can not tell what sequences they may contain; and you need

a solution of 500 ng/ml (and perhaps 0.2 to 1 ml of that, depending on your curette) to reach an absorbency of 0.01, the usual limit of detection.

Each of the four nucleotide bases has a slightly different absorption spectrum, and the spectrum of DNA is the average of them (Fig. 3.3).

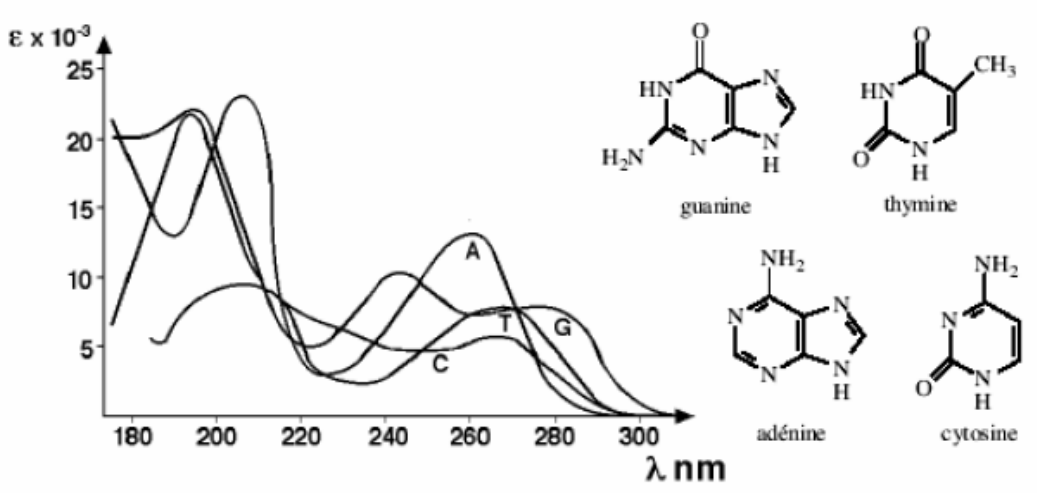

Fig. 3.3: Absorption spectra of DNA bases. Each base has unique absorption peak at range between 250 to 290nm. The absorption of DNA is the average of all those four base absorption peaks and results in 260nm absorption. [3.7]

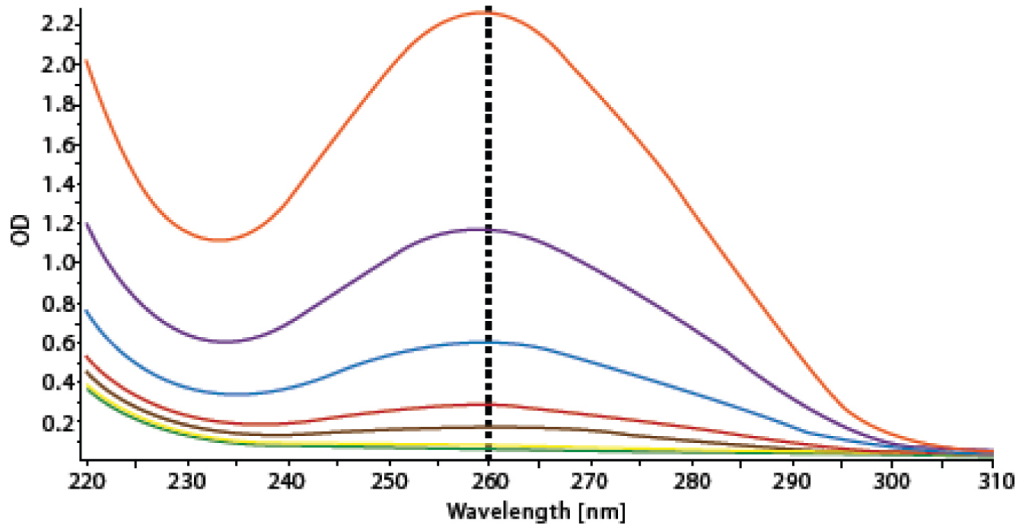

Fig. 3.4: Absorbance spectrum of different DNA concentrations. Detection range is between 220 and 310 nm and resolution was set at 1 nm.

Measurement of solution absorbance at 260 nm (A260) is one of the most common methods for nucleic acid detection due to the fact that nucleic acids have an absorption maximum at this UV wavelength. Although a relatively simple and fast method, A260 suffers from low sensitivity and interference from nucleotides and single-stranded nucleic acids.

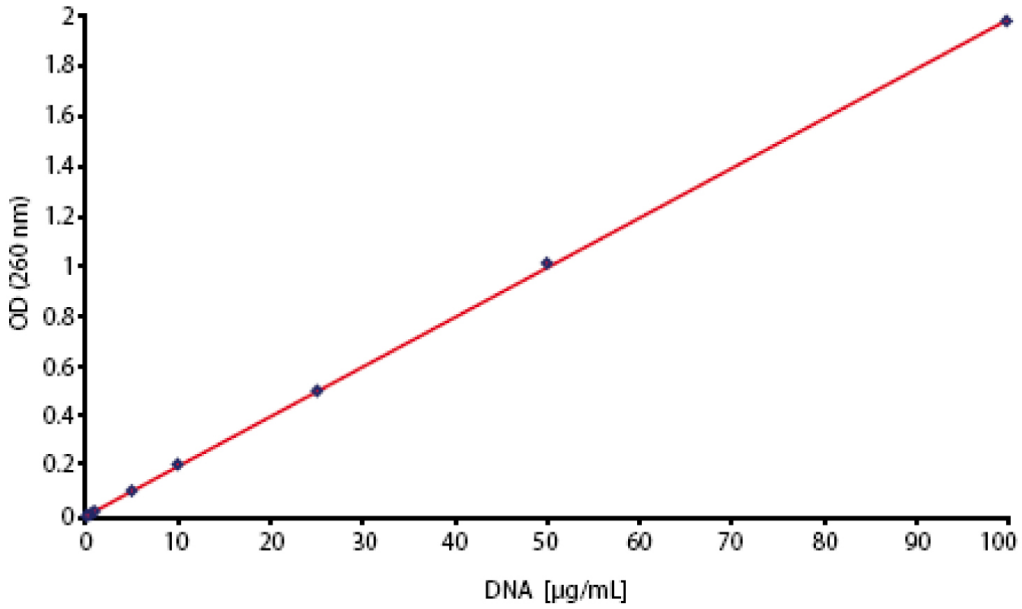

Fig. 3.5: Linear regression fit performed on the DNA standard curve in the concentration range from 0.1 to 100 µg/mL. [3.8]

3.1.3 Mass Change (mechanical)

3.1.3.1 Quartz Crystal Microbalance QCM

A quartz crystal microbalance (QCM) consists of a thin piezoelectric plate with electrodes deposited on both sides. Due to the piezo-effect, an AC voltage across the electrodes induces a shear deformation. The electro-mechanical coupling provides a way to detect the resonance.

A quartz crystal microbalance (QCM) measures a mass per unit area by measuring the change in frequency of a quartz crystal resonator. It is useful for monitoring the rate of deposition in thin film deposition systems under vacuum.

In liquid, it is highly effective at determining the affinity of molecules (proteins, in particular) to surfaces functionalized with recognition sites. It is easy to measure mass densities down to a level of below 1 μg/cm^2.

The QCM method is based on the Sauerbey equation; the mass change (Δm) is determined by the frequency variety of the QCM. Thus, the immobilization, hybridization, and hydrolytic cleavage of DNA can be monitored in situ from the change in QCM frequency [3.9-3.11]

$$\Delta f = \frac{-2\Delta m f_0^2}{A\sqrt{\rho_q \mu_q}} = -\frac{2f_0^2}{A\sqrt{\rho_q \mu_q}}\Delta m \qquad \text{(eq. 3.5)}$$

f_0 – Resonant frequency (Hz)
Δf – Frequency change (Hz)
Δm – Mass change (g)
A – Piezoelectrically active crystal area (Area between electrodes, cm^2)
ρ_q – Density of quartz
μ_q – Shear modulus of quartz for AT-cut crystal
v_q – Transverse wave velocity in quartz (m/s)

The Sauerbrey equation was developed for oscillation in air and only applies to rigid masses attached to the crystal. It has been shown that quartz crystal microbalance measurements can be performed in liquid, in which case a viscosity related decrease in the resonant frequency will be observed:

In the liquid, the differential equation describing the shear waves is the diffusion equation, having as solutions highly damped sinusoidal shear waves traveling in the z direction, away from the resonator. This shear wave can be written in terms of the instantaneous velocity of the liquid layer located at z, v(z,t)

$$v_x(z,t) = Ae^{-k(z-l)} \cos\left[k(z-l) - \omega t\right] \qquad \text{(eq. 3.6)}$$

A is the amplitude of the wave at the interface z = l. The characteristic distance describing the envelope of the decay function is 1/k, the reciprocal of the propagation constant.

The propagation constant can be written in terms of the density p and the absolute viscosity η of the liquid

$$k = (\omega\rho/2\eta)^{1/2} \quad \text{(eq. 3.7)}$$

Requiring that the transverse velocity of the surface of the quartz resonator at z = l be identical with that of the adjacent liquid, and that the force exerted by the liquid on the crystal be equal and opposite to the force exerted by the crystal on the liquid, leads to the condition for the shift A_f in the resonant frequency f_o

$$\Delta f = - f_0^{3/2}(\eta_l\rho_l/\pi\rho_q\mu_q)^{1/2} \quad \text{(eq. 3.8)}$$

where ρ_l is the density of the liquid and η_l is the viscosity of the liquid (Kanazawa and Gordon 1985)

QCM is utilized for the detection of a micro-change on an electrode's surface and has become one of the most effective techniques of molecular biology and microchemistry because it offers the advantages of simple, rapid, and real-time monitoring, as well as high sensitivity and specificity. An example of QCM (surface modified with probe ssDNA) vibration frequency shift in solution when complementary target ssDNA introduced is shown in Fig. 3.6

QCM DNA-biosensors have been already used in many fields of human interest: genetic diagnosis [3.10], detection of genetically modified organisms [3.11], bacteria detection [3.12] and toxicology. Moreover, they have been successfully used to investigate various biomolecular mechanisms: DNA surface hybridization kinetics [3.13], DNA polymerase chain reaction [19–21], DNA cleavage reaction [3.14, 3.15]

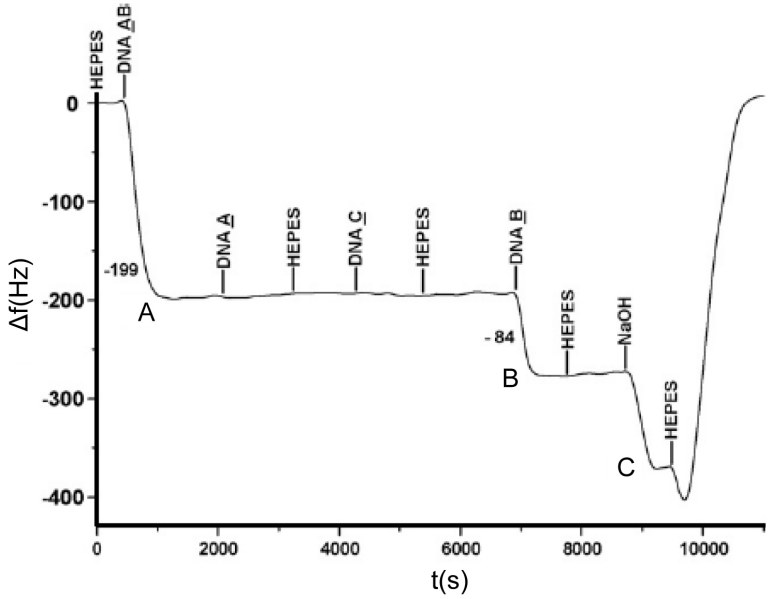

Fig. 3.6: Real time measurement of surface modified QCM as a DNA biosensor. When thiolated probe ssDNA AB is inject into the system, a frequency drop to A means the probe is modified on the QCM surface. The later introduced DNA A, DNA C is not complementary to the probe, no hybridization occur and no frequency drop. Complementary ssDNA B is injected into system and hybridize with probe and cause a drop of frequency to point B. [3.9]

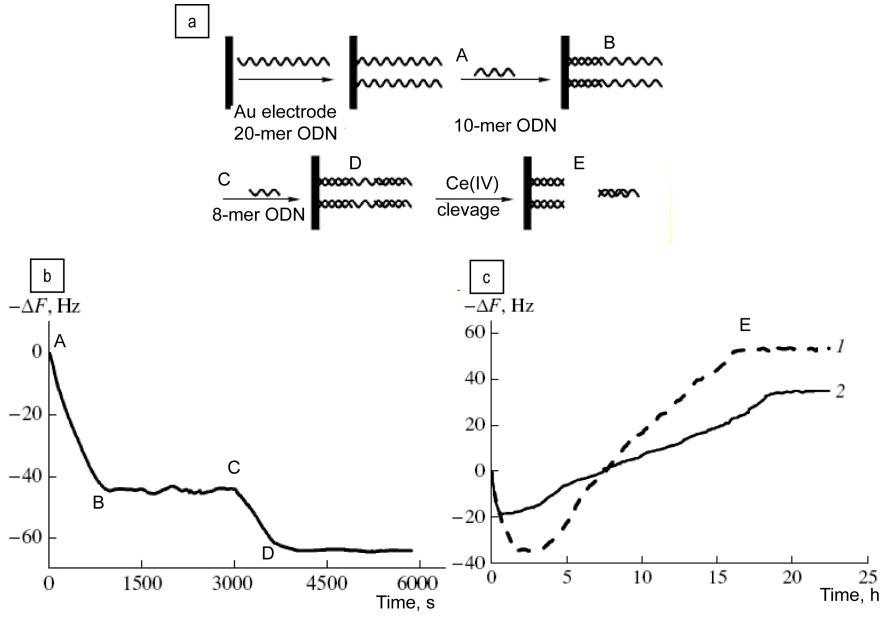

Fig. 3.7: Real time measurement of DNA hybridizes on the probe modified QCM surface. (a) Sketch of the measurement steps. (b) QCM measurement for step A→D. (c) QCM measure of cleavage step E, Frequency response versus time for spontaneous cleavage (curve1) and for site-specific cleavage (curve2)(30℃). [3.16]

3.1.3.2 Microcantilever

Microcantilever biosensor is basically one of the applications by modified atomic force microscopy (AFM). A laser spot is focus on the tip of microcantilever and be reflected to a position sensitive detector (usually a photo diode). The movement (or vibration amplitude change) of microcantilever tip will cause the reflect laser beam movement change and can be translate as information of surface roughness, force between tip and surface. AFM is a very high-resolution type of scanning probe microscopy and piezoelectric elements that facilitate tiny but accurate and precise movements on (electronic) command enable the very precise scanning.

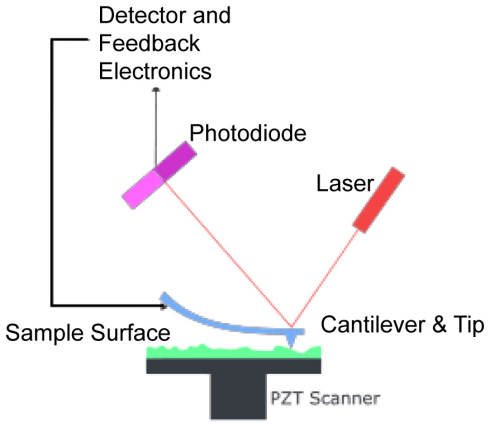

Fig. 3.8: Microcantilever working principle.

The recent discovery of the origin of nano-mechanical motion generated by DNA hybridization and protein–ligand binding [3.17] provided some insight into the specificity of the technique. In addition, its use for DNA–DNA hybridization detection, including accurate positive/negative detection of one–base pair mismatches, was also reported [3.18]

The basic ideal for microcantilever used as biosensor is: (1) Modified the back side of microcantilever with probe biomolecules. (2) While biomolecule recognization process, the bending of the microcantilever caused by mass, electrostatic force or stress change due to the probe biomolecules binding can be detected. The sketch of how microcantilever can be used as biosensor is shown at Fig. 3.9.

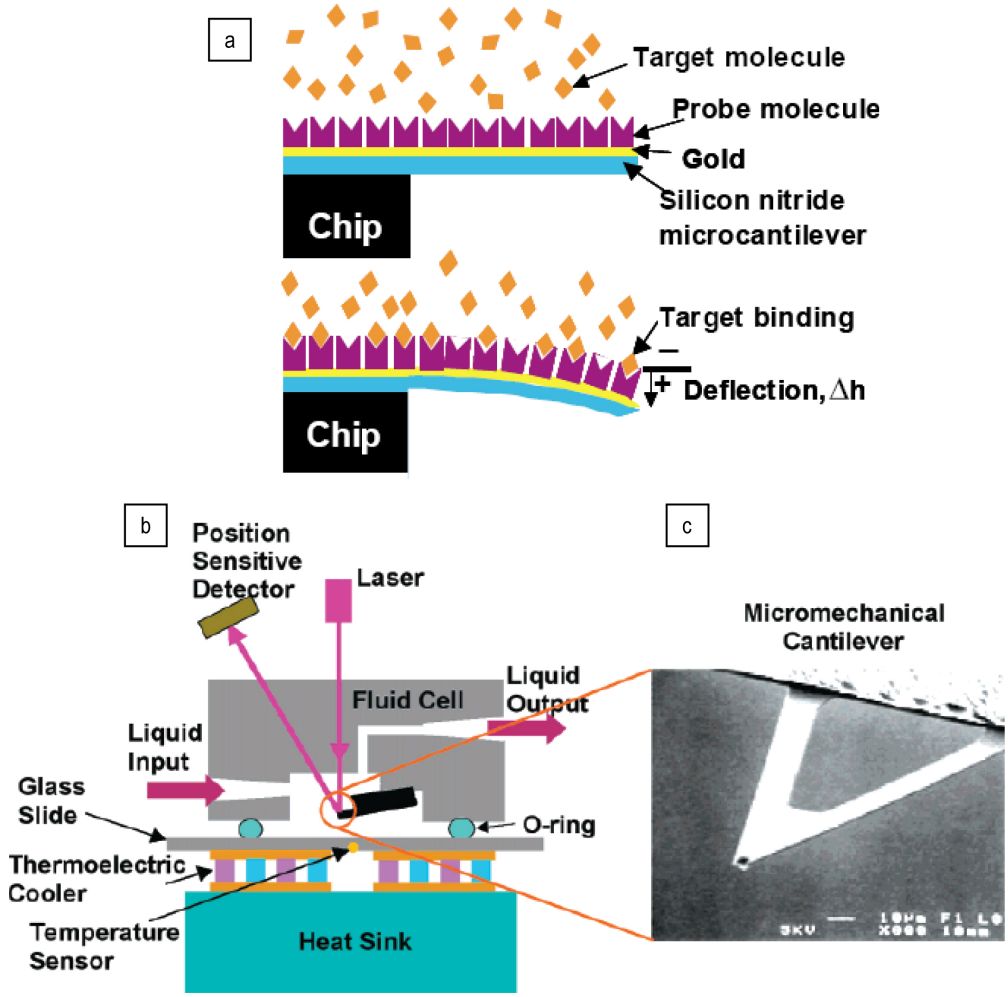

Fig. 3.9: Microcantilever biosensors: (a) Diagram of interactions between target and probe molecules on cantilever beam. This can produce a sufficiently large force to bend the cantilever beam and generate motion. [3.19] (b) Schematic diagram of experimental setup showing a fluid cell within which a microcantilever beam was mounted. (c) SEM micrograph on right shows geometry of cantilever beam. [3.20]

For microcantilever used as DNA biosensor, the hybridization event occurs between target (from solution) and probe (immobilized on the back side of cantilever) will cause not only the mass change, but also the electrostatic repelling between DNA increasing. The charge density of dsDNA is higher than ssDNA and therefore, dsDNA are more repulsive with each other compares to ssDNA.

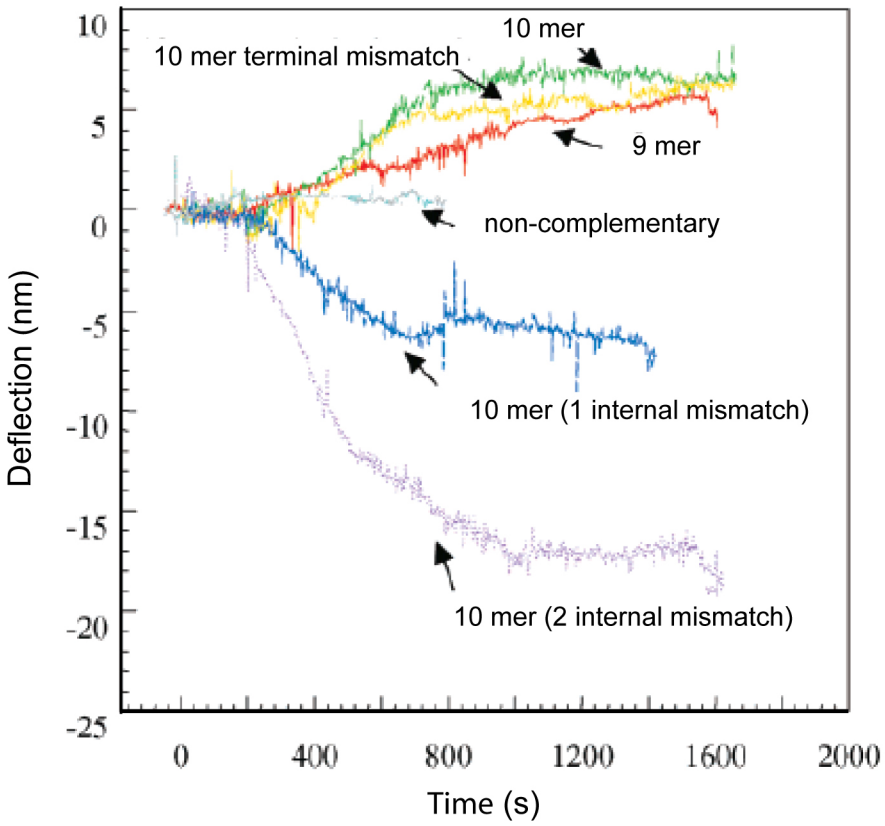

Fig. 3.10: Cantilever deflection for hybridized oligonucleotides. Cantilever surfaces functionalized with thiolated 20-mer probe 1 and challenged with complementary, mismatch, and non-complementary target oligonucleotides. (Measured by Fig. 3.9 (b) and (c))

From one of the measurement result [3.20], the microcantilever is modified with 20-mer probe. And they claim the upward bending of the cantilever for hybridization with complementary 9-mer and 10-mer is due to the reduction of compress force. They explain that, at this situation, the configuration entropy (steric effect) is domain over the increase in electrostatic repulsion due to the additional negative charge in the target ssDNA that hybridizes with the probe. Before hybridization, ssDNA are coiled and highly flexible, whereas dsDNA is present in rod-like configuration. For non-complementary oligomer, there is no hybridization and

therefore, no change of the micro cantilever. For internal mismatch 10-mer with 1 and 2 mismatches are introduced into the system. The hybridization occurs between probe and mismatched 10-mer, however, the cantilever bends downward. They do not have a clear explanation about why the cantilever will bend downward, but compare to 1 base pair mismatch and 2 base pair mismatch, the 2 base mismatch situation cause larger bend downward than 1 base pair which indicate the bend downward do caused by mismatch existence.

In short, the microcantilever is very sensitive to the force change on the cantilever surface in the experiment. For DNA biosensor, those forces changes during the hybridization process including repulsive electrostatic force between DNA, steric force, configuration entropy and mass change. And the result of the cantilever deformation is the sum of all the forces above.

3.1.4 Electrochemical Properties Change

Electrochemical biosensors are normally based on enzymatic catalysis of a reaction that produces or consumes electrons (such enzymes are able to be called as redox enzymes). The sensor substrate usually contains three electrodes; a reference electrode, an active electrode and a sink electrode. An auxiliary electrode (also known as a counter electrode) may also be present as an ion source. The target analyte is involved in the reaction that takes place on the active electrode surface, and the ions produced create a potential which is subtracted from that of the reference electrode to give a signal. We can either measure the current (rate of flow of electrons is now proportional to the analyte concentration) at a fixed potential or the potential can be measured at zero current (this gives a logarithmic response). Note that potential of the working or active electrode is space charge sensitive and this is often used. Further, the label-free and direct electrical detection of small peptides and proteins is possible by their intrinsic charges using bio-functionalized ion-sensitive field-effect transistors [3.21].

Electrochemical transducers have often been used for detecting DNA hybridization due to their high sensitivity, small dimensions, low cost, and compatibility with micromanufacturing technology.

Label-free electrochemical detection is based on modifications of properties, such as capacitance, conductance, or an intrinsic electrochemical response due to DNA (e.g., oxidation of guanines). DNA-based electrochemical sensors take advantage of nanoscale interactions between the target in solution, the recognition layer and a solid electrode surface. Numerous approaches to electrochemical detection have been developed, including (1) direct electrochemistry of DNA, (2) electrochemistry of DNA-specific redox reporters, (3) electrochemical amplifications with nanoparticles. We will mainly focus on (1) direct electrochemistry properties of DNA hybridization without any label in this section, the others (with label, enzyme or redox reporter) will be discuss in the later indirect detection section.

All the molecular-based biosensors rely on highly specific recognition events to detect their target analytes. The role of the biosensor is to provide a suitable platform that probe-target complex can be formed and this binding event triggers a usable signal for electronic readout. That is to say, the basic elements of electrochemical biosensor include a molecular recognition layer and a signal transducer that can be coupled to an appropriate readout device. DNA is one of the bio-molecules that suitable for the bio-sensing applications because the base-pairing interactions between complementary sequences are both specific and robust.

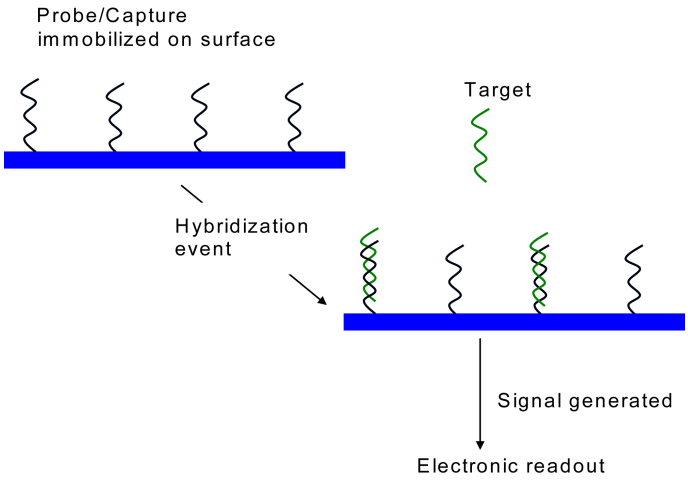

Fig. 3.11: The sketch of electrochemical bio-molecule detection principle. The probe or capture molecule need to be immobilized on the surface first. The way of immobilization may affect the detection efficiency. Second, the hybridization event occur on the surface, signals are generated and been detected by the electronic device.

3.1.4.1 MOSFET DNA Biosensor

Fig. 3.12 shows an example of electrochemistry DNA biosensor without and modification of Target ssDNA. This MOSFET type sensor utilizes the characteristic of gate electrode sensitive to the electron environment. The gold gate electrode surface is modified with probe ssDNA and used as sensing area. Thiolated probe ssDNA were immobilized on the gate electrode surface through thiol-Au bonding.

With a P-channel MOSFET, when the negative bias applied to gate electrode, the drain current increase due to the width increase of p-channel. The hybridization events can be sensed due to the variation of drain current. DNA hybridization on the gate electrodes cause the negative charge increasing due to the phosphate groups of DNA have a negative charge, and therefore the gate potential of PMOSFET is affected.

Fig. 3.12 shows the drain current increased when thiolated ssDNA and target DNA were injected into the solution, because of the field effect due to the electrical charge of DNA molecules. The basic principle of P-channel MOSFET is briefly described below:

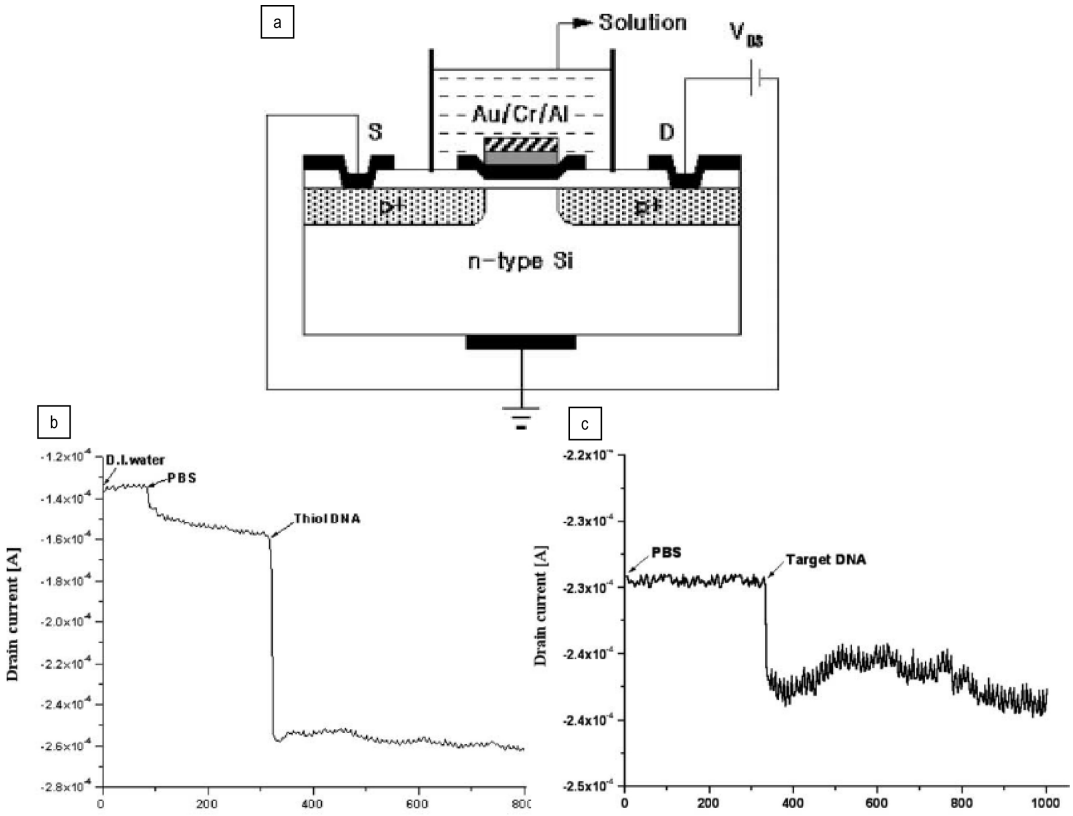

Fig. 3.12: An example of label-free electrochemical DNA biosensor utilizing MOSFET. (a) Structure of MOSFET and DNA charge sensor. This is p-channel MOSFET for negative charged DNA molecule detection. (b) Real time detection of DNA sequence according to the variation of drain current. Plot of drain current versus time after thiolated c-ssDNA injection (c) Plot of drain current versus time after injection t-ssDNA [3.22].

If the MOSFET is a p-channel or p-MOS FET, then the source and drain are 'p+' regions and the body is a 'n' region. When a negative gate-source voltage (positive source-gate) is applied, it creates a p-channel at the surface of the n region. Therefore, the drain current will increase while negative bias is applied on the gate electrode.

Fig. 3.12(b) and (c) show the real time drain current increasing immediately after PBS buffer, thiolated ssDNA and target ssDNA. However, thiolated ssDNA modified gold gate electrode requires certain time, and time is also required for the target ssDNA hybridize with probe. We believe that is because gold gate electrode is very sensitive to the electron environment of whole solution, not just DNA molecules attach or close to the electrode surface.

Therefore, the immediately drain current drop might not because the probe-target DNA interaction and this can be proven by the injection of PBS buffer solution. When PBS buffer is injected into the solution, there is no modification for the electrode, but the ions will be trapped on the gold electrode surface (metal surface in the electrolyte will form electric double layer) and cause the accumulation of anions. This is to say, no matter there is a chemical bonding or DNA hybridization on the surface, as long as the charged molecules come close to the electrode surface, the drain current will be affected.

3.1.4.2 Solid State Nanopore

Another example of label-free electrochemistry DNA sensor is “nanopore” sensor. The DNA sequence can be determined by measuring how the force interact between target DNA and probe DNA molecules, and also ion currents through the nanopore, change as the molecules pass through the nanopore. Nanopores are functionalized with a probe of hair-pin loop DNA can selectively transport short lengths of t-ssDNA that are complementary to the probe under an applied electrical field. With a single base mismatch between the probe and target results in longer translocation pulses and a significantly reduced number of translocation events. [3.23, 3.24] Also, by measure the current (ions pass through nanopore), the different I-V behavior of the existence of whether complementary ssDNA or 1 base pair mismatched ssDNA are shown at Fig. 3.13 (b) and 3.13 (c). While complementary target ssDNA path through the hairpin loop DNA modified nanopore, the hair pin loop DNA will open and hybridize with target ssDNA. The hair pin loop probes can catch target ssDNA by strong interaction between them and block the pathway for ions, therefore, a larger drop of current is observed (Fig. 3.13 (c)) compared to the mismatched ssDNA (Fig. 3.13 (b)).

Although this article claim their approach is CMOS compatible and has the ability to count every single molecule pass through nanopores directly from electrical signal, but there are still something we need concern about.

First, it is not easy to get uniform 20nm size channels through CMOS technology, the signal will be varied a lot with very little variation of diameter of channel size. Then, due to the small size of channels, the large molecules can not path through the channels and get stacked there and cause the failure of nanopore channels. This is to say, the pre-filter is required to reject all the other large molecules in the sample which is inconvenient [3.25]. Third, although this method can get the signal from individual DNA chain, but the DNA sample solution is required to have relatively high concentration as 1pM and large volume (~10 ml).

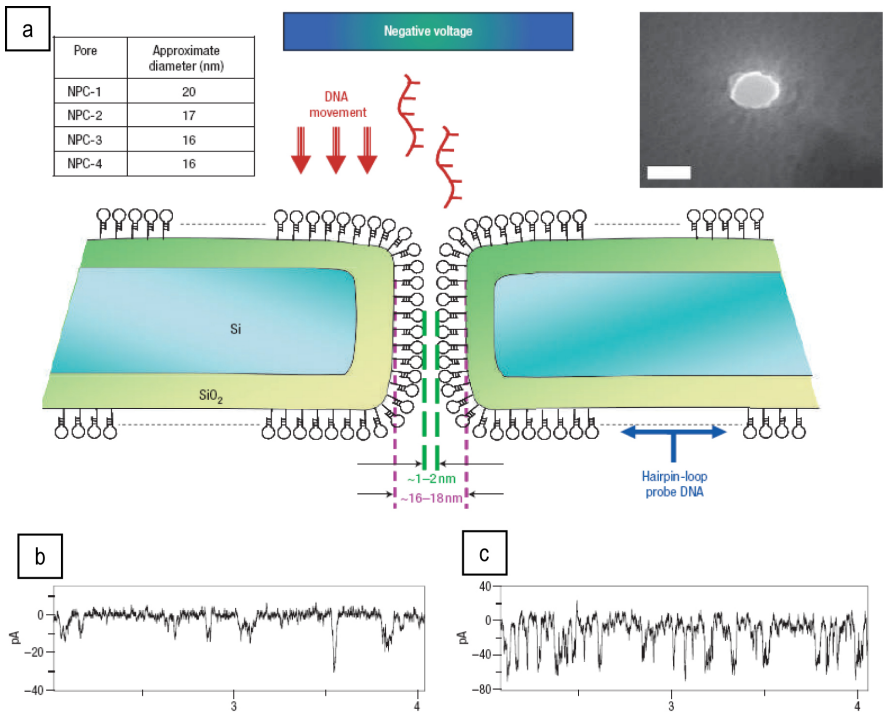

Fig. 3.13: Nanopore DNA sensor (a) Cross-section of the solid-state Nano-Pore Channel functionalized with HPL-DNA molecules (not drawn to scale). The inset table shows dimensions of the various NPCs used in this study. The inset TEM image shows the NPC-2 before functionalization (scale bar, 20 nm). (b, c), Current–time representative data for 1mismatch-DNA (b) and perfect complementary-DNA (c) translocation through NPC-1. A higher number of narrower and deeper pulses are observed for the PC-DNA (c) (note change in scale of vertical axes) [3.25].

3.1.4.3 Solid Nanowire or Nanotube Sensor [3.26-3.28]

Nanowire (NWs) or Nanotube (NTs) is very sensitive to the electrical environment. This is to say, the conductance of nanowire or nanotube type FET is very sensitive to environment and can be use as a sensor. When the FET is made use NWs or NTs as a channel for carriers pass through from source to drain, the electrical environment of this channel would affect the conductance and the conductance change can be read as electrical signals of environment sensing. In this article, the surface of Si nanowire is modified with probe-ssDNA, and the device is immersed into micro-fluidic channel. When the charged biomolecules are injected into micro-fluidic channel, the degree of conductance change can be though as the intensity of biomolecules-p-ssDNA interaction. The complementary ssDNA gives the conductance change larger than that of mismatch ssDNA, and the sensitivity of this sensor is claimed as high as 10 femto-mol.

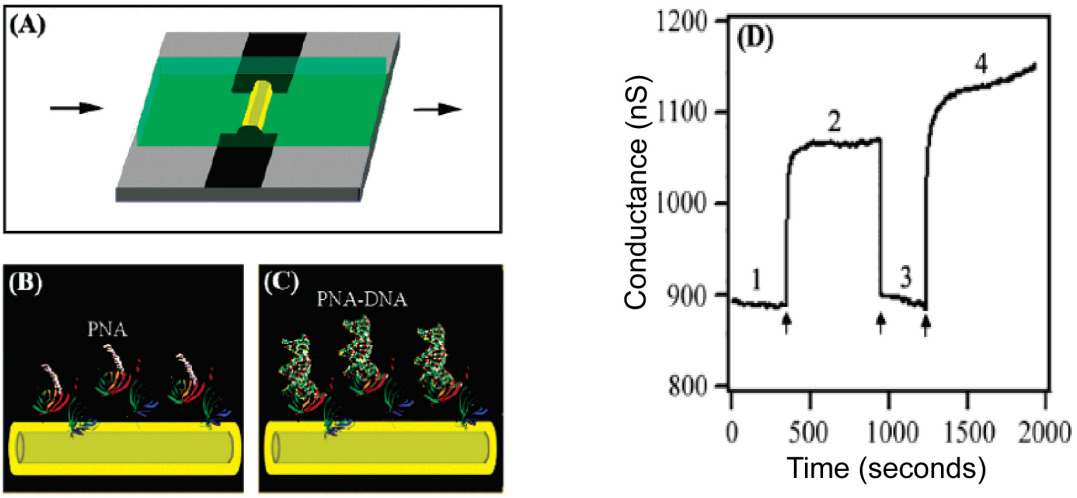

Fig. 3.14: Nanowire biosensor. (a) Schematic of a sensor device consisting of a SiNW (yellow) and a micro-fluidic channel (green), where the arrows indicate the direction of sample flow. (b) The SiNW surface with PNA receptor. (c) PNA-DNA duplex formation. d): Conductance versus time for PNA-functionalized NW device during flow of DNA-free solution (1), 100 fM MU DNA (2), DNA-free solution (3), and 100 fM WT DNA [3.29].

However, the first serious issue is that, it is very difficult to align the nanowire or nanotube on the wafer to make a device. This difficulty directly hinders this type of sensors from mass productive CMOS technology and the device is difficult to make. Fig. 3.14(d) shows the

conductance change when the device is under DNA-free micro-fluidic (stage 1 and 3), 100fM mismatch ssDNA (stage 2) and 100fM complementary ssDNA. This figure tell us that, although the sensitivity of this device is high, but no matter what kind of charged molecules in the micro-fluidic will affect the conductance.

3.2 Indirect Detection

There are many different kinds of labels can be applied into DNA detection method. Some of them are used as reporter, signal amplifier or both. Those labels include fluorescence label, Magnetic label, Quantum dot, Dye and gold nanoparticle. With the help of those easy detected labels, we can achieve high sensitivity of DNA detection by detecting the label instead of detecting DNA hybridization event itself.

3.2.1 Fluorescence label

Fluorescent dyes have been used for decades to stain biomolecules for imaging and detection applications. Many of these dyes bind to DNA and RNA, causing the nucleic acids to become fluorescent and therefore readily detected in a fluorescence microscope

The detection of fluorescence label require a fluorescence microscope which is expensive and the signal need to be convert from optical to electrical signal. There are three different approached of utilizing fluorescence molecules to assist DNA hybridization detection. (1) Directly modified fluorescence label on target or on later introduced reporter ssDNA which can also hybridize with part of target ssDNA. (2) Choose certain fluorescence which will selectively bind to dsDNA (intercalator). (3) Choose certain fluorescence which will bind to ssDNA, and change the fluorescence wavelength due to the electron environment change after hybridization.

The benefit of approach (2) compares to (1) is that: for approach (1), only one fluorescence label for individual target hybridizes with probe. But for approach (2), many

fluorescent molecules can insert in one dsDNA, and the fluorescent labels can generate many times brighter than individual fluorescent dye molecules.

Fluorescence microscope is an optical microscope used to study properties of organic or inorganic substances using the phenomena of fluorescence and phosphorescence instead of, or in addition to, reflection and absorption.

3.2.1.1 Ethidium Bromide Fluorescence

Ethidium bromide is an intercalating agent commonly used as a fluorescent tag (nucleic acid stain) in molecular biology laboratories for techniques such as agarose gel electrophoresis. It is commonly abbreviated as "EtBr", which is also an abbreviation for bromoethane. When exposed to ultraviolet light, it will fluoresce with an orange colour, intensifying almost 20-fold after binding to DNA.

RNA and DNA can both be stained by ethidium bromide (in a solution of 1 microgram ethidium bromide/ml). The increase in fluorescence occurs when ethidium bromide (EtBr) binds to deoxyribonucleic acid (DNA) and ribonucleic acid (RNA).

This can be used to quantities the amount of nucleic acid present [3.30~3.32]. Using a pH between 6 and 8.8 where the double-strand helical arrangement of the nucleic acid, which is necessary for intercalation of the dye, is maintained and a salt concentration of 0.1-0.2 M, they were able to measure 0.01ug/ml of DNA. RNA gave about one-third the fluorescence of an equal amount DNA. The “EtBr-DNA complex” emits fluorescence at 620 nm after excitation at 360 nm. DNA fluorescence in the presence of EtBr requires the presence of double-stranded DNA. This is shown by the fact that heating DNA to 95 ^{o}C causes it to lose fluorescence when added while hot to EtBr. This fluorescence appears spontaneously and reaches base line values in about 5 min as the solution is allowed to return to room temperature.

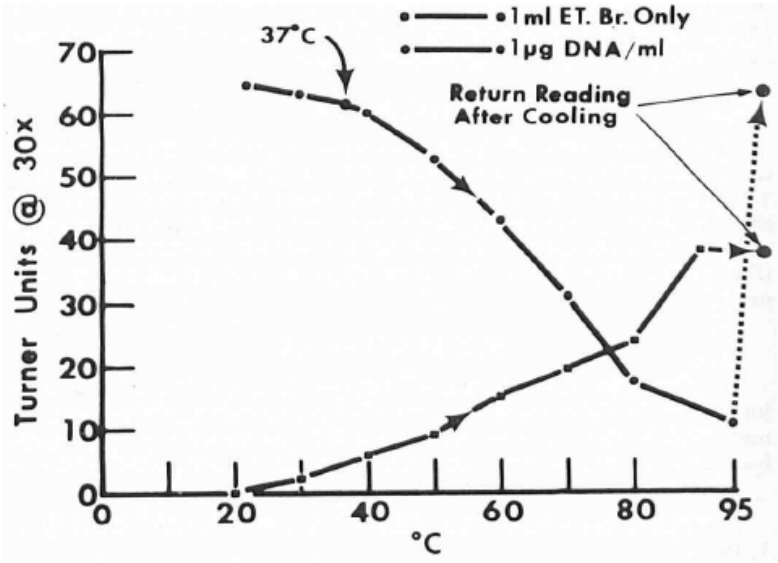

Fig. 3.15: Loss of DNA + ethidium bromide fluorescence on heating. The fluorescence of 1 ug DNA in ethidium bromide solution was measure at room temperature. The solution was heated to 90 ^{o}C and then allowed to return to room temperature. [3.30]

If the ethidium bromide is used in conjunction with gel electrophoresis, the two nucleic acids are not easily confused, and 10 to 50 ng of DNA can be readily detected in a single band. This method has an advantage in measuring the size (mobility on a gel) of your DNA, which provides the information on the identity of the DNA. For gel electrophoresis, DNA samples must be concentrated in bands to achieve the most sensitive levels of detection -- if sample is a random collection of sizes, the fluorescence will spread out over a greater area. If the sample is pure, we can use ethidium bromide without resorting to a gel, by making spots of your DNA sample (mixed with ethidium bromide) on a piece of plastic wrap. By comparing the fluorescence of your DNA dilutions against a standard of known concentration, we can estimate the concentrations of samples that are too valuable to use in spectroscopy.

3.2.1.2 Fluorescence label attach on target DNA

The principle of target ssDNA detection through fluorescence microscope is that: t-ssDNA is modified with fluorescence molecule and hybridized with c-ssDNA which is then fixed

on the substrate into the scan area. The fluorescence intensity in hybridization area is proportional to the concentration of t-ssDNA [3.33].

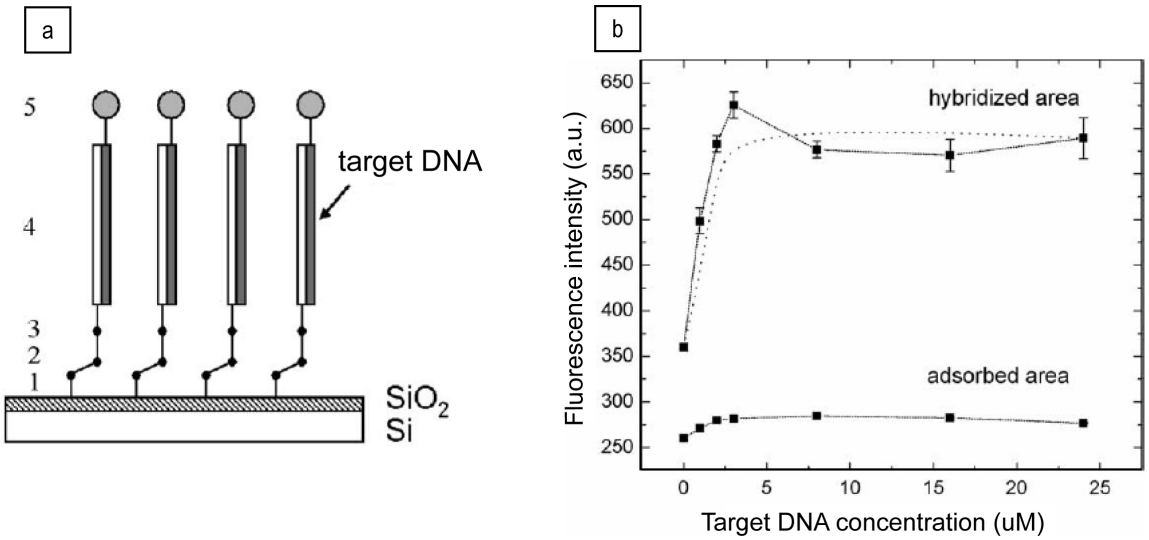

Fig. 3.16: Schematic diagrams of DNA biosensor with fluorescence molecules modified t-ssDNA. (a) Fluorescent detection-based sensor in which a SiO2-covered substrate is first activated with a piranha solution (1), functionalized with a silane (2) and via a cross-linker (3) attached to a ssDNA probe (4). Hybridisation Hybridization with fluorescently labeled complementary target ssDNA (5) provides the detection signal. (b) Fluorescent intensity of hybridized and adsorbed target ssDNA as a function of the concentration of the target DNA. [3.33]

Though the principle this approach is simple but the measurement equipment is expensive and not easy to use. And the fluorescence molecules are expensive and will degrade after scanning.

3.2.2 Magnetic nanoparticle label

The principle of their approach is: first, modify magnetic nanoparticles (MNPs) surface with c-ssDNA, and modify GNP probes surface with p-ssDNA. Then t-ssDNA will hybridize with both c-ssDNA and p-ssDNA; the GNP probes are connected to the MNPs through DNA hybridization. And then separate MNPs from t-ssDNA solution with magnetic field and let GNP probes released from MNPs through DNA denature process [3.34]. Lastly separate GNP probes

and enlarge the size through silver coating on the GNP probes surface to enhance the light scattering.

The result shows that without silver coating enhancement, the sensitivity is low. But with silver coating enhancement, the sensitivity can reach to 10fM.

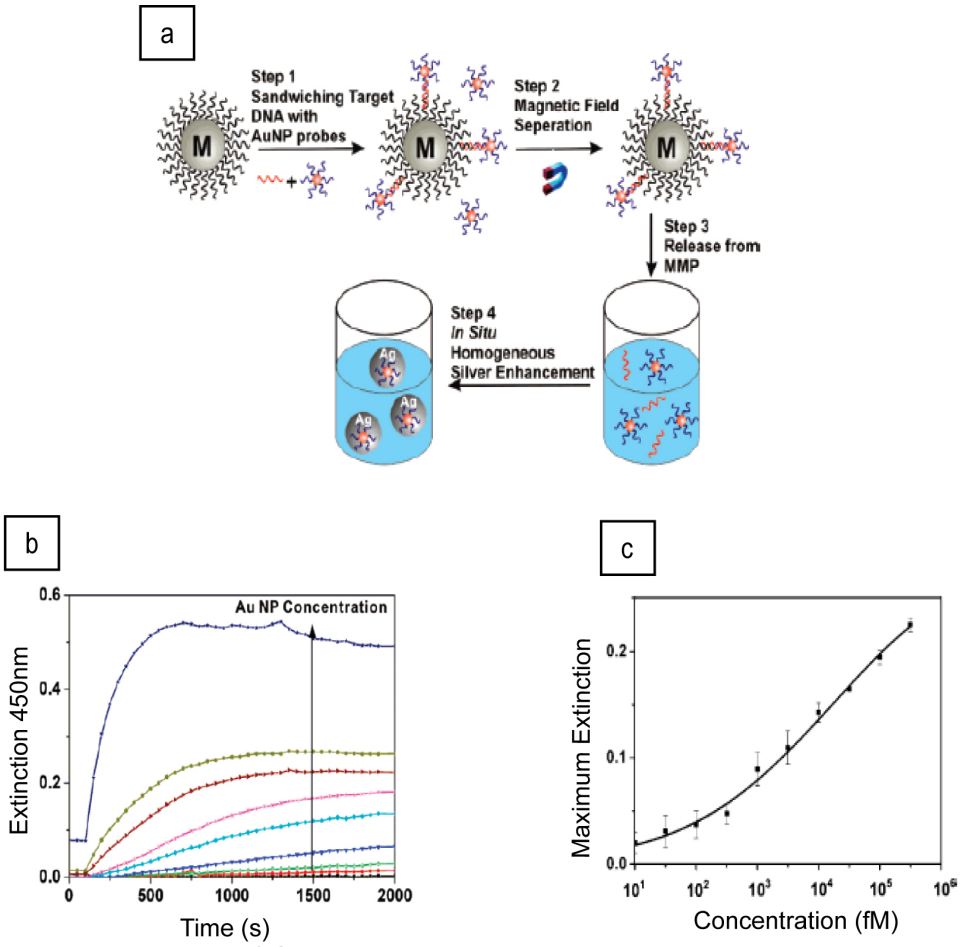

Fig. 3.17: (a) The scheme of silver coating enhancement GNP probes for DNA detection through light scattering. (b) The data of light scattering with 450nm wave length versus time. The concentrations shown above are (top to bottom: 10 nM, 1 nM, 100 pM, 10 pM, 1 pM, 100 fM, 10 fM, no particles. (c) Detection results of Maximum Extinction versus t-ssDNA concentration for DNA target concentrations in the 10 fM-1 nM range. [3.34]

However, this kind of approach is not a simple process and contains a lot of errors originating from operation while processing. It requires a lot of steps of centrifuging, extraction and re-suspension during the whole process. Errors may occur at each step and is not easy to prevent. In our study, we want to have an easy-use device which is simply processing the

sample with immersing into c-ssDNA, t-ssDNA, p-ssDNA and GNPs solution then get the concentration data from I-V measurement.

3.2.3 Gold nanoparticle label

The most direct detection of labeled DNA hybridization event is the conduction changes between two electrodes after metal nanoparticle modified target ssDNA hybridize with probe ssDNA immobilized between two electrodes. Gold nanoparticle in one of the best choice among other metal nanoparticle because it's affinity to biomolecules and is easy to be modified. The thiolat modified ssDNA is well established, easily available and well commercialized.

Gold nanoparticle label can be used as for conductance enhancement label, or can be also used as for light scattering. Also, while DNA modified nanoparticles were linked by linker ssDNA, the color change due to the size of GNP change can also be used as a indicator of hybridization event.

3.2.1.2 Multi-layer GNPs Bridge

Conductivity increases when Gold Nanoparticles (GNPs) are connected through DNA hybridization and form multiple layers of GNPs between two electrodes as a bridge [3.35]. In this approach, the GNPs are fixed in between two gold electrodes 350nm apart using thiol group terminated MPTMS (3-mercapto-propyl-trimethoxy-silane) SAMs. Then the thiolated c-ssDNA is added to modify the surface of the gold nanoparticles as well as the surface of the gold electrodes. And then the c-ssDNA and the thiolated P-ssDNA are hybridized with t-ssDNA so that a layer of thiol group is formed on top of gold surface of GNPs and electrodes. At this stage, the conductivity between two electrodes is low due to the wide separation between electrodes and GNPs. The sample is then immersed in gold colloid again to form second layer of GNPs for conductivity enhancement. The principle for their design is the conductivity between two electrodes will vary with the concentration of t-ssDNA.

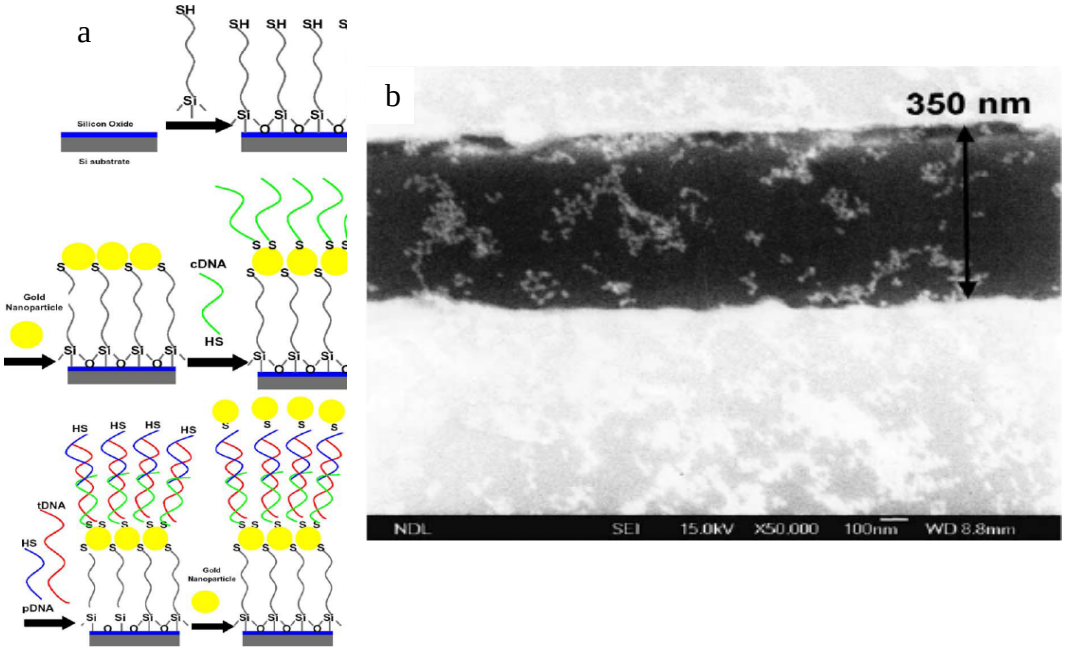

Fig. 3.18: Multilayer GNP bridge DNA sensor. a) Flow chart of multi-layer GNPs formation between two gold electrodes. b) SEM image of multi-layer GNPs in-between 350nm gap gold electrodes. [3.35]

However, some obvious drawbacks of this approach are: 1) With only MPTMS SAMs modification, the thiol group will also react with gold electrode surface and silane group is exposed at gold electrode surface which causes a lot of GNP agglomeration on the Au electrode surface. 2) Second layer of GNPs can react with un-reacted thiol group on the MPTMS SAMs, thiol modified p-ssDNA on gold electrode surface or thiol modified p-ssDNA on SiO2 surface between electrodes. We can not tell whether the increasing of conductivity after we apply second layer of GNPs is due to t-ssDNA or due to the aggregation of GNPs.

The reason why our approach is expected to have much higher sensitivity compared to this is we modified gold electrode surface with negative charged 16MHDA SAMs which prevents the GNPs precipitate onto the gold electrodes surface. This is important because the first GNPs will act as receptors of c-ssDNA, and the first layer GNPs outside the gap between electrodes will greatly reduce the sensitivity. The first layer GNPs in our study will be attached only in the center area between two electrodes. The second layer GNPs will only react with the

thiol group of p-ssDNA which is fixed on top of first layer GNPs through hybridization with t-ssDNA. In our study, the number of second layer GNPs fixed on the sample is directly proportional to the concentration of t-ssDNA and also directly related to the current passing through two electrodes.

3.2.1.2 Single-layer GNPs bridge with Silver Coating Enhancement

Due to the low or no signal can be detected with little number of GNPs between electrodes which is caused by very low t-ssDNA concentration, the silver coating enhancement is required to amplify the signal. Conductivity increases when Gold Nanoparticles are fixed between two electrodes through DNA hybridization, and silver coating enhancement is applied to form a bridge between two electrodes [3.36-3.38].

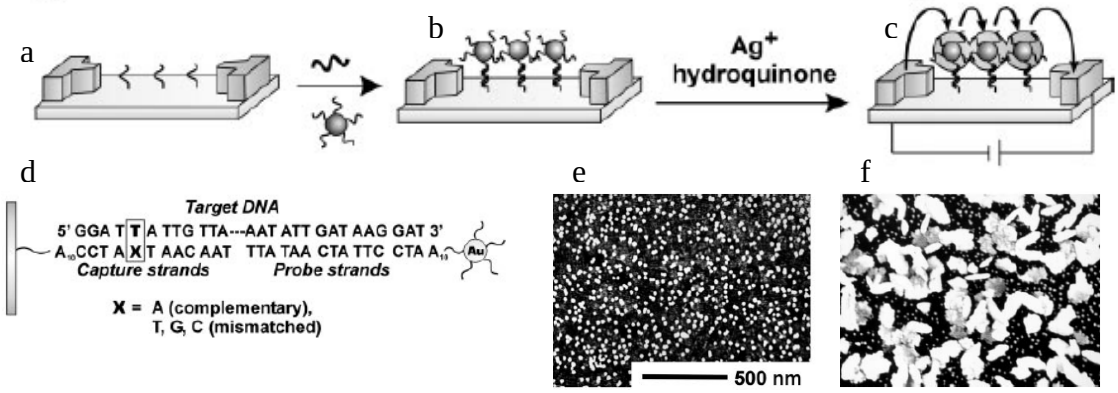

Fig. 3.19: Scheme of DNA electrical detection concept: (a) 20um gap between two 60nm thick gold electrodes on top of 5nm titanium oxide, c-ssDNA is fixed on top of titanium oxide substrate. (b) p-ssDNA modified GNPs was fixed on substrate through c-ssDNA, t-ssDNA and p-ssDNA hybridization. (c) Silver coating enhancement of conductivity between two gold electrodes. (d) Structure of c-ssDNA, t-ssDNA and p-ssDNA. (e) SEM image of (b). (f) SEM image of (c).

In this approach, the substrate modified with c-ssDNA is hybridized with t-ssDNA. Then, prepare p-ssDNA modified GNPs and hybridize with t-ssDNA which is fixed on the substrate between two gold electrodes. Apply silver coating on GNPs surface to enlarge the size of particle and increase the conductivity between two gold electrodes. The sensitivity of this method is clamed as 500fM.

Compared to this approach, our approach of DNA detection does not need silver enhancement to amplify the electrical signal and we also expect the sensitivity (~ atto-mol) which is much higher than this method.

3.3 DNA Microarray

DNA microarray is a multiplex technology used in molecular biology and in medicine which simultaneously measure multiple analytes in a single assay. DNA microarray consists of an arrayed series of thousands features of DNA oligonucleotides microscopic spots which containing around picomoles (~10^{-12} mole) of a specific DNA sequence (probe). Probe can be a short segment of a gene or other DNA element that can be used to hybridize with complementary Target DNA or RNA sample. Probe-Target hybridization is usually detected and quantified by fluorophore-, silver-, or chemiluminescence-labeled targets to determine relative among of nucleic acid sequences in the target. DNA microarray can accomplish many genetic tests in parallel and therefore dramatically accelerated many types of investigation. The microarrays may have from a hundred to many thousands of test sites that can range in size from 10 to 500 microns. High-density microarrays may have up to 10^6 test sites in a 1–2-cm^2 area.

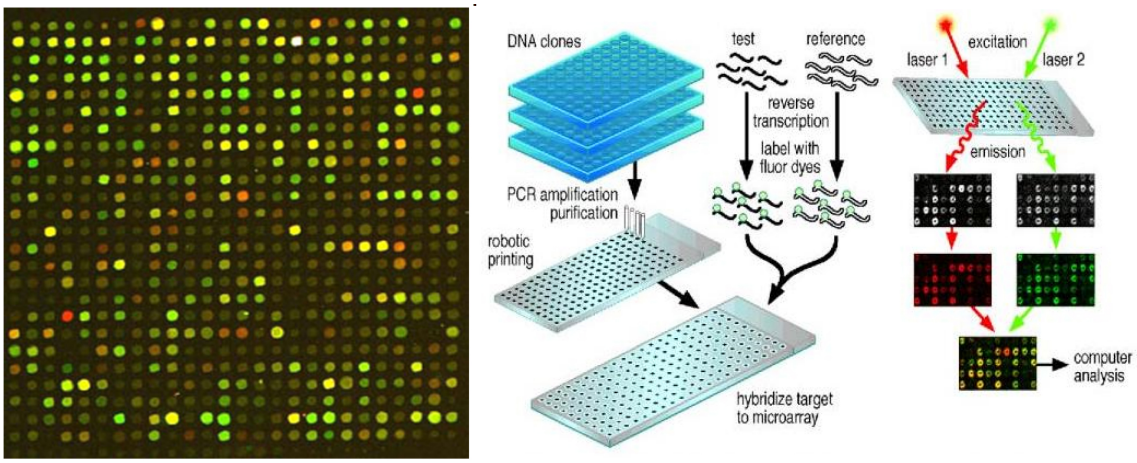

Fig. 3.20: Example of microarray hybridization. [3.40]

In standard situation, probes are attached to a solid surface by a covalent bond. Solid surface can be glass or silicon chip in which are commonly known as gene chip. The core principle of DNA microarray is hybridization between two ssDNA strands. Complementary nucleic acid sequences pair with each other specifically by forming hydrogen bonds. After washing off non-specific bonding sequences, only strongly paired strands will remain hybridized. The fluorescently labeled target sequences that bind to a probe sequence generate a signal that depends on the strength of the hybridization determined by the number of paired bases, the hybridization conditions (such as temperature), and washing after hybridization.

The patterns obtained from microarray experiments have helped researchers to understand genetic mechanisms and progress of diseases [3.41, 3.42], to predict molecular functions of genes [3.43, 3.44], to build functional pathways [3.45], and to identify novel genes or splice variants [3.46].

The successful implementation of DNA microarray technologies requires the development of methods and techniques for the fabrication of microarrays, the selection of probes to spot, the quantification of hybridization, and data analysis [3.47-3.49]. Currently, DNA microarrays are manufactured using either cDNA or oligonucletides as gene probes. cDNA microarrays are usually created by spotting amplified cDNA fragments in a high density pattern onto a solid surface such as a glass slide [3.50, 3.51]. Probes for oligonucletides arrays are either spotted or synthesized directly onto a glass or silicon surface using various technologies including photolithography, ink-jets, and some other technologies [3.52-3.54].

There are two schemes to detect differently expressed targets when comparing an experimental sample with a reference sample: one- and two-color schemes as shown in Fig. 3.21. In one-color case, images are obtained on a different chip for each sample using a single fluorescent label. Different images are then compared to obtain differentially expressed targets. In two-color format, two RNA samples (reference and experimental) are labeled separately with different fluorescent tags (for example, cyanine 3 and cyanine 5 (Cy3, Cy5)), then hybridized to a single microarray and scanned to generate fluorescent images from the two channels. A two-

color graphical overlay can then be used to visualize targets that are up-regulated or down-regulated.

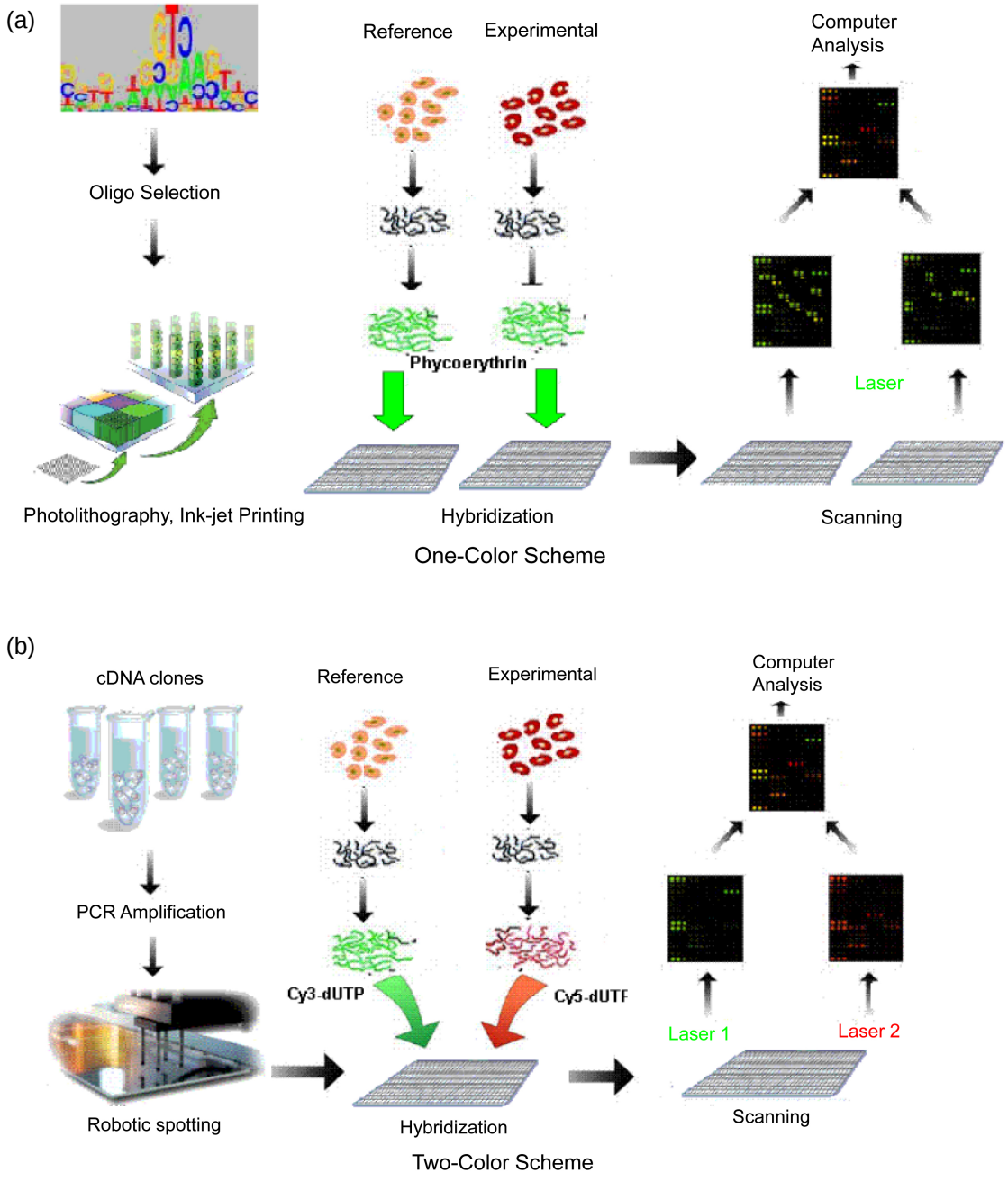

Fig. 3.21: Two different type of DNA micro array detection. [3.50] (a)One-color scheme. (b) Two-color Scheme

The major spotting techniques used in microarray systems are: pin-based fluid transfer system [3.55], piezo-based inkjet dispenser systems [3.56, 3.57], photolithography for the in situ synthesis of high-density DNA microarrays [3.58] and electronic-based addressing of microarrays.

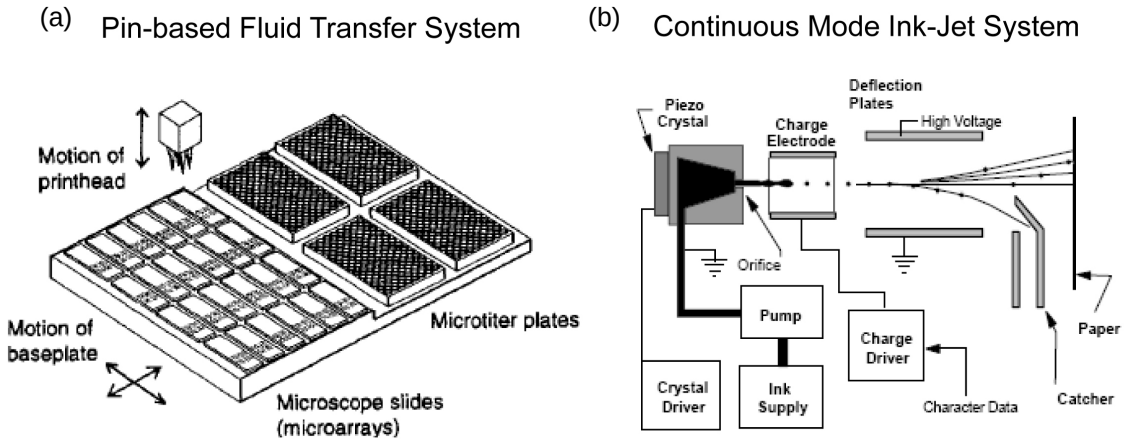

Fig. 3.22: Pin-based and Ink-Jet spotting system [3.55, 3.56]. (a) Pin based fluid transfer system. (b) Continuous mode Ink-Jet system

3.4 Common Method of Immobilize DNA on Substrate

There are a lot of different methods of DNA immobilization on the substrate surface through chemical linker. Instead of probe immobilized on the substrate surface by physical absorption, a chemical linkage is preferred due to the configuration of how probe DNA is on the substrate surface. Fig. 2.10 shows that the probe DNA lies down flat on the substrate by physical absorption including electrostatic force (base pair face up) or by van der Waals' force (base pair face down). When the base pair of oligonucleotide is face up, the hybridization can still occur but with less hybridization efficiency due to the distortion of double helix structure. When the base pair is face down, the hybridization reaction can not occur. This is to say, to immobilize probe DNA on the surface is not favorable by just physical absorption.

A favored immobilization method is the use of a self-assembled monolayer (SAM) on the substrate surface, which increases the degrees of freedom of the probe and, consequently, those of binding target molecules.

With the chemical linkage, the probe DNA can “stand straight” and the hybridization behavior is more like free DNA chain in the solution. Therefore, by modifying the surface and probe DNA with different functional groups and the reaction between those functional groups can provide the chemical linkage between probe DNA and substrate surface.

We can form SAMs layer on different substrate with different tail functional group (such as: $-NH_2$, -OH, -COOH, -SH...) and react with different function group modified DNA probe molecules (such as: $-NH_2$, -SH, -OH (at 3’end)…). We will discuss some of the most commonly used DNA probe immobilization methods.

3.4.1 Thiol Modified DNA Probe

SAMs can be formed by thiol-modified biomolecules, e.g. DNA (Manera et al., 2008) and RNA (Piliarik et al., 2008) sequences, directly attached to the gold surface by exploiting its high affinity with thiol groups. Thiol modification is commercially available for both DNA 5’ end and 3’ end with different length of spacer ($-(CH_2)_n-$). The spacer for 3’ end thiolation is $(CH_2)_3$, and spacer for 5’ end thiolation is $(CH_2)_6$. The detail structure of 3’-end and 5’-end thiol group modified DNA are shown at Fig. 3.23. This method can directly form a self assembled monolayer direct and is commonly used in either modify gold surface or gold nanoparticle surface. Also, the DNA-DNA interspacing can be control by mixing alkanethiol with thiolated DNA in the solution. The SAMs formed will have the same ratio with alkanethiol/thiolated DNA.

DNA hybridization efficiency is strongly affected by the surface probe density for the heterogeneous hybridization; therefore, utilizing short chain alkanethiol and thiolated ssDNA mixture, we can control the surface probe density and having better DNA hybridization efficiency.

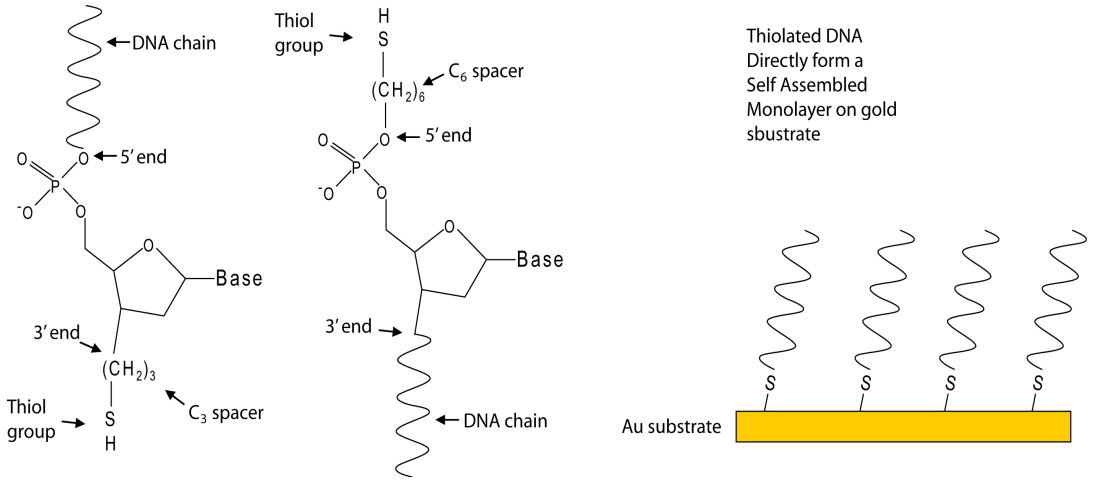

Fig. 3.23: Thiolated ssDNA SAMs. 3'-end and 5' end thiolated DNA can directly form self assembled monolayer on gold substrate through thiol-gild reaction.

3.4.2 Amnio Tail Group React with 5' Phosphate Group of Probe DNA

Gold surface is immersed into 5 mM aminoethanethiol hydrochloride/ethanol solution for 10 hours at room temperature. Follow by rinsing with distilled water and ethanol and air-dried. The sample then immersed in N-methylimidazole buffer (0.1 M, pH 6.0) containing 0.1 M 1-ethyl-3-(3-dimethylaminopropril) carbodiimide (EDAC) and 7.0 mM of the oligonucleotide probe. The electrode was incubated for 3 hours at 25oC. The 5'-phosphate groups of the probe can form a phosphoramidate bond (R-NH-P$(OR)_2$O) with the amine groups on the crystal. The modified surface was washed three times with a solution of sodium dodecylsulphate (SDS) 0.25% with NaOH 0.4 M for 5 min to remove adsorbed oligonucleotides [3.39]. Fig. 3.20 shows the whole reaction mechanism. The major benefit of this method is that, the immobilized oligonucleotide do not required any modification.

This method can also be applied on SiO_2 surface with APTES (H_2N-$(CH_2)_3$-Si$(OC_2H_5)_3$) SAMs layer which can modified SiO_2 surface with amine tail group.

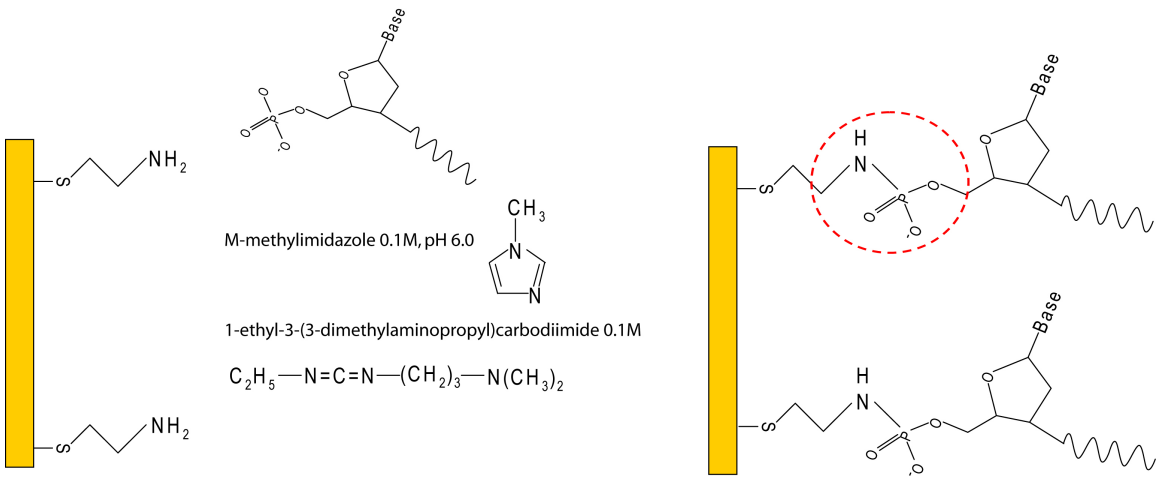

Fig. 3.24: The reaction of 5'-end phosphate group react with amine tail group on the substrate.

3.4.3 Amino Tail Group React with R-N=C=S Function Group

3'-end or 5'-end amine modification is also a commonly used DNA modification. The reaction between isothiocyanate group (R-N=C=S) and amine group ($R\text{-}NH_2$) is shown at Fig. 3.25. The gold substrate surface is first modified with amine terminated alkanethiol and then reacts with diisothiocyanate (S=C=N-R-N=C=S) (ex: Phenylene diisothiocyanate). The R-N=C=S functional group can react with amine group and form R-NH-CS-NH-R' linkage. The other exposed isothiocyanate group can then react with amine modified DNA and probe oligonucleotide can be immobilized on the substrate. This method can be also applied on SiO_2 substrate modified by amine tail group SAMs (ex: APTES).

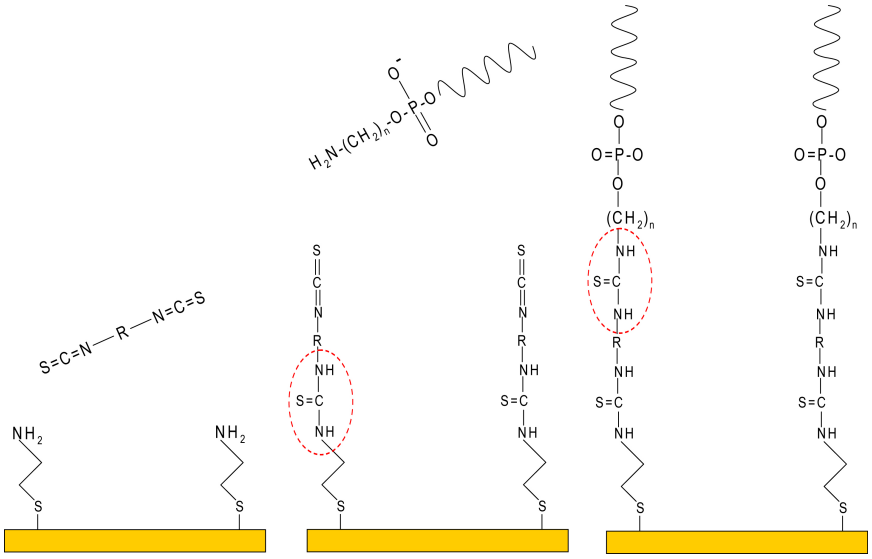

Fig. 3.25: Reaction mechanism of SAMS with amine tail group reacts with isothiocyanate functional group.

3.4.4 Amino Tail Group React with Aldehyde (OHC-R) Function Group

Amine group can also react with aldehyde (R-CH=O) function group. The detail reaction mechanism is shown at Fig. 3.26:

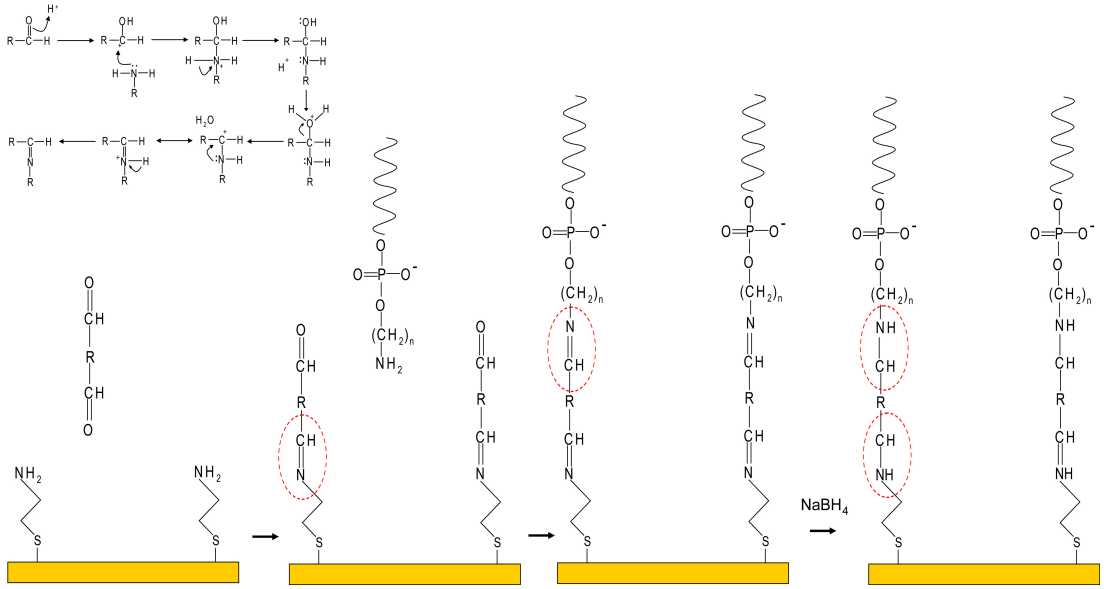

Fig. 3.26: Reaction mechanism of amine functional group reacts with aldehyde.

3.4.5 Thiol Tail Group React with Thiolated DNA probe

(3-Mercaptopropyl)trimethoxysilane (MPTMs), ($HS-(CH_2)_3-Si(OCH_3)_3$) is used to modified SiO_2 surface and form SAMs layer with thiol tail group (-SH). The reaction condition is: SiO_2 substrate immersed in 5mM MPTMs/Isopropanol solution (3 drops of water added) for 40^oC/1hr following by rinsing with isopropanol and dry with N_2 gas.

Thiolated ssDNA sample usually have a chemical cap (R-S-) to protect thiol group of thiol functional group (R-S-S-R'). This chemical cap will be replaced when react with thiol tail group of MPTMS SAMs as shown at Fig. 3.27.

Again, this reaction mechanism can be applied to gold substrate by replace MPTMs with di-thiol molecules.

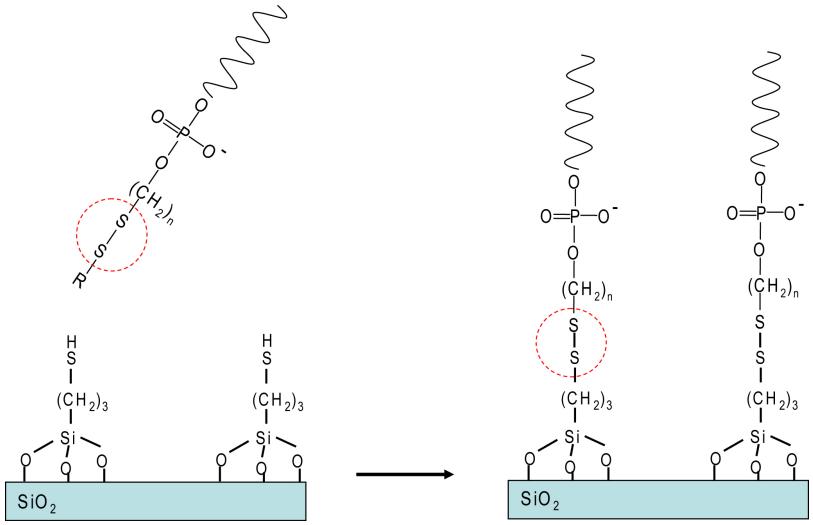

Fig. 3.27: The thiolated probe oligonucleotide with chemical cap protection (R-S-S-DNA) reacts with thiol tail group

CHAPTER 4

BACKGROUND KNOWLEDGE OF SELF ASSEMBLED MONOLAYER AND DLVO THEORY

4.1 Self-Assembled Monolayers

A self assembled monolayer (SAM) is an organized layer of amphiphilic (a chemical compound possessing both hydrophilic (water-loving) and hydrophobic (fat-loving) properties) molecules in which one end of the molecule, the “head group” shows a special affinity for a substrate. SAMs also consist of a tail with a functional group at the terminal end which far from the substrate.

SAMs are created by the chemi-sorption of hydrophilic “head groups” onto a substrate from either the vapor or liquid phase followed by a slow two-dimensional organization of “tail groups”.

The adsorbate molecules form either a disordered mass of molecules or form a lying down phase in the initial state first, and begin to form crystalline or semi-crystalline structures on the substrate surface later. The alkyl chains become closer during the formation of SAMs. Therefore, the inter-chain van der Waals interactions become effective, which leads to formation of a close-packed “ordered” or “solid-like” state. Areas of close-packed molecules nucleate and grow until the surface of the substrate is covered in a single monolayer. The surface energy of substrate is lowered during the SAMs formation.

There are different kinds of head functional groups that can modify different kind substrate. Also, the tail functional group of SAMs can be varied and therefore can provide various surface properties for the modified substrate.

Disulfide (R-S-S-R'), sulfide (S^{2-}) or thiol (R-SH) coordinate are very strongly onto a variety of metals, e.g., gold, silver, platinum or copper. The structure of a self-assembled monolayer depends on the morphology of the metal (Au (111) is mostly applied for the formation of monolayers). Typically, head groups are connected to an alkyl chain in which the terminal end can be functionalized (i.e. adding –OH, $–NH_3$, or –COOH groups) to vary the wetting and interfacial properties.

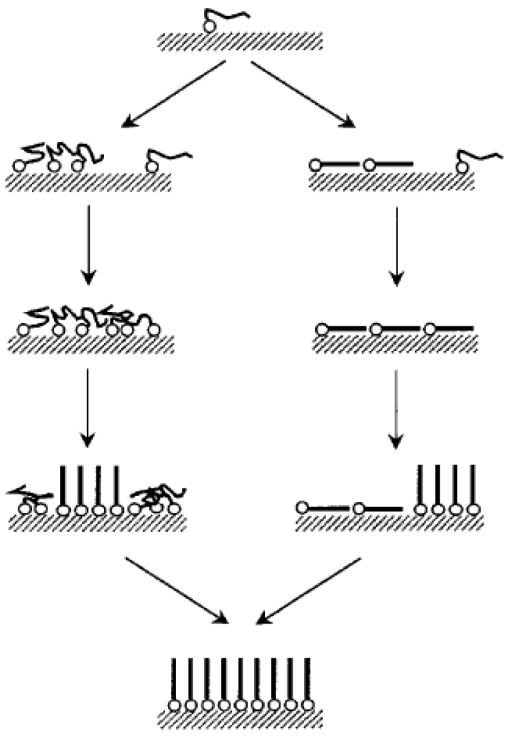

Fig. 4.1: Sketch of SAMs formation. Molecules are first adsorbed on the substrate in a short time, and then gradually form an ordered phase (slow process) [4.1]

4.1.1 Thiol Head Group

Alkanethiols are the most commonly used molecules for SAMs. Alkanethiols are molecules with an alkyl chain, $(C\text{-}C)_n$ chain, as the back bone, a tail group, and a S-H head group. Alkanethiols from dilute solution form a densely packed monolayer in less than 1 h [4.1].

The adsorption time seems to be independent of the chain length, but high concentrations lead to shorter adsorption times. The mole ratio of a mixture of thiols in solution results in the same ratio in the mixed SAM. The two components do not phase segregate into islands [4.2]. Although dense monolayers assemble quickly, well ordered monolayers can take days to form [4.3]. The assembling kinetics of a monolayer is biphasic: the diffusion-controlled adsorption is followed by a slow (re-)crystallization process.

Thiol groups are deprotonated upon adsorption [4.4]. The assumed formation of a gold–thiolate bond is:

$$\bar{R}SH + Au \rightleftharpoons RS{-}Au + e^- + H^+ \qquad \text{(eq. 4.1)}$$

Monolayers of w-substituted alkanethiols (n > 10) are densely packed crystalline-like structures, exhibiting a typical tilt angle in the range of 28–40° from the surface normal and a twist of chain axes of approximately 55°[4.5].

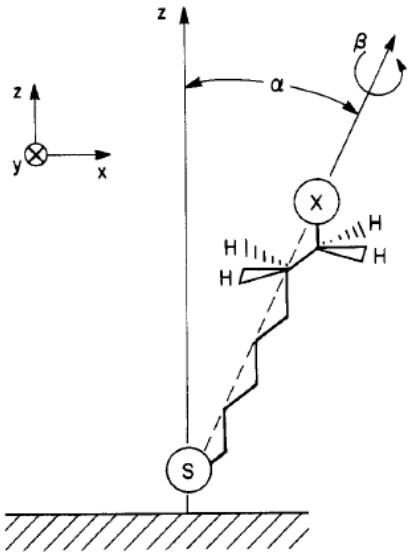

Fig. 4.2: Tilting and rotation of an all-trans alkyl chain in surface coordinates. The initial configuration of the chain is with the main axis parallel to Z and the CCC plane parallel to X,Z plane. The tilt and rotation angles are α and β, respectively [4.5].

4.1.2 Silane Head Group

The silane group is also a common used head group which has highly reactive and silanizes the surface by forming covalent bonds with surface atoms.

Usually, the SAMs that utilized silane as head group are formed spontaneously by immersing the Si substrates into an active solution, e.g. surfactant molecules R(CH2)nSiX3 (X = Cl, OCH3 or OC2H5) dissolved in alkane/carbon tetrachloride. Forms the chemical bond with surface atoms of the substrate (exothermic: ~40–45 kcal/mol or ~1.7 eV) causing the pinning of surfactant molecule to the substrate.

On a silicon oxide surface, three classes of molecules, namely, silanes ($RSiX_3$, with X= Cl, OMe, OEt), organometallics (RLi or RMgX), and alcohols (ROH) are widely used for the formation of self assembled monolayers.

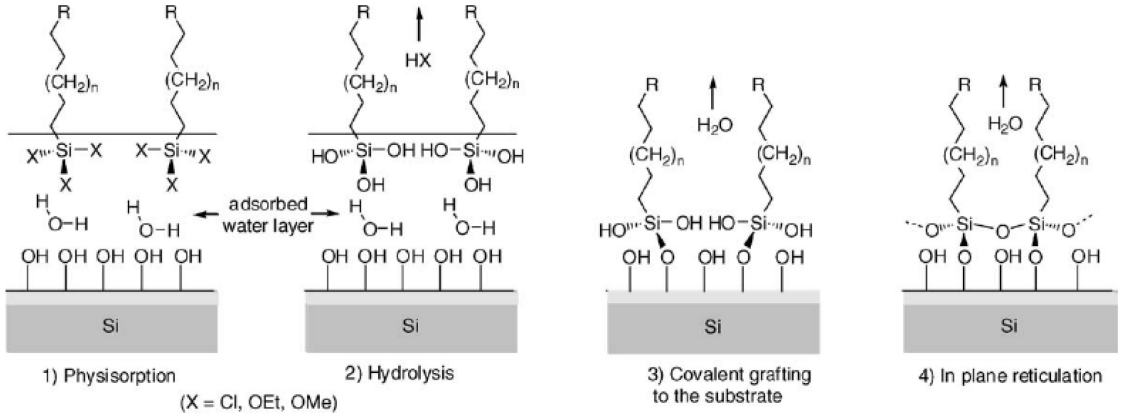

Fig. 4.3: Schematic showing different steps involved in the mechanism of SAM formation on a hydrated silicon surface [4.7]. (1), (2) molecules are attracted to the surface by physisorption. (3) Chemical bonding formation between siliane group and surface hydroxyl group. (4) cross linking process between siliane group.

4.1.3 Tail Group

The methylene groups exhibit strong van der Waals interactions and stabilize the monolayer. Methylene groups are ordered (crystalline like) at low temperatures and less ordered (semi-crystalline) at room temperature [4.6]. Tail group such as -NH2, -OH is relatively

small, the orientation of the monolayer is not influenced. More bulky groups such as COOH, decrease the density of packing and ordering.

Aliphatic amino groups ($R\text{-}NH_2$) have a pK of approximately 10.6. Although the close packing of the aliphatic amino groups on the AP-mica surface decreases the pK, the surface will still be positively charged in solution at neutral pH.

4.1.4 Characterization of APTES SAMs

3-Aminopropyltriethoxysilane (APTES) is a commonly used self-assembled monolayer on silicon substrate. APTES film formation on a silicon substrate is that silanization begins with the hydrolysis of ethoxy groups in APTES, a process catalyzed by water, leading to the formation of silanols. APTES silanols then condense with surface silanols forming a monolayer of APTES via a lateral siloxane network in which amino groups are oriented away from the underlying silicon surface.

The structure and thickness of APTES films are affected by preparation conditions such as the deposition time and the choice of reaction solutions. In an anhydrous toluene solution, APTES films grow by both covalent and non-covalent adsorption of APTES. However, APTES films grow by electrostatic interactions/or hydrogen bonding when deposited from aqueous solutions. [4.8]

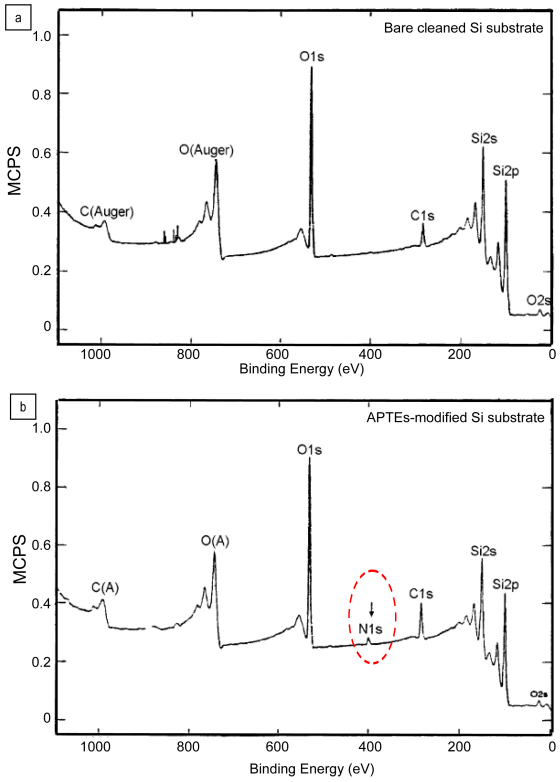

Fig. 4.4: XPS survey spectra of substrate and SAMs (a) the bare Si; (b) the APTES modified Si. Arrow shown in (b) indicates the peak of N1s due to the adsorption of APTES SAM onto the Si surface. [4.9]

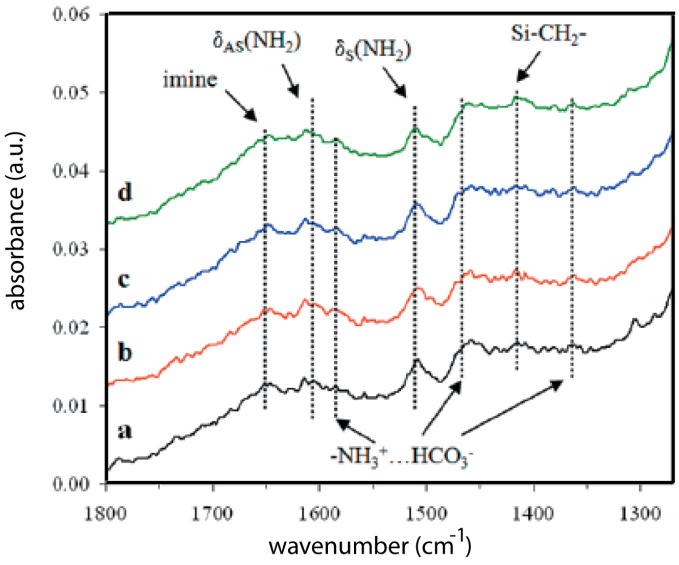

Fig. 4.5: FTIR spectra of APTES films. APTES film is produced in PBS with the deposition time of 15 min (a), 1 h (b), 4 h (c), and 24 h (d) following a 20 min sonication in phosphate buffered water. Measured thicknesses of these films were about 8, 9, 10, and 13 Å, respectively.

4.1.5 Characterization of 16MHA SAMs

16-mercaptohexadecanoic acid is a commonly used SAMs with thiol head group and carboxyl tail group. Thiol head group form chemical bonding with gold substrate and carboxyl tail group is exposed to the surface.

In the case of COOH-terminated SAMs, the effect of the intramonolayer hydrogen bonding between the neighboring carboxyl groups in the SAMs had been considered with respect to their surface property, such as wettability and surface acidity (pK_a) of the carboxyl groups [4.10-4.12].

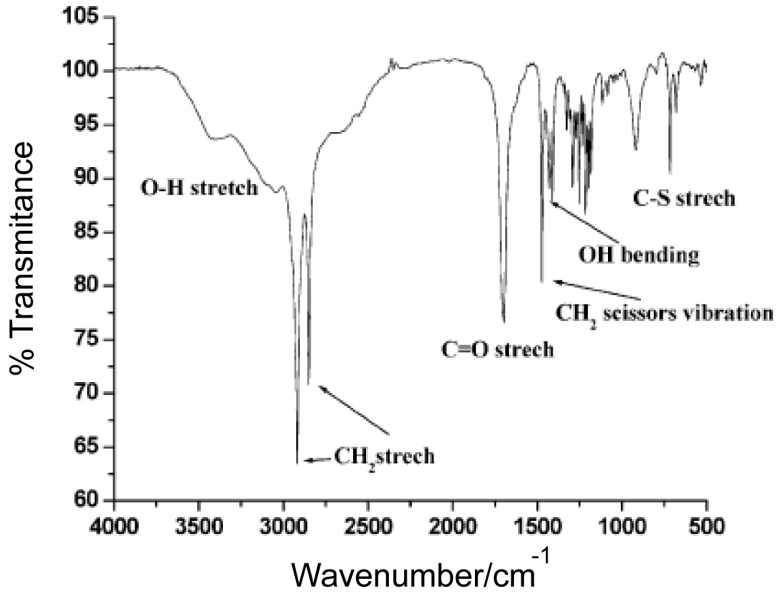

Fig. 4.6: FT-IR spectra of 16-mercaptohexadecanoic acid in KBr cell. [4.12]

4.2 Electric Double Layer theory and DLVO theory

The principle behind this nanoparticles are aligned by the guiding structure is the interaction between charged nanoparticles and charged guiding structure surface.

When a solid emerges in a polar solvent or an electrolyte solution, a surface charge will be developed through one or more of the following mechanisms: (1) Preferential adsorption of

ions. (2) Dissociation of surface charged species. (3) Accumulation or depletion of electrons at the surface. (4) Physical adsorption of charged species onto the surface. (5) Isomorphic substitution of ions.

4.2.1 Surface Charge Density

For a given solid surface in a given liquid medium, a fixed surface electrical charge density or electrode potential, E, will be established, which is given by the Nernst equation:

$$E = E_0 + \left(R_g T / n_i F\right) \ln a_i \qquad \text{(eq. 4.2)}$$

where E_o is the standard electrode potential when the concentration of ions is unity, n_i is the valence state of ions, R_g is the gas constant and T is temperature, F is the Faraday's constant, and a_i is chemical activity.

The surface charge in oxides is mainly derived from preferential dissolution or deposition of ions. Ions adsorbed on the solid surface determine the surface charge, and thus are referred to as charge determining ions, also known as co-ions. In the oxide systems, typical charge determining ions are protons and hydroxyl groups and their concentrations are described by pH (pH = -log $[H^+]$). As the concentration of charge determining ions varies, the surface charge density changes from positive to negative or vice versa. The concentration of charge determining ions corresponding to a neutral or zero-charged surface is defined as a point of zero charge (p.z.c.).

At pH > p.z.c., the oxide surface is negatively charged, since the surface is covered with hydroxyl groups, OH^-, which is the electrical determining ion. At pH < p.z.c., H^+ is the charge determining ions and the surface is positively charged. The surface charge density or surface potential, E in volt, can then be simply related to the pH and the Nernst equation (eq. 4.1) can be written as

$$E = 2.303 R_g T\left[\left(p.z.c.\right) - pH\right] / F \qquad \text{(eq. 4.3)}$$

Table 4.1: A List of z.p.c. of Some Common Oxides in Water

Solids	z.p.c.
WO_3	0.5
V_2O_5	1-2
d-MnO_2	1.5
b-MnO_2	7.3
SiO_2	2.5
SiO_2 (quartz)	3.7
TiO_2	6
TiO_2 (calcined)	3.2
SnO_2	4.5
Al-O-Si	6
ZrO_2	6.7
FeOOH	6.7
Fe_2O_3	8.6
ZnO	8
Cr_2O_3	8.4
Al_2O_3	9
MgO	12

4.2.2 Electric Double Layer in Electrolyte

When a surface charge density of a solid surface is established, there will be an electrostatic force between the solid surface and the charged species in the proximity to segregate positive and negatively charged species. However, there also exist Brownian motion and entropic force, which homogenize the distribution of various species in the solution. In the solution, there always exist both surface charge determining ions and counter-ions, which have opposite charge of the determining ions. Although charge neutrality is maintained in a system, distributions of charge determining ions and counter-ions in the proximity of the solid surface are inhomogeneous and very different. The distributions of both ions are mainly controlled by a combination of the following forces: (1) Coulombic force or electrostatic force (2) Entropic force or dispersion (3) Brownian motion [4.15].

The combined result is that the concentration of counter ions is the highest near the solid surface and decreases as the distance from the surface increases, whereas the concentration of determining ions changes in the opposite manner. Assuming surface charge is positive. Such inhomogeneous distributions of ions in the proximity of the solid surface lead to

the formation of so-called double layer structure. The double layer consists of two layers, Stern layer and Gouy layer (also called diffuse double layer) which are separated by the Helmholtz plane [4.16, 4.17].

Stern layer is an inner sub-layer that built by the counter-ions specifically adsorb near the surface (between the solid surface and the Helmholtz plane), where the electric potential drops linearly through the tightly bound layer of solvent and counter-ions.

Diffuse layer is the outer part of the screening layer (beyond the Helmholtz plane until the counter ions reach average concentration in the solvent), where the counter ions diffuse freely and the electric potential does not reduce linearly.

The diffuse layer, or at least part of it, can move under the influence of tangential stress. There is a conventionally introduced slipping plane that separates mobile fluid from fluid that remains attached to the surface. Electric potential at this plane is called zeta potential (denoted as ζ-potential).

The electric potential drops approximately following

$$E \propto e^{-\kappa (h-H)} \qquad \text{(eq. 4.4)}$$

κ^{-1} is known as the Debye-Hückel screening strength and is also used to describe the thickness of double layer (Fig. 4.7).

$$\kappa = \{(F^2 \Sigma_i C_i Z_i^2)/(\varepsilon_r \varepsilon_o R_g T)\}^{1/2} \qquad \text{(eq. 4.5)}$$

F is Faraday's constant = N_A e = 6.02 x 10^{23}(mol^{-1}) x 1.602 x 10^{-19} (C) = 96485 (C/mol)
ε_o is the permittivity of vacuum = 8.854 x 10^{-12} (F/m)
ε_r is the dielectric constant of the solvent
C_i and Z_i are the concentration and valence of the counter-ions of type I
R is ideal gas constant =8.314 (N m/mol K)

The electric potential at the proximity of solid surface decreases with increased concentration and valence state of counter-ions, and increases with an increased dielectric constant of the solvent exponentially. Higher concentration and valence state of counter-ions would result in a reduced thickness of both Stern layer and diffuse double layer.

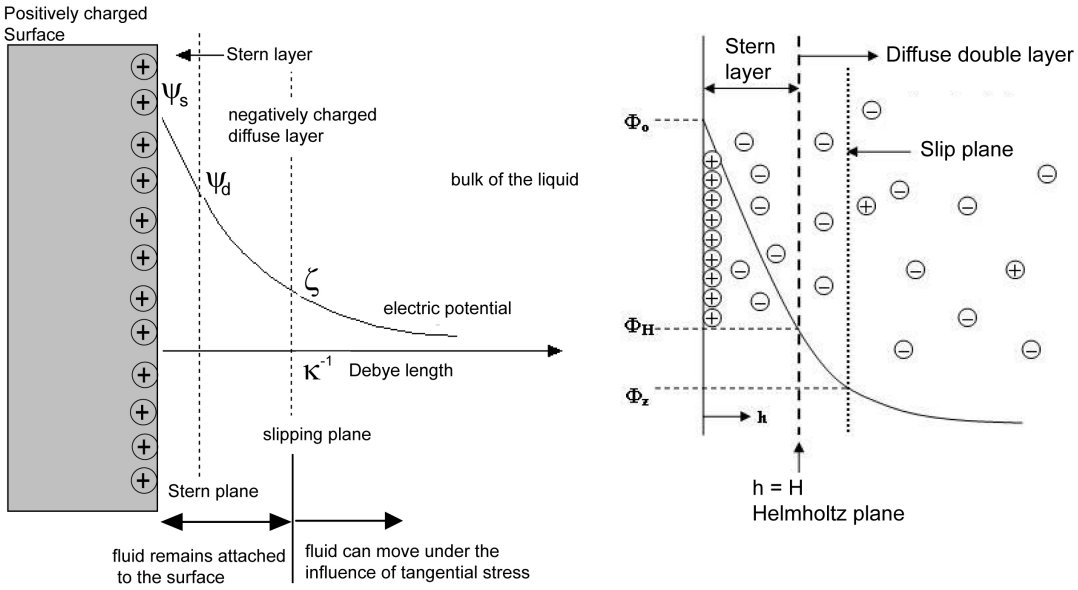

Fig. 4.7: Electric double layer for the plane surface [4.18].

Although, the above discussion has been focused on a flat solid surface in an electrolyte solution, the concepts are applicable to curved surfaces as well. Assuming that the surface is smooth and thus the surface charge is distributed uniformly. Also, the surface charge density is constant, so that the electric potential in the surrounding solution can be described using eq. 4.2 and 4.3, too. Such assumptions are certainly valid for spherical particles, particles are dispersed in an electrolyte solution and the distance between any two particles are large enough so that the charge distribution on particle surface is not influenced by other particles.

The electrostatic repulsion between two particles arises from the electric surface charges, which are attenuated to a varied extent by the double layers. When two particles are far apart, there will be no overlap of two double layers and electrostatic repulsion between two particles is zero. However, when two particles approach one another, double layer overlaps and a repulsive force develops. An electrostatic repulsion between two equally sized spherical particles is:

$$\Phi_R = 2 \pi \varepsilon_r \varepsilon_o r E^2 \exp(-\kappa S) \qquad \text{(eq. 4.6)}$$

S: separation distance between particles.

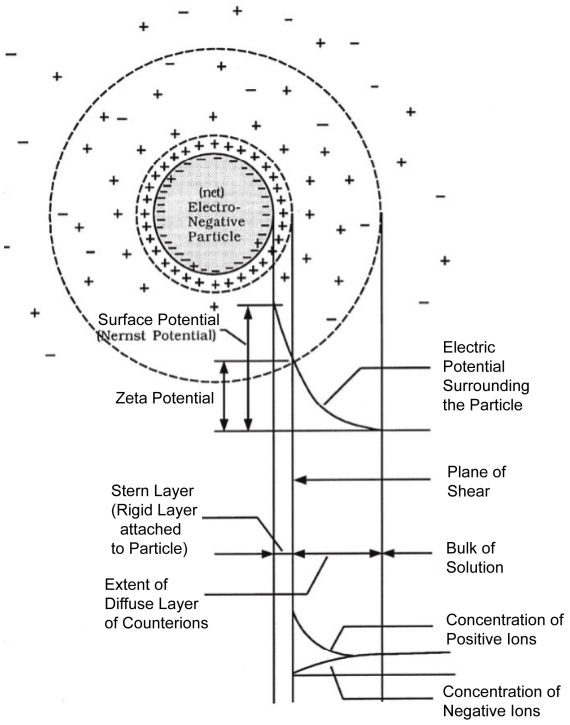

Fig. 4.8: Electric double layer for particle surface. [4.18]

4.2.3 Van Der Waals Force

When particles are small, typically in micrometers or less, and are dispersed in a solvent, van der Waals attraction force and Brownian motion play important roles, whereas the influence of gravity becomes negligible. Van der Waals force is a week force and becomes significant only at a very short distance. Brownian motion ensures the nanoparticles colliding with each other all the time. The combination of van der Waals attraction force and Brownian motion would result in the formation of agglomeration of the nanoparticles. Van der Waals interaction between two nanoparticles is the sum of the molecular interaction for all pair of molecules composed of one molecule in each particle, as well as to all pairs of molecules with one molecule in a particle and one in the surrounding medium such as solvent.

Integration of all the van der Waals interactions between two molecules over two spherical particles of radius, r, separated by a distance, S, gives the total interaction energy or attraction potential

$$\Phi_A=-A/6\ \{2r^2/(S^2+4rS)+2r^2/(S^2+4rS+4r^2)+\ln[(S^2+4rS)/(S^2+4rS+4r^2)]\} \quad \text{(eq. 4.7)}$$

Negative sign: the attraction nature of the interaction between two particles
A: positive constant termed the Hamaker constant

The total interaction between two particles, which are electrostatic stabilized, is the combination of van der Waals attraction and electrostatic repulsion:

$$\Phi = \Phi_A + \Phi_R \quad \text{(eq. 4.8)}$$

The following tables give the common useful parameters that required for the van der Waals force calculation.

Table 4.2: Simple Formulas for the Van der Waals Attraction Between Two Objects [4.13]

Particles	Φ_A
Two spheres of equal radius, r*	$-A\,r/12S$
Two spheres of unequal radii, r_1 and r_2*	$-A\,r_1 r_2/6S(r_1+r_2)$
Two parallel plates with thickness of δ, interaction per unit area	$-A/12\pi[S^{-2} + (2\delta+S)^{-2} + (\delta+S)^{-2}]$
Two blocks, interaction per unit area	$-A/12\pi S^2$

*: r, r_1 and r_2 >> S

Table 4.3: Hamaker Constants for Some Common Materials [4.13]

Materials	A_i (10^{-20}J)
Metals	16.2-45.5
Gold	45.3
Oxides	10.5-15.5
Al_2O_3	15.4
MgO	10.5
SiO_2 (fused)	6.5
SiO_2 (quartz)	8.8
Ionic crystals	6.3-15.3
CaF_2	7.2
Calcite	10.1
Polymers	6.15-6.6
Polyvinyl chloride	10.82
Polyethylene oxide	7.51
Water	4.35
Acetone	4.20
Carbon tetrachloride	4.78
Chlorobenzene	5.89
Ethyl acetate	4.17
Hexane	4.32
Toluene	5.40

4.2.4 DLVO Theory

The electrostatic stabilization of particles in a suspension is successfully described by the DLVO theory, named after Derjaguin, Landau, Verwey, and Overbeek. The interaction between two particles in a suspension is considered to the combination of van der Waals attraction potential and the electric repulsion potential. There are some important assumptions in the DLVO theory: (1) Infinite flat solid surface, (2) Uniform surface charge density, (3) No re-distribution of surface charge, i.e., the surface electric potential remains constant. (4) No change of concentration profiles of both counter-ions and surface charge determining ions, i.e., the electric potential remains unchanged, and (5) Solvent exerts influences via dielectric constant only, i.e., no chemical reactions between the particles and solvent [4.14].

It is very clear that some of the assumptions are far from the real picture of two particles dispersed in a suspension. For example, the surface of particles is not infinitely flat, and the surface charge density is most likely to change when two charged particles get very close to

each other. However, in spite of the assumptions, the DLVO theory works very well in explaining the interactions between two approaching particles, which are electrically charged, and thus is widely accepted in the research community of colloidal science.

At a distance far from the solid surface, both van der Waals attraction potential and electrostatic repulsion potential reduce to zero. Near the surface is a deep minimum in the potential energy produced by the van der Waals attraction. A maximum is located a little farther away from the surface, as the electric repulsion potential dominates the van der Waals attraction potential. The maximum is also known as repulsive barrier. If the barrier is greater than ~10 kT, where k is Boltzmann constant, the collisions of two particles produced by Brownian motion will not overcome the barrier and agglomeration will not occur.

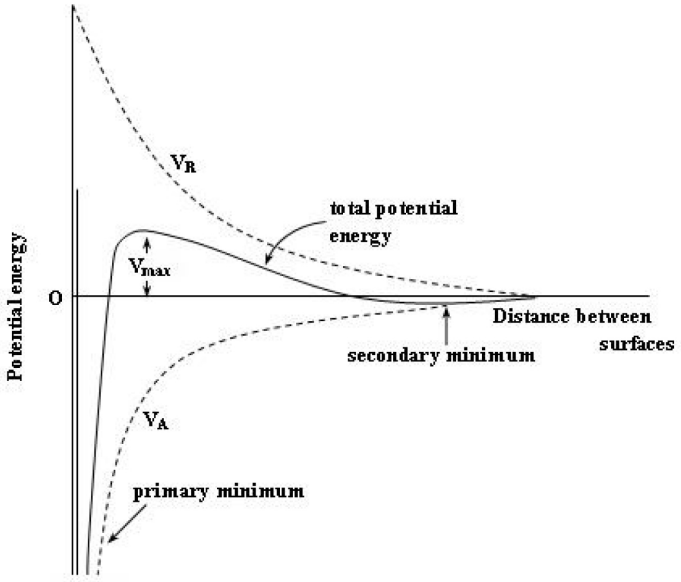

Fig. 4.9: Interaction potential energy of DLVO theory. Van der Waals attraction potential and electric repulsion potential between two charged particles in electrolyte environment [4.14].

Since the electric potential is dependent on the concentration and valence state of counter-ions as given in eq. 4.5 and 4.6 and the van der Waals attraction potential is almost independent of the concentration and valence state of counter-ions, the overall potential is strongly influenced by the concentration and valence state of counter-ions. An increase in concentration and valence state of counter-ions results in a faster decay of the electric potential.

As a result, the repulsive barrier is reduced and its position is pushed towards the particle surface.

It should be noted that the repulsion is not directly due to the surface charge on solid particles; instead it is the interaction between two double layers. The other is the osmotic flow. When two particles approach one another, the concentrations of ions between two particles where two double layers overlap, increase significantly, since each double layer would retain its original concentration profile. As a result, the original equilibrium concentration profiles of counter ions and surface charge determining ions are destroyed. To restore the original equilibrium concentration profiles, more solvent needs to flow into the region where the two double layers overlap. Such an osmotic flow of solvent effectively repels two particles apart, and the osmotic force disappears only when the distance between the two particles equals to or becomes larger than the sum of the thickness of the two double layers.

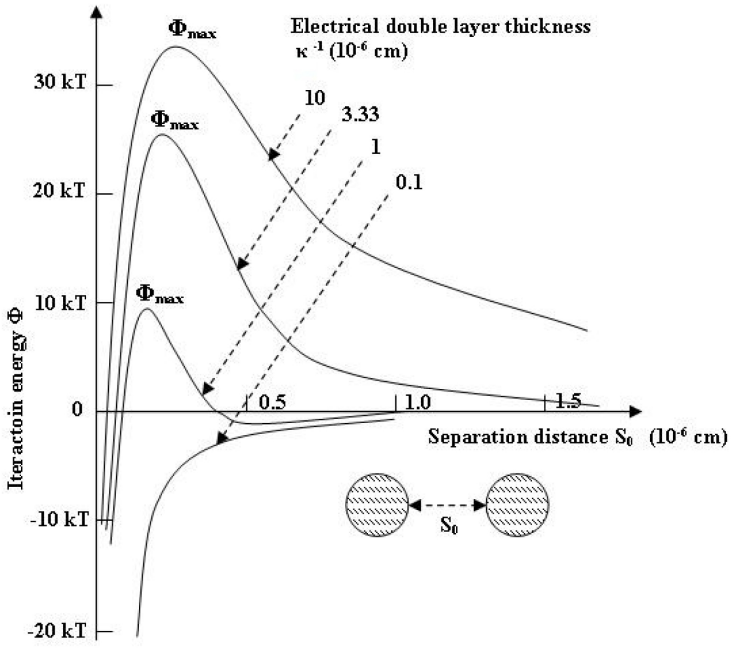

Fig. 4.10: The influence of interaction energy by concentration and valence state of counter-ions [4.15].

CHAPTER 5

EXPERIMENT STEPS

5.1 Device Design

The DNA detecting device is prepared by E-beam lithography, metal deposition and lift-off process in our study, but the real device can be manufactured by current CMOS techniques at wafer scale.

We create a simple pattern with square SiO_2 ring (100um in length, 90nm in width of the ring) between inside and outside gold electrodes on SiO_2 substrate. Inside and outside gold surface can be used as source and drain electrodes (Fig. 5.3). The square SiO_2 ring width is decided due to the gold nanoparticle size we use in the experiment. Our DNA detection method is based on the hybridization events that occur between C-50au and T-P-30au. When complementary T-ssDNA exist, Capture-ssDNA modified 50nm GNP and Probe-ssDNA modified 30nm GNP can be linked together and form 50au-C-T-P-30au. This 50au-C-T-P-30au is the GNP bridge in our detection mechanism which provides an electrical pathway for electrons flowing from source electrode to drain electrode. Therefore, the width of square SiO_2 ring should be suitable for the GNP bridge size. In order to have best detection sensitivity, we wish to detect T-ssDNA through the 50au-C-T-P-30au formed from every single hybridization event; therefore, the SiO_2 gap is chosen for ~90nm width.

The relationship between SiO_2 band width and 50au-C-T-P-30au GNP bridges are shown at Fig. 5.1. When the SiO_2 width is larger than 120nm, the GNP bridge can not form even with more than one hybridization events (Fig. 5.1 (a1)-(a4)). When SiO_2 width is 120nm, GNP bridge can be formed only when C-50au located in the center with more than two

hybridization events. When the SiO_2 width is around 90nm width, GNP bridge can be formed in most of the situations even with only one hybridization event, except for the case of Fig. 5.1 (c1). However, Fig 5.1 (c1) is usually not the real case in our experiment because we heat C-50au solution up to 50^{o}C during the C-50au positioning process to prevent C-50au aggregation. The thermal energy can cause the deviation on C-50au alignment in the center of SiO_2 band. This is to say, 90nm gap width is the best width we can choice to achieve high detection sensitivity. Also, if the gap is smaller than 90nm, the positioning of C-50au will be very difficult due to the repelling force provided from gold electrode surface can strongly affect the attraction force from APTES on SiO_2 surface.

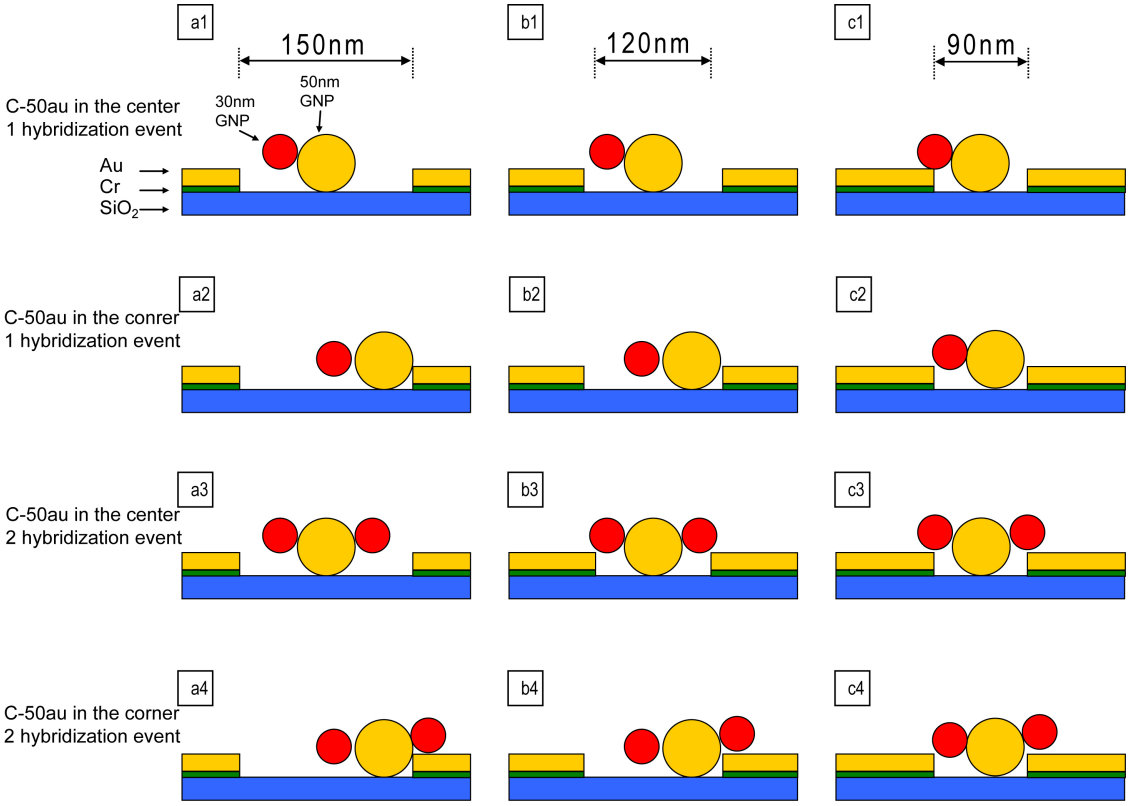

Fig. 5.1: The relationship between SiO_2 band width and 50au-C-T-P-30au GNP bridge. (a1)~(a4), SiO_2 gap >120nm, C50au-T-P-30au can not form GNP bridge even with more than one hybridization events. (b1)~(b4) SiO_2 gap = 120nm, GNP bridge can be form only when C-50au is in the center with more than one hybridization event. (c1)~(c4) SiO_2 gap = 90nm, GNP bridge can be form at (c2), (c3), (c4) situation, but can not form at (c1)situation. But in the real experiment, instead of (c1) and (c3), (c2) and (c4) are usually the real situations because we heat C-50au solution to 50^{o}C during C-50au positioning to prevent aggregation between C-50au. The thermal energy will cause the deviation of C-50au from the gap center.

5.2 Patterned Device Preparation

After the size of DNA detection device is decided, we can now fabricate the device with e-beam lithography. Again, we want to emphasize that the real devices can be fabricated using current photolithography techniques at wafer scale.

5.2.1 E-beam Lithography, Metal Deposition and Lift-Off Process

We first spin coating a layer of negative e-beam resist, AR-N 7520, with 8000rpm/2min on a Si wafer with ~1um thermal oxidation SiO_2 layer on the surface, the thickness of resist is around 500nm. The sample is then baked on a hot plate with 85^{o}C/1min and cool down to room temperature. After e-beam writing, the sample is immersed in developer for 1min developing and then immersed in DI water for rinsing. After drying the sample with N2 gas, we deposit 5nm Cr and 15nm Au on both sides of sample using e-beam evaporation process, then we immerse samples into acetone and sonicate for at least 30min (lift-off process). 5nm Cr is used as an adhesive layer in between

The negative resist is chosen for two reasons: (1) With negative resist, the writing area is small (the exposed SiO_2 band area). (2) The profile of negative resist pattern is good for lift-off process. Fig. 5.2 shows the bad side wall generated due to the profile of positive resist pattern. While metal deposition, the deposited metal will form a continuous thin film on the side wall of resist, too. Therefore, during lift-off process, the continuous thin file on the side wall can not be removed totally, especially for the ductile metal as Cr and Au.

The reason why the smooth side wall is important to us is: the roughness of side wall might provide false signal for the DNA detection. The protrusion of remained metal thin film may contact with nanoparticles and provide a pathway between two gold electrodes.

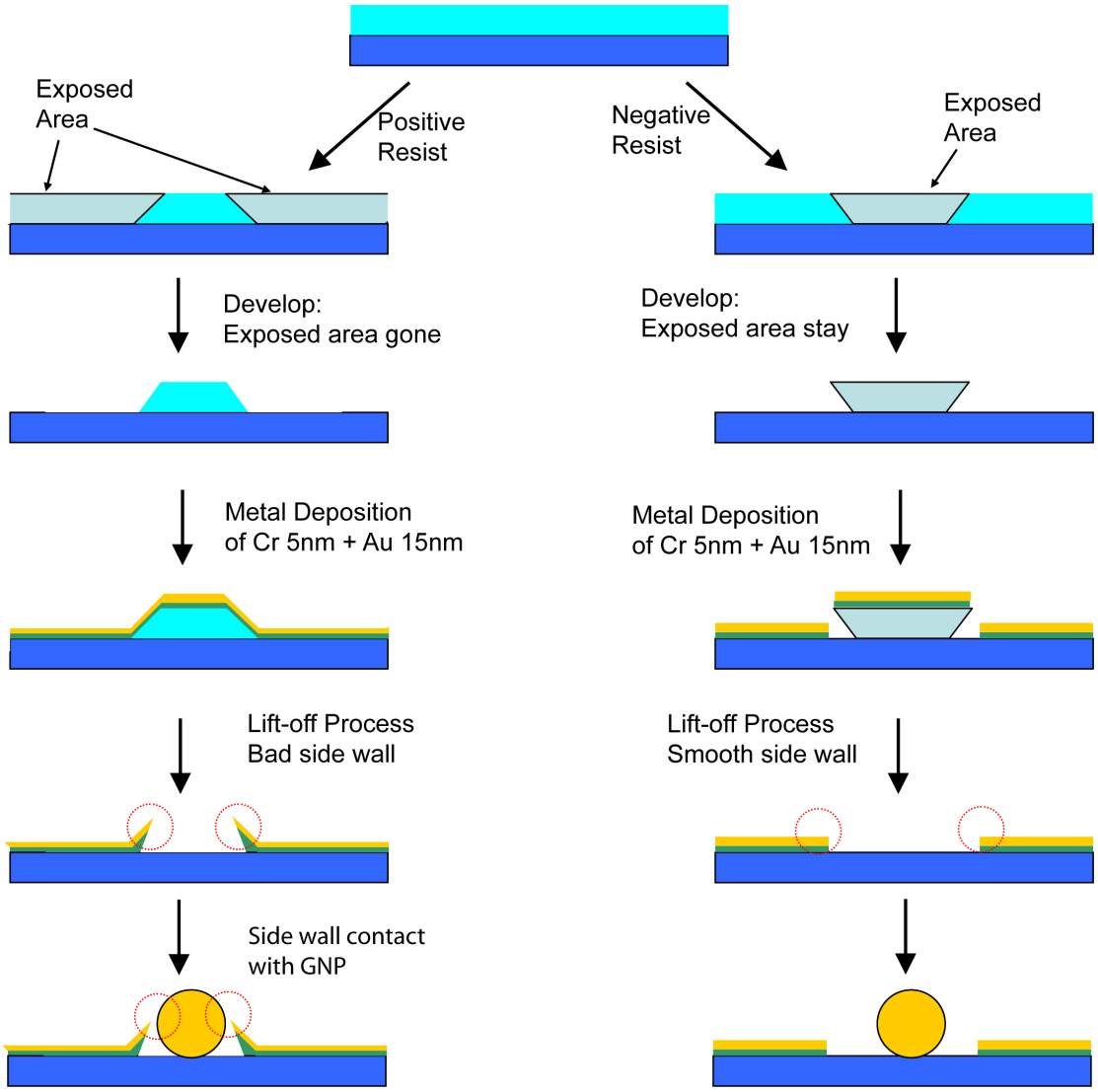

Fig. 5.2: The sketch of sample side wall smoothness prepared by positive or negative photo/e-beam resists. Negative resist is suitable for lift-off process due to the relatively smooth side wall.

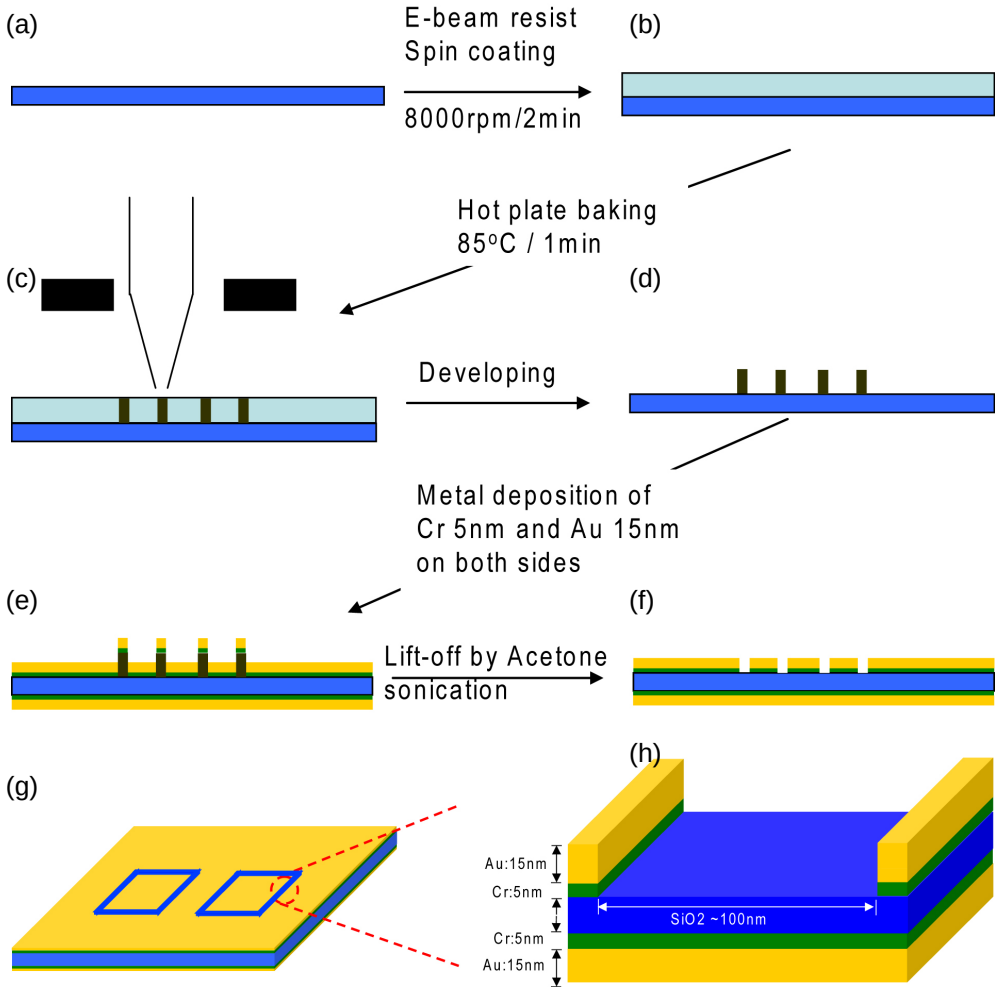

Fig. 5.3: Sample preparation process. (a)~(d): E-beam lithography. (e) Metal deposition on both side with 5nm Cr and 15nm Au. (f) Lift-off process, acetone sonication for 30~40mins. (g)-(h) The structure of the DNA detecting device

5.2.2 Sample Cleaning

After lift-off, the samples go through a cleaning procedure including acetone rinsing, UV-Ozone 90~120min, followed by immersion in Ethanol for overnight, and then the samples are dried with N2 gas and stored in nitrogen box.

The cleaning procedure is very important for our DNA detection method due to the following reasons: (a) Residuales from photo or e-beam resist, which are organics with variety of functional group. Those residues will cause serious problems not only for the sample surface itself, but can also contaminate the DNA solution while the sample immersion. (b) The residue will seriously affect the formation of SAMs layer. Without good SAMs layer, the accurate positioning of GNPs can not be done.

Instead of using oxygen plasma to burn out the residual organics, we use UV-Ozone to clean the sample. UV-Ozone is a photo-sensitized oxidation process in which the contaminant molecules of photo resists, cleaning solvent residues and flux are excited and/or dissociated by the absorption of short-wavelength UV radiation. Atomic oxygen is simultaneously generated when molecular oxygen is dissociated by 184.9 nm and ozone by 253.7 nm UV. The 253.7 nm UV radiation is absorbed by most hydrocarbons and also by ozone. The products of this excitation of contaminant molecules react with atomic oxygen to form simpler, volatile molecules which desorbs from the surface. Therefore, when both UV wavelengths are present atomic oxygen is continuously generated, and ozone is continually formed and destroyed.

All the samples require another cleaning procedure including acetone rinse, UV-Ozone cleaning (20~30mins) and ethanol immersion (2~3hrs) to remove gold oxide formed during UV Ozone process.

Usually acetone sonication and UV-Ozone cleaning is good enough for the normal photo/e-beam resist cleaning, however, there are some kinds of e-beam resist which are difficult to clean. PMMA is a commonly used e-beam resist, which is difficult to clean by just acetone sonication and UV-Ozone, a Dichlorobenzene (DCB) immersion for overnight is required to clean the sample surface efficiently.

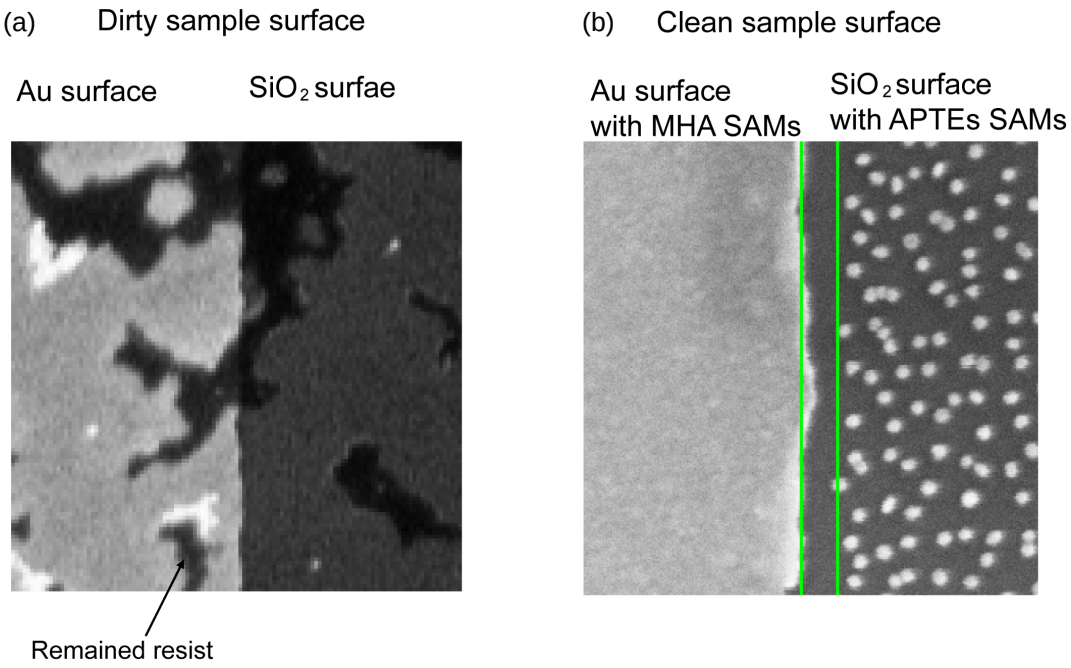

Fig. 5.4: Dirty surface and clean surface. (a) Dirty surface after lift-off process without future cleaning, the black broken film-like contamination cover the sample surface and affect the SAMs formation, colloidal gold nanoparticle stability and GNP attachment. The aggregation of GNP is founded. (b) Clean surface of lithography patterned sample with UV-Ozone cleaning followed by EtOH immersion. The SAMs layer quality is good and colloidal gold nanoparticle is stable and attach only on SiO_2 surface.

5.3 Single Strand DNA Modified Gold Nanoparticles Preparation

There are two DNA modified Gold Nanoparticles (GNP) we need in our experiment, Capture single strand DNA modified 50nm GNP (C-50au) and Probe single strand DNA modified 30nm GNP (P-30au). All the single strand oligo-nucleotides are purchased from Alpha-DNA. The DNA sequences and modifications are listed below.

Table 5.1: ssDNA Sequence and Modification

Name	Sequence
Capture	5'-AACTACTCCTCTACTGCG-TTTTTTTTT-3'-$(CH_2)_3$-SH'
Target	5'-CGCAGTAGAGGAGTAGTTGTTAGGGAGTGTGGATGG-3'
Probe	HS-$(CH_2)_6$-5'-TTTTTTTTT-CCATCCACACTCCCTAAC-3'
3mm	5'-CGCAGGAGTGGCGTAGTTGTTAGGGAGTGTGGATGG-3'

Capture (C-ssDNA): 3' end thiol modified single strand DNA:

C-ssDNA is 18 base pair single strand DNA with 9 base pair poly T as spacer and thiolated at 3' end. C-ssDNA is the DNA we use to modified 50nm gold nanoparticles (50nm GNP) through thiol-gold reaction and form C-ssDNA-50nm GNP (C-50au).

Probe (P-ssDNA): 5' end thiol modified single strand DNA:

P-ssDNA is 18 base pair single strand DNA with 9 base pair poly T as a spacer and thiolated at 5' end. P-ssDNA is the DNA we use to modified 30nm GNP through thiol-gold reaction and form P-ssDNA-30nm GNP (P-30au)

Target (T-ssDNA):

T-ssDNA is 36 base pair single strand DNA without any modifications. Half of T-ssDNA is complementary to C-ssDNA, and the other half is complementary to P-ssDNA.

3mm (3mm-ssDNA): three base pair mismatch single strand DNA:

3mm-ssDNA is the DNA we use as an indication between specific and non-specific hybridization. Half of 3mm-ssDNA has three base pair mismatch to C-ssDNA, but the other half is complementary to P-ssDNA.

5.3.1 C-ssDNA Modified 50nm GNP (C-50au) Preparation

1 tube of dried C-ssDNA sample (~45 nmole) is first centrifuge at 3000rpm/3min. Add 2ml TE buffer (pH 7.4) and shaking for 2-3hrs (C-ssDNA/TE) at room temperature. Take 0.2ml of this C-ssDNA/TE and add into 2ml 50nm gold colloid, shaking for 2days at room temperature (C-50au). Add NaCl = 0.1M into C-50au solution and heat up to 50^{o}C for overnight, collect top pink clean solution and dispose of any black precipitation at the tube bottom. The black precipitation on the bottom is usually the aggregated not well-modified GNPs, which are unstable due to the high salt concentration environment. The well modified GNP is still remaining stable due the covalent bond formation between ssDNA and GNP surface through thiol-gold reaction.

After collect top pink clean solution which contains C-50au, excess C-ssDNA and NaCl, we need a purify step to collect only C-50au.

In order to ensure all the 50nm GNP can be well modified by thiolated C-ssDNA, the amount of C-ssDNA we add into 50nm GNP is much more than we need. In other words, we have now a lot of excess C-ssDNA and NaCl exist in the C-50au solution. In order to remove those excess C-ssDNA and NaCl, we use centrifuge and wash steps and repeat for 8~10 times.

Centrifuge and wash steps include: a) Centrifuge C-50au solution at 8000rpm/5min to spin down C-50au. b) Remove top clean solution which contains excess C-ssDNA and NaCl. c) Re-suspend bottom red oil-like C-50au into 2ml TE buffer solution.

However, the experiment results show that there are still a lot of excess C-ssDNA remain in the C-50au solution. The P-30au preparation is the same as C-50au.

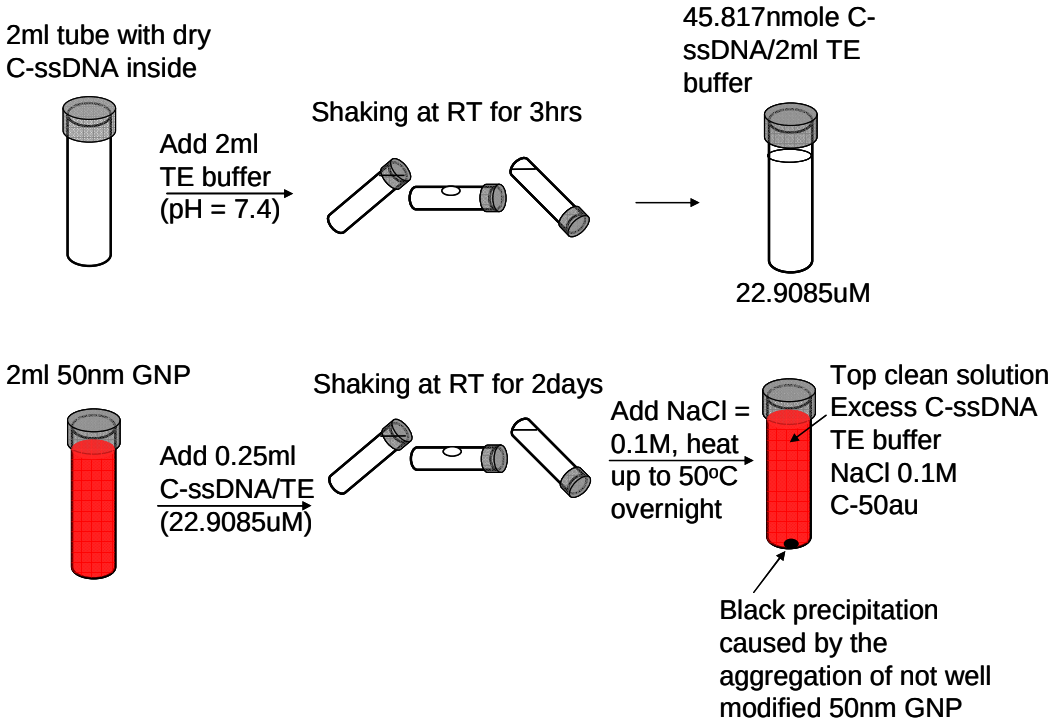

Fig. 5.5: ssDNA modified GNP preparation steps. C-ssDNA or P-ssDNA is thiol modified artificial DNA, and dried to the powder form in the sample tube for shipping. 3000rpm/3min centrifuge is preferred before add TE buffer solution to dissolve ssDNA. After add TE buffer solution (pH 7.4) into sample tube, shaking at room temperature (or at 4^{o}C is preferred if cold room is available) for 2~3 hours before mixing with GNP solution. Mix thiolated ssDNA with GNP in the sealed tube and shaking for 2 days for surface modification process. Thiol group of thiolated ssDNA will form chemical bond to the GNP surface.

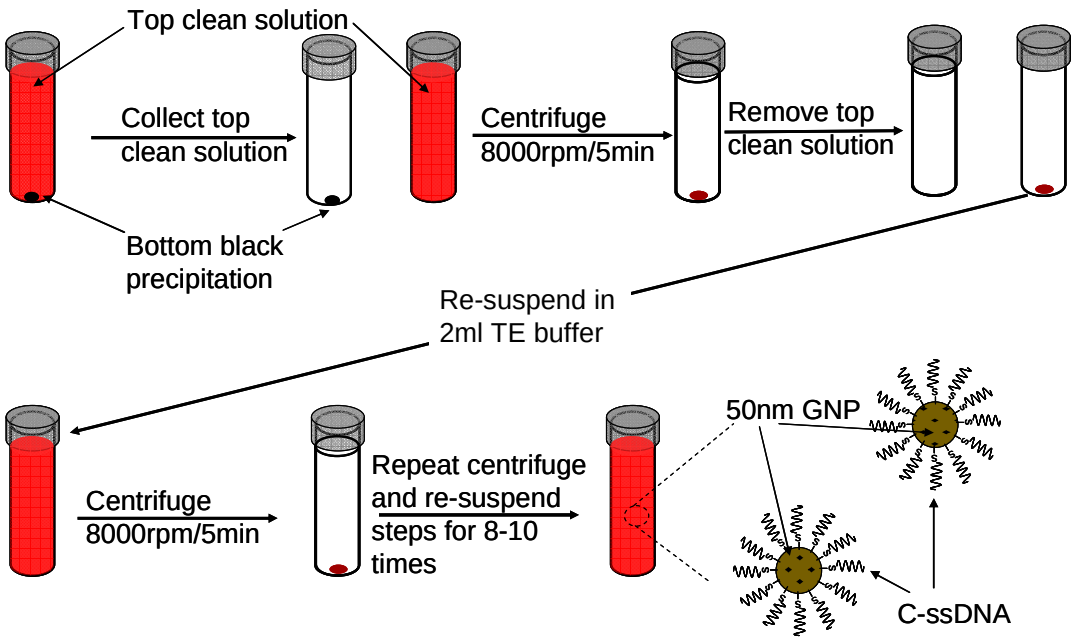

Fig. 5.6: Centrifuge/Wash step: To remove excess C-ssDNA and NaCl we added into the ssDNA modified GNP solution, we need a centrifuge/wash steps. C-50au can be centrifuge down to the bottom and form red oil-like precipitation with 8000rpm/5min, which P-30au requires 10000rpm/10min. After centrifuge, the top clean colorless solution containing salt and excess DNA is removed. And the bottom red oil-like C-50au is re-suspended into 2ml TE buffer.

5.4 C-50au Placement

In our design, we need C-50au be placed into ~90nm SiO_2 area between two gold electrodes only. In order to accurately guild C-50au in the position we want, two different SAMs are applied. The SiO_2 surface is functionalized with positively charged amine group terminated APTES SAMs and gold electrode surface is functionalized with negatively charged carboxyl terminated 16MHDA SAMs. The interaction force between SAMs and DNA modified GNPs is related to: (1) Surface charge density of APTES and 16MHDA SAMs. (2) Ion concentration. (3) Distance between charged object.

The SAMs modification steps are as follow:

1. Samples are processed with UV-Ozone 30min and then immersed into EtOH for 2hrs, use N_2 gas dry before use.
2. Sample immerse in APTES solution (0.4ml APTES+80ml EtOH) for 1hr, RT
3. Take out the sample and rinse in EtOH (add NaOH, pH=12) for 10sec
4. Rinse with EtOH, and then dry with N_2 gas.
5. Immerse into 16-MHA solution (0.05g 16-MHA + 80ml EtOH) for 3hrs, RT
6. Rinse sample into 1% HCl/EtOH for 10sec
7. Rinse sample with EtOH and then dry with N_2 gas

After processing with SAMs, we immerse the sample into 50nm colloidal gold solution, the negative charged GNPs will attracted to SiO2 surface by the attraction force originated from positively charged amine group of APTES SAMs, and be further pushed toward the center of SiO2 by negatively charged carboxyl group of 16MHDA SAMs on gold surface.

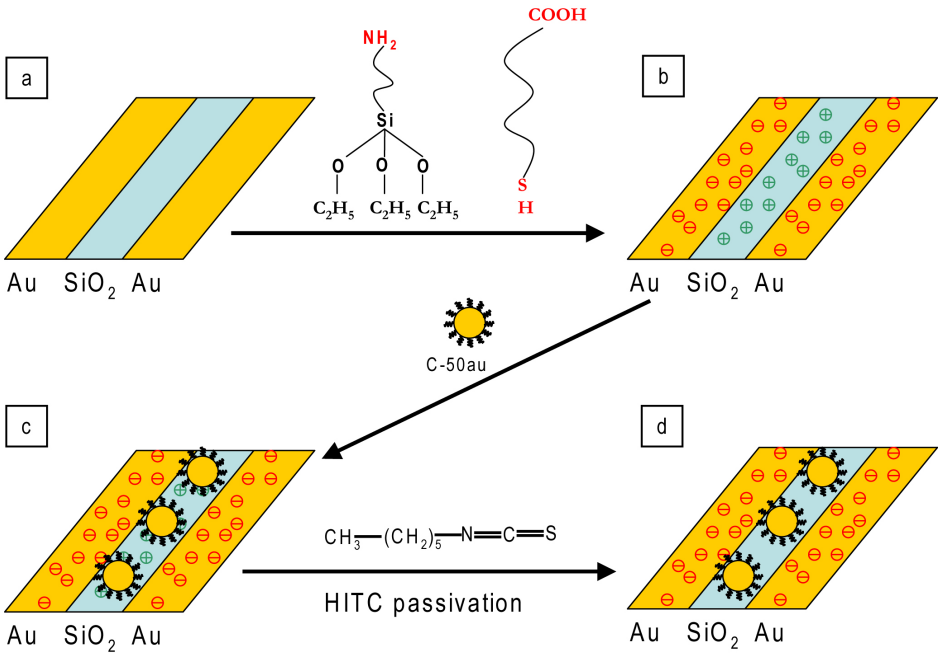

Fig. 5.7: Accurate control of charged nanoparticle placement. (a) Sample with Au and SiO_2 surface. (b) After modification of APTES and MHA SAMs, Au surface is now negatively charge due to the carboxyl group of MHA dissociation (-COOH→-COO^-). SiO2 surface is positively charged due to the amine group of APTES dissociation (-NH_2 → -NH_3^+). (c) C-50au is negatively charged due to the phosphate ssDNA back bone dissociation (-PO_4^-) and therefore can be guided into positively charged surface only. (d) The passivation reaction using HITC react with APTES.

5.5 Passivation of Excess APTES

Hexyl isothiocyanate (HITC) is used to react with the excess amino group on APTES SAMs which is not occupied by C-50au. To make a passivation solution, we mix 0.1ml HITC with 45ml DMSO and 5ml pyridine and pre-heat up to 45°C. Samples with APTES SAMs and DNA modified GNPs are immersed into the passivation solution for 4-5hrs at 45°C followed by rinse with autoclaved DI water and dry with N_2 gas.

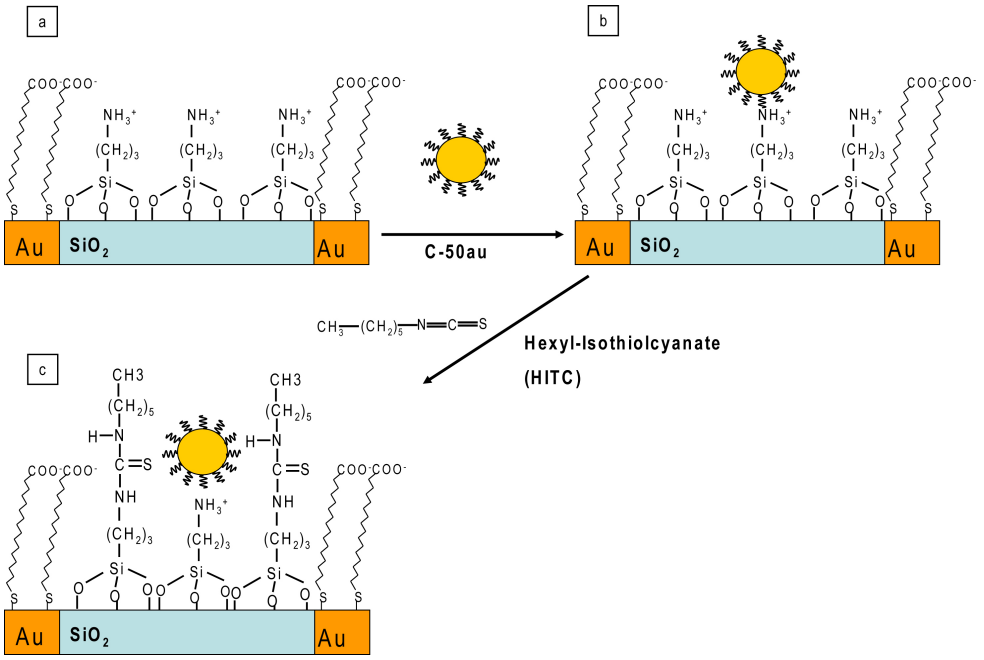

Fig. 5.8: Passivation step. (a) Patterned sample functionalized with APTES and 16MHA SAMs. (b)C-50au is guided into APTES/SiO_2 area. (c) HITC react with unoccupied amine ($-NH_3^+$)

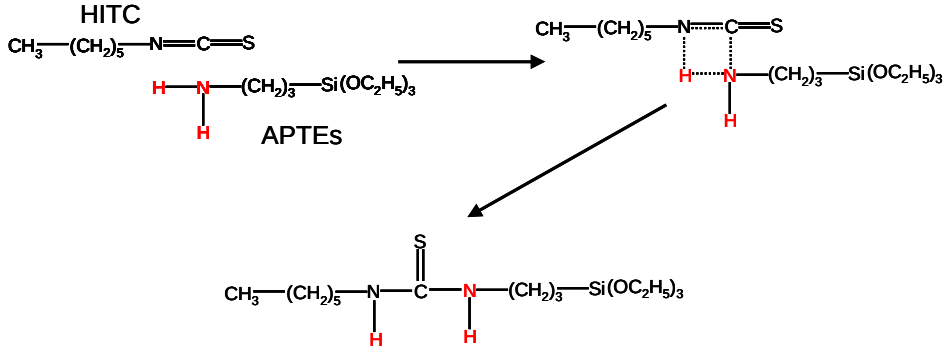

Fig. 5.9: Detail reaction mechanism of HITC react with APTES. R-N=C=S functional group of HITC will react with $-NH_2$ functional of APTES [5.1, 5.2].

5.6 T-P-30au hybridization

We apply three-ssDNA system in our study, C-ssDNA, T-ssDNA and P-ssDNA. We first let T-ssDNA hybridize with P-30au and form T-P-30au in the homogeneous liquid phase and then hybridize T-P-30au with C-50au which is fixed on the device surface (heterogeneous hybridization). We add 10% (v/v) Hybridization Buffer in the P-30au solution for hybridization and let 20nM T-ssDNA hybridize with P-30au for 3hrs at 45^{o}C. After T-P-30au is made, we put our sample with C-50au fixed on the device surface into T-P-30au for 3hrs at 45^{o}C. After heterogeneous hybridization of C-50au with T-P-30au, the sample is immersed into Washing Buffer 1, 45^{O}C/20min then Washing Buffer 2, 45^{o}C/overnight.

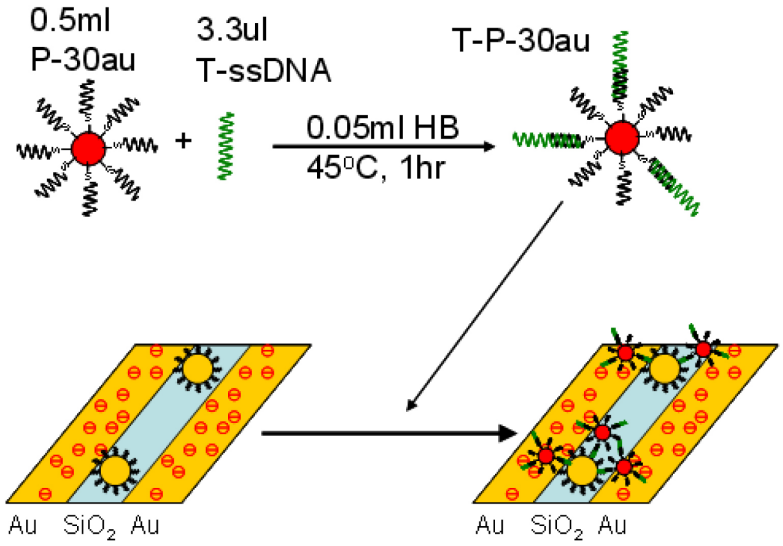

Fig. 5.10: T-P-30 hybridize with C-50 on narrow trench area. T-P-30au is made in the liquid phase by mixing T-ssDNA and P-30au with 10% v/v hybridization buffer. Sample with C-50au and passivation step is immersed into T-P-30 solution for T-P-30au and C-50au hybridization.

5.7 Chemicals Used in Experiment

50 nm Colloidal gold: 4.5 x 10^{10} particles/ml (Ted Pella)

30 nm Colloidal gold: 2.0 x 10^{11} particles/ml (Ted Pella)

20 nm Colloidal gold: 7.0 x 10^{11} particles/ml (Ted Pella)

DI water: ultra pure water, 18.2 MΩ

Ethanol: 200 proof, anhydrous, ≥99.5% (Sigma-Aldrich), CAS: 64-17-5

Isopropanol: anhydrous, 99.5% (Sigma-Aldrich), CAS: 67-63-0

Acetone: CHROMASOLV® Plus, for HPLC, ≥99.9% (Sigma-Aldrich), CAS: 67-64-1

DMSO: Dimethyl sulfoxide, BioReagent, for molecular biology, ≥99.9% (Sigma), CAS: 67-68-5

Dichloromethane: anhydrous, ≥99.8%, contains 50-150 ppm amylene as stabilizer (Sigma-Aldrich), CAS: 75-09-2

Pyridine: biotech. grade, ≥99.9% (Sigma-Aldrich), CAS: 110-86-1

TE buffer solution: Tris-EDTA buffer solution, BioUltra, for molecular biology, pH 7.4 (Fluka), EC: 231-791-2

APTES: (3-Aminopropyl)triethoxysilane, ≥98% (Sigma-Aldrich), CAS: 919-30-2

16MHA: 16-Mercaptohexadecanoic acid, 90% (Aldrich), CAS: 69839-68-5

ODT: 1-Octadecanethiol, 98% (Aldrich), CAS: 2885-00-9

PITC: Phenyl isothiocyanate, ≥99% (GC), liquid (Sigma), CAS: 103-72-0

HITC: Hexyl isothiocyanate, 95% (Aldrich), CAS: 4404-45-9

Denhardt's solution: BioReagent, for molecular biology, lyophilized powder (Sigma). reconstitution with 5 mL of water yields a 50× concentrate.

SDS: Sodium dodecyl sulfate solution, for molecular biology, 10% in 18 megohm water (Sigma), CAS: 151-21-3

SSC: BioReagent, for molecular biology, 20x concentrate (Sigma)

SSPE: for molecular biology, 20× concentrate (Sigma),

Tritonx-102: (Sigma-Aldrich), CAS: 9002-93-1

All ssDNA are purchas from Alpha DNA

3’ end thiolated Capture ssDNA: 5’-AACTACTCCTCTACTGCGTTTTTTTTT-3’-$(CH_2)_3$-SH

Target ssDNA: 5’-CGCAGTAGAGGAGTAGTTGTTAGGGAGTGTGGATGG-3’

5’ end thiolated Probe-ssDNA: HS-$(CH_2)_6$-5’-TTTTTTTTTCCATCCACACTCCCTAAC-3’

3 base pair mismatched ssDNA: 5’-CGCAGGAGTGGCGTAGTTGTTAGGGAGTGTGGATGG

CHAPTER 6

RESULTS AND DISCUSSION

The basic working principles of our DNA detection mechanism are: (1) 30nm GNP which is modified by 5' end thiolated P-ssDNA act as signal amplifier. (2) When hybridization event occur, T-P-30au will attach to C-50au (located between two electrodes) and form a bridge that provides a pathway for current to pass through. (3) Mis-matched DNA (3mm-P-30au) can not or only very few hybridize with C-50au and therefore, no bridge can be formed between two electrodes. I-V measurement of the device with mis-matched DNA will show open circuit.

In order to reach the high sensitivity and lower the detection limit (be able to detect Target ssDNA in a very low concentration range), there are some requirement for our DNA detecting mechanism: (1) Accurate control of C-50au placement, C-50au can only be located in between two gold electrodes which is separated by ~100nm SiO_2 layer. (2) Using C-50au as a GNP bridge base and therefore DNA hybridization only occur on the C-50au surface. (3) When t-ssDNAs exist, P-30au work as signal amplifier and form GNP bridge by hybridize with C50au. Electrons can pass from source to drain through this GNP bridge. (4) Gold nanoparticles are the major object contribute to conductivity increasing, not DNA itself.

To fulfill the requirements mentioned above, there are some techniques need to be applied in our experiment. First, we place C-50au only in between two gold electrodes by applying two different SMAs layer on the device surface. One SAMs has positively charged amine group at the exposed end (APTES) and can modify SiO_2 surface which separates two gold electrodes. The other SAMs has negatively charged carboxyl group at the exposed end and can modify gold electrode surface with thiol group at the other end. With the technique, we

create attraction and repelling force on our device and are able to guild negatively charged ssDNA modified GNPs into SiO_2 area only (modified by positively charged APTES SAMs).

Second, to ensure that T-P-30au can only reach to the device surface by hybridizing with C-50au, we have to convert positively charged amine group of APTES in to non-attractive functional group. Therefore the negatively charged T-P-30au or P-30au will not be attracted to SiO_2 surface by APTES and will be repel by the negatively charged MHA SAMs on gold electrode surface. Therefore, the only way for T-P-30au to be fixed on the device surface is through hybridizing with C-50au. To passivate unoccupied APTES, HITC (Hexyl isothiocyanate) is chosen to react with amine group of APTES and convert amine terminal into non-attractive methyl group. The detail reaction mechanism will be discussed later.

Third, to avoid false signal of our DNA detection while mis-matched ssDNA exist, we need choose a proper hybridization condition by varying the hybridization temperature and add hybridization buffer solution to increase the selectivity of hybridization. The 3 base pair mis-matched ssDNA (3mm-ssDNA) have three base pair mismatch with capture ssDNA, which means half part of 3mm-ssDNA can still hybridize with P-ssDNA (modified on 30nm GNP surface) and form 3mm-P-30au.

There are four basic situations of how DNA modified GNPs behave on our DNA detection device. (a) C-50au and P-30au forms a GNP bridge through ssDNA hybridization in between two electrodes, which contribute to conductivity increasing. (b) C-50au and P-30au located on the SiO_2 trench separately. (c) C-50au and P-30au forms a GNP bridge outside the SiO_2 trench area. (d) C-50au and P-30au located outside of SiO_2 trench area separately. (b) ~ (d) are the situations which are not contributing to conductivity increasing and will reduce the sensitivity of the DNA detection device due to the waste of target. We will discuss how each situation occurs and how to avoid situation b)-d) separately.

We modified negatively charged MHA SAMs on gold electrodes surface, and theoretically will repelling negatively charged DNA modified due to the interaction of electric

double layer. However, if sample is not clean enough before processing, the SAMs formation will not good and cause DNA modified GNP can attach to the gold surface (Fig. 6.1 (b), (c)).

The positively charged APTES SAMs on SiO_2 surface will process with passivation reaction and convert amine group into methyl group after C-50au is immobilized on the SiO_2 surface. However, if the passivation reaction is not complete, the remain un-passivate APTES can still attract later introduced T-P-30au (Fig. 6.1 (d)).

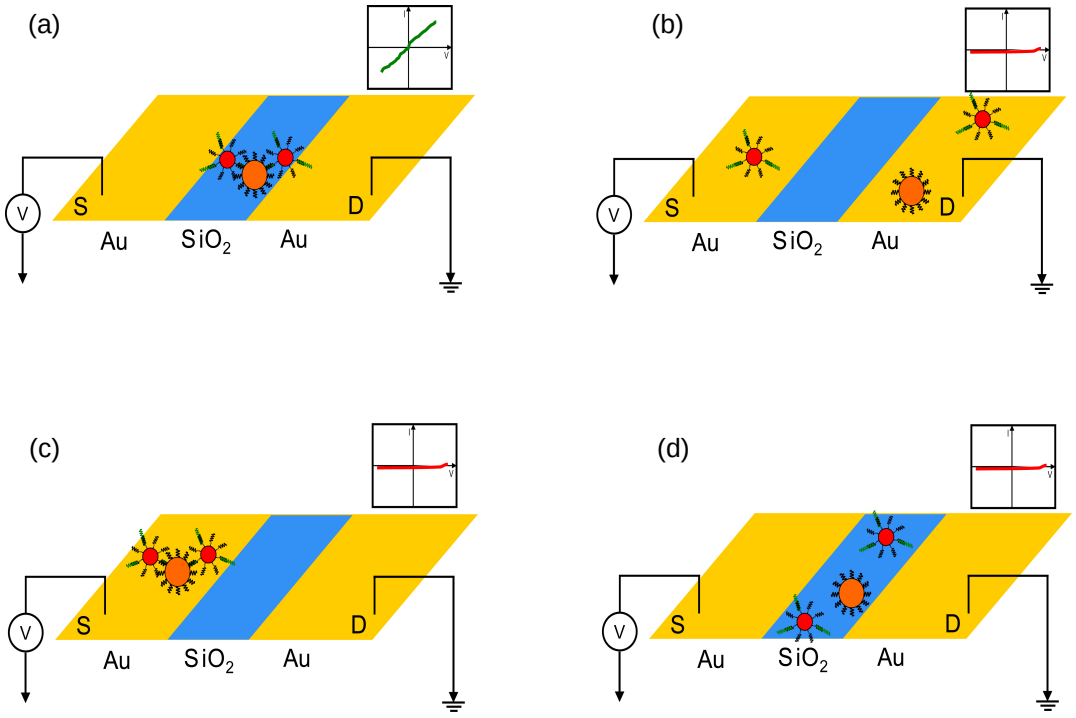

Fig. 6.1: Sketch of DNA modified GNP on device surface. (a) GNP bridge form between two electrodes. (b) C-50au or P-30au located between two electrodes. (c) GNP bridge form on other place. (d) C-50au or P-30au locates on other place. Only (a) can provide a linear I-V curve when measuring I-V signal of the device. (b)-(d) can only show open circuit behavior.

6.1 Accurate Placement of C-50au in between Source and Drain Electrodes

In order to accurate control C-50au positioning only on the ~100nm SiO_2 trench area, we apply two different kinds of SAMs layers in our experiment. One is APTES, which has amino group terminal at one end and silane group at the other end. Silane group can react with SiO_2 surface and form chemical bonding Si-O-Si; amino group can provide a positively charged surface ($R\text{-}NH_2 \rightarrow R\text{-}NH_3^+$) on SiO_2 trench surface. The other SAMs is 16MHA, which has carboxylic acid (R-COOH) terminal at one end and thiol group (R-SH) at the other end. Thiol group can react with gold electrode surface and form chemical bonding R-S=Au; carboxylic acid group can provide negatively charged surface (R-COOH → R-COO-) on gold electrodes surface.

With these two SAMs, we can create a device with positively and negatively charged surfaces and the negatively charged nanoparticles can be guided into the position by the attracting and repelling force provided by those two SAMs layer accurately. The detail of how negatively charged nanoparticles or ssDNA modified nanoparticles can be guided into the target position will be discuss later.

The results of different nanoparticle alignment are shown below.

6.1.1 One Dimension Alignment of GNP

We have done two different kind of 1-D alignment on the patterned wafer, on the sandwich structure side wall, and on the plane surface.

The basic idea for 1-D alignment of negatively charged GNP is: by creating proper guiding feature and apply repelling and attracting force on the feature surface by SAMs layer modification, the negatively charged GNP (surrounding by a physical absorption citric ion) can be guided into the attracting area. In our experiment, gold surface is modified by negatively charged SAMs layer, MHA, which means the repelling for GNP. Also, SiO_2 surface is modified by positively charged APTES layer, which means the attracting for GNP. This is so called

electrostatic funneling. The sketch of this approach about 1-D alignment of GNP on side wall or on flat surface is shown at Fig. 6.2.

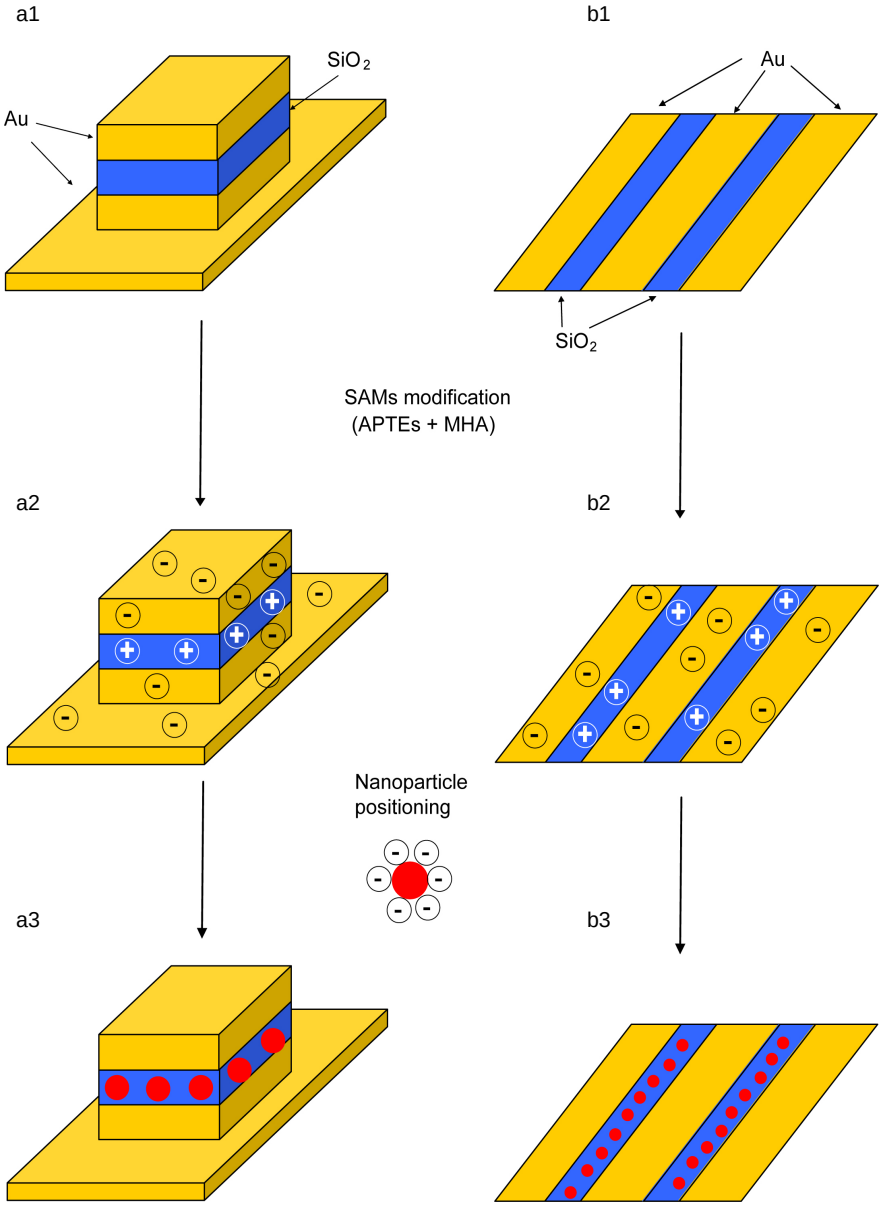

Fig. 6.2: Sketch of how to align nanoparticle in one dimension. By creating a proper guiding structure and apply positively and negatively charged SAMs on different pattern surface, charged nanoparticles can be guided and align in order. (a1)~(a3) show the nanoparticles can be aligned in the side wall structure. (b1)~(b3) show the nanoparticles can be aligned on the flat surface. The width of SiO_2 layer decides the size of nanoparticle that can be aligned.

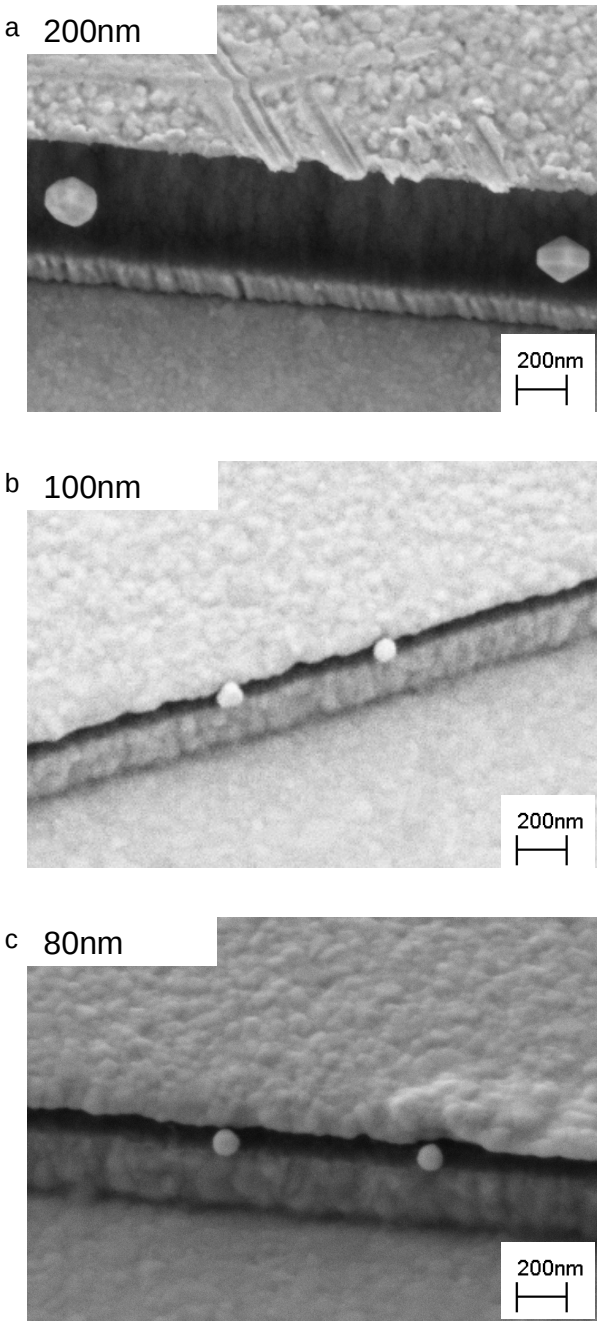

Fig. 6.3: Side wall 1-D alignment by of Au/Cr/SiO2/Cr/Au side wall structure. (a) 200nm GNP attach to the side wall. Black area is SiO_2 substrate. (b) 100nm GNP. (c) 80nm GNP. The thicknesses of SiO2 layer are 450nm, 100nm, and 90nm.

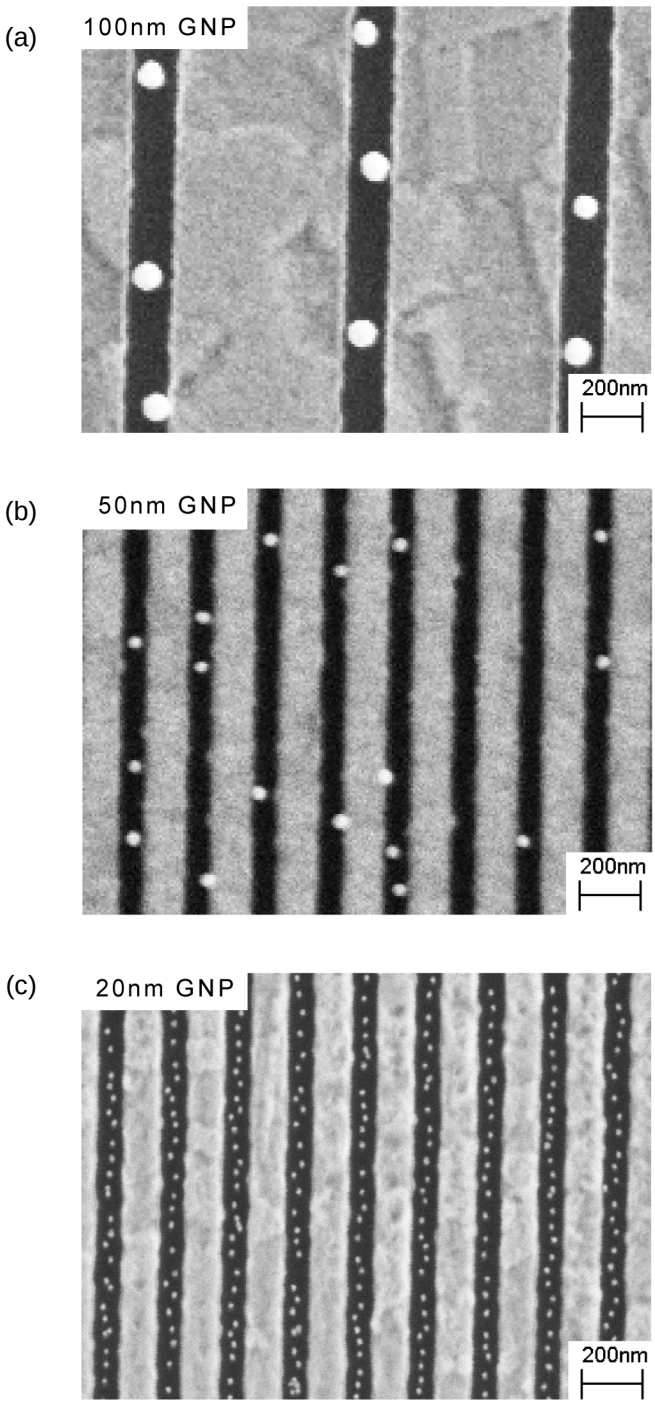

Fig. 6.4: 1-D alignment in the trench guiding structure. (a) 100nm GNP aligned between two gold lines. Black area is SiO_2 substrate. (b) 50nm GNP alignment (c) 20nm GNP alignment.

(The following section is re-organized from L.-C. Ma, R. Subramanian, H.-W. Huang, V. Ray, C.-U. Kim, and S. J. Koh,. Nano Lett. 7, 439 (2007) [6.25] till the end of section 6.1.1) The electrostatic funneling concept is illustrated by an example in Fig. 6.5, where a substrate having a surface pattern of alternating lines is functionalized with positively and negatively charged molecules. When the substrate is immersed into a colloidal solution containing charged nanoparticles, the substrate and nanoparticles interact in the liquid medium via electrical double-layer interaction [6.1-6.3].

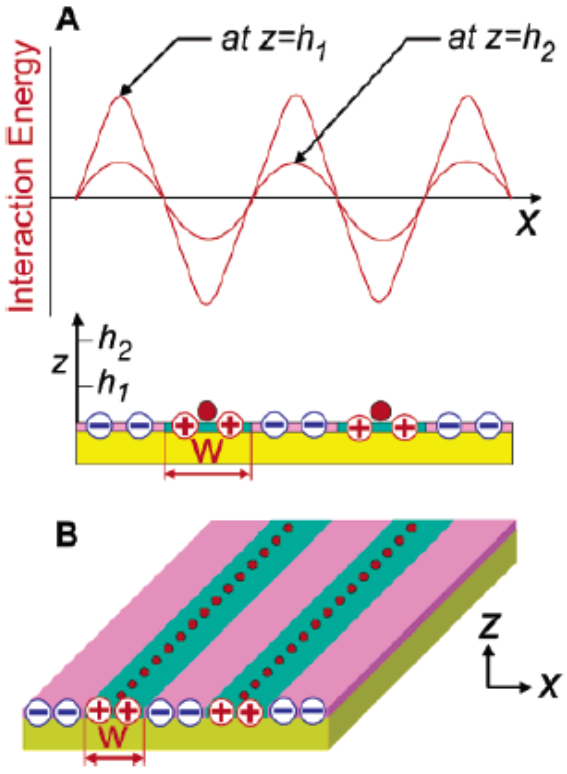

Fig. 6.5: Wafer-scale nanoparticle placement with electrostatic funneling. (A) A schematic of the electrostatic interaction energy in an aqueous solution for a negatively charged nanoparticle near a substrate surface functionalized with positively and negatively charged molecules. (B) The nanoparticles (red dots) are guided to the centers of positively charged lines (of width W) where the interaction energy is minimum [6.25].

Simple electrostatic consideration shows that, near the substrate surface, the interaction energy between a negatively charged nanoparticle and the substrate has minima and maxima as displayed in Fig. 6.5. When the charged nanoparticle is being attracted to a

positively charged line, the gradient of the interaction energy in a direction parallel to the substrate (x direction in Fig. 6.5) produces lateral forces that push it toward the center of the positively charged line, a low-energy site. When the interaction energy gradient is sufficiently strong, nanoparticles can be placed along a line with nanometer scale precision even though the guiding structures are defined in much larger scale, on the order of ~100 nm.

Electrostatic interactions between the particle and substrate surface are believed to be the dominant mechanism for the guided particle placement seen in Fig. 6.5. First, we want to point out that the capillary forces, which have been successfully implemented for nanoparticle placement by other research groups [6.4-6.6] are not likely to be responsible for the guided placement shown in Fig. 6.4. Capillary force driven assembly requires the existence of an air-water interface at the surface patterns, but our experimental procedures do not produce this condition [6.7].

The importance of electrostatic interaction is clearly seen in Fig. 6.6, where we compare two wafers functionalized with SAMs of differing charge combinations. For one wafer (Fig. 6.6 (A)), silicon oxide and gold patterns were functionalized with positively and negatively charged molecules, using the SAMs described earlier (i.e., APTES and MHA, respectively). For the other wafer (Fig. 6.6 (B)), the same positively charged APTES SAMs were placed on the silicon oxide surface, but the negatively charged SAMs on the gold surface were replaced with nonpolar SAMs using n-octadecanethiol (ODT, $HS\text{-}(CH_2)_{17}\text{-}CH_3$)

When the two samples were immersed into a colloid of Au nanoparticles (~20 nm diameter), the former set of SAMs created denuded zones with width of ~70 nm, Fig. 6.6 (A). On the other hand, no denuded zone was found for the latter set of SAMs, Fig. 6.6 (B). These images provide evidence of the importance of the magnitude of the electrostatic interaction energy gradient (in a direction parallel to the substrate) in guiding nanoparticles to the surface. Where the gradient is strong, the nanoparticles are funneled away from the boundary toward the center of the positively charged area, and where the gradient is weak, they are not.

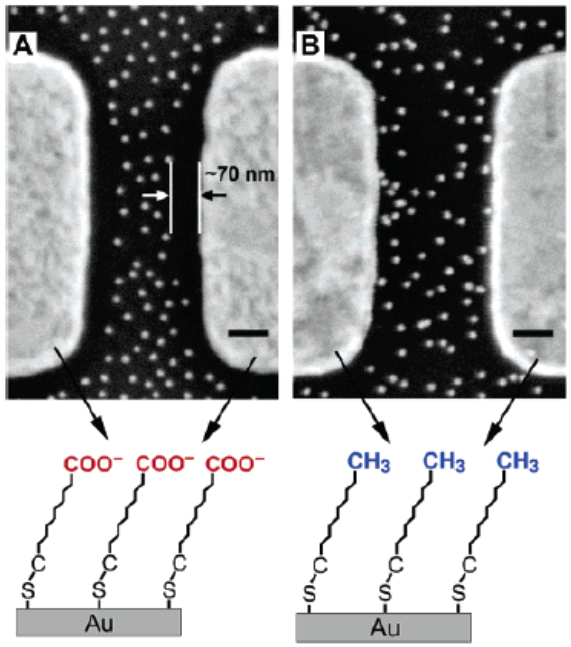

Fig. 6.6: Control of guiding electrostatic interaction energy with different combinations of SAMs. (A) The gold surfaces (bright in the SEM image) were negatively charged with SAMs of MHA (-COO^- terminated) while the silicon oxide surface (dark in the SEM image) was positively charged with SAMs of APTES (-NH_3^+ terminated). When immersed into the Au colloidal solution, Au nanoparticles (negatively charged, diameter ~20 nm) were guided away from gold surfaces and attracted onto silicon oxide surface, creating denuded zones with width of ~70 nm. (B) Under exactly the same conditions except that the gold surfaces were functionalized with nonpolar SAMs using ODT (-CH_3 terminated), we observe no denuded zone due to the absence of appreciable gradient of interaction energies in a direction parallel to the substrate. Scale bars: 100 nm [6.25].

The observations in Fig. 6.4 and Fig. 6.6 (A) clearly indicate that the interactions between Au nanoparticles and charged substrate are electrostatic and of long range, extending at least over tens of nanometers. To get a more quantitative picture of this long-range nanoparticle-substrate interaction, we have calculated the interaction energies based on DLVO theory.[6.2, 6.3, 6.8] We first calculate the interaction energy between a Au nanoparticle and an infinite surface functionalized with either MHA or APTES (geometry in parts A and B of Fig. 6.7, respectively). The interaction energy $V_j(z)$ is a sum of electrical double-layer interaction energy $\Phi_j(z)$ and van der Waals interaction energy $W_j(z)$, where j represents the surface type (functionalized with either MHA or APTES)

$$V_{MHA}(Z) = \Phi_{MHA}(Z) + W_{MHA}(Z)$$
$$V_{APTES}(Z) = \Phi_{APTES}(Z) + W_{APTES}(Z) \quad \text{(eq. 6.1)}$$

The double-layer interaction energies, $\Phi_{MHA}(z)$ and $\Phi_{APTES}(z)$, can be calculated using linear superposition approximation [6.9-6.11] (LSA) and given by

$$\Phi_{MHA}(Z) = 4\pi\varepsilon\varepsilon_0 a(kT/e)^2 Y_{Au} Y_{MHA} \exp(-\kappa z)$$
$$\Phi_{APTES}(Z) = 4\pi\varepsilon\varepsilon_0 a(kT/e)^2 Y_{Au} Y_{APTES} \exp(-\kappa z) \quad \text{(eq. 6.2)}$$

where ε is the dielectric constant of water, ε0 is the permittivity of free space, a is the radius of a Au nanoparticle, k is the Boltzmann constant, T is the absolute temperature, e is the unit charge of an electron, and Y_{Au}, Y_{MHA}, and Y_{APTES} are effective reduced surface potentials [6.9, 6.12, 6.13] of an isolated Au nanoparticle, an isolated MHA functionalized substrate, and an isolated APTES functionalized substrate, respectively. κ is the inverse Debye length defined by [6.2]

$$\kappa = \left[\left(1000e^2 N_A / \varepsilon\varepsilon_0 kT\right)\sum_i z_i^2 M_i\right]^{1/2} \quad \text{(eq. 6.3)}$$

where N_A is Avogadro's number, z_i is the valency of ion species i and M_i is the molar ion concentration of ion species i. From eq 3, the Debye length κ^{-1} of our Au colloid [6.14] is calculated to be 81.5 nm.

Each of Y_{Au}, Y_{MHA}, and Y_{APTES} can be obtained by solving nonlinear Poisson-Boltzmann equations when ion concentrations M_i, valencies z_i, and surface charge densities σ_{Au}, σ_{MHA}, and σ_{APTES} are given. No exact analytical solution to the nonlinear Poisson-Boltzmann equations exists except for a planar geometry, but numerical solutions [6.15] as well as approximate analytic expressions [6.16, 6.17] are available. Using the approximate analytic expressions by Ohshima, [6.16, 6.17] along with known ion concentrations45 and available surface charge densities σ_{Au}, σ_{MHA}, and σ_{APTES}, [6.18-3.20] we obtain Y_{Au}, Y_{MHA}, and Y_{APTES} as -1.59, -5.62, and 1.07, respectively. By inserting Y_{Au}, Y_{MHA}, and Y_{APTES} along with κ into eq. 6.2, we obtain

double-layer interaction energies $\Phi_{MHA}(z)$ and $\Phi_{APTES}(z)$, which are plotted in parts A and B of Figure 5, respectively. The van der Waals interaction energies $W_{MHA}(z)$ and $W_{APTES}(z)$ are given by [6.2].

$$W_{MHA}(z) = -A_{MHA}a/6z$$
$$W_{APTES}(z) = -A_{APTES}a/6z \quad \text{(eq. 6.4)}$$

where A_{MHA} and A_{APTES} are the Hamaker constants for the system of Au/MHA/water/Au and SiO2/APTES/water/Au,[6.21, 6.22] the reported values of which are 2.5 x 10^{-19} and 5.7 x 10^{-20} J, respectively [6.23, 6.24]. From eq 4, the van der Waals interaction energies $W_{MHA}(z)$ and $W_{APTES}(z)$ were obtained and are plotted in parts A and B of Fig. 6.7, respectively.

From eqs 6.1-6.4, the total interaction energies $V_{MHA}(z)$ and $V_{APTES}(z)$ were obtained and are plotted in parts A and B of Fig. 6.7. The calculation results shown in these plots reveal the nature of guiding forces seen in our experiments. The total interaction energies $V_{MHA}(z)$ and $V_{APTES}(z)$ are dominated by the electrostatic double-layer interactions as long as the nanoparticle-surface separation is more than 10 nm. For MHA functionalized substrates, the interaction with a Au nanoparticle is repulsive (positive interaction energies), and for APTES functionalized substrates, the interactions are attractive (negative interaction energies), as expected from the surface charge states of Au nanoparticles, MHA, and APTES. Most importantly, the plots clearly indicate that the interactions are indeed of long range: for the interaction of a Au nanoparticle with MHA functionalized substrates, the interaction energy $V_{MHA}(z)$ reaches the room temperature thermal energy (~25 meV) at ~370 nm away from the substrate (beyond the axis range in Fig. 6.7 (A)). For the interaction with APTES functionalized substrates, $V_{APTES}(z)$ reaches the thermal energy (ca. -25 meV) at ~270 nm. With the interaction energies $V_{MHA}(z)$ and $V_{APTES}(z)$ obtained, we now can get a more quantitative picture for the observed denuded zone in Fig. 6.7 (A). When two surfaces functionalized with MHA and APTES are adjacent to each other (geometry in Fig. 6.7 (C)), we can semi-quantitatively plot the interaction energy $V(x,z = h)$ between a Au nanoparticle and the substrate as follows. First, we

note that when the nanoparticle is appreciably away from the MHA-APTES boundary (when $|x|$ is large), $V(x,z = h)$ assumes the value $V_{MHA}(h)$ or $V_{APTES}(h)$ because the influence of the other charged surface diminishes. Second, near the interface (when $|x|$ is small), $V(x,z = h)$ deviates from both $V_{MHA}(h)$ and $V_{APTES}(h)$ and assumes a value between them because the influence of negatively and positively charged surfaces overlaps. If we assume that variation of $V(x,z = h)$ is constant, i.e., $dV(x,z = h)/dx$ is constant, we obtain a plot for $V(x,z = h)$ as in Fig. 6.7 (D).

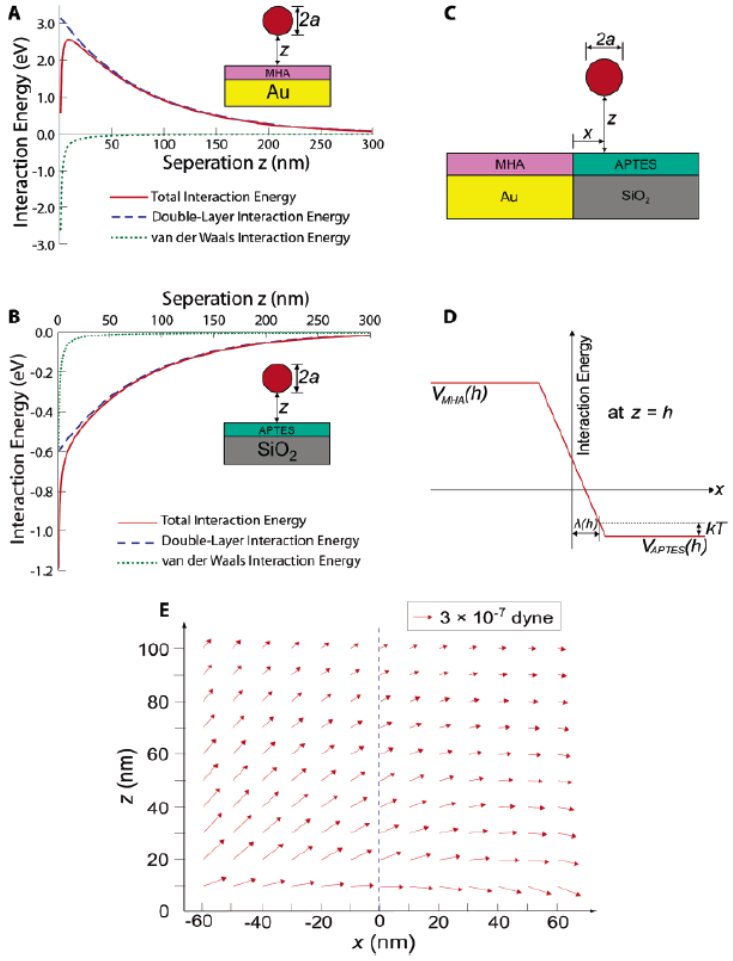

Fig. 6.7: Calculation of the interaction energies. (A) Interaction energy between a 20 nm Au nanoparticle (a = 10 nm) and a MHA functionalized substrate. (B) Interaction energy between a 20 nm Au nanoparticle (a = 10 nm) and an APTES-functionalized substrate. (C) A geometrical schematic for a nanoparticle interacting with a substrate functionalized with MHA for one side and APTES for the other side. (D) A schematic of the interaction energy as a function of x for a fixed z (=h) under the geometry in C. (E) Forces exerted on a 20 nm diameter Au nanoparticle under the geometry in C for $|x| < 70$ nm and $z \leq 100$ nm. The MHA-APTES boundary is located at x = 0 and indicated by the dotted line [6.25].

According to Fig. 6.7 (D), the nanoparticle can approach the MHA-APTES boundary only up to $x = \lambda(h)$ because of the energy barrier. This effect produces the denuded zone observed in Fig. 6.6 (A).

We can further estimate the lateral force F_L ($=-\partial V(x,z)/\partial x\big|_{z=h}$) exerted on the Au nanoparticle. From geometrical consideration of Fig. 6.7 (D), we get the relationship between $\partial V(x,z)/\partial x\big|_{z=h}$ and λ(h) as

$$\partial V(x,z)/\partial x(\text{at } x = h) = -\{(V_{MHA}(h) - V_{APTES}(h))/2 - kT\}/\lambda(h) \qquad \text{(eq. 6.5)}$$

6.1.2 Zero Dimension Alignment of GNP

From previous work done in our group, we utilize modified positively charged APTES SAMs layer and negatively charged MHA SAMs layer on SiO_2 and Au surface which act as a guiding structure that can confine the negatively charged nanoparticle positioning. We observe an exclusive zone for negatively charged nanoparticles alone the negatively charged Au surface where no particle can attach to the SiO_2 surface in the range. The principle behind this exclusive zone is the DLVO theory which is discussed in the previous section. In short, charged surface or particle in the electrolyte environment will form an electric double layer, the combination of both electric double layer interaction and Van der Waals force between charged nanoparticles and charged surface determine whether the force between two charged object is attracting or repulsing when they are separated in certain distance.

The formation of exclusive zone we observe in our experiment is the result of negatively charged gold nanoparticle that attracted by the positively charged SiO_2 surface but repelled away from the negatively charged Au surface alone the Au surface edge.

By utilizing this principle, we can successfully achieve either one dimension alignment of nanoparticles or even individual nanoparticle positioning by varying the ion concentration of the gold nanoparticle solution (varying the exclusive zone thickness with a given guiding

structure), or varying the size of guiding structure (varying the area that is not affected by repulsive force with a given ion concentration).

The following figure shows two different approach of control the number of nanoparticle positioning in the target area (Fig. 6.8, Fig. 6.9 and Fig. 6.10).

We also demonstrate the Single Particle Placement (SPP) using ~20 nm Au nanoparticles and circular guiding patterns as a model system. Theoretical calculations show that the self-limiting behavior in SPP is due to significant increase in the free energy barrier upon placement of the first nanoparticle on a target location, preventing the approach of the other nanoparticles.

Fig. 6.11 schematically displays the SPP concept. First, an electrostatic guiding structure, the electrostatic funnel [6.25], is formed by functionalizing the substrate surface and the pattern on it with SAMs having different polarities (in Fig. 6.11, the circle is positively charged, the rest of the surface negatively charged). When the substrate is immersed in a colloidal solution, a nanoparticle (negatively charged) is electrostatically guided onto a target location, the circle center (Fig. 6.11 (a)). Once a nanoparticle occupies the circle, however, it alters the electrostatic potential landscape in such a way that the approach of other nanoparticles to the substrate surface is prohibited, resulting in self-limiting SPP (Fig. 6.11 (b)).

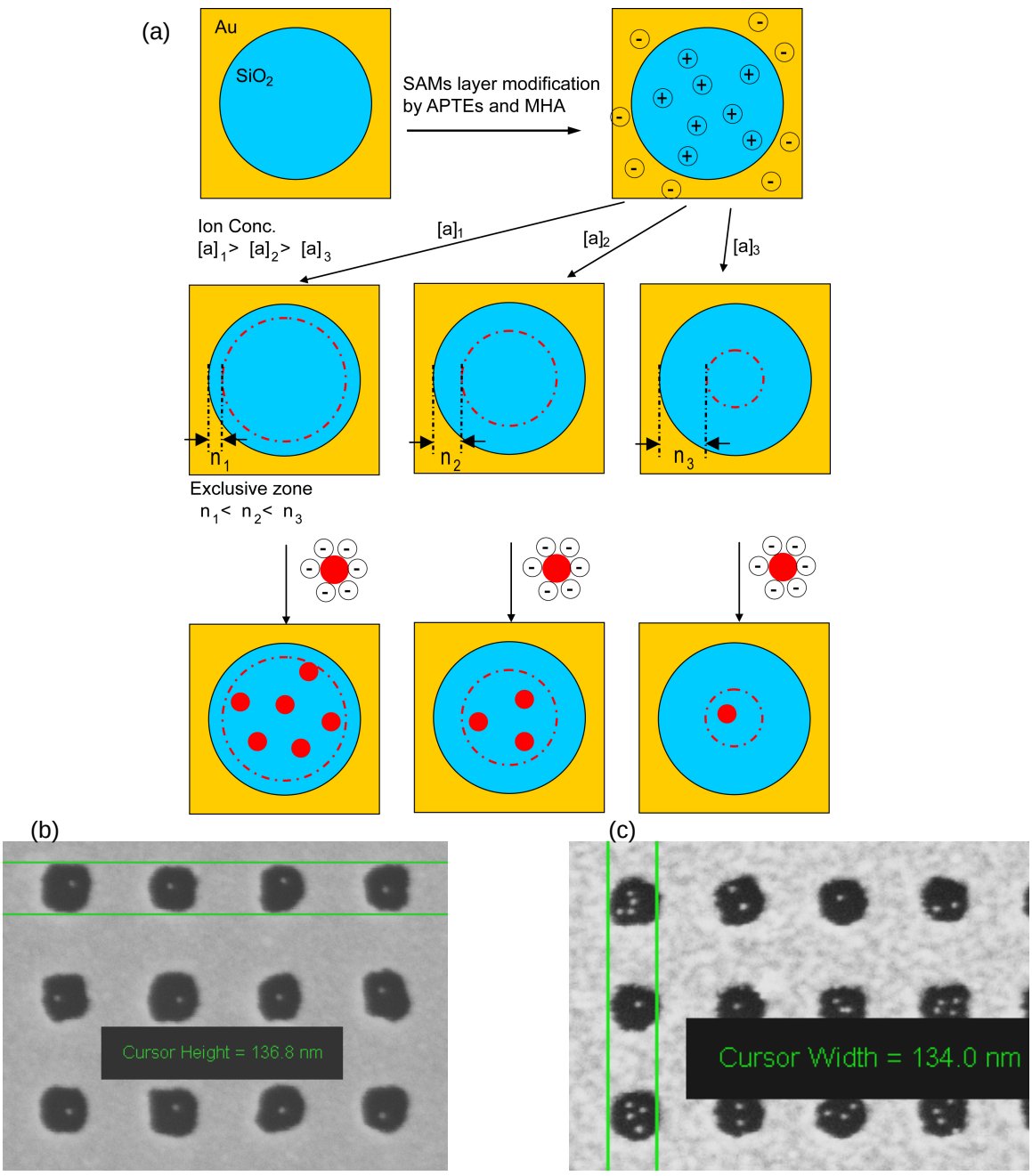

Fig. 6.8: Control the number of GNP attach to the guiding structure by very the ion concentration of gold nanoparticle solution. (a) Sketch of how the exclusive zone thickness varied with varied ion concentration. (b) With diluted gold nanoparticle solution (less ion concentration), the exclusive zone confined GNP attaching area is limited for only one 20nm GNP can fill in each SiO_2 hold. (c) With concentrated gold nanoparticle solution (higher ion concentration), the exclusive zone is reduced and therefore, more 20nm GNP can be filled into the similar size SiO_2 hold.

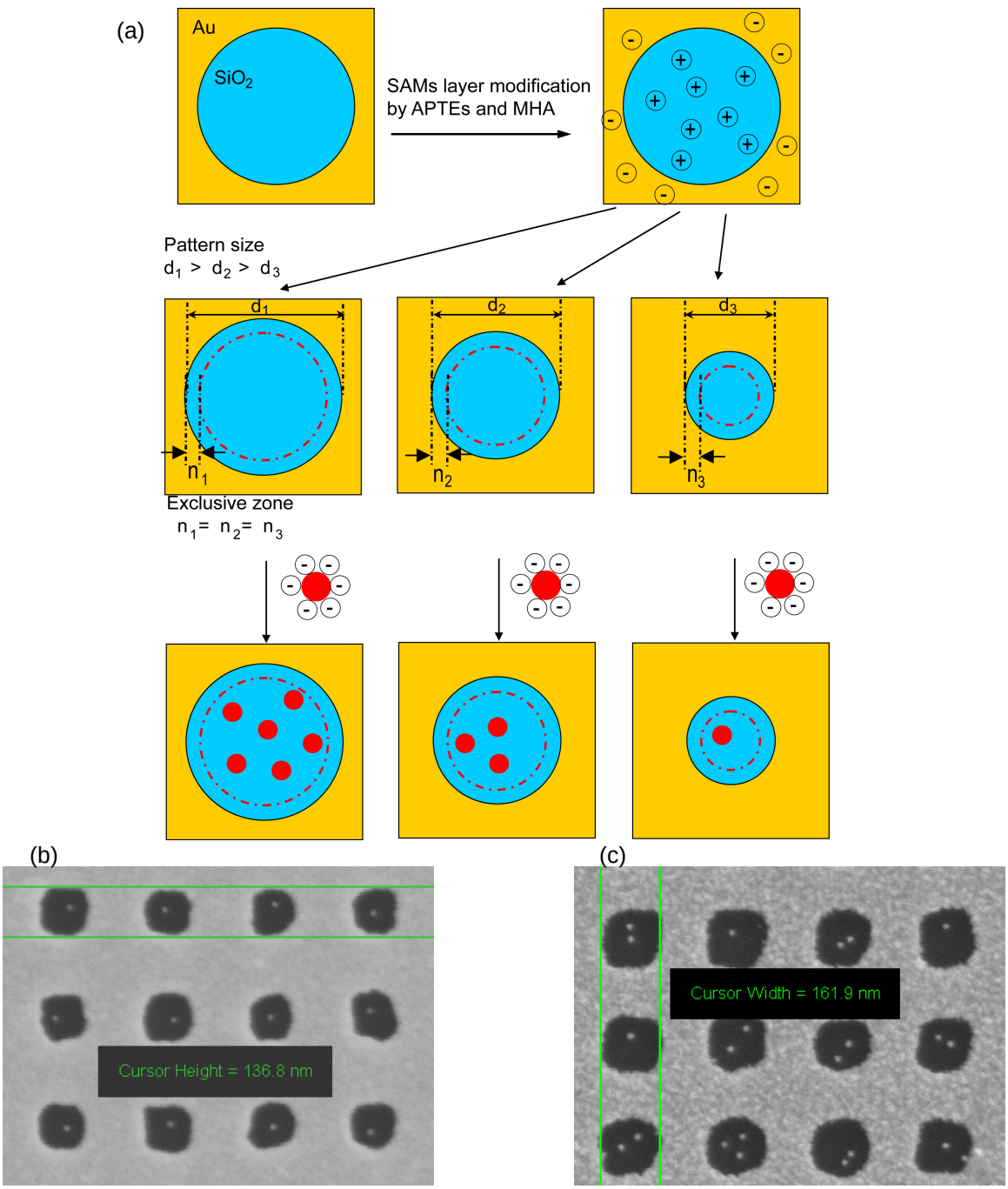

Fig. 6.9: Control the number of GNP attach to the guiding structure by very the feature size. (a) Sketch of how the attachable area for GNP varied with varied feature size when ion concentration is fixed. (b) With diluted gold nanoparticle solution and ~136nm feature size, only one 20nmm GNP are allowed to fill into the SiO_2 hold. (c) With diluted gold nanoparticle solution (same as (b)), larger size of the feature allow more 20nm GNP can fill into SiO_2 hold.

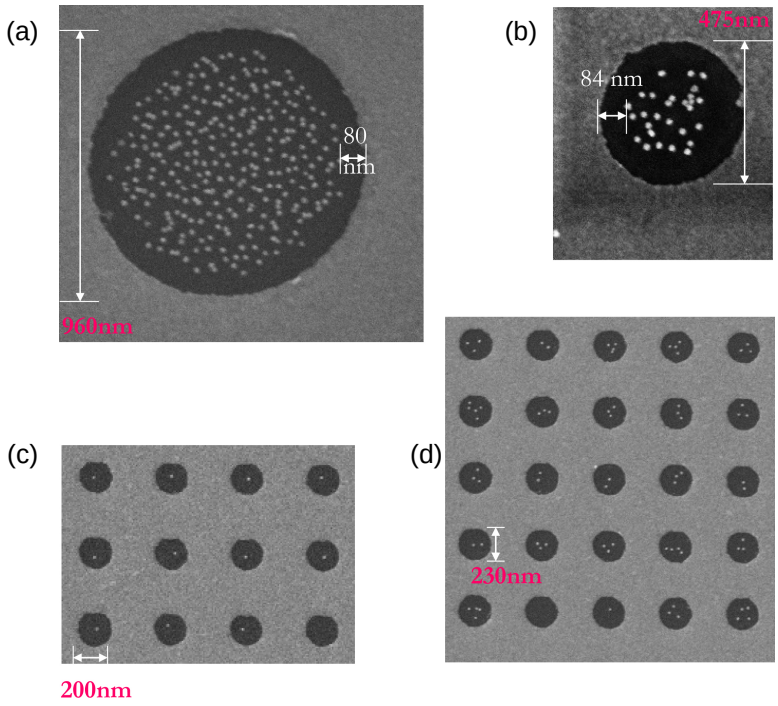

Fig. 6.10: Another example of how guiding feature size can help control the number of nanoparticle fills into the SiO_2 circle area. (a) 960 nm feature size with ~80nm exclusive zone thickness. (b) 475 nm feature size with ~84nm exclusive zone thickness, the number. (c) 200 nm feature size with ~80nm exclusive zone thickness, only one 20nm GNP can fill into SiO_2 circle. (d) 230nm feature size, more than one 20nm GNP can fill into SiO_2 circle. All the ion concentration of gold nanoparticle solution are the same (exclusive zone thickness are similar).

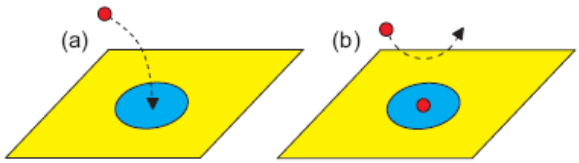

Fig. 6.11: Concept of SPP. Inside the circle: positively charged; outside the circle: negatively charged; and nanoparticle: negatively charged. (a) A nanoparticle (in a colloidal solution) is electrostatically guided onto a target position (circle center). (b) Once the circle is occupied by a nanoparticle, the approach of other nanoparticle is prohibited [6.26].

(The following section is re-organized from H-W Huang, P. Bhadrachalam, V. Ray, and Seong Jin Koh,. APPLIED PHYSICS LETTERS 93, 073110 (2008) [6.26] till the end of section 6.12) Fig. 6.12 shows a SEM image of a 10x10 array, demonstrating the effectiveness of SPP. We find 97 circles in the array containing exactly one Au nanoparticle. Only three circles,

indicated by arrows in Fig. 6.12, had either no nanoparticle or two Au nanoparticles. The self-limiting behavior in the nanoparticle positioning is evident in Fig. 6.12, as it is in great contrast to the saturated nanoparticle attachment on the silicon oxide surface outside the patterned arrays (Fig. 6.12). We also examined four 10x10 circle arrays (including the one in Fig. 6.12) and counted the number of Au nanoparticles positioned on each circular pattern. The data are summarized in a histogram in Fig. 6.12, which shows SPP works consistently well over all the four arrays. Overall, 364 circles out of 400 (91%) contained exactly one nanoparticle, convincingly demonstrating the self-limiting capability in the nanoparticle positioning.

Beyond the capability of allocating single nanoparticles to each circular pattern, it is also desirable to place them onto accurate target positions, i.e., the center of each circle. In Fig. 6.12 (a), we observe that nanoparticles are placed close to the centers of the circular patterns. For further assessment of the accuracy of SPP, we examined the positions of the single nanoparticles relative to each circle center for the 364 circles that contained exactly one nanoparticle. (The circle centers were defined for each 10x10 array as the cross points of equally spaced 10 horizontal and 10 vertical lines.) Fig. 6.12 (d) displays the positions of the single nanoparticles superimposed in one plot. We find that ~90% of nanoparticles are located within 20 nm (the width of a single Au nanoparticle) from the circle center. The average distance of the nanoparticle position from the circle center, i.e., the precision of the SPP was measured to be 12.1 nm. [6.26]

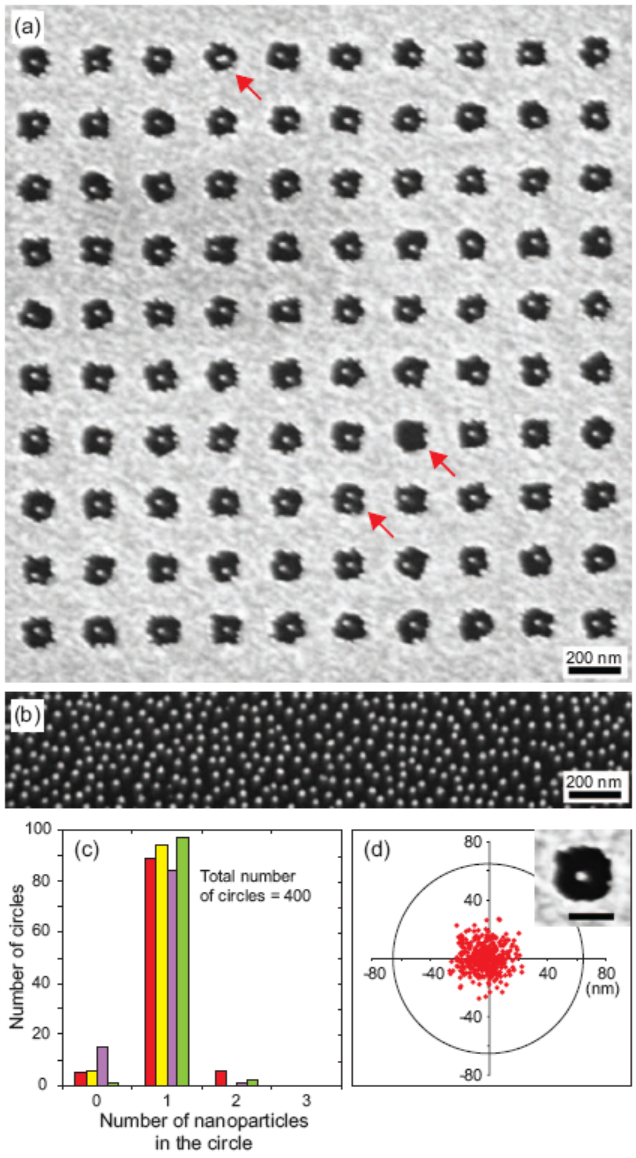

Fig. 6.12: Large scale of SPP. (a) SEM image of SPP. Bright dots: ~20 nm Au nanoparticles; dark circular patterns: silicon oxide surface functionalized with SAMs of APTES; and bright area: Au surface functionalized with SAMs of MHA. The arrows indicate the defects. (b) Saturated nanoparticle attachment on silicon oxide surface outside the patterned area. (c) Histogram showing the statistics for number of nanoparticles positioned on the circular pattern. Data from four 10x10 circle arrays with number count from each 10x10 array displayed by a different color. (d) Superimposed plot for the positions of single nanoparticles. Inset: SEM image of a circular pattern containing one Au nanoparticle. Scale bar: 100 nm. [6.26]

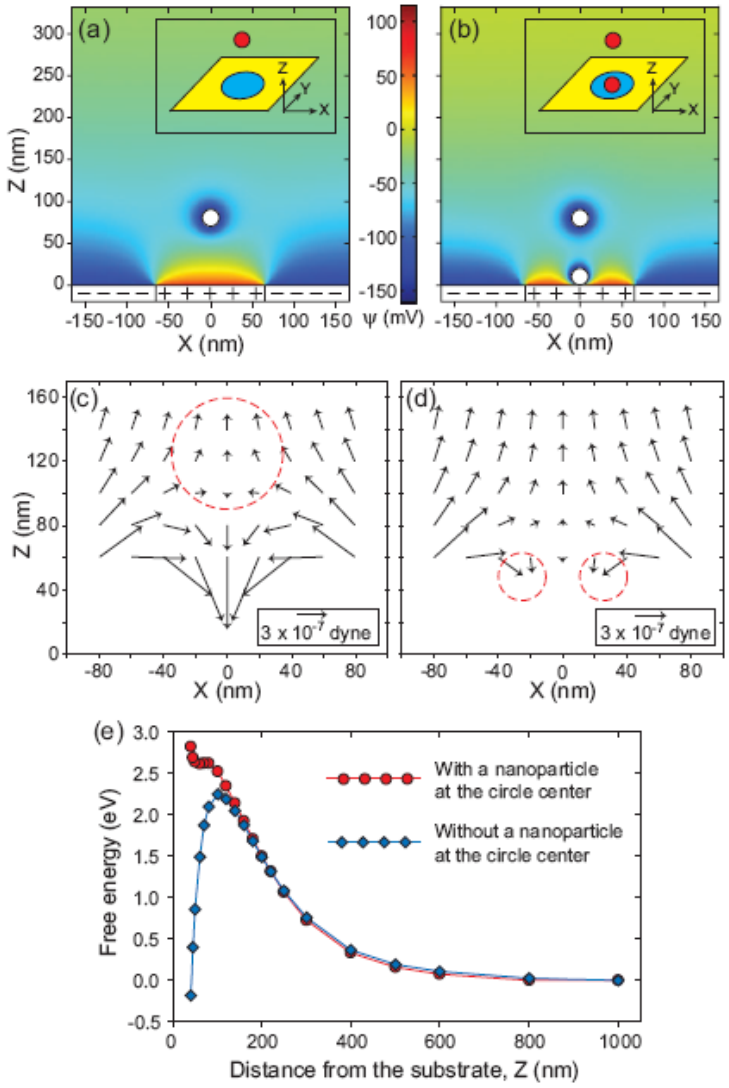

Fig. 6.13: Calculated electrostatic potentials $\Psi(\vec{r})$ when a 20 nm Au nanoparticle is located at $\vec{R}$=(0,0,80 nm), (a) without and (b) with presence of one 20 nm Au nanoparticle at the circle center, respectively. (c) and (d) Forces $\vec{F}(\vec{R})$ exerted on a 20 nm Au nanoparticle positioned at various $\vec{R}$, (c) without and (d) with presence of one 20 nm Au nanoparticle at the circle center, respectively. (e) Free energy of interaction $V(\vec{R})$ between a 20 nm Au nanoparticle at $\vec{R}$=(0,0,*z*) and the substrate surface. Blue diamonds and red circles are for the cases without and with presence of one 20 nm Au nanoparticle at the circle center, respectively. The calculation parameters: circle diameter=130 nm; *p*H=6.6; ion concentrations: $[Na^+]=4.2\times10^{-6}M$, $[C_6O_7H_7^-]=9.7\times10^{-9}M$, $[C_6O_7H_6^{2-}]=6.5\times10^{-7}M$, $[C_6O_7H_5^{3-}]=1.0\times10^{-6}M$, $[H3O^+]=2.5\times10^{-7}M$, and $[OH^-]=4.0\times10^{-8}M$; surface potentials: -134, 72, and -159 mV for MHA functionalized Au surface, APTES functionalized silicon oxide surface, and citratepassivated Au nanoparticle surface, respectively. [6.26]

Again, to accurate control charged nanoparticle positioning is the most basic and most important part for our DNA detection method. In our DNA detection mechanism, Capture-ssDNA modified 50nm GNP (C-50au) is also negatively charged due to the ionization phosphate group of DNA back bone. Therefore, the method we applied to control nanoparticle positioning can be also suitable for DNA modified GNP.

Immobilize C-50au only in the SiO_2 band area (between two gold electrodes) in the most important step for the whole detection mechanism. C-50au is the base for the GNP bridge formation when T-P-30au attach to C-50au by hybridization. There will be no contribution to the conductivity change if C-50au located outside the SiO_2 band area even with a lot of T-P-30au hybridize with C-50au.

6.2 Passivation of APTES

Passivation of unoccupied APTES (not taken by C-50au) is also important because ssDNA and dsDNA are also negatively charged molecules at pH 2~14 and can be attracted to the positively charged APTES SAMs. Also, instead of hybridization between T-P-30au and C-50au, T-P-30au can also be attracted by the unoccupied APTES and therefore reduce the detection sensitivity (T-P-30au attach to SiO_2 surface will not contribute to the conductivity increasing).

In our real DNA detecting device, the total SiO_2 surface area between two gold electrodes is around $40um^2$ (4x100umx0.1um), and only around ten C-50au are placed into SiO_2 area. Which means, the useful sensing area of our device is the top half surface area of C-50au ($4\pi r^2 / 2 = 3925nm^2 = 0.0039\ um^2$). That is to say, the probability of T-P-30au to meet C-50au in the SiO_2 surface is only 0.00975% ($0.0039\ um^2 / 40um^2$). This is just a rough estimate the probability by the ratio of sensing area and SiO_2 area. If we take χ (the probability of T-P-30au that can successfully hybridize with C-50au for each collision) into account, the chance of

T-P-30au can successfully hybridize with C-50au without passivate un-occupied amine group of APTES will be even lower than 0.00975%.

Therefore, we need a passivation reaction to convert positively charged amine group of APTES into non-attractive function group (such as $-CH_3$, $-C_6H_6$) or repulsive functional group (such as $-COO^-$, $-PO_4^-$).

In our study, we choose to convert positively charged amine group of APTES into non-attractive functional group because the repulsive functional group will also increase the difficulty for T-P-30au approaching C-50au.

We have three different ways to convert amino group of APTES into non-attractive functional group:

(a) Acetic acid: 18mM DCC (Dicyclohexylcarbodiimide) + 18mM Acetic acid +

70ml Dichloromethane → 40°C, 3hr

Mix Glacial acetic acid with 70ml Dichloromethane and make acetic acid 18mM. Add DCC (solid) 18mM as catalyst into the solution and heat the solution to 40°C, 3hours in the sealed beaker for reaction. After reaction, the exposed amine terminal of APTES can be converted into methyl group (Fig.6.14 (b)).

(b) Phenyl isothiocyanate: 0.4ml PITC + 5ml Pyridine + 45ml DMSO → 45°C, 5hr

Mix 0.4ml PITC with 45ml DMSO, and add 5ml Pyridine as catalyst, pre-heat the solution to 45°C before sample immersing. The sample need immersed into PITC/DMSO solution and react at 45°C for 5hours in the sealed beaker. The Ph-N=C=S can react with R-NH_2 of APTES and form Ph-NH-CS-NH-R and the exposed amine group can be converted into phenyl group (Fig. 6.14 (c)).

(c) Hexyl isothiocyanate: 0.4ml HITC + 5ml Pyridine + 45ml DMSO → 45°C, 5hr

Similar to PITC passivation, the R-N=C=S functional group of HITC is also react with amine group of APTES with Pyridine as catalyst in DMSO environment. The reaction condition is the same as PITC passivation reaction, 45°C, 5 hours in sealed beaker (Fig. 6.14 (d)).

All the passivation methods can effectively passivate positively charged ATPEs by convert amine group into non-attractive methyl group or phenyl group. Considering DNA might be damaged during Acetic acid passivation procedure (DNA might be damaged at high pH or low pH value), HITC passivation is applied to our experiment.

R-N=C=S functional group is very commonly used functional group to react with amine modified DNA and therefore immobilize the amine modified DNA on the substrate.

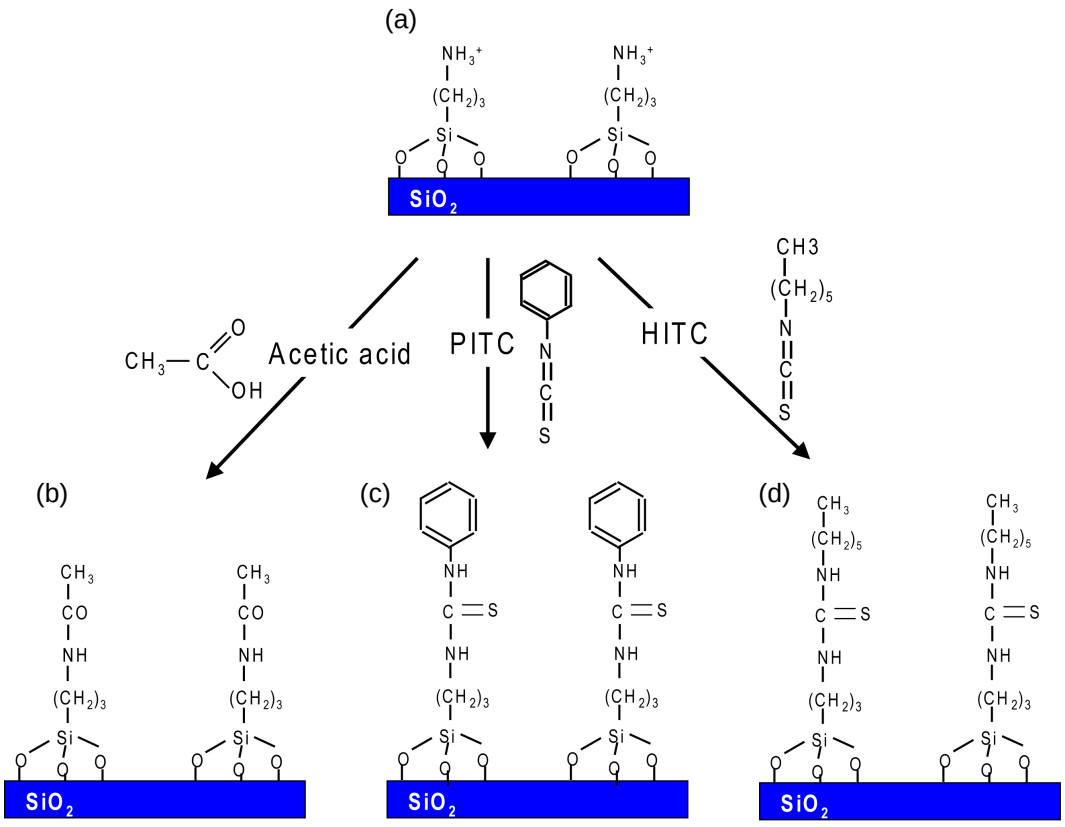

Fig. 6.14: Three different method of APTES passivation reaction. (a) APTES SAMs modified SiO_2 surface. (b) Passivate APTES with acetic acid, R-NH_2 react with HOOC-R' and form R-NH-CO-R'. Methyl group is the exposed functional group. (c) Passivate APTES with PITC, R-NH_2 react with S=C=N-Ph and form R-NH-CS-NH-Ph. Phenyl group is the exposed functional group. (d) Passivate APTES with HITC, R-NH_2 react with S=C=N-R' and form R-NH-CS-NH-R'. Methyl group is the exposed functional group.

6.2.1 Passivation Reaction: HITC React with Amine group of APTES

In order to make sure the passivation reaction between HITC and APTES is success, we design an experiment with two different sizes GNPs to check. We first prepare two samples with SiO_2 surface and modify the surface with APTES SAMs (0.5ml APTES/80ml EtOH, 1hr, RT) (Fig.6.15 (a)). Then immerse both samples into 50nm colloidal gold for 30minutes (immersion time is not enough for 50nm GNPs to fully cover the APTES SAMs surface) (Fig. 6.15 (b)). After 50nm GNP attachment, one sample is directly immersed into 20nm colloidal gold solution (Fig. 6.15 (d)) and the other process with HITC passivation reaction first (Fig. 6.15 (c)), and then immerse into 20nm colloidal gold solution (Fig. 6.15 (e)). If the passivation reaction is success, we should not observe 20nm GNP on the HITC passivation sample.

From Fig. 6.16 (b), we observe both 50nm GNP and 20nm GNP on SiO_2 surface by SEM. When the sample is immersed in the 50nm gold nanoparticle solution for 30minutes, the immersion time is not enough for 50nm GNP to fully cover the whole surface and there are still a lot of unoccupied APTES on the SiO_2 surface for 20nm GNP to attach. However, if the sample process with HITC passivation after 50nm GNP attachment, almost all the exposed amino group of APTES SAMs are passivated and the surface now is functionalized with non-attractive methyl group. From Fig.6.16 (a), we can find very little amount of 20nm GNP attach to the SiO_2 surface and that proves the passivation reaction of HITC is success.

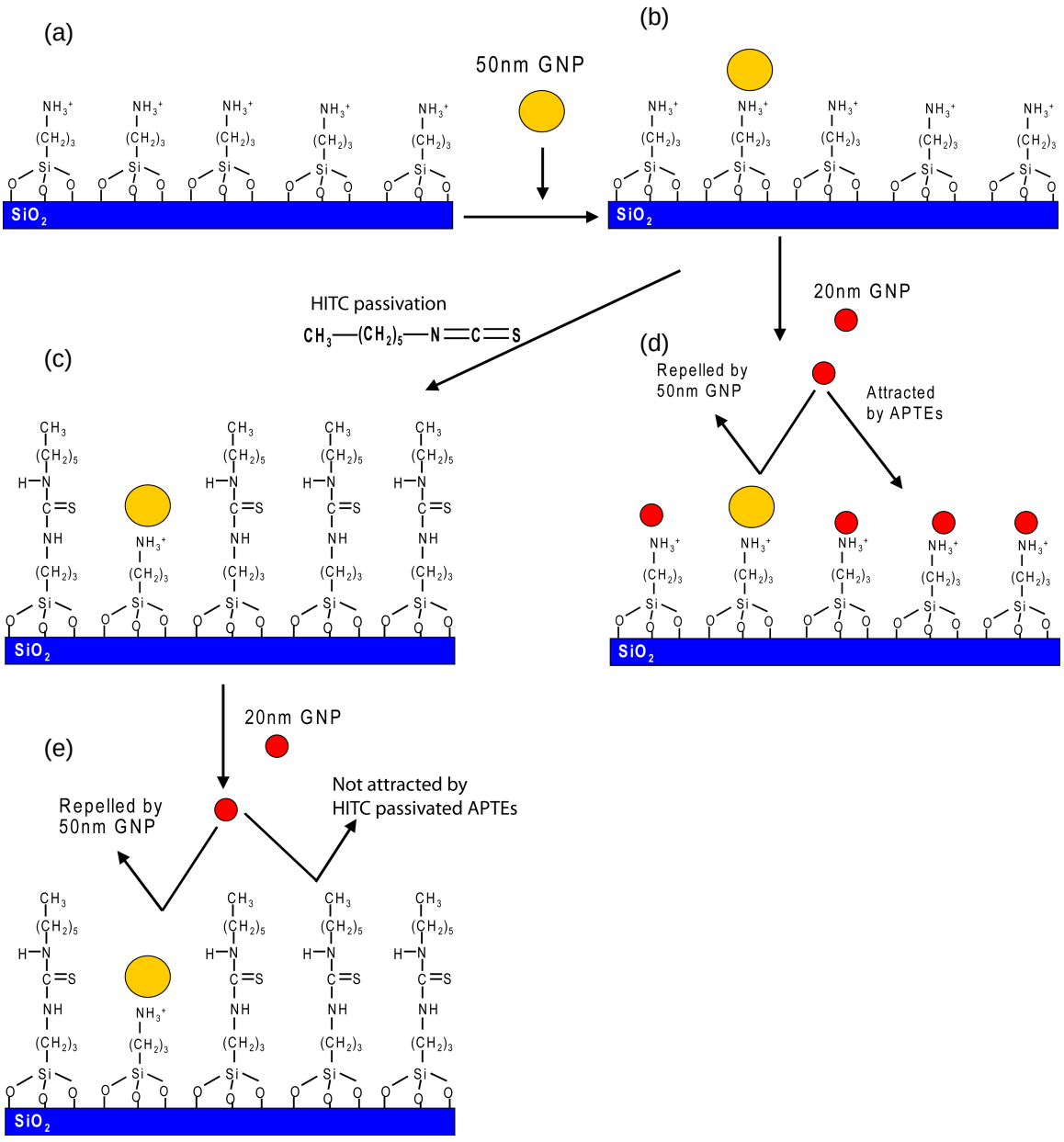

Fig. 6.15: Sketch of passivation reaction experiment steps. (a)→(b) 50nm GNP is attracted and fixed on the APTES modified SiO_2 surface. (b)→(c)→(e) Sample process with HITC passivation after 50nm GNP is fixed on the APTES SAMs modified SiO_2 surface. 50nm GNP will still stay on the surface, but all the un-occupied APTES is passivated and converted into non-attractive methyl group. The later introduced 20nm GNP can not attach to SiO_2 surface because the absence of positively charged amine group. (b)→(d) Without passivation reaction, the later introduced 20nm GNP can still occupy exposed amine group and attach to the SiO_2 surface. The purpose of this experiment is to show the HITC passivation reaction is success by examining the existence of later introduced 20nm GNP.

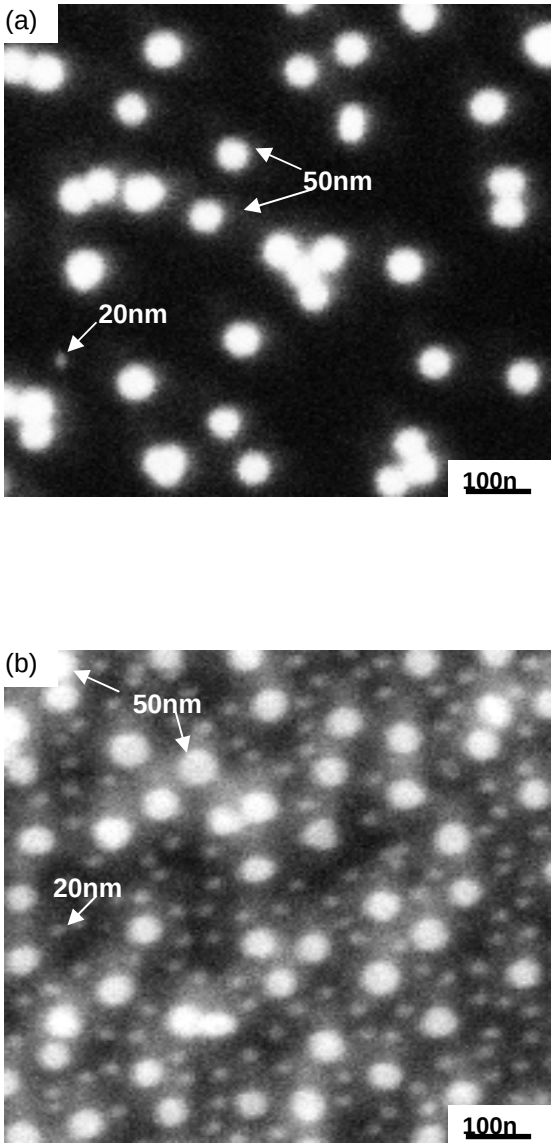

Fig. 6.16: SEM image of experiment described in fig. 6.15. (a) The SEM image of sample which process with HITC passivation reaction (fig. 6.15 (b)→(c)→(e)). Almost no 20nm GNP can be found on blank SiO_2 surface. (b) The SEM image of sample which do not process with HITC passivation (fig 6.15 (b)→(d)). 20nm GNP can still attach to the SiO_2 surface due to the attraction force between amine group of APTES (not taken by 50nm GNP) and 20nm GNP. Note that the 50nm GNP and 20nm GNP are not contact with each other due to the protection of citric ion which is physically absorbed on the nanoparticle surface.

6.2.2 HITC Passivation Reaction and C-50au T-P-30au Hybridization

After we make sure the passivation reaction between HITC and APTES is success, we have to make sure that HITC passivation reaction does not damage DNA molecules and does not affect the hybridization reaction between C-50au and T-C-30au (exp11/22/09). We now prepare two samples with APTES SAMs on SiO_2 substrate and immersed into C-50au/TE buffer solution for 1hrs at 50^{o}C (the reason why we heat up C-50au/TE buffer solution to 50^{o}C is to prevent aggregation between C-50au through non-specific hybridization between C-50au) (Fig. 6.17 (a)). We also prepare T-P-30au by hybridizing T-ssDNA with P-30au in the liquid phase at the same time (20nM T-ssDNA + 0.5ml P-30au + 1/10 HB at 45^{o}C, 2hr). After C-50au attach to the sample surface, one sample directly immersed into T-P-30au/TE buffer solution for hybridization at 45^{o}C, 2hr (Fig. 6.17(c)). The other sample process with HITC passivation at 45^{o}C, 5hr first (Fig. 6.17(b)), then hybridize with T-P-30au (Fig. 6.17(d)). The SEM images are shown as Fig. 6.17(e) for the process without HITC passivation, and Fig. 6.17 (f) for the process with HITC passivation.

Compare Fig. 6.16(b) with Fig. 6.18(a), 20nm GNP in Fig. 6.16 (b) can not attach to 50nm GNP surface due to the repelling force between citric-ion stabilized GNPs, but T-C-30au in Fig. 6.18 (a) can attach to C-50au due to some attraction force between C-50au and T-P-30au. We believe this attraction force comes from the hybridization reaction between T-P-30au and C-50au. However, to future confirm that hybridization reaction do occur between C-50au and T-P-30au, we will have another experiment which use three base pair mismatched ssDNA to replace complementary target ssDNA and will discuss later.

Compare Fig 6.16 (a) and Fig. 6.18 (b), we observe a lot of T-P-30au attach to SiO_2 substrate in Fig 6.16 (a) which means DNA modified T-P-30au can also be attracted by positively charged APTES SAMs. However, we also find some T-P-30au attach to HITC passivated SiO_2 surface in Fig. 6.18 (b) which is not preferred. Compare Fig 6.16 (a) and Fig 6.18 (b), all the un-occupied APTES should be passivated by HITC; however, T-P-30au can still attach to the SiO_2 surface, which means T-P-30au is still attracted by something we do not

expect. There two possibilities: (a) HITC passivation is not complete, still some positively charged amine groups are not passivated and therefore can attract T-P-30au. (b) Something occupied APTES site, and can attract T-P-30au.

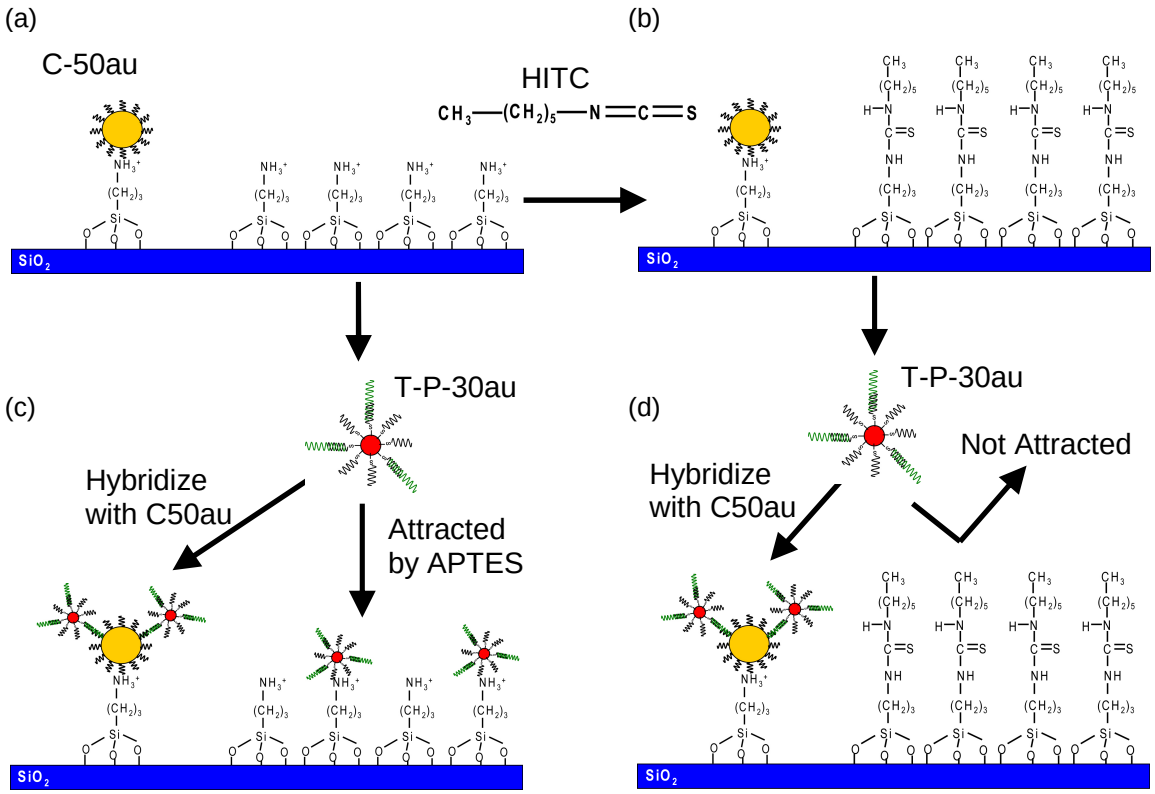

Fig. 6.17: Sketch of experiment steps for C-50au fixed on the solid substrate first, and then hybridizes with T-P-30au. (a)→(b)→(d) HITC passivation is applied after C-50au is fixed on SiO_2 surface by APTES SAMs and the later introduced T-P-30au can only attach to the surface by hybridizing with C-50au. The un-occupied APTES should be passivated according to the previous experiment (Fig. 6.15, and Fig. 6.16), therefore, no T-P-30au is expected to be found on the SiO_2 surface other than attach to C-50au. (a)→(c) No HITC passivation is applied after C-50au fixed on SiO2 surface by APTES SAMs. Later introduced T-P-30au can attach to the sample surface through either hybridizing with C-50au or occupying the exposed amine group (positively charged) of APTES.

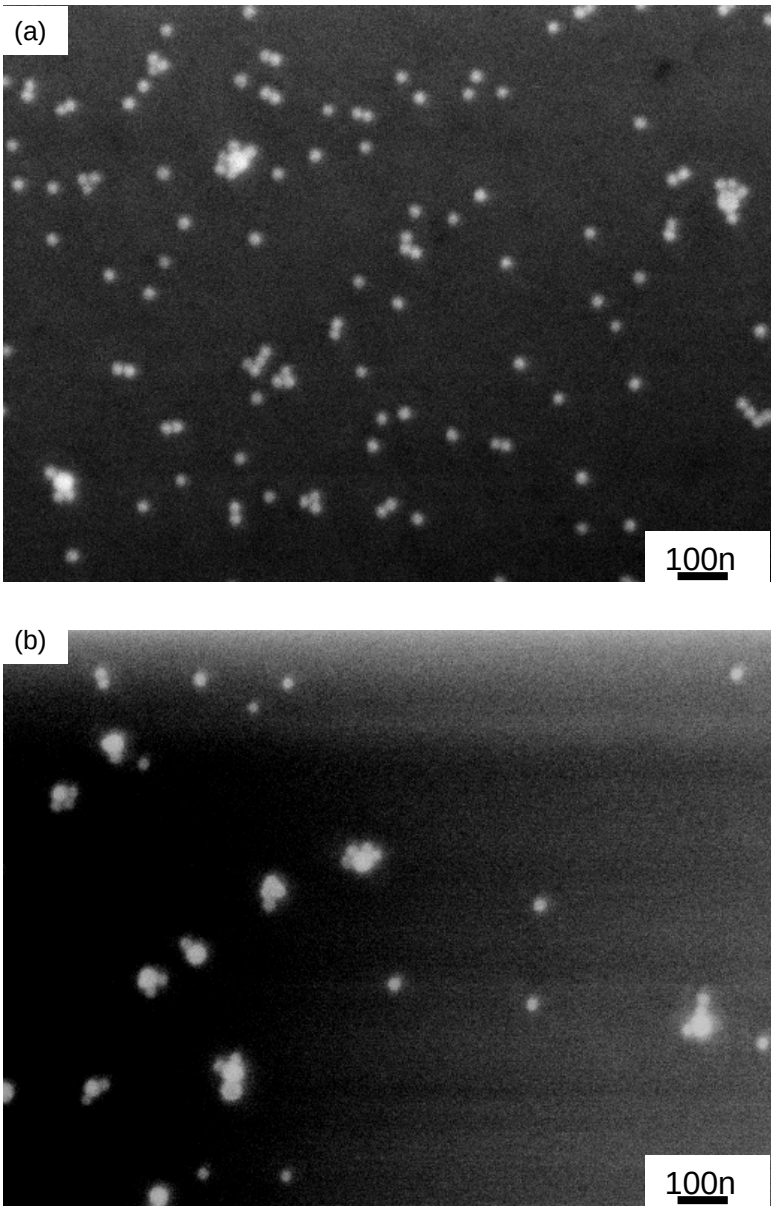

Fig. 6.18: SEM image of experiment results described at Fig. 6.17. (a) SEM image of sample process without HITC passivation (Fig. 6.17 (a)→(c)). T-P-30au can attach to the surface by either hybridizing with C-50au or occupying exposed APTES. (b) SEM image of sample process with HITC passivation (Fig. 6.17 (a)→(b)→(d)). T-P-30 attach to C-50au through hybridization is expected, but attach to SiO_2 surface is unexpected. The possible reason for T-P-30au can still attach to SiO_2 surface even process with HITP passivation is investigated and explained at next section.

6.2.3 Excess C-ssDNA Remain in C-50au Solution

To investigate the reason why T-P-30au can still attach to the HITC passivated SiO_2 surface, we design another experiment which including passivation reaction and C-50au hybridizing with T-P-30au, 3mm-P-30au and C-30au (exp 12/01/09). The reaction conditions are shown on the table 6.1 and SEM image of sample 1, 2, and 3 are shown at Fig. 6.19.

Table 6.1: Reaction Condition of C-50au Hybridize with T-P-30au, 3mm-P-30au and P-30au

Sample	SAMs	C-50au/TE	HITC Passivation	Hybridization
1	0.5ml APTES + 80ml EtOH 1hr, RT	0.5ml C-50au, 50oC, 1hr	0.5ml HITC + 5ml Pyridine + 45ml DMSO, 45oC, 5hr	T-P-30au
2				3mm-P-30au
3				P-30au

From the results of this experiment, we found an interesting situation that only T-P-30au can attach to the HITC passivated SiO_2 surface, but 3mm-P-30au and P-30au can. These results prove that the HITC passivation is success and T-P-30au attach to SiO_2 surface is not due to the un-passivated APTES but something else.

Also, only T-P-30au can attach to C-50au surface, but 3mm-P-30au and P-30au can not. This result is what we expect because C-ssDNA can hybridize with complementary T-ssDNA and form more stable double helix structure compares to 3mm-ssDNA (3 base pair mis-match). With proper hybridization condition, we can make T-P-30au easily to hybridize with C-50au and form stable satellite structure but not for the 3mm-P-30au and P-30au.

Therefore, we can conclude that the attraction force for T-P-30au to attach C-50au surface and HITC passivated SiO_2 surface is the same, which comes from C-ssDNA hybridize with T-P-30au.

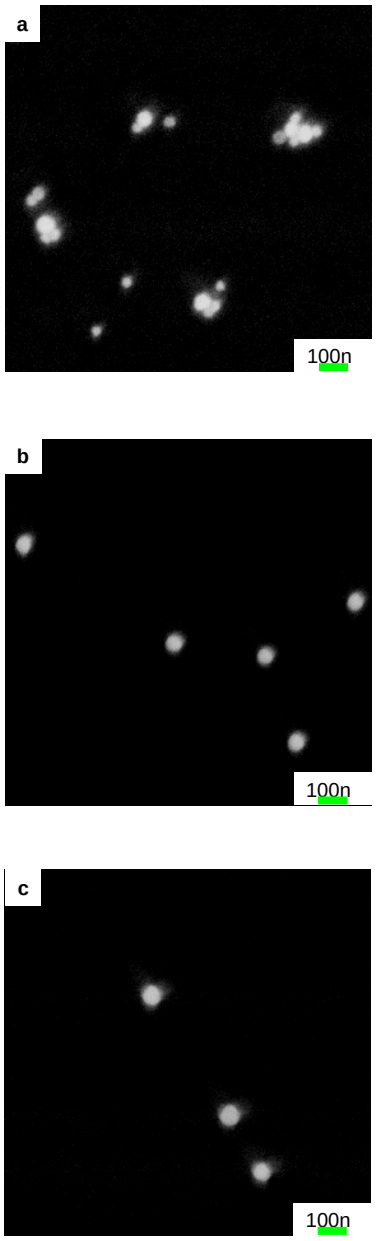

Fig. 6.19: SEM image of experiment sample described at table 6.1. (a) Sample process with HITC passivation after C-50au fixed on SiO_2 surface. The later introduced T-P-30au can attach to C-50au through hybridization and also can attach to SiO_2 surface due to the excess C-ssDNA remained in C-50au solution which occupied APTES site and provide a possible hybridization site. (b) Instead of T-P-30au, 3mm-P-30au is introduced after C-50au positioning and HITC passivation. Almost no 3mm-P-30au can be found on either C50au or SiO_2 surface. Which means 3mm-P-30au is not allowed to hybridize with C-ssDNA at given hybridization condition. (c) Instead of T-P-30au, only P-30au is introduced after C-50au positioning and HITC passivation. No hybridization event is expected and no P-30au can be found on the sample surface.

This is to say, when there are some C-ssDNA molecules remained in C-50au/TE buffer solution. When we immerse the sample of APTES modified SiO_2 surface into C-50au/TE buffer solution, not only C-50au is attracted and fixed of the SiO_2 surface, but also excess C-ssDNA attached to the SiO_2 surface (Fig. 6.20(b)).

After HITC passivation (Fig. 6.20(c)), although positively charged amine group of APTES are passivated and become non-attractive to negatively charged ssDNA modified GNPs, but excess C-ssDNA molecules trapped by APTES still provide active hybridization sites for complementary target ssDNA hybridization (T-P-30au) (Fig. 6.20(e), Fig. 6.19(a)). This is the most possible reason we can conclude from those experiment which well explains why we can not find 30nm GNPs on the SiO2 surface or connect with 50nm GNP under SEM when we introduce three base pair mis-matched ssDNA (3mm-P-30au) (Fig. 6.20(f), Fig. 6.19(b)) and only P-30au (Fig. 6.20(d), Fig. 6.19(c)).

The excess C-ssDNA molecules remaining in the C-50au/TE buffer solution can provide another hybridization site for T-P-30au; however, this hybridization event can not contribute to the conductivity changing in our design and will reduce the sensitivity of our detection.

While preparing C-50au, we add much more 3'-end thiolated C-ssDNA than needed to modify 50nm GNP and remove the excess C-ssDNA by centrifuge process mentioned at previous chapter (Chp 5.).

In order to ensure all the C-50au nanoparticles are well modified, we add much more 3' end thiolated C-ssDNA than we need to modify 50nm GNPs. After two days modification at room temperature, we add NaCl (=0.1M) and do not observe any 50nm GNP aggregation/precipitation (the highest density of thiolated DNA modified GNP is close to 1ssDNA/3nm^2). Theoretically, the highest ssDNA/GNP modification ratio is 2616 ssDNA/ 50nm GNP (30000 ssDNA/ 50nm GNP in our process); 942 ssDNA/ 30nm GNP (3100 ssDNA/ 30nm GNP in our process). Therefore, we expect to have a lot of excess ssDNA remain in the solution and try to remove them by several times repeating centrifuge/wash steps. However, it seems still have some remained.

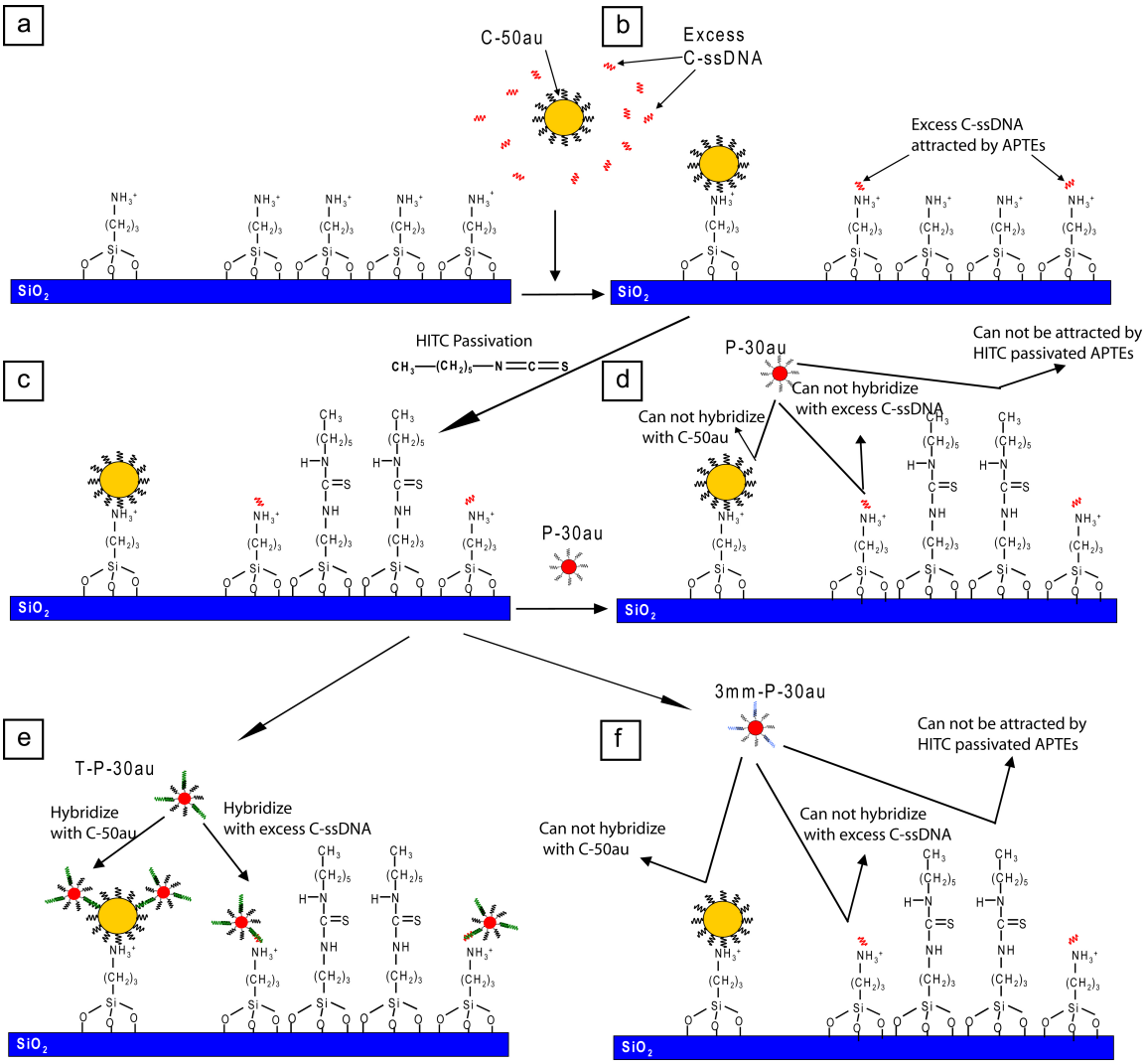

Fig. 6.20: How excess C-ssDNA affect the HITC passivation reaction and hybridization with T-P-30au. (a) SiO_2 surface with APTEs SAMs, (b) C-50au with excess C-ssDNA attach to APTEs surface, (c) passivate un-occupied APTEs SAMs, (d) introduced P-30au will not attach to surface by hybridizing with C-50au or excess C-ssDNA, (e) introduced T-P-30au will attach to surface by hybridizing with C-50au and excess C-ssDNA, (f) 3mm-P-30au will not attach to surface by hybridizing with C-50au or excess C-ssDNA.

6.3 Real DNA Sensing Device SEM Image and I-V measurement

After all the experiment steps required for a successful DNA detection are confirmed, our DNA detection method can now be applied to a real DNA detection device. The structure of the DNA detection device is described at the following section.

6.3.1 DNA detection Device

The basic DNA detection device for our method contains two parts: (1) a sensing area which is a dielectric layer separates two gold electrodes. (2) Two gold electrodes, one is used as source electrode and the other is used as drain electrode.

The simplest structure that fulfills both requirements is described at experiment steps section (Chp. 5). And here is the sketch with real SEM image.

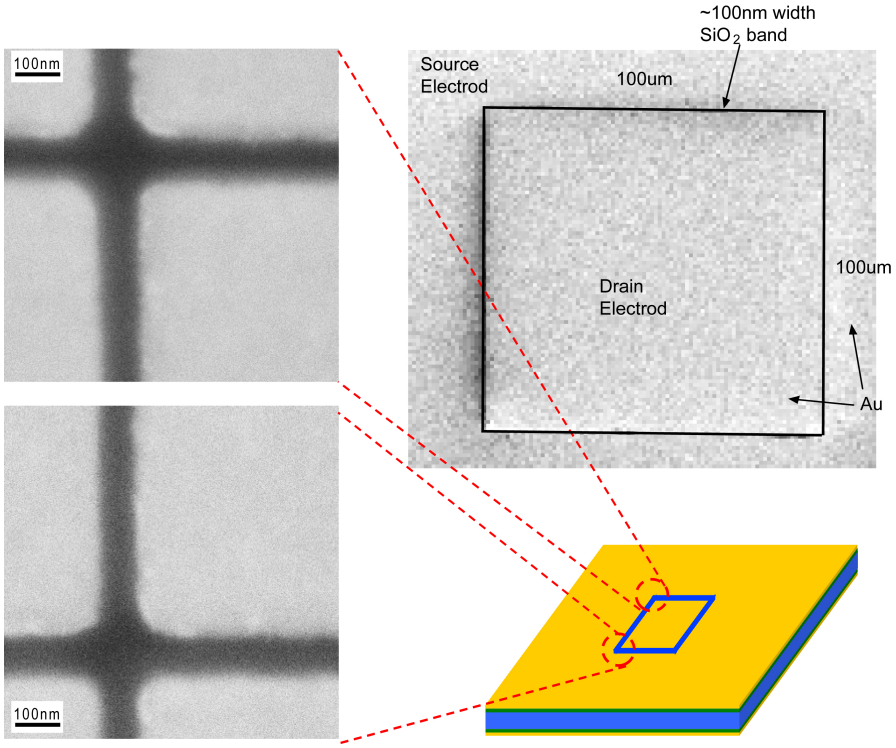

Fig. 6.21: SEM image for the real DNA detection device. The width of SiO_2 band is around ~100nm, the length of SiO_2 band is around 100um. Two gold electrodes (inside Au surface and outside Au surface) are separated by the SiO_2 band.

An exposed SiO_2 square band area with ~100nm width is created on the SiO_2 substrate, all other area is covered by gold. The gold surfaces outside and inside SiO_2 square band can be used as Source and Drain respectively. When there is no GNP bridge formed in the SiO_2 square band area (between two gold electrodes), the device shows open circuit.

The gold electrode surface is covered with 16MHA SAMs and SiO_2 surface is covered with APTES SAMs. All the samples before I-V measurement required a 10min UV Ozone to burn out those organic SAMs. Due to the ability of accurate controlling of nanoparticle placement as described at chapter 6.1, we are able to confine that all the DNA modified GNP and even DNA molecules can only be placed in the SiO_2 square band area.

The SEM image (Fig. 6.21) shows just one of our DNA detecting devices, but the whole idea can be applied as a DNA micro array. In other ward, with current CMOS technology, our DNA detecting device can be made by photolithography at entire wafer scale. Also, many devices can be placed in a small piece of wafer and form micro array. Each device can be treated as a pixel for entire micro array which give us the ability of massive detection information at one experiment compares to other DNA detection method.

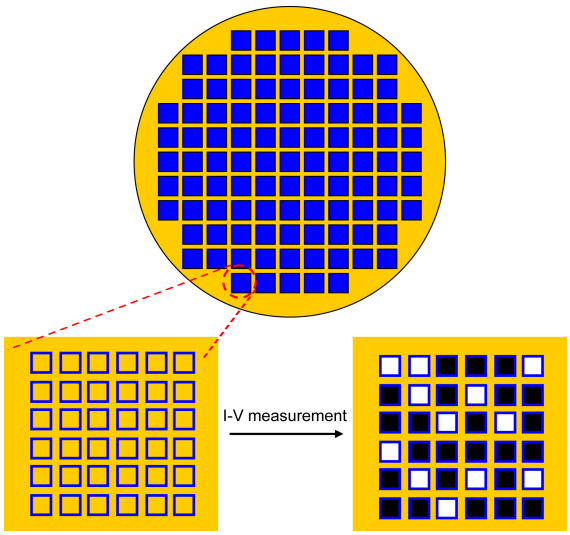

Fig. 6.22: Sketch of micro array made by our DNA detection mechanism. White squares represent device with resistive circuit (with Target DNA, GNP bridges formed), black squares represent open circuit (no Target DNA, no GNP bridge). The current intensity can be used as an indication of the concentration of Target DNA

6.3.2 Analysis and Estimation of Tm for DNA and DNA modified GNP

Melting temperature is important for the DNA hybridization experiment because hybridization temperature is usually 10~15 ^{o}C lower than the melting temperature. Also, we introduce a three-base-pair mismatched ssDNA (3mm-ssDNA) as a contrast experiment compare to complementary Target ssDNA, therefore, it is very important to choose the hybridization temperature which lower than the Tm of T-ssDNA but higher than the Tm of 3mm-ssDNA. This means, this hybridization temperature will allow complementary Target to hybridize with Capture ssDNA, but almost not for the 3mm ssDNA.

In order to have some estimation of melting point of the DNA we use in the experiment. An online tool provided by IDT (https://www.idtdna.com/analyzer/Applications/OligoAnalyzer/) is applied for the Tm estimation. The factors that affect Tm of DNA were discussed in the previous chapter, but we just briefly describe here again. The concentration of ssDNA and the concentration of salt are the main factors for the Tm variation in the DNA hybridization system. We have estimate the Tm for our Capture ssDNA and Probe ssDNA from a range of [DNA] = 10nM ~ 500nM, and [Na^{+}] = 0.01M~0.15M. The estimation plots are shown at Fig. 6.23 and Fig. 6.24.

Although the estimation of free DNA melting temperature in the free solution environment (calculated by simulation software provided by IDT) can not represent the real situation of DNA modified GNP melting behavior, but the estimation still provide some ideal about the roughly range that is suitable for our experiment conditions. The melting temperature of DNA linked GNP in the liquid phase will shift lower but sharper compares to the free DNA due to the interaction between nanoparticles as discuss on previous section. And if one DNA modified GNP is fixed on the substrate and the other DNA modified GNP is from free solution, the Tm will be also different compares to the liquid phase DNA linked GNP.

The purpose of all the discussion above is to illustrate the reason why we can not have the accurate hybridization before hybridization directly by estimation or calculation, but need do some experiment and find the best hybridization temperature first.

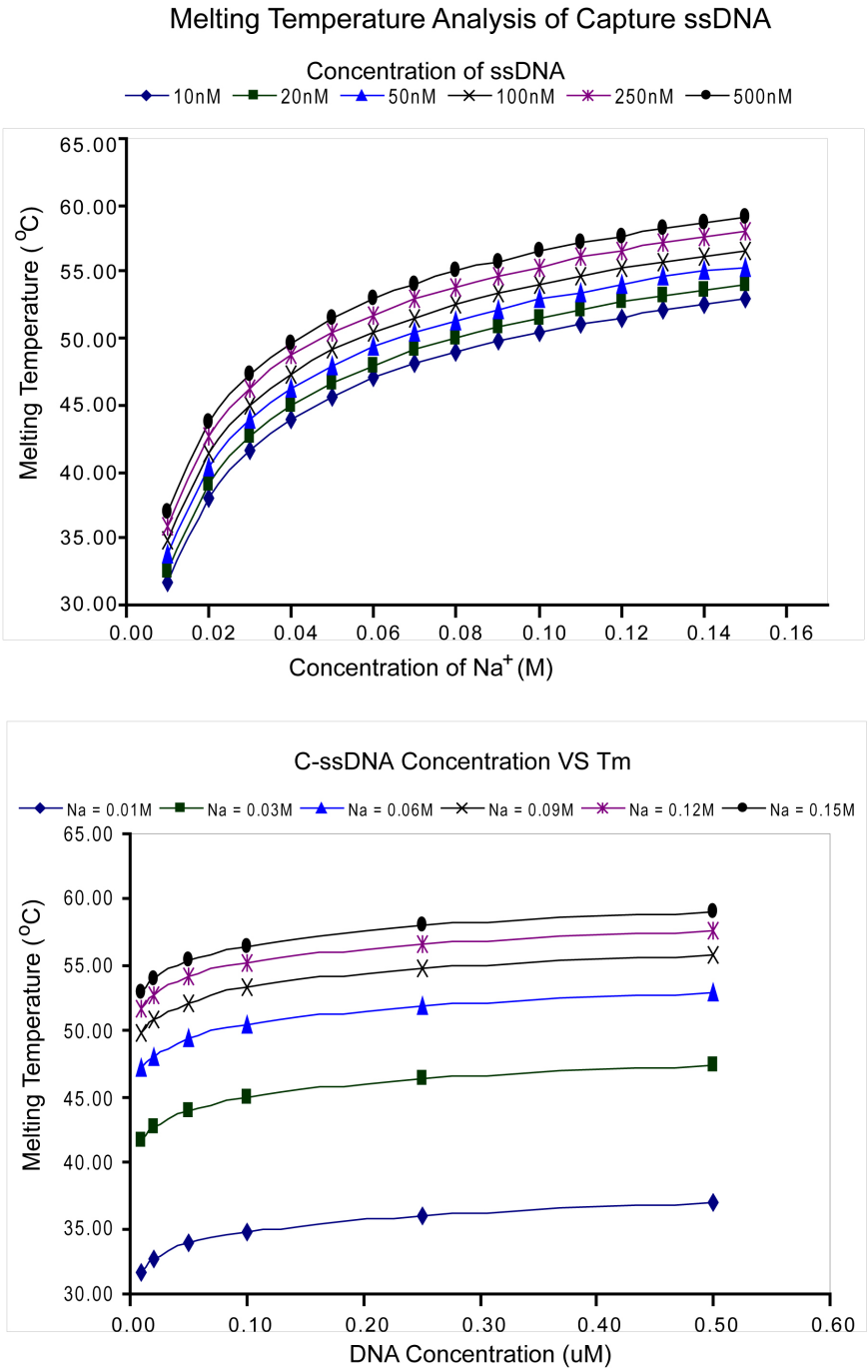

Fig. 6.23: Estimation of C-ssDNA Tm at different DNA concentration and Na^+ concentration.

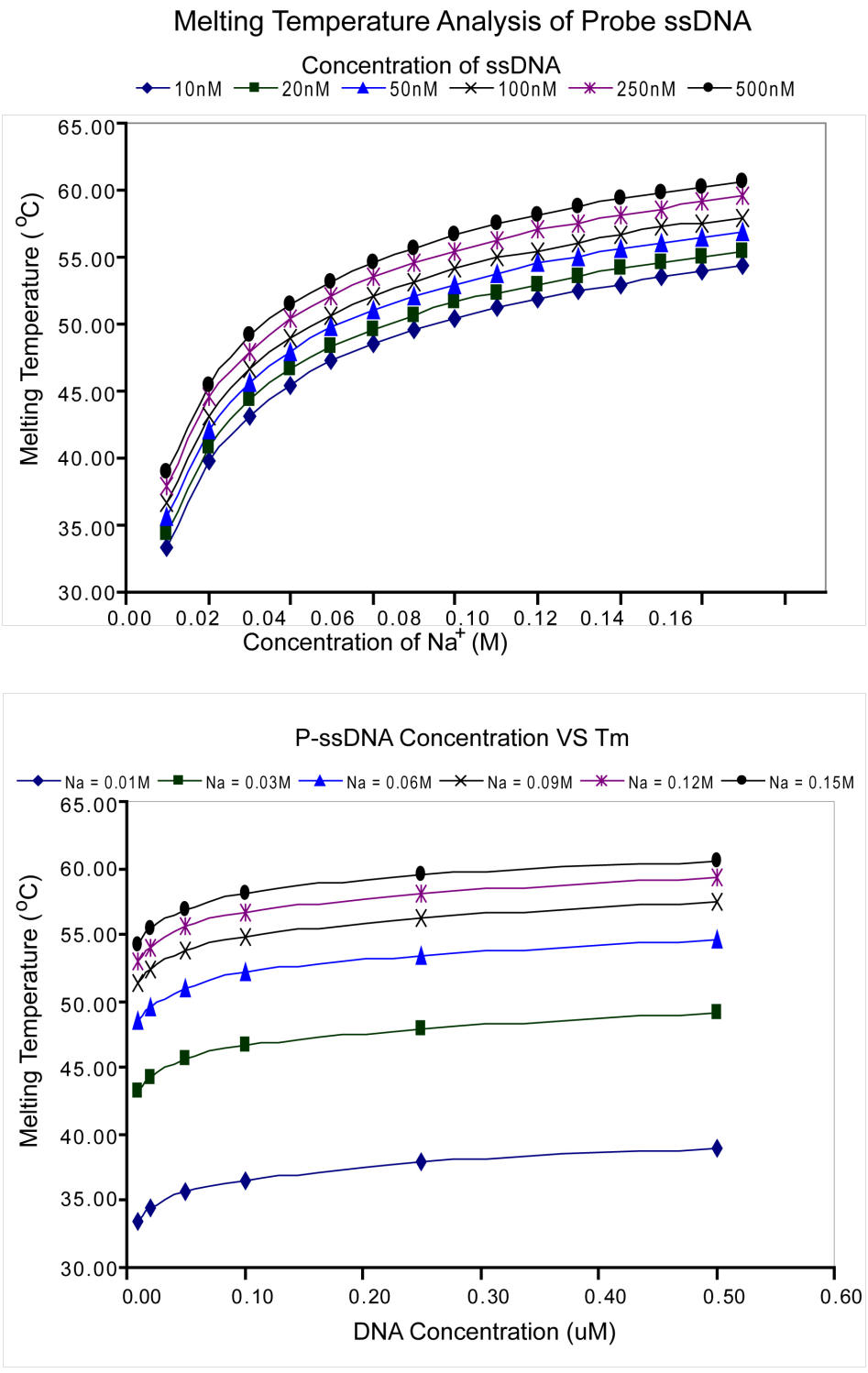

Fig. 6.24: Estimation of P-ssDNA Tm at different DNA concentration and Na^+ concentration.

6.3.3 Liquid Phase Hybridization of C-50 and T-P-20

In order to have roughly idea about the hybridization we should choose for ssDNA modified GNP hybridization, we design a set of experiment for ssDNA modified GNP hybridization in liquid phase with different temperature. We can directly observe weather DNA modified GNP is linked through DNA hybridization reaction or not by observe the color change of DNA-GNP solution from red to dark blue or precipitation on the bottom. The experiment steps are illustrated by Fig. 6.25. We mix 0.5ml C-50au with (a) 0.5ml T-P-20au, (b) 0.5ml 3mm-P-20au and (c) 0.5ml P-20au and add 0.1ml Hybridization buffer. Those mixtures are hybridized in water bath with different temperature (T1, T2 and T3) for 2~3hours. When hybridization reaction occurs, nanoparticle will linked together through DNA hybridization and aggregate. The aggregation of GNP will cause the solution color change from red-pink to light pink and finally gray or dark blue. Also, black of dark blue precipitation will show on the bottom due to the aggregated GNP precipitate from solution.

The temperature we choose for T1 (55^oC) is 5^oC higher than the melting temperature of C-ssDNA in free solution (50^oC, $[Na^+]$ =0.1M, [T-ssDNA] =20nM). In this set of experiment (Fig. 6.25 (a1), (b1), (c1)), we do not expect to observe and color change of the solution or any precipitation. That means there should be no hybridization between C-50au with T-P-20au, 3mm-P-20au or P-20au. This set of experiment is to confirm that GNP aggregation must caused by DNA hybridization events, not by other factor. (All the DNA modified are proven stable even at 60^oC overnight.)

T2 (45^oC) is chosen as 5^oC lower than free DNA melting temperature. We know that the melting temperature of DNA linked GNP will be different from free DNA melting due to the extra interaction between nanoparticles. But how much shift of Tm compares to free DNA melting temperature depends on the distance between nanoparticles. In the work done by Storhoff and Mirkin et al (2000), Y.Sun and C.-H. Kiang et al (2005) [2.22, 2.23] suggest that for nanoparticles separated by 24 base pair, the Tm of DNA linked GNP is lowered by around 15^oC (for 3-DNA system). If the separation is 12 base pair, Tm of DNA linked GNP is lowered by

26^{o}C (for 2-DNA system). And if the separation is 24 base pair in 2-DNA system, the Tm of DNA linked GNP is similar to Tm of free DNA [2.23]. Seems 3-DNA system will increase the Tm shifting while GNPs are closed. And for 2-DNA system, 24 base pair provides good enough separation to minimize the GNP interaction effect.

In our situation, we apply 3-DNA system (capture, target and probe ssDNA), the total separation between nanoparticles is 36 base pair + 9 poly T spacer + C_9H_{18} linker. We can assume the separation between C-50au and P-20au should be far enough to minimize the GNP interaction, therefore, the melting temperature of our DNA linked GNPs should be roughly close to the free DNA melting temperature. (Consider at high salt concentration environment for DNA hybridization, electric double layer interaction for C-50au and P-20au should be reduced and will not affect Tm much.)

However, we still do not know the accurate melting temperature for 3mm-ssDNA; therefore, in order to make sure the hybridization temperature can provide a good environment for complementary Target-ssDNA hybridize with C-ssDNA, but prohibit 3 base pair mismatched 3mm-ssDNA hybridize with C-ssDNA, we choose T2 (hybridization temperature) is only 5^{o}C lower than the Tm of free DNA.

From experiment result shown at Fig. 6.25, we observe solution color change (red to light pink) and black precipitation on the bottom (Fig. 6.25(a2)) within given hybridization time (2 hours), and no precipitation and color change for the C-50 + 3mm-T-P20au (Fig. 6.18(b2)).

If we immerse a piece of APTES modified SiO_2 sample into (a2) and (b2) and check if the hybridization do occur or not, the SEM image is shown at Fig. 6.26.

T3 is chosen as 30^{o}C, which is 20^{o}C lower than the free DNA melting temperature. The experiment results show that both C-50 hybridize with T-P-20au and 3mm-P-20au. Therefore, at this hybridization temperature, we can not have the selectivity of hybridization between complementary Target ssDNA and 3 base pair mismatched ssDNA.

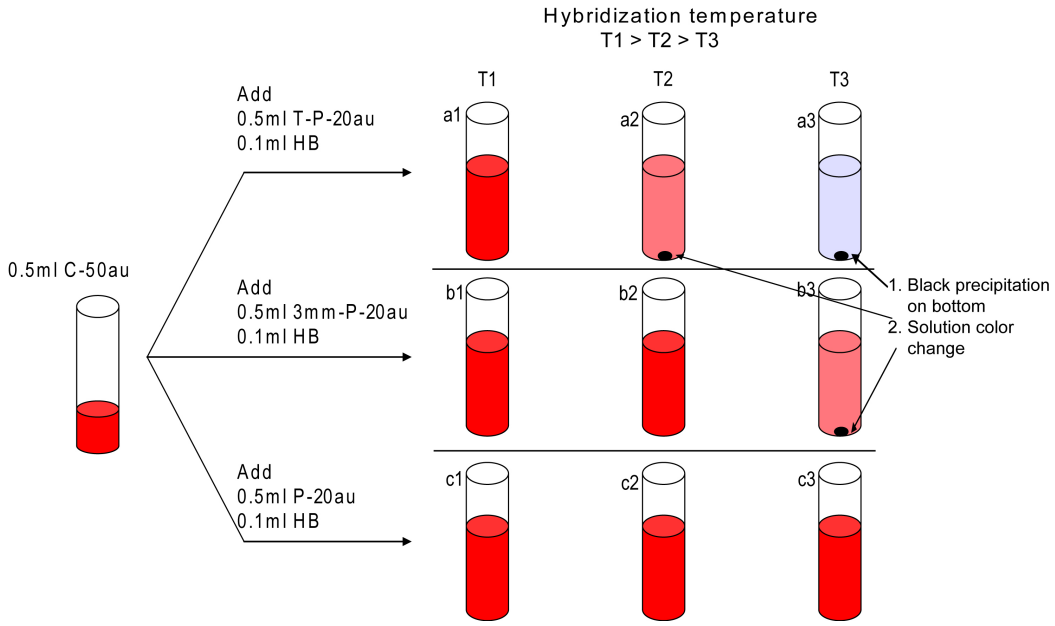

Fig. 6.25: Liquid phase hybridization experiment steps. (a1)(a2)(a3) C-50au mix with T-P-20au and hybridized at different temperature T1, T2 and T3. (b1)(b2)(b3) C-50au mix with 3mm-P-20au and hybridized at different temperature T1, T2 and T3. (c1)(c2)(c3) C-50au mix with P-20au and hybridized at T1, T2 and T3. Black precipitation occur on the bottom (a2, a3, b3) means the GNPs are linked with each other and aggregate together through DNA hybridization. When GNP aggregate, the size of particle increase which cause the color change from red to dark blue.

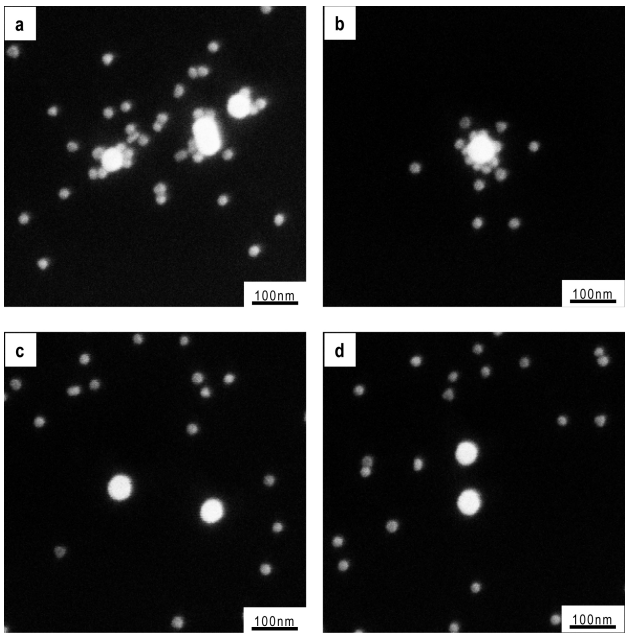

Fig. 6.26: SEM image of Fig. 6.25. (a)(b)SEM image of Fig. 6.25 (a2). (c) SEM image of Fig. 6.25 (b2), (d) SEM image of Fig. 6.25 (c2)

6.3.4 C50au hybridize with T-P-20au in narrow trench area

Science we have confirmed all the DNA detection experiment steps are working successfully, the next step is to determine the time required for C-50au aligned in the narrow trench area (100~90nm width), and the time required for hybridization.

The repelling force between charged surface and charged nanoparticle will be affected due to the change of guiding structure on the surface. Also, the ion concentration is an important factor, too.

We design following experiment with (1) interparticle distance affected by ion concentration of gold nanoparticle solution (2) different time to observe the time required for nanoparticle get into the narrow trench area.

Fig. 6.27 shows different interparticle distance with different dilution ratio.

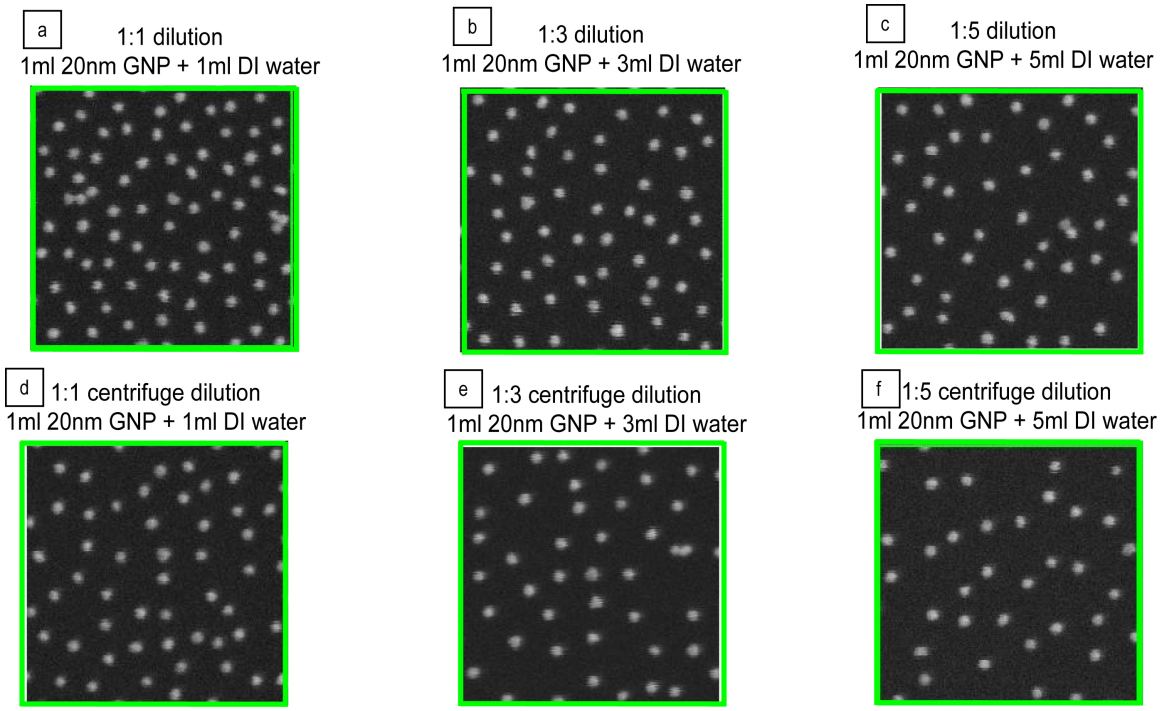

Fig. 6.27: Interparticle distance varying with ion concentration. (a) ~ (c): direct dilute 20nm gold nanoparticle solution with DI water, the interparticle spacing increase with dilution ratio. (d)~(e): the gold nanoparticle solution is centrifuge first and remove top layer clean solution before add DI water to dilute gold nanoparticle solution, the ion concentration should be lower than (a)~(c) at same dilution ratio (exp 04/13/2007).

The analysis result of how interparticle spacing varying with different concentration are shown at Fig. 6.28

Table 6.2: Interparticle Distance with Different Ion Concentration

Conditions (Au colloid/DI water)	No. of particles	Inter-particle distance (nm)
1:1 Dilution	76	55.61
1:3 Dilution	55	65.80
1:5 Dilution	49	69.36
1:1 centrifuge Dilution	52	66.72
1:3 centrifuge Dilution	44	73.99
1:5 centrifuge Dilution	36	79.69

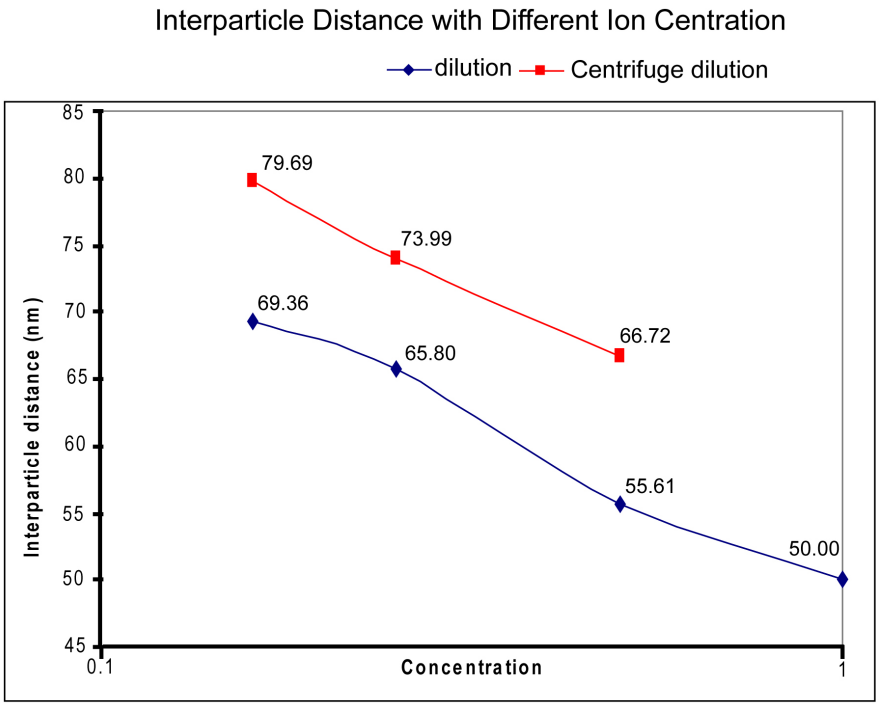

Fig. 6.28: The interparticle distance varying with ion concentration of gold nanoparticle solution.

The diluted gold nanoparticle solution has lower ion concentration, although we do not know the accurate ion concentration, but we can just compare with different dilution ratio and have a roughly ideal. The centrifuge dilution (red square curve) means we centrifuge down of

the nanoparticles first, and remove the top clean solution which contains most of the ions and stabilizers for gold nanoparticle (Fig. 6.27 (d)~(f)). In this way, we can future reduce the ion concentration compares to the diluted only sample (Fig. 6.27 (a)~(c)).

For the whole experiment describe above, we let gold nanoparticle have enough time to attach on the surface (24hr, RT) and reach the saturation situation (highest density). The attachment of GNP to the APTES SAMs modified SiO_2 substrate is not reach the highest density at once, but attach to the surface with low density and then gradually increasing.

It is important to notice that the time require for C-50au get into a narrow trench area is varied with (1) the width of trench, (2) the concentration of C-50au, and (3) the ion concentration of C-50au solution. We fix those three factors and observe the C-50au attachment with different time of C-50au solution immersion. Fig. 6.29 (a) shows the C-50au attachment for 17hrs immersion and Fig. 6.29 (b) shows the attachment for only 10hrs immersion. And from the experiment, we choose 17hrs C-50au immersion time for our experiment condition.

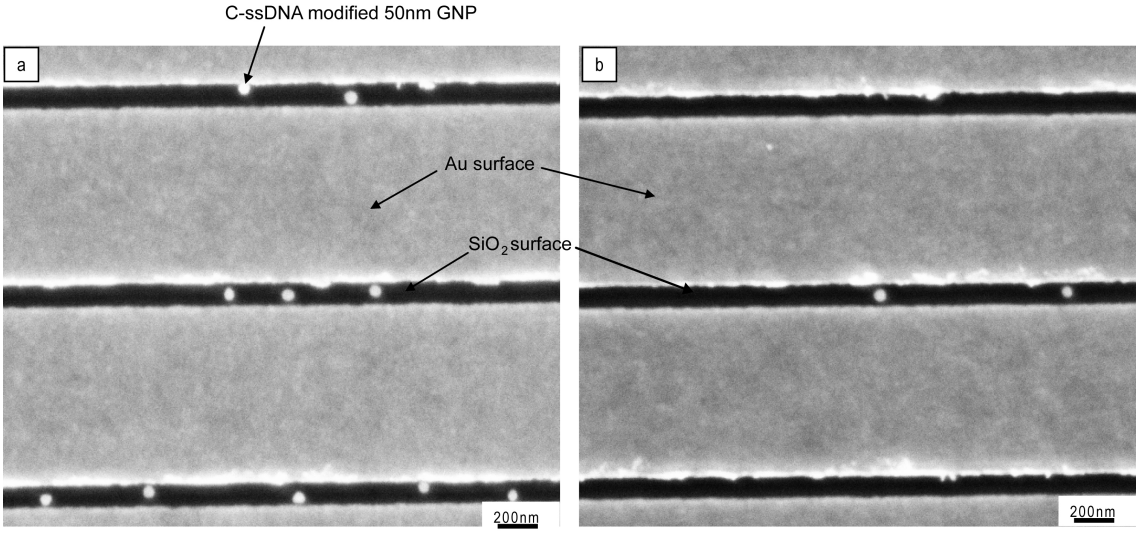

Fig. 6.29: Time required for C-50au to enter the narrow trench SiO_2 band. (a) 17hrs immersion for C-50au enter ~100nm trench SiO_2 band. (b) 10hrs immersion. The number of C-50au in the trench is much less compares to (a).

For the hybridization time estimation, we find out that the ion concentration for hybridization is high enough to greatly reduce the Debye length of electric double layer, therefore the 3hrs hybridization time for T-P-30au to hybridize with C-50au (located in the trench area) can allowed enough DNA bridge formation.

6.3.5 Real DNA sensing Device Experiment and I-V measurement

The real DNA detecting device we designed is a simple SiO_2 square band with ~90nm in width and 100um in length which separate gold substrate into two parts, inside the square and outside. The separated inside and outside gold surface can be used as source-drain electrodes and measuring the conductivity change after hybridization. The simple experiment steps are: (1) Modified sample surface with APTES and MHA. (2) Immerse sample into C-50au solution, C-50au will fill into the SiO_2 square band only. (3) Passivate sample with HITC (hybridize 20nM T-ssDNA or 3mm-ssDNA with P-30au during passivation reaction). (4) Hybridize T-P-30au or 3mm-P-30au with C-50au on sample surface. (5) Immerse sample in washing buffer for overnight washing at hybridization temperature.

After all the process, the SEM image is taken and shown at Fig. 6.30 ~ Fig. 6.33. There are some experiment settings should be noticed.

(1) The concentration of C-50au: The number of 50nm GNP is around $4.5x10^{10}$ / ml and we expect ~20-30% 50nm GNPs will be lost during C-ssDNA modification and centrifuge wash process. Although we add excess C-ssDNA to modified 50nm GNP and therefore no precipitation occur after add [NaCl] = 0.1M and heat to $50^{o}C$ overnight for aging. But, during the centrifuge wash process (centrifuge down the nanoparticles, and remove top layer clean solution by pipette then followed by add fresh TE buffer solution to re-suspend C-50au), we will lose part of C-50au while remove the top clean solution. The more repeating times of the centrifuge steps, the more C-50au will be lost. However, in order to remove excess C-ssDNA as much as possible, we repeat this step for 10 times. By control the concentration of C-50au and

the C-50au positioning time, we can control the number of C-50au filled into SiO2 squire band area. In this set of experiment, there are around ten C-50au in each device.

(2) The concentration of P-30au: same situation for P-30au compares to C-50au. The number of 30nm GNP is around $2.0x10^{11}$ /ml, and will lose 20~30% after repeating centrifuge process for 10 times.

(3) The concentration of T-P-30au: We add T-ssDNA into 0.5ml P-30au and make the concentration of T-ssDNA is 20nM. This means we have ~$6x10^{12}$ T-ssDNA in the 0.5ml P-30au solution. Assuming we do not lose any 30nm GNP during P-30au preparation. Therefore, each P-30au can have at least 30 T-ssDNA ($6x10^{12}$ / $2x10^{11}$) for hybridizing.

The number of P-ssDNA modified on 30nm GNP should be more than 300 (max. DNA modified GNP density is 42pmole/cm^2 = 0.25/nm^2, which means ~700 ssDNA/30nmGNP)[ref" A fluorescence-based method for determining the surface coverage and hybridization efficiency"]. Therefore, the number of P-ssDNA on the 30nm GNP is much more than the number of T-ssDNA. And it should be safe to assume all the T-ssDNA is hybridized by P-30au in the liquid phase.

From Fig. 6.30~ Fig. 6.33, we successfully demonstrate a new DNA sensing method which hybridization events can be accurate controlled on the specific sensing area (C-ssDNA modified 50nm GNP surface). The uniqueness of our work is that every single DNA hybridization event might be able to be detected by our method. By accurate controlling of C-50au placement, C-50au is placed only between two gold electrodes. The following passivation of positively charged APTES SAMs on SiO_2 surface ensures that the only place which T-P-30au can attaches is C-50au surface by hybridization. This is to say, every hybridization event between C-50au and T-P-30au is taking place in the effective sensing area and have a good chance to be detected by forming GNP bridges across two gold electrodes (separated by ~90nm SiO_2 band).

Our experiment results show that GNP bridges (formed by C-50au and T-P-30au) formed across two gold electrodes provide strong signal even with very limited among of GNP

bridges (four GNP bridges between two electrodes provide ~0.5uA current signal at 0.1V). Which means our detection method is able to detect the existence of Target ssDNA even with only a few hybridization events between C-50au and T-P-30au and therefore the theoretical sensitivity can be reached is ~zM (10^{-21} M). And the control experiment with 3 base-pair-mismatched ssDNA shows no GNP bridge formation which means our detection method provide good selectivity between complementary Target ssDNA and mis-matched ssDNA.

We have proved our concept working fine with Target ssDNA concentration at 20nM, but the detection sensitivity can be greatly improved by applying other hybridization assistant system such as hybridization chamber and microfluidic system.

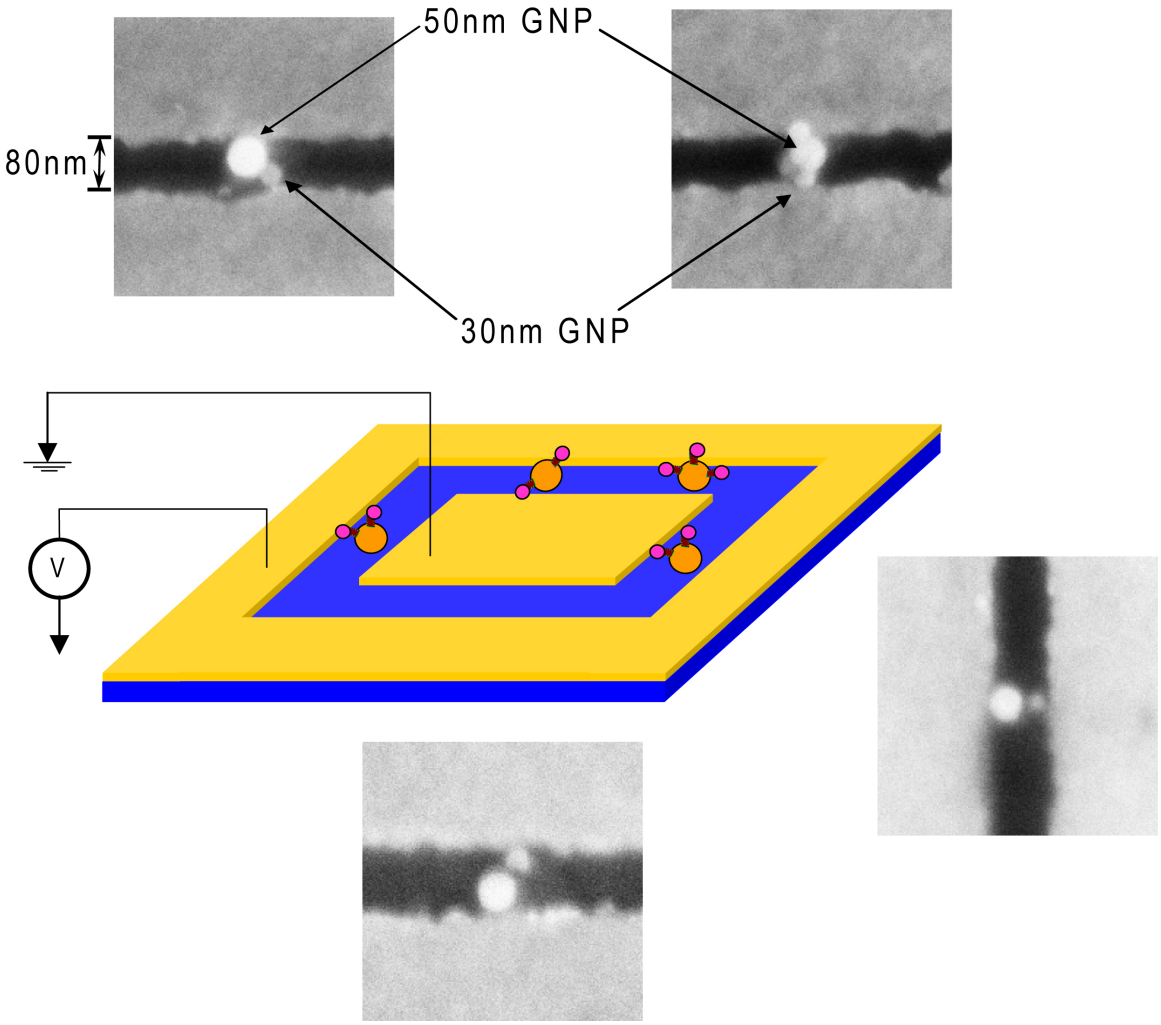

Fig. 6.30: SEM image of 20nM T-P-30au hybridize with C-50au in the SiO_2 square band area. The band width is ~90nm, depth is around 20nm (lower than the Au electrode surface on both side). Due to the concentration of C-50au and the SiO_2 band width we use in this experiment, around 6 C-50au are able to fill into the SiO_2 band and 4 GNP bridge was found. I-V measurement is shown at Fig. 6.33.

.

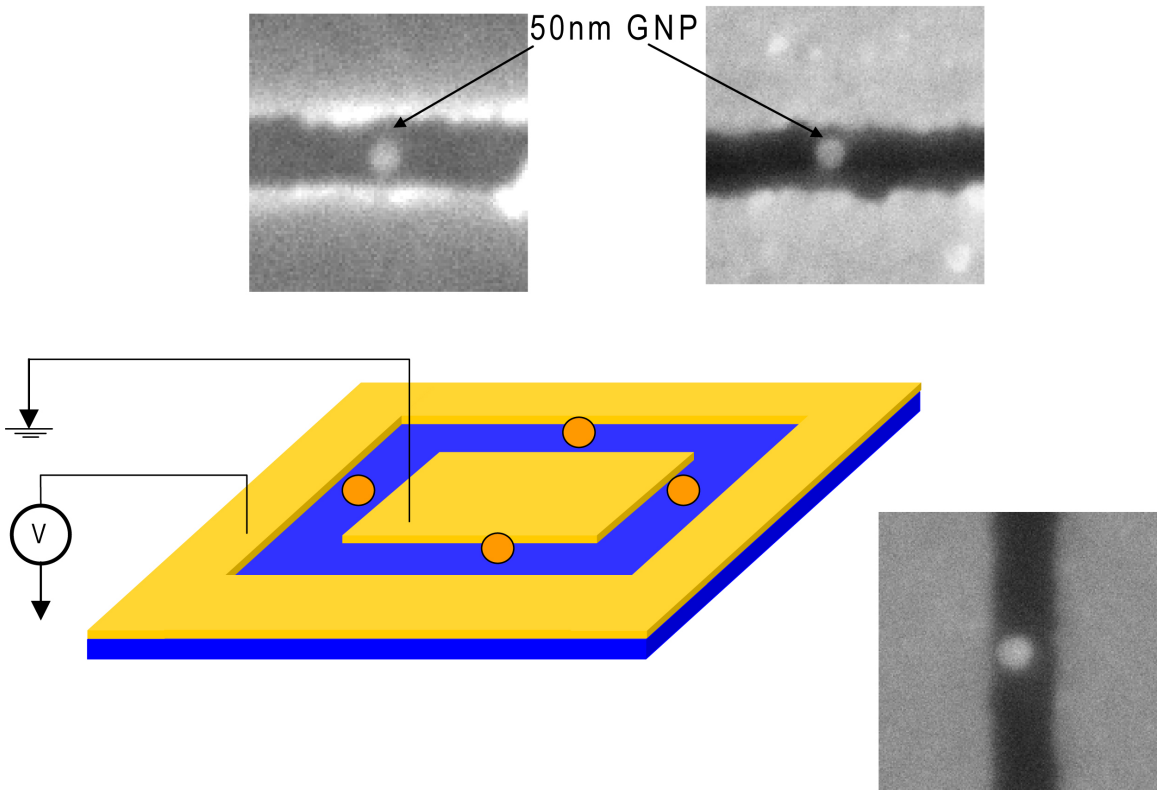

Fig. 6.31: SEM image of 20nM 3mm-P-30au hybridize with C-50au in the SiO_2 square band area. Due to the hybridization temperature we chose (45^{o}C) is not suitable for 3mmssDNA hybridize with C-ssDNA, no 30nm GNP is expected to attach on 50nm GNP surface through C-50 and 3mm-P-30au hybridization. There are around 10 C-50au found in the whole SiO_2 area without any 3mm-P-30au attached. I-V measurement shows open circuit and is shown at Fig. 6.33.

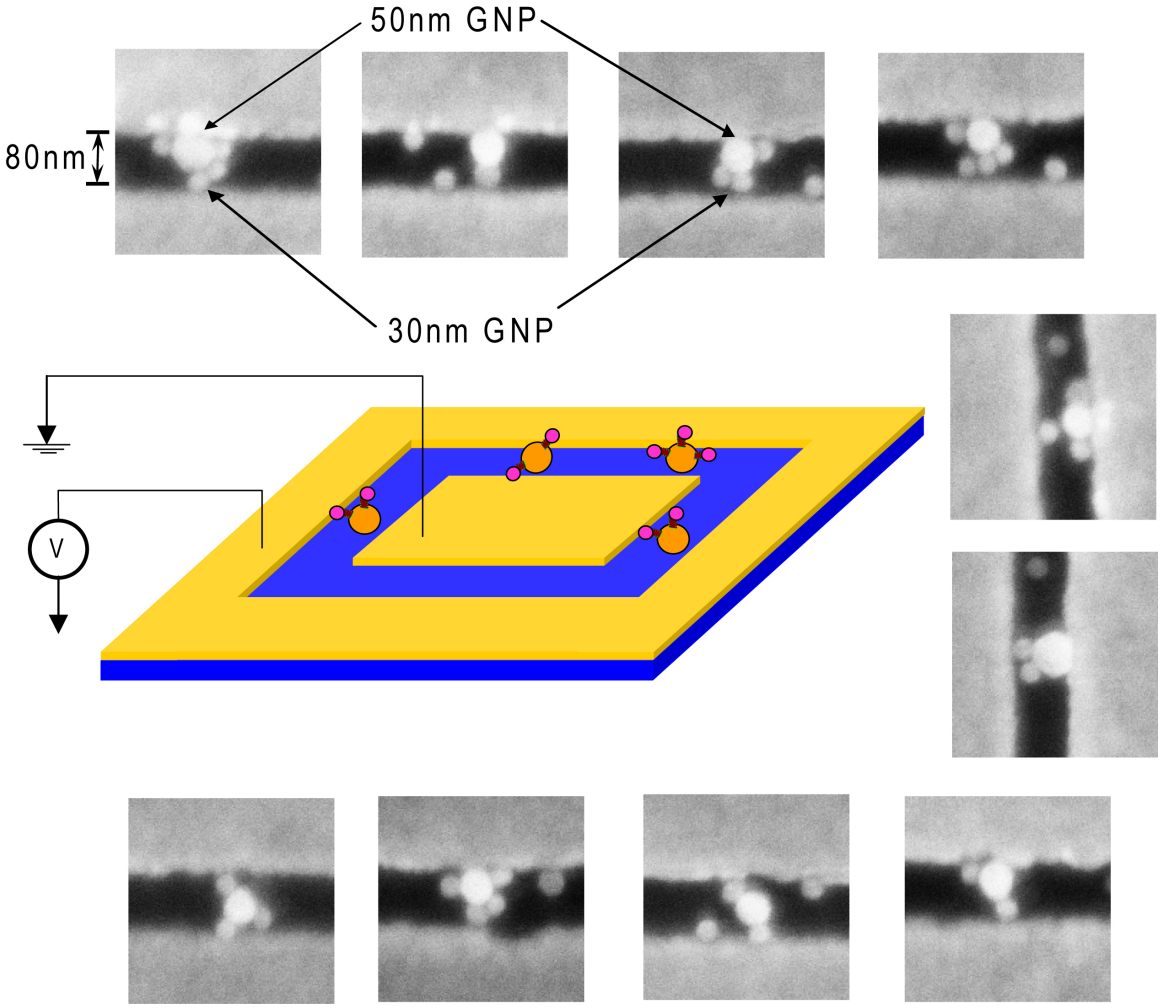

Fig. 6.32: SEM image of 20nM T-P-30au hybridize with high concentration of C-50au in the SiO_2 square band area. The band width is ~90nm, depth is around 20nm (lower than the Au electrode surface on both side). The concentration of C-50au in this sample is 4 times higher that Fig 4.21 and the SiO_2 band width we use in this experiment, around 20 C-50au are able to fill into the SiO_2 band and 10 GNP bridge was found. I-V measurement is shown at Fig. 6.33.

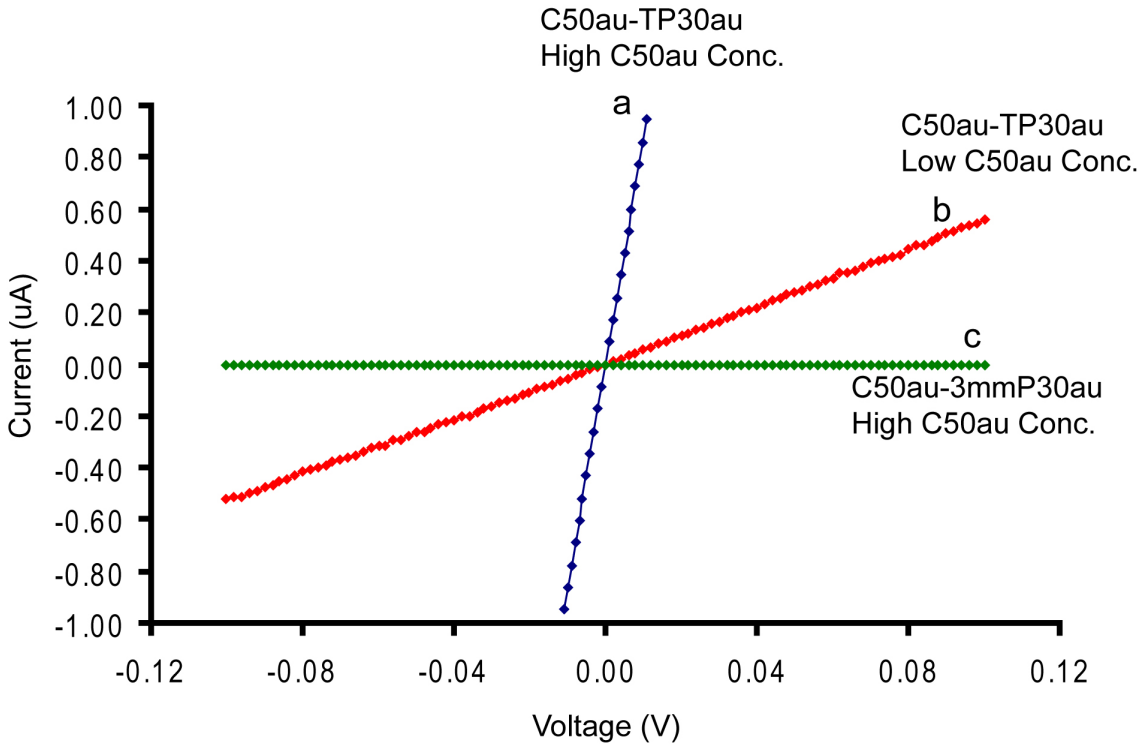

Fig. 6.33: I-V measurement of DNA detection device shown at Fig. 6.30, Fig. 6.31 and Fig. 6.32. (a): Sample process with high concentration C-50au and hybridize with 20nM T-P-30au (Fig. 6.32). (b) Sample process with low concentration C-50au (Fig. 6.30) and hybridize with 20nM T-P-30au. (c) Sample process with low concentration C-50au and hybridize with 20nM 3mm-P-30au (Fig. 6.31).

CHAPTER 7

CONCLUSION AND FUTURE WORK

7.1 Conclusion

In this study, a new DNA sensing method is successfully demonstrated in which DNA hybridization events lead to the formation of nanoparticle satellites that bridge two electrodes and are detected electrically. The hybridization events are exclusively carried out only on specific locations, the surfaces of C-ssDNA modified 50 nm GNPs by controlling the C-50au positioning and passivation reaction of un-occupied APTES SAMs. The uniqueness of this work is that only a small number of T-ccDNA molecules (<10) is required to form the nanoparticle satellites, allowing ultra-sensitive DNA sensing. The principle of this new DNA sensing technique has been demonstrated using target DNA and three-base-pair-mismatched DNA in 20nM concentrations with a great selectivity.

The advantages of our work are described as following sections.

7.1.1 Three ssDNA system

Three-DNA system is applied in our detection mechanism. The major benefit of applying three-ssDNA system (Capture, Target, and Probe ssDNA) compares to two-DNA system (Probe and Target) is that no modification is required for the Target. Modification process for target ssDNA usually will cause the lost of the target sample during the purification process. If the target sample is only with limited among, another PCR process is required to amplify the target ssDNA concentration which is not very convenient.

Three-DNA system which including: (a) Capture ssDNA which is immobilized on the substrate surface or nanoparticle surface (in our approach). (b) Target ssDNA which is the

sample DNA we want detect. (c) Probe ssDNA which can be modified with signal amplifier such as fluorescence label or nanoparticles (in our approach). Both C-ssDNA and P-ssDNA are artificial synthesized oligonucleotide.

7.1.2 DNA Modified GNP

Instead directly immobilize C-ssDNA on the sensing area (SiO_2 surface between two gold electrodes); we immobilize C-ssDNA on the nanoparticle surface (50nm GNP in our case). The reason for this is because the melting transition behavior for DNA linked GNP is sharper than that of free DNA [2.22, 2.23]. It is important to have a sharp melting transition for preventing false signal when both mismatched ssDNA and complementary ssDNA exist in the detection system. If the melting temperatures for complementary and mismatched DNA are similar (which is usually the case when only 1 or couple base pair mismatch), and the melting transition is a broad range of temperature, the overlapping of the melting temperature will usually provide the false signal due to the mismatched DNA still have chance to hybridize.

Hybridization temperature is usually 10~15^{o}C lower than melting temperature in order to have a good hybridization efficiency for complementary DNA hybridization. However, this hybridization temperature might also allow mismatched DNA hybridization, too. These mismatched DNA hybridization events will cause a serious problem when we want have high sensitivity detection at very low target-ssDNA low concentration situation.

High sensitivity means that even with very low concentration target and very small among of hybridization events, the device can still collect enough signal for the readout. Therefore, for high sensitivity DNA detection, false signals provide by mismatched DNA hybridization can lead to the misjudgments.

Therefore, to have a sharp melting transition curve is very important which allows us to have high hybridization efficiency to the complementary hybridization event, but very low for the mismatched hybridization (as discussed at chapter 2.14, Fig. 2.18).

Thiolated ssDNA modified gold nanoparticle is robust and can be applied in many DNA detection applications such as optical detection methods (light scattering, light absorption, surface plasmon), electrical detection methods (I-V measurement) and mechanical detection methods (QCM, micro-cantilever). Gold nanoparticle is easy to be modified and can be use as a signal amplifier.

7.1.3 Accurate Control of GNP Positioning and Passivation reaction

Another important reason why we chose to modified C-ssDNA on 50nm GNP is we can control the C-50au positioning accurately "only" between two electrodes by applying attracting APTES SAMs and repelling MHA SAMs. After C-50au positioning, attracting APTES SAMs is passivated and converted to non-attractive methyl functional group.

This means, the only place that T-P-30au hybridization events can occur is on the C-50au surface. And there is no other place for T-P-30au to attach on the substrate by either hybridization or other attraction force. This is to say, instead of treating SiO_2 band between two electrodes as the sensing area, C-50an is the real sensing area in our detection design. As long as couple (2~3) hybridization event occur on the sensing area surface, the GNP bridge can be form and provide enough conductivity variation from open circuit to resistive circuit.

7.1.4 Theoretical Detection Sensitivity

Detection sensitivity in DNA detection usually means the smallest number of target DNA hybridization events required for instrument to receive distinguishable signal (signal with enough strength). In our detection mechanism, we combine both accurate C-50au positioning and passivation process which ensure every C-50au and T-P-30au hybridization only occur on the C-50au surface immobilized between two gold electrodes separated by ~90nm SiO_2 band and form GNP bridge across two gold electrodes. From experiment data, the device with only 4 GNP bridges provides the resistive circuit with resist around 160 kΩ. And for the device with 10 GNP bridges, the resist is lowered to 10 kΩ.

From the experiment results of SEM image and I-V measurement, we can say that even with only few (less than 10) hybridization events occur, we are able to detect. This is to say, the detection limit for our detection method should be able to reach ~zM range (10^{-21} M) theoretically if the hybridization efficiency between immobilized C-50au and T-P-30au can be improved.

7.2 Future Work

In principle, our detection sensitivity should be able reach to a molecular level; however, the lowest concentration we can detect is ~nM range so far. When we lower the T-ssDNA concentration to 20pM, the SEM image shows no T-P-30au hybridize with C-50au on the device. This indicates that the hybridization efficiency is low. Therefore, the most important thing for improving our detection performance is to increasing the hybridization efficiency between C-50au and T-P-30au, or between T-ssDNA and P-30au in the liquid phase.

Also, to remove excess C-ssDNA or P-ssDNA after preparation of ssDNA modified GNP (C-50au and P-30au) is important.

7.2.1 Remove Excess ssDNA from DNA Modified GNP Solution

For remove excess C-ssDNA and P-ssDNA, instead of repeating centrifuge/wash steps many times, Liquid Chromatography (LC) or high pressure liquid chromatography (HPLC) system might be a good choice. Gel filtration is a simple and reliable chromatographic method for separating molecules according to size. This is to say, by applying proper pore size of filter, P-30au and C-50au can flow through LC column faster compares to the small ssDNA molecular. Large DNA modified GNP (C-50au and P-30au) can not flow into the pore in the filter, but can only flow through the gaps between filters. Small molecules such as C-ssDNA and P-ssDNA (18 base pair + 9 poly T spacer + C_6 modification spacer = ~ 12nm) can flow through those pore inside the filter, therefore, the pathway for small molecules (excess ssDNA) is much

longer than that of DNA modified GNPs and take longer time for excess ssDNA to flow through the LC column.

7.2.2 Improve the Hybridization Efficiency

For improving the hybridization efficiency, there might be three things we can investigate: (a) Lower the DNA modification density of C-50au and P-30au by mixing short chain alkane with one end thiolated. It is known that the high ssDNA modification density is not suitable for ssDNA hybridization due to the volume required for double helix formation. If the surface DNA modification density is high (0.25 ssDNA/nm^2), only 4% can be hybridized, but with density around 0.1 ssDNA/nm^2, 33% can be hybridized (Linette M. Demers, Chad A. Mirkin, et al, 2000).

(b) Utilize hybridizing chamber for heterogeneous hybridization reaction between C-50au and T-P-30au. The way we process heterogeneous hybridization reaction in our experiment is immerse the whole sample into a tube with at least 0.3~0.5ml T-P-30au solution. However, as we discussed above, we only need 20~30 hybridization events to get a measureable I-V signal. That is to say, almost 99% of T-P-50au (~10^{11}) is wasted. By hybridizing T-P-30au with C-50au in the hybridization chamber, we need only less than 10ul T-P-30 to cover whole sample surface. we can first apply small among of P-30au to hybridize target ssDNA first, then concentrate T-P-30au by centrifuge, and the put 10ul concentrate T-P-30au on sample surface.

Also, with very limited among of T-P-30au volume, the frequency of T-P-30 can reach to the sample surface will increase significantly and therefore, increase hybridization efficiency.

(c) Reduce the repelling force from sample surface. We provide MHA SAMs on gold electrode surface which has carboxyl tail group (R-COOH $\rightarrow$R-COO^-) and provide repelling electrostatic force to the negatively charged DNA modified GNPs. To reduce this repelling force, instead applying MHA SAMs, we can mix MHA with alkane thiol such as Octadecanethiol (ODT). The head group of alkane thiol same as MHA which is thiol group (-SH), there the ratio

of MHA/ODT in the formation of SAMs on gold electrodes will follow the concentration ratio in the solution. Therefore, with mixing non-repulsive alkane thiol with repulsive carboxyl thiol, we can reduce the surface repelling force.

Also, we may increase the [Na^+] in the hybridization solution which can reduce the electric double layer interaction and reduce the repelling force.

REFERENCES

[1.1]: Epstein, J.R., Biran, I. and Walt, D.R., “Fluorescence-based nucleic acid detection and microarrays”. Anal. Chom. Acta 469, 3-36 (2002)

[1.2]: McDonnell, J.M. “Surface Plasmon resonance: toward an understanding of the mechanisms of biological molecular recognition”. Curr. Opin. Chem. Biol. 5, 572-577 (2001)

[1.3]: Storhoff, J.J., Elghanian, R., Mucic, R.C., Mirkin, C.A. and Letsinger, R.L. “One-pot colorimetric differentiation of polynucleotides with single base imperfections using gold nanoparticle probes”. J. Am. Chem. Soc. 120, 1757-1760 (2000)

[1.4]: Wang, J., Jiang, M. and Palecek, E., “Real-time monitoring of enzymatic cleavage of nucleic acid using a quartz crystal microbalance”. Bioelectrochem. Bioenergetics 4, 477-480 (1999)

[1.5]: Fritz, J. et al.,”Translating biomolecular recognition into nanomechanics”. Science 288, 316-318 (2000)

[1.6]: Plecek, E., “Oscillographic polarography of highly polymericed deoxyribonucleic acid”, Nature 188, 656-657 (1960)

[1.7]: Palecek, E., “Adsorptive transfer stripping voltammetry-determination of nanogram quantities of DNA immobilized at the electrode surface. Anal. Biochem. 170, 421-431 (1988)”

[2.1]: Gerald Weissmann and Robert. “Cell membranes : biochemistry, cell biology, & pathology”, New York : HP Pub. Co., c1975, 1981 printing.

[2.2]: Saenger, Wolfram (1984). Principles of Nucleic Acid Structure. New York: Springer-Verlag. ISBN 0387907629.

[2.3]: Alberts, Bruce; Alexander Johnson, Julian Lewis, Martin Raff, Keith Roberts and Peter Walters (2002). Molecular Biology of the Cell; Fourth Edition. New York and London: Garland Science. ISBN 0-8153-3218-1.

[2.4]: Butler, John M. (2001). Forensic DNA Typing. Elsevier. ISBN 978-0-12-147951-0. OCLC 45406517 223032110 45406517. pp. 14–15.

[2.5]: Mandelkern M, Elias J, Eden D, Crothers D (1981). "The dimensions of DNA in solution". J Mol Biol 152 (1): 153–61.

[2.6]: Gregory S; Barlow, KF; McLay, KE; Kaul, R; Swarbreck, D; Dunham, A; Scott, CE; Howe, KL et al. (2006). "The DNA sequence and biological annotation of human chromosome 1". Nature 441 (7091): 315–21.

[2.7]: Gordon !. Leonard, William N. Hunter, and Tom Brown. “Studies of the structure and stability of base pair mismatches, base pairs involving modified bases, and DNA drug complexes” J. of Chemical Crystallography, Vol. 24, No. 1, 1994

[2.8]: V. Chan, S.E. McKenzie, S. Surrey, P. Fortina, D.J. Graves, J. Colloid Interface Sci. 203 (1998) 197.

[2.9]: Golub, A. A., Zubenko, A. I., and Zhmud, B. V., J. Colloid Interface Sci. 179, 482 (1996).

[2.10]: M. Bezanilla, S. Manne, D.E. Laney, Y. Lyubchenko, H.G. Hansma, Langmuir 11 (1995) 655.

[2.11]: Alain Carre, Valerie Lacarriere, and William Birch.,” Molecular interactions between DNA and an aminated glass substrate ” J. Colloid and Interface Science 260 (2003) 49–55

[2.12]: C.R. Cantor, P.R. Schimmel, Biophysical Chemistry I. The Conformation of Biological Macromolecules, Freeman, New York, 1980.

[2.13]: Ganachaud, F., Elaissari, A., Pichot, C., Laayoun, A., and Cros, P., 54. Ma, C., and Bloomfield, V. A., Biophys. J. 67, 1678–1681 (1994) .Langmuir 13, 701–707 (1997)

[2.14]: Chrisey, L. A., et al., Mater. Res. Soc. Symp. Proc. 330, 179–185 57 (1994).

[2.15]: J. Marmur and P. Doty, “Determination of the base composition of deoxyribonucleic acid from its thermal denaturation temperature” J. Mol. Biol. (1962) 5, 109-118

[2.16]: Roger M. Wartell and Albert S. Benight “Thermal denaturation of DNA molecules: A comparison of theory with experiment“ PHYSICS REPORTS-REVIEW SECTION OF PHYSICS LETTERS Volume: 126 Issue: 2 Pages: 67-107 Published: 1985

[2.17]: Scott G. Delcourt and R. D. Blake, “Stacking Energies in DNA”, J. of Biol. Chem. Vol. 266, No. 23, pp. 15160-15169, 1991.

[2.18]: Philip N. Borer, Barbara Dengler, Ignacio Tinoco Jr., “Stability of Ribonucleic acid Double-stranded Gelices”, J. Mol. Biol. (1974) 86, 843-853

[2.19]: Richard Owczarzy, Bernardo G. Moreira, Yong You, Mark A. Behlke, and Joseph A. Walder., “Predicting Stability of DNA Duplexes in Solutions Containing Magnesium and Monovalent Cations”. Biochemistry 2008, 47, 5336–5353

[2.20]: Richard Owczarzy, Yong You, Bernardo G. Moreira, Jeffrey A. Manthey, Lingyan Huang, Mark A. Behlke, and Joseph A. Walder. “Effects of Sodium Ions on DNA Duplex Oligomers: Improved Predictions of Melting Temperatures”, Biochemistry 2004, 43, 3537-3554

[2.21]: 21 Demers, L.M.,Mirkin, C.A.,Mucic, R.C., Reynolds, R.A., Letsinger, R.L., Elghanian, R., and Viswanadham, G.: Anal. Chem., 2000, 72, pp. 5535–5541

[2.22]: Rongchao Jin, Guosheng Wu, Zhi Li, Chad A. Mirkin,* and George C. Schatz,” What Controls the Melting Properties of DNA-Linked Gold Nanoparticle Assemblies?” J. AM. CHEM. SOC. 2003, 125, 1643-1654

[2.23]: Y. Sun, N.C. Harris, C.-H. Kiang, “melting transition of directly linked gold nanoparticle DNA assembly” Physica A 350 (2005) 89-94.

[2.24]: Gold-nanoparticle-assisted oligonucleotide immobilization for improved DNA detection; C. Minard-Basquin, R. K.ugler, N.N. Matsuzawa and A. Yasuda, IEE Proc.-Nanobiotechnol., Vol. 152, No. 2, April 2005

[2.25]: Organic Reactions in Ionic Liquids Ionic Liquid-promoted Efficient Synthesis of Disubstituted and Trisubstituted Thioureas Derivatives. Chinese Chemical Letters Vol. 16, No. 2, pp 201-204, 2005

[2.26]: Kinetic study of DNA/DNA hybridization with electrochemical impedance spectroscopy. Delan Li a,b, Xiangqin Zou a, Qing Shen b, Shaojun Dong a,* Electrochemistry Communications 9 (2007) 191–196

[2.27]: A.B. Steel, T.M. Herne, M.J. Tarlov, Anal. Chem. 70 (1998) 4670.

[2.28]: R. Levicky, T.M. Herne, M.J. Tarlov, S.K. Satija, J. Am. Chem. Soc. 120 (1998) 9787.

[2.29]: Laidler, K. J., Chemical Kinetics, 3rd edn, Harper Collins, New York 1987, p. 231.

[3.1]: Catterall, R. W., "Chemical Sensors". 1997, Oxford, UK: Oxford University Press.

[3.2]: Thevenot D. R., Toth K., Durst R. A., Wilson G. S., "Electrochemical Biosensors: Recommended Definitions and Classification". Pure Appl. Chem, 1999, 71,2333-2348

[3.3]: Lakard B., Herlem G., Lakard S., Antoniou A., Fahys B., "Urea potentiometric biosensor based on modified electrodes with urease immobilized on polyethylenimine films". Biosens. Bioelectron. 2004, 19, 1089-1096

[3.4]: Jiri Homola, "Present and future of surface plasmon resonance biosensors". Anal. Bioanal. Chem. (2003) 377:528-539

[3.5]: Snyder AW, Love JD (1983) Optical waveguide theory. Chapman and Hall, London

[3.6]: Parriaux O, Voirin G (1990) Sens Actuators A 21–23:1137

[3.7]: Avraham Rasooly and Keith E. Herold. "Biosensors and biodetection : methods and protocols", New York : Humana Press, c2009

[3.8]: www.bmglabtech.com

[3.9]: M. Lazerges , H. Perrot , N. Zeghib , E. Antoine, C. Compere, "In situ QCM DNA-biosensor probe modification " Sensors and Actuators B 120 (2006) 329–337

[3.10]: A. Bardea, A. Dagan, I. Ben-Dov, B. Amit, Amplified microgravimetric quartz-crystal-microbalance analyses of oligonucleotide complexes: a route to a Tay-Sachs biosensor device, Chem. Commun. (1998) 839–840

[3.11]: I. Mannelli, M. Minunni, S. Tombelli, M. Mascini, Quartz crystal microbalance (QCM) affinity biosensor for genetically modified organism (GMOs) detection, Biosens. Bioelectron. 18 (2003) 129–140.

[3.12]: X.-T. Mo, Y.-P. Zhou, H. Lei, L. Deng, Microbalance-DNA probe method for the detection of specific bacteria in water, Enzyme Microb. Technol. 30 (2002) 583–589.

[3.13]: H. Su, M. Thompson, Kinetics of interfacial nucleic acid hybridization studied by acoustic network analysis, Biosens. Bioelectron. 10 (1995) 329–340.

[3.14]: K. Niikura, H. Matsuno,Y. Okahata, Direct monitoring of DNA polymerase reactions on a quartz-crystal microbalance, J. Am. Chem. Soc. 120 (1998) 8537–8538.

[3.15]: H. Matsuno, H. Furusawa, Y. Okahata, Kinetic studies of DNA cleavage reactions catalyzed by an ATP-dependent deoxyribonuclease on a 27-MHz quartz-crystal microbalance, Biochemistry 44 (2005) 2262–2270.

[3.16]: L. Zhu, Y. Gao, H. Shen, Y. Yang, and L. Yuan, “A Quartz Crystal Microbalance (QCM) Study of Single-Strand DNA Hybridization and Hydrolytic Cleavage”, Journal of Analytical Chemistry, Vol. 60, No. 8, 2005, pp. 780–783.

[3.17]: Wu, G. et al. Origin of nanomechanical cantilever motion generated from biomolecular interactions. Proc. Natl. Acad. Sci. USA 98, 1560–1564 (2001).

[3.18]: Hansen, K.M. et al. Cantilever-based optical deflection assay for discrimination of DNA single nucleotide mismatches. Anal. Chem. 73, 1567–1571 (2001).

[3.19]: Guanghua Wu, Ram H. Datar, Karolyn M. Hansen, Thomas Thundat, Richard J. Cote, and Arun Majumdar, “Bioassay of prostate-specific antigen (PSA) using microcantilevers” nature biotechnology • VOLUME 19 • SEPTEMBER 2001 856-860

[3.20]: Karolyn M. Hansen, Hai-Feng Ji, Guanghua Wu, Ram Datar, Richard Cote, Arunava Majumdar, and Thomas Thundat, “Cantilever-Based Optical Deflection Assay for Discrimination of DNA Single-Nucleotide Mismatches” Anal. Chem. 2001, 73, 1567-1571

[3.21]: S.Q. Lud, M.G. Nikolaides, I. Haase, M. Fischer and A.R. Bausch (2006)."Field Effect of Screened Charges: Electrical Detection of Peptides and Proteins by a Thin Film Resistor" ChemPhysChem 7(2), 379-384

[3.22]: Dong-Sun Kim, Yong-Taek Jeong, Hey-Jung Park, Jang-Kyoo Shin, Pyung Choi , Jong-Hyun Lee , Geunbae Lim, “An FET-type charge sensor for highly sensitive detection of DNA sequence”, Biosensors and Bioelectronics 20 (2004) 69–74

[3.23]: Chang, Hung; Iqbal, Samir M.; Stach, Eric A.; King, Alexander H.; Zaluzec, Nestor J.; Bashir, Rashid. ”Fabrication and characterization of solid-state nanopores using a field emission scanning electron microscope”, Applied Physics Letters (2006), 88(10)

[3.24]: Samir M. Iqbal, Demir Akin and Rashid Bashir. “Solid-state nanopore channels with DNA selectivity”, Nature Nanotechnology, (2007), pp243-248

[3.25]: Young-Rok Kim, Junhong Min, In-Ho Lee, Suhyeun Kim, Ah-Gi Kim, Kuihyun Kim, Kak Namkoong, Christopher Ko. “Nanopore sensor for fast label-free detection of short double-stranded DNAs”, Biosensors and Bioelectronics 22 (2007) 2926-2931

[3.26]: Tang, Xiaowu; Bansaruntip, Sarunya; Nakayama, Nozomi; Yenilmez, Erhan; Chang, Ying-lan; Wang, Qian. “Carbon Nanotube DNA Sensor and Sensing Mechanism.” Nano Letters (2006), 6(8), 1632-1636

[3.27]: Hahm, Jong-in; Lieber, Charles M.. “Direct ultrasensitive electrical detection of DNA and DNA sequence variations using nanowire nanosensors.” Nano Letters (2004), 4(1), 51-54

[3.28]: Cui Y; Wei Q; Park H; Lieber C M;” Nanowire nanosensors for highly sensitive and selective detection of biological and chemical species.” Science (New York, N.Y.) (2001), 293(5533), 1289-92.

[3.29]: Vladimir V. Tsukruk and Valery N. Bliznyuk, “Adhesive and Friction Forces between chemically Modified Silicon and Silicon Nitride Surfaces” Langmuir (1998), 14,446-455

[3.30]: Stevenson P, Sones KR, Gicheru MM, Mwangi EK. (1995). "Comparison of isometamidium chloride and homidium bromide as prophylactic drugs for trypanosomiasis in cattle at Nguruman, Kenya.". Acta Trop. 59 (2): 257–258.

[3.31]: Diaz F, Bayona-Bafaluy MP, Rana M, Mora M, Hao H, Moraes CT. (2002). "Human mitochondrial DNA with large deletions repopulates organelles faster than full-length genomes under relaxed copy number control.". Nucleic Acids Res. 30 (21): 4626–33.

[3.32]: Huang Q, Fu WL (2005). "Comparative analysis of the DNA staining efficiencies of different fluorescent dyes in preparative agarose gel electrophoresis". Clin. Chem. Lab. Med. 43 (8): 841–2.

[3.33]: Daniel Berdat, Annick Marin, Fernando Herrear, Martin A.M. Gijs, “DNA biosensor using fluorescence microscopy and impedance spectroscopy”, Sensors and Actuator B 118 (2006) 53-59.

[3.34]: Lisa M. Dillenback, Glenn P. Goodrich, and Christine D. Keating, “Temperature-Programmed Assembly of DNA:Au Nanoparticle Bioconjugates”, Nano Letters Vol. 6, No. 1, pp16-23, (2006)

[3.35]: Yi-Ting Cheng, Ching-Chin Pun, Chien-Ying Tsai, Ping-Hei Chen∗ , “An array-based CMOS biochip for electrical detection of DNA with multilayer self-assembly gold nanoparticles”, Sensors and Actuators B 109 (2005) 249–255.

[3.36]: So-Jung Park, T. Andrew Taton,* Chad A. Mirkin, “Array-Based Electrical Detection of DNA with Nanoparticle Probes”, Science, Vol. 295, (2002) pp.1503-1506.

[3.37]: L. Moreno-Hagelsieb, P.E. Lobert, R. Pampin, D. Bourgeois, J. Remacle, D. Flandre, “Sensitive DNA electrical detection based on interdigitated Al/Al2O3 microelectrodes”, Sens. Actuators B 98 (2004) 269–274.

[3.38]: J. Li, M. Xue, Z. Lu, Z.K. Zhang, C.G. Feng, M.S. Chan, “A highdensity conduction-based micro-DNA identification array fabricated with a CMOS compatible process”, IEEE Trans. Electron Dev. 50 (2003) 2165–2170.

[3.39]: S. Tombelli, M. Mascini, A.P.F. Turner, « Improved procedures for immobilization of oligonucleotides on gold coated piezoelectric quartz crystals «, Biosensors and Bioelectronics 17 (2002) 929_/936

[3.40]: Valerie Reinke, Department of Genetics, Yale University, New Haven, CT 06520 USA

[3.41]: Miklos, G.L. and R. Maleszka, Microarray reality checks in the context of a complex disease. Nat Biotechnol, 2004. 22 (5): p. 615-21.

[3.42]: Breitling, R., A. Amtmann, and P. Herzyk, Iterative Group Analysis (iGA): a simple tool to enhance sensitivity and facilitate interpretation of microarray experiments. BMC Bioinformatics, 2004. 5: p. 34.

[3.43]: Park, J.C., H.S. Kim, and J.J. Kim, Bidirectional incremental parsing for automatic pathway identification with combinatory categorial grammar. Pac Symp Biocomput, 2001: p. 396-407.

[3.44]: Spellman, P.T., G. Sherlock, M.Q. Zhang, V.R. Iyer, K. Anders, M.B. Eisen, P.O. Brown, D. Botstein, and B. Futcher, Comprehensive identification of cell cycle-regulated genes of the yeast Saccharomyces cerevisiae by microarray hybridization. Mol Biol Cell, 1998. 9 (12): p. 3273-97.

[3.45]: Roberts, C.J., B. Nelson, M.J. Marton, R. Stoughton, M.R. Meyer, H.A. Bennett, Y.D. He, H. Dai, W.L. Walker, T.R. Hughes, M. Tyers, C. Boone, and S.H. Friend, Signaling and circuitry of multiple MAPK pathways revealed by a matrix of global gene expression profiles. Science, 2000. 287 (5454): p. 873-80.

[3.46]: Shoemaker, D.D., E.E. Schadt, C.D. Armour, Y.D. He, P. Garrett-Engele, P.D. McDonagh, P.M. Loerch, A. Leonardson, P.Y. Lum, and G. Cavet, Experimental annotation of the human genome using microarray technology. Nature, 2001. 409: p. 922-927.

[3.47]: Schena, M., DNA Microarrays: A Practical Approach. 1999: Oxford University Press.

[3.48]: Mills, J.C., K.A. Roth, R.L. Cagan, and J.I. Gordon, DNA microarrays and beyond: completing the journey from tissue to cell. Nat Cell Biol, 2001. 3 (8): p. E175-8.

[3.49]: Allison, D.B., X. Cui, G.P. Page, and M. Sabripour, Microarray data analysis: from disarray to consolidation and consensus. Nat Rev Genet, 2006. 7 (1): p. 55-65.

[3.50]: Hegde, P., R. Qi, K. Abernathy, C. Gay, S. Dharap, R. Gaspard, J.E. Hughes, E. Snesrud, N. Lee, and J. Quackenbush, “A concise guide to cDNA microarray analysis. Biotechniques,” 2000. 29 (3): p. 548-50, 552-4, 556 passim.

[3.51]: Schena, M., D. Shalon, R.W. Davis, and P.O. Brown, “Quantitative monitoring of gene expression patterns with a complementary DNA microarray.” Science, 1995. 270 (5235): p. 467-70.

[3.52]: Pease, A.C., D. Solas, E.J. Sullivan, M.T. Cronin, C.P. Holmes, and S.P. Fodor, “Light-generated oligonucleotide arrays for rapid DNA sequence analysis.” Proc Natl Acad Sci U S A, 1994. 91 (11): p. 5022-6.

[3.53]: Hughes, T.R., M. Mao, A.R. Jones, J. Burchard, M.J. Marton, K.W. Shannon, S.M. Lefkowitz, M. Ziman, J.M. Schelter, and M.R. Meyer, “Expression profiling using microarrays fabricated by an ink-jet oligonucleotide synthesizer.” Nature Biotechnology, 2001. 19: p. 342-347.

[3.54]: Nakano, Y.I., M. Okamoto, and T. Nishida, “Enriching agent animations with gestures and highlighting effects.” Intelligent Media Technology for Communicative Intelligence, 2004. 3490: p. 91-98.

[3.55]: Schena M. 1996. “Genome analysis with gene expression microarrays.” Bioessays 18(5):427–31

[3.56]: Marshall A, Hodgson J. “DNAchips: an array of possibilities. Nat. Biotechnol.” 16:27–31, 1998.

[3.57]: Patrick Cooley, David Wallace, Bogdan Antohe, MicroFab TechnoloApplications of Ink-Jet Printing Technology to BioMEMS and Microfluidic Systems gies, Inc. “Applications of Ink-Jet Printing Technology to BioMEMS and Microfluidic Systems.” Proceedings, SPIE Conference on Microfluidics and BioMEMS October, 2001

[3.58]: Fodor SP, Read JL, Pirrung MC, Stryer L, LuAT, Solas D. “Light-directed, spatially addressable parallel chemical synthesis.” Science 251:767–73,1991.

[4.1]: Th. Wink, S. J. van Zuilen, A. Bult and W. P. van Bennekom ”Self-assembled Monolayers for Biosensors” Analyst, April 1997, Vol. 122 (43R-50R)

[4.2]: Bain, C. D., and Whitesides, G. M., J. Am. Chem. Soc., 1989, 111, 7164.

[4.3]: Dubois, L. H., and Nuzzo, R. G., Annu. Rev. Phys. Chem., 1992, 43, 437.

[4.4]: Widrich, C. A., Chung, C., and Porter, M. D., J. Electroanal. Chem.,1991, 310, 335.

[4.5]: Nuzzo, R. G., Dubois, L. H., and Allara, D. L., J. Am. Chem. Soc.,1990, 112, 558.

[4.6]: Strong, L., and Whitesides, G. M., Langmuir, 1988, 4, 546.

[4.7]: D.K. Aswal, S. Lenfant, D. Guerin , J.V. Yakhmi , D. Vuillaume, ‘’ Self assembled monolayers on silicon for molecular electronics’’ Analytica Chimica Acta 568 (2006) 84–108

[4.8]: Joonyeong Kim, “Investigation of the Formation and Structure of APTES Films on Silicon Substrates”, www.Piketech.com (instrument menu)

[4.9]: Wei ZQ, Wang C, Zhu CF, Zhou CQ, Xu B, Bai CL, ” Study on single-bond interaction between amino-terminated organosilane self-assembled monolayers by atomic force microscopy”, Surface Science 459 (2000) 401–412

[4.10]: J. Zhao, L. Luo, X. Yang, E. Wang, and S. Dong, Electroanalysis, 1999, 11, 1108.

[4.11]: K. Aoki and T. Kakiuchi, J. Electroanal. Chem., 1999, 478, 101.

[4.12]: K. Kim and J. Kuwak, J. Electroanal. Chem., 2001, 512, 83.

[4.13]: P.C. Hiemenz, Principles of Colloid and Surface Chemistry, Marcel Dekker, New York, 1977.

[4.14]: G.D. Parfitt, in Dispersion of Powders in Liquids with Special Reference to Pigments, ed. G.D. Parfitt, Applied Science, London, p.1, 1981.

[4.15]: J.T.G. Overbeek, J. Colloid Interf. Sci. 58, 408 (1977).

[4.16]: C.J. Brinker and G.W. Scherer, Sol-Gel Science: The Physics and Chemistry of Sol-Gel Processing, Academic Press, San Diego, CA, 1990.

[4.17]: Lyklema, J. “Fundamentals of Interface anA.C. Pierre, Introduction to Sol-Gel Processing, Kluwer, Norwell, MA, 1998. d Colloid Science”, vol.2, page.3.208, 1995

[4.18]: A.C. Pierre, Introduction to Sol-Gel Processing, Kluwer, Norwell, MA, 1998.

[5.1] Sang-Woo Joo" Characterization of self-assembled phenyl and benzyl isothiocyanate thin films on Au surfaces", Surf. Interface Anal. 2006; 38: 173–177

[5.2]: Zhang Gao LE, Zhen Chu CHEN, Yi HU, Qin Guo ZHENG, "Organic Reactions in Ionic Liquids: Ionic Liquid-promoted Efficient Synthesis of Disubstituted and Trisubstituted Thioureas Derivatives", Chinese Chemical Letters Vol. 16, No. 2, pp 201-204, 2005

[6.1]: The electrical double layer is formed due to rearrangement (screening) of ions that are present in the liquid medium. Its electrostatic potentials and charge densities are described by the Poisson-Boltzmann equation. When the nanoparticles come very close to the substrate, the van der Waals interaction also contributes to the interaction energy. More details can be found in the later part of this paper. See also refs 38-39.

[6.2]: Israelachvili, J. Intermolecular and Surface Forces, 2nd ed.; Academic Press: London; San Diego, 1991.

[6.3]: Verwey, E. J. W.; Overbeek, J. T. G. Theory of the Stability of Lyophobic Colloids; Elsevier: Amsterdam, 1948. 27-29

[6.4]: Cui, Y.; Bjork, M. T.; Liddle, J. A.; Sonnichsen, C.; Boussert, B.; Alivisatos, A. P. Nano Lett. 2004, 4, 1093-1098.

[6.5]: Xia, Y. N.; Yin, Y. D.; Lu, Y.; McLellan, J. AdV. Funct. Mater. 2003, 13, 907-918.

[6.6]: Gordon, M. J.; Peyrade, D. Appl. Phys. Lett. 2006, 89, 053112.

[6.7]: First, both MHA and APTES functionalized surfaces are hydrophilic, so that when the sample is removed from the aqueous solution of gold colloid, the sample is completely covered with a film of water and produces no water-air interface near the surface patterns. Second, while the sample is entirely covered with the water film, it is immediately immersed into a large volume of pure methanol to rinse unattached nanoparticles from the substrate. When the sample is finally removed from the methanol for drying with nitrogen, no unattached nanoparticles are present to contribute to capillary force driven assembly. Also, if the capillary force were instrumental in the observed

nanoparticle placement, the amount of immersion time in the Au colloidal solution would be irrelevant. However, if the immersion time is reduced to a few minutes (<_4 min), with everything else kept exactly the same, we find almost no attachment of Au nanoparticles on the substrate. This serves as another direct evidence that capillary forces are not responsible for the observed nanoparticle placement.

[6.8]: Hiemenz, P. C. Principles of Colloid and Surface Chemistry; Marcel Dekker: New York, 1977.

[6.9]: Bell, G. M.; Levine, S.; McCartney, L. N. J. Colloid Interface Sci. 1970, 33, 335-359.

[6.10]: Warszynski, P.; Adamczyk, Z. J. Colloid Interface Sci. 1997, 187, 283-295.

[6.11]: Adamczyk, Z.; Warszynski, P. AdV. Colloid Interface Sci. 1996, 63, 41-149.

[6.12]: Loeb, A. L.; Overbeek, J. T. G.; Wiersema, P. H. The Electrical Double Layer Around a Spherical Colloid Particle; MIT Press: Cambridge, 1960.

[6.13]: Ohshima, H. J. Colloid Interface Sci. 1995, 174, 45-52.

[6.14]: The aqueous gold colloidal solution contains Na+, citrate ions ($C_6O_7H_7^-$, $C_6O_7H_6^{2-}$, $C_6O_7H_5^{3-}$), Cl^-, H_3O^+, and OH^-. Their concentrations are (from the measured pH of 6.6, known dissociation constants of citrate ions, and private communication with Ted Pella Inc.): $[Na^+] = 7.8 \times 10^{-6}$ M, $[C_6O_7H_7^-] = 1.5 \times 10^{-8}$ M, $[C_6O_7H_6^{2-}] = 1.0 \times 10^{-6}$ M, $[C_6O_7H_5^{3-}] = 1.6 \times 10^{-6}$ M, $[Cl^-] = 1.2 \times 10^{-6}$ M, $[H_3O^+] = 2.5 \times 10^{-7}$ M, $[OH^-] = 4.0 \times 10^{-8}$ M.

[6.15]: Loeb, A. L.; Overbeek, J. T. G.; Wiersema, P. H. The Electrical Double Layer Around a Spherical Colloid Particle; MIT Press: Cambridge, 1960.

[6.16]: Ohshima, H. J. Colloid Interface Sci. 1995, 174, 45-52.

[6.17]: Ohshima, H. J. Colloid Interface Sci. 1995, 171, 525-527.

[6.18]: Biggs, S.; Mulvaney, P.; Zukoski, C. F.; Grieser, F. J. Am. Chem. Soc. 1994, 116, 9150-9157.

[6.19]: Kane, V.; Mulvaney, P. Langmuir 1998, 14, 3303-3311.

[6.20]: Kumagai, S.; Yoshii, S.; Yamada, K.; Matsukawa, N.; Fujiwara, I.; Iwahori, K.; Yamashita, I. Appl. Phys. Lett. 2006, 88, 153103.

[6.21]: The value of the Hamaker constant is dominated by substrate materials and medium, and the effect of SAMs on Hamaker constant is negligible as long as the separation is larger than ~5 nm. See, for example, ref [6.22].

[6.22]: Israelachvili, J. N.; Tabor, D. Proc. R. Soc. London, Ser. A 1972, 331, 19-38.

[6.23]: Biggs, S.; Mulvaney, P. J. Chem. Phys. 1994, 100, 8501-8505.

[6.24]: Barten, D.; Kleijn, J. M.; Duval, J.; von Leeuwen, H. P.; Lyklema, J.; Stuart, M. A. C. Langmuir 2003, 19, 1133-1139.

[6.25]: L.-C. Ma, R. Subramanian, H.-W. Huang, V. Ray, C.-U. Kim, and S. J. Koh, “Electrostatic Funneling for Precise Nanoparticle Placement: A Route to Wafer-Scale Integration”. Nano Lett. 7, 439 (2007).

[6.26]: Hong-Wen Huang, Pradeep Bhadrachalam, Vishva Ray, and Seong Jin Koh, “Single-particle placement via self-limiting electrostatic gating”. APPLIED PHYSICS LETTERS 93, 073110 (2008)

BIOGRAPHICAL INFORMATION

Hong-Wen Huang, raised in Pingtung, Taiwan, graduated in 1994 from high school. He entered National Cheng Kung University at autumn as a Chemical Engineering major with an emphasis in polymer synthesis and analysis. He graduated and received his B.S. degree in 1999. He entered National Taiwan University at autumn, 1999 as a Material Science and Engineering major and kept focusing on rigid-rod epoxy resin synthesis and analysis. He visited Dr. Wei-Ping Pan in Western Kentucky University as a visiting scholar for one semester at Fall, 2000. He got trained for many thermal analysis tools in Dr. Pan's thermal analysis lab and experienced first snow in his life. He received his M.S. degree in Material Science and Engineering from National Taiwan University in 2002.

After 2 year alternative military service in Ping-Tung environment protection bureau, he joined Ph.D program in UT Arlington as a Material Science and Engineering major, in Fall, 2004. He set up his future research field related to nanotechnology and biotechnology and joined Dr. Seong Jin Koh's group in Spring, 2005. He participated the project of accurate controlling of nanoparticle placement in one-dimension and zero-dimension. After nanoparticle placement project finished, he started his own project of developing a new DNA detection mechanism.

He finished all the course work with GPA 4.0 and got "Graduate Student Seminar Award" at Feb 22, 2008 from Materials Science and Engineering Department, UT Arlington. He got First Place of "Best Student Paper Award in Nanomaterials" during TMS 2008 Annual Meeting and Exhibition (March 9-13, 2008). And he got "University Scholar award" at President's Convocation for Academic Excellence, April 23, 2009, UT Arlington.

The expected date for him to receive his Ph. D. degree is May, 2010.